LARS Information Note 052875

Geometric Analysis and Restitution of Digital Multispectral Scanner Data Arrays

by

J. R. Baker
and
E. M. Mikhail

Published by the
Laboratory for Applications of Remote Sensing
and the
School of Civil Engineering
Purdue University
Lafayette, Indiana 47907

This work was sponsored by the National Aeronautics and Space Administration under Grant No. NGL-15-005-112 and Contract No. NAS9-14016 and the Purdue School of Civil Engineering. T-1039/4.

ACKNOWLEDGMENTS

The author wishes to express his appreciation to his advisor, Dr. Edward M. Mikhail, for his active interest and assistance in this undertaking. Also he would like to thank Dr. G. Warren Marks, Dr. Philip Swain, and Dr. Leroy Silva for their guidance and recommendations, as well as Dr. John Trinder, who collaborated in the early stages of the investigation, and Mr. Paul Anuta for his able advice during the investigation. The author is also indebted to the Laboratory for Applications of Remote Sensing, which sponsored the research and provided the basic data.

TABLE OF CONTENTS

TABLE OF CONTENTS, cont.

TABLE OF CONTENTS, cont.

LIST OF TABLES

LIST OF TABLES, cont.

LIST OF FIGURES

LIST OF FIGURES, cont.

LIST OF FIGURES, cont.

ABSTRACT

Baker, James Richard. Ph.D., Purdue University, May 1975. GEOMETRIC ANALYSIS AND RESTITUTION OF DIGITAL MULTISPECTRAL SCANNER DATA ARRAYS. Major Professor: Edward M. Mikhail.

This thesis contains the results of an investigation performed in order to define causes of geometric defects within digital multispectral scanner (MSS) data arrays, to analyze the nature of the resulting geometric errors, and to investigate restitution methods to correct or reduce such geometric errors.

The thesis includes a review of digital multispectral scanning systems, including the recording and digital form for computer aided analysis. Causes of geometric errors within the data arrays are presented, and previous investigations of geometric aspects of remote sensing systems are reviewed.

The introduction of geometric transformation relationships for scanned data, from which collinearity equations for MSS may be derived, serves as the basis of parametric methods of analysis and restitution of MSS digital data arrays. The linearization of these collinearity equations is presented, including consideration of the functional assumptions made in order to model the stochastic changes in the exterior orientation of the sensor down the flight line.

Parametric algorithms for analysis and restitution based upon the above analytical treatment which were considered are: the direct use of MSS collinearity equations, and the use of piecewise polynomials based upon the linearized collinearity equations. In addition, nonparametric algorithms for restitution are introduced, as an alternative to the parametric algorithms.

A proposed system for the geometric analysis and restitution of MSS digital data arrays is introduced. This procedure was used to test the methods of analysis and restitution, utilizing actual MSS data arrays from two aircraft flights. The results of these tests indicate that the collinearity equations can yield acceptable results when utilized for the analysis and restitution of such arrays. The investigation indicates that the piecewise polynomial algorithms are in general inferior to other methods of restitution. The nonparametric algorithms show great promise for the restitution of these arrays since the resulting accuracy of restitution is comparable to or better than that using collinearity, and they possess definite advantages in computational efficiency. The arithmetic mean algorithm appears to perhaps represent a particularly efficient nonparametric algorithm for restitution of MSS digital data, at least for the arrays tested.

INTRODUCTION

This introduction serves to define the problem to be investigated. The objectives of the research are presented, and the scope of the investigation is defined. An outline of the thesis is included as an aid to the reader.

Statement of the Problem

Computer aided analysis of digitally recorded multispectral scanner (MSS) data arrays with the aid of high speed digital computers has made great progress recently. However, the digital data arrays which serve as the basis for these investigations are subject to geometric distortions, which are presently ignored or subordinated to the interpretation aspects. Consequently, the research problem of this thesis is to investigate the geometric distortions present within digital MSS arrays, and to formulate procedures for reducing the geometric errors present within the data.

Research Objectives

Based upon the problem statement above, the following research objectives were formulated.

1.) To systematically review the methods of recording MSS data, generating digital MSS data arrays, and performing computer

aided analysis, in order to define the context within which the geometric aspects of these data are considered.

2.) To define the geometric distortions present within the data arrays.

3.) To analyze the transformation equations of MSS data recording and derive from them functional forms for investigating geometric errors within these data and algorithms for reducing these errors.

4.) To introduce nonparametric methods not based upon these transformation relationships as an alternate method of reducing geometric error within the arrays.

5.) To identify the problems associated with these methods when working with digital rather than continuously recorded information and to present methods to deal with these problems.

6.) To test the analysis methods of 3. and 4. above on real MSS digital data arrays.

Scope of the Investigation

To satisfy the research objectives above, the investigation is limited to evaluation of MSS digital data arrays obtained by airborne multispectral scanners. However many of the concepts and procedures presented will be applicable to data gathered from spacecraft. The investigation was limited to actual data arrays presently existing. No simulation of data was attempted. The investigation includes both theoretical modeling and numerical analysis by computer as an integral part of the research.

Outline of the Thesis

The thesis is organized in such a manner as to provide a logical sequence, in general progressing from the more theoretical aspects of analysis to the more practical applications utilizing the relationships introduced. In Chapter 1 a brief introduction to the field of remote sensing, the most widely used remote sensing systems, and basic radiometric concepts common to many of them is given. The physical configuration of the multispectral scanner and the processing of the information gathered by the scanner into digital data arrays are presented. Techniques of computer aided analysis utilizing the digital arrays thus generated are introduced. Also included in this chapter are derivations of the basic sources and types of geometric errors which have been included in the arrays. The chapter concludes with a review of previous investigations of the geometric aspects of remote sensing systems.

Chapter 2 begins with the introduction of a general remote sensing transformation, including both radiometric and geometric information. The geometric portion of this transformation is derived in its most general form for the MSS system. From this basic geometric transformation, the collinearity equations for multispectral scanners are derived. The procedure for linearizing these equations by Taylor's series for performing resection by least squares is presented. This linearization includes the dynamic effects of time varying orientation parameters.

In Chapter 3 restitution methods for MSS data arrays are discussed. The purpose of these restitution methods is to process the data to

form arrays which are essentially orthographic projections. First, simple resampling algorithms are presented which are useful as pre-processing steps. The direct use of MSS collinearity equations as a restitution method is next presented. The use of polynomial forms for restitution is given, and a discussion follows of some of the problems associated with using piecewise polynomials and the collinearity equations. A completely different approach to restitution of MSS digital data arrays is then introduced, that of nonparametric methods. The basic forms for these nonparametric restitution algorithms are presented along with the major advantages and disadvantages of each. The chapter next deals with the unique problems associated with transforming digital data arrays into the desired form. The chapter concludes with a discussion of the problems associated with determining elevations within digital data arrays which have been obtained from singly scanned areas.

Chapter 4 deals with the testing of the above methods of analysis and restitution on actual MSS data arrays. Two flight lines of data were obtained and analyzed using each of the above methods. The results are statistically analyzed and compared.

The thesis concludes in Chapter 5 by summarizing the research effort, stating the conclusions drawn from the investigations performed, and enumerating recommendations for further research in this area.

1. THE MULTISPECTRAL SCANNING (MSS) SYSTEM

This chapter is intended to provide the background material required for an understanding of the investigation. A brief introduction to the discipline of remote sensing, and a brief survey of remote sensing systems is provided. The basic radiometric concepts required for an understanding of recording data by multispectral scanners is described, and the physical configuration of the scanner is presented. The digital aspects of multispectral scanning (MSS) systems are presented, including a brief introduction to the field of machine aided interpretation utilizing digitally recorded data. The basic geometric distortions inherent in the digital arrays are presented in order to obtain an appreciation of geometric defects within the data. The chapter concludes with a review of previous investigations in geometric analysis of remote sensing systems.

1.1 Introductory Remarks

The term "remote sensing" may be applied to virtually any activity in which information is gathered without physical contact. As generally used, however, the term is usually applied to those systems which yield data about the Earth's surface and its resources from a considerable distance. References [1] through [4] contain definitions of remote sensing systems by persons prominent in this

field. The definition from [4] is one of the most descriptive: "Remote sensing denotes the joint effects of employing modern sensors, data processing equipment, information theory and processing methodology, communications theory and devices, space and airborne vehicles, and large systems theory and practice for the purpose of carrying out aerial or space surveys of the Earth's surface." It may be seen from this definition that the existing disciplines of photogrammetry, radargrammetry, hologrammetry, and many other activities can be considered as divisions within remote sensing.

Remote sensing systems may be classified according to many different criteria [5]: geometric properties, stationary or moving platform, image forming or non image forming, and passive or active with respect to the source of a carrier field such as electromagnetic energy, sound, or gravity. Figure 1.1 depicts the various classification schemes, ending with examples of sensors which fall into the various categories.

An active-passive differentiation between sensor types depends upon whether the sensor generates its own energy source for the carrier field (active) or relies upon an external source for the carrier field (passive). Both active and passive systems may have image forming capabilities. Classification as regards geometry would include area recording (e.g. frame camera), line recording (e.g. panoramic and continuous strip cameras), or point recording (e.g. optical mechanical scanners). References [6], [7], and [8] contain other classification schemes or tabular data concerning the properties of remote sensors.

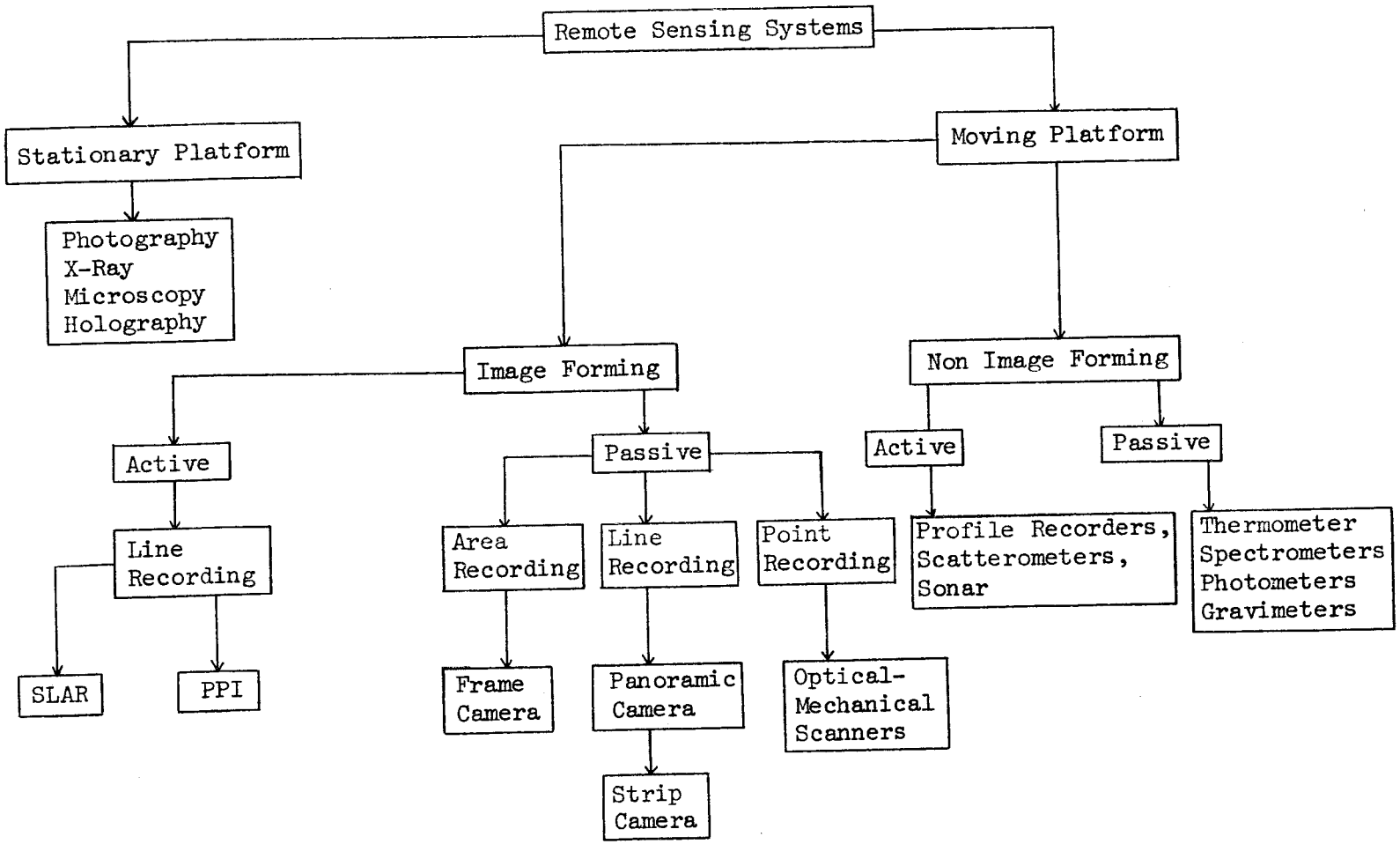

Figure 1.1. Remote Sensing Systems

The subject of this investigation, the multispectral scanner, is a passive system operating from a moving platform (either aircraft or spacecraft) with potential image formation and records in a point by point mode. The term "point" is used here to mean a small but finite area representing the system's resolution element as will be explained in detail later in this chapter. Scanning modes for MSS systems may be linear about a near vertical axis, linear about an axis tilted with respect to vertical, or conical about an axis which may be vertical or tilted. This investigation will be limited to the case of linear scanning about a near vertical axis in a direction normal to that of the motion of the platform.

The carrier field for the MSS system is composed of electromagnetic waves. Figure 1.2 presents the spectrum of the electromagnetic fields. The human eye is sensitive to the visible portion of the spectrum, between the wavelengths of 0.4 to 0.7 micrometers. The entire band between 0.3 and 15 micrometers is referred to as the optical portion of the electromagnetic spectrum, since electromagnetic waves may be refracted and focused using lenses and prisms in this region. It is within this range that most passive remote sensing systems operate. The region of the spectrum between 0.3 and 1.0 micrometers is called the photographic region where photographic emulsions may be used to record data. Wavelengths below 0.4 micrometers are in the ultraviolet region of the spectrum, and that portion above 0.7 micrometers is the infrared portion. The region between 0.7 and 3 micrometers is referred to as the reflective

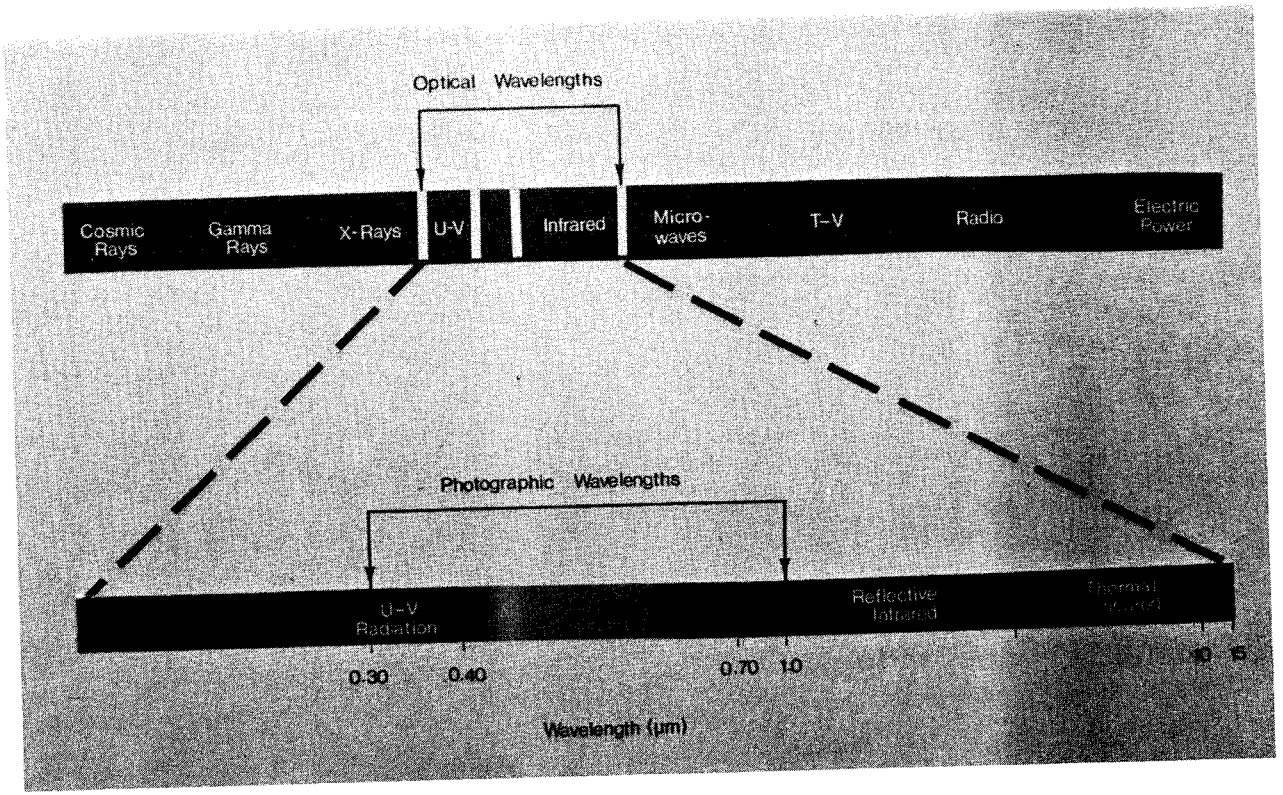

Figure 1.2. The Electromagnetic Spectrum [1]

infrared region, and the region from 3 to 15 micrometers is called the emissive region, since energy in these wavelengths is dominated by emission from a body as a result of thermal activity at temperatures of approximately 300° K, rather than being reflected.

For the subsequent discussion of basic radiometric relationships, the term power is used to denote the time rate of energy emanating from an object, or incident upon some sensor. Radiation power would then denote the time rate of energy due to reflected and/or emitted electromagnetic energy. Radiance may be defined as the radiation power per unit area directed into a unit solid angle from an object. Irradiance is used to denote the radiant power per unit area incident upon an object or sensor. Reflectance is a unitless quantity between zero and one and represents the portion of energy incident upon an object which is reflected from it.

The source of the energy incident upon the sensor's detectors is reflected and emitted radiant energy from the scene being sensed. All energy coming to Earth from the sun is either reflected, scattered or absorbed and subsequently emitted by objects on Earth. The total radiance from an object is composed of two components, reflected radiance and emitted radiance. In general, it may be stated that the reflected radiance forms a dominant portion of the total radiance from an object at shorter wavelengths of the electromagnetic spectrum, while the emissive radiance becomes greater at longer wavelengths [9, 4]. Figure 1.3 depicts in schematic form the interaction between the radiant energy emanating from the sun and a ground scene. In this figure, E denotes emitted radiation, and R denotes reflected radiation.

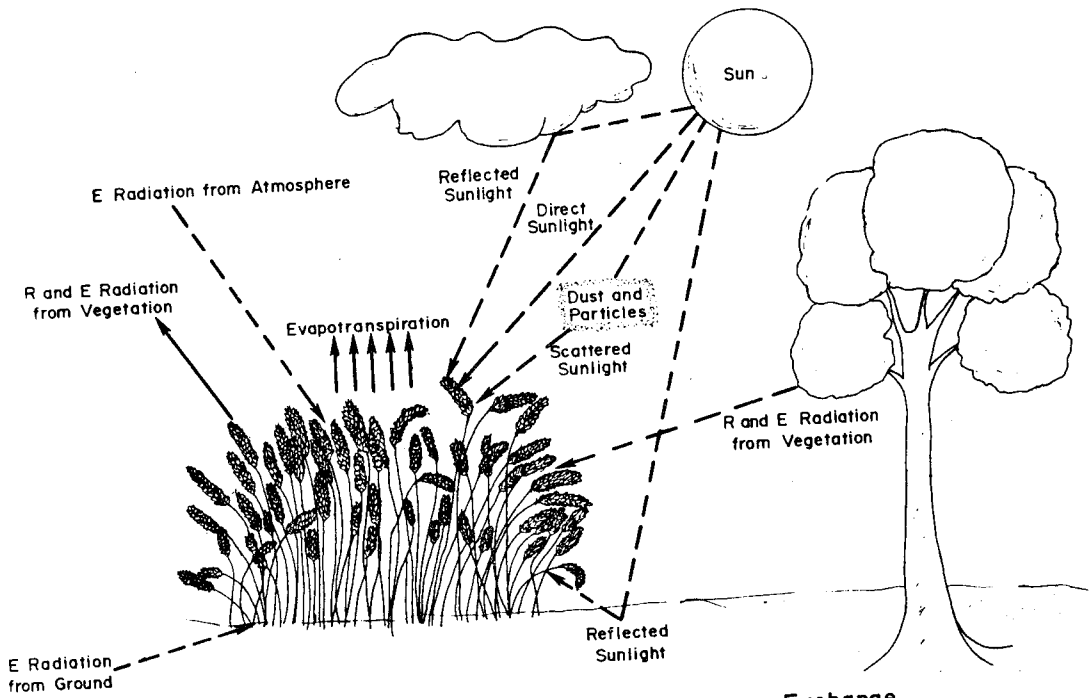

Figure 1.3. Interaction of Electromagnetic Energy at the Earth's Surface [1]

The spectral radiance, in watts/sq. cm-steradian-micrometer from a scene in the reflectance region may be given as [9]

$$L_\lambda = \frac{1}{\pi} E_\lambda \rho \cos\theta_s \tag{1.1}$$

in which E_λ is the solar irradiance in watts/sq. cm incident on the object at a wavelength λ, θ_s the sun angle and ρ the reflectance of the scene, a unitless quantity. Figure 1.4 shows a plot of radiance versus wavelength for typical agricultural scene, in the reflectance region, having wavelengths between 0.3 and 3.0 micrometers [9]. The figure shows the reflected radiance as it would be recorded near ground level. For this plot, ρ is assumed equal to 0.1, a reasonable assumption for vegetation in the visible portion of the electromagnetic spectrum or for soils in the near infrared portion of the spectrum.

In the emissive region of the spectrum, the radiance from an object may be represented by Planck's Law,

$$L_\lambda = \frac{(1.19 \times 10^4)\varepsilon}{\lambda^5[\exp(14338/\lambda T)-1]} \tag{1.2}$$

in which T represents the absolute temperature of the object in degrees Kelvin, and ε represents the emissivity, a unitless coefficient which is unity at all wavelengths for objects called black bodies. Objects are called gray bodies if their emissivity is a constant between zero and one. Most objects however, are neither black bodies nor gray bodies, and the emittance may be a complicated function

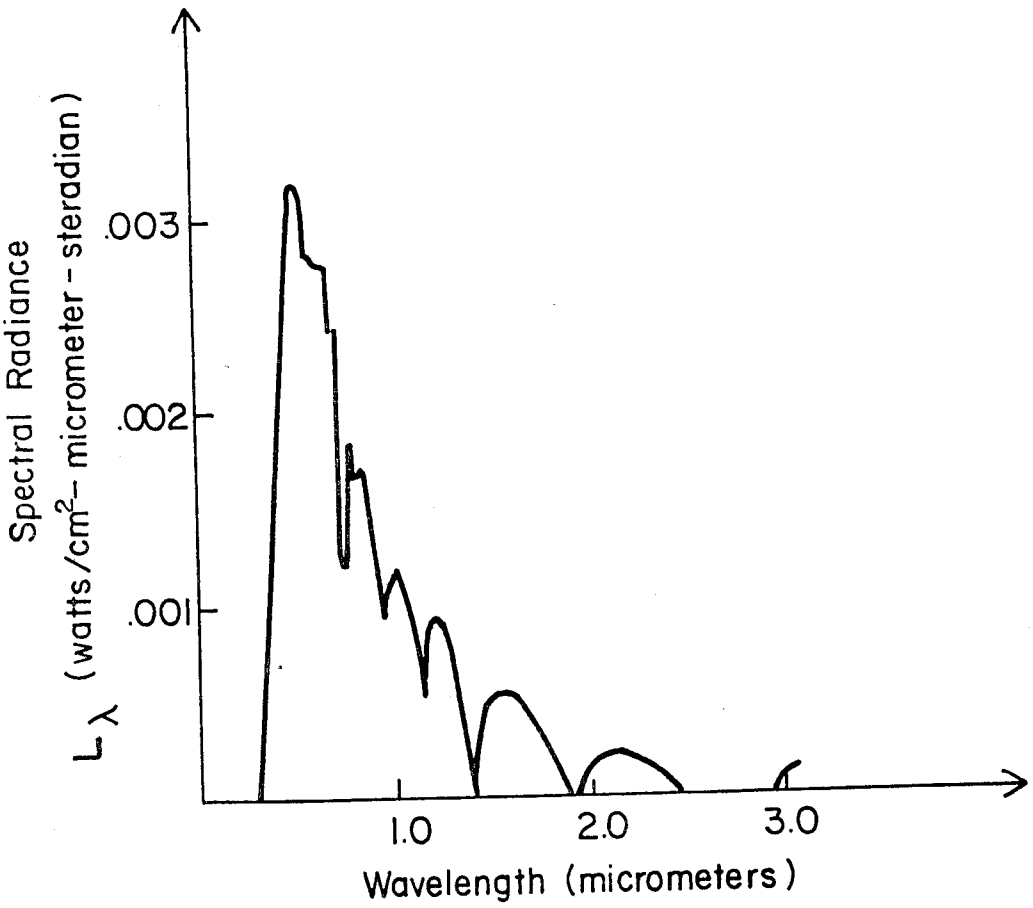

Figure 1.4. Spectral Radiance in the Reflected Region [9]

of wavelength. Figure 1.5 shows a plot of spectral radiance for a typical black body, emittance equal 1, at an absolute temperature of 300° K.

The combination of two curves from the reflectance and emittance regions, then, would represent the total spectral response of the object. Figure 1.6 shows a simplified example in which the agricultural scene represented in the reflective region by Figure 1.4, is assumed to behave as a black body in the emissive region, represented in Figure 1.5. It is this plot which represents the "spectral signature" of an object, and it is the difference between such signatures for different objects which allows the differentiation between objects using the multispectral approach of remote sensing.

The summation of the preceding plots will yield the magnitude of radiance emanating from an object. In order to evaluate the energy, or power (time rate of energy) incident at the sensor, however, the transmission through the atmosphere must also be considered. The atmosphere will attenuate and modify energy very significantly by molecular absorption for many spectral wavelengths. There are, however, spectral intervals at which the atmoshpere is reasonably "transparent" to electromagnetic radiation. These transparent spectral regions are called "windows", and sensing from a remote location requires that these spectral intervals be utilized. Figure 1.7 presents a graph of the transmission of the atmosphere for the wavelengths of the optical portion of the spectrum. The plot does not include the effects of atmospheric scattering. Table 1.1 summarizes some of the more important atmospheric windows which have

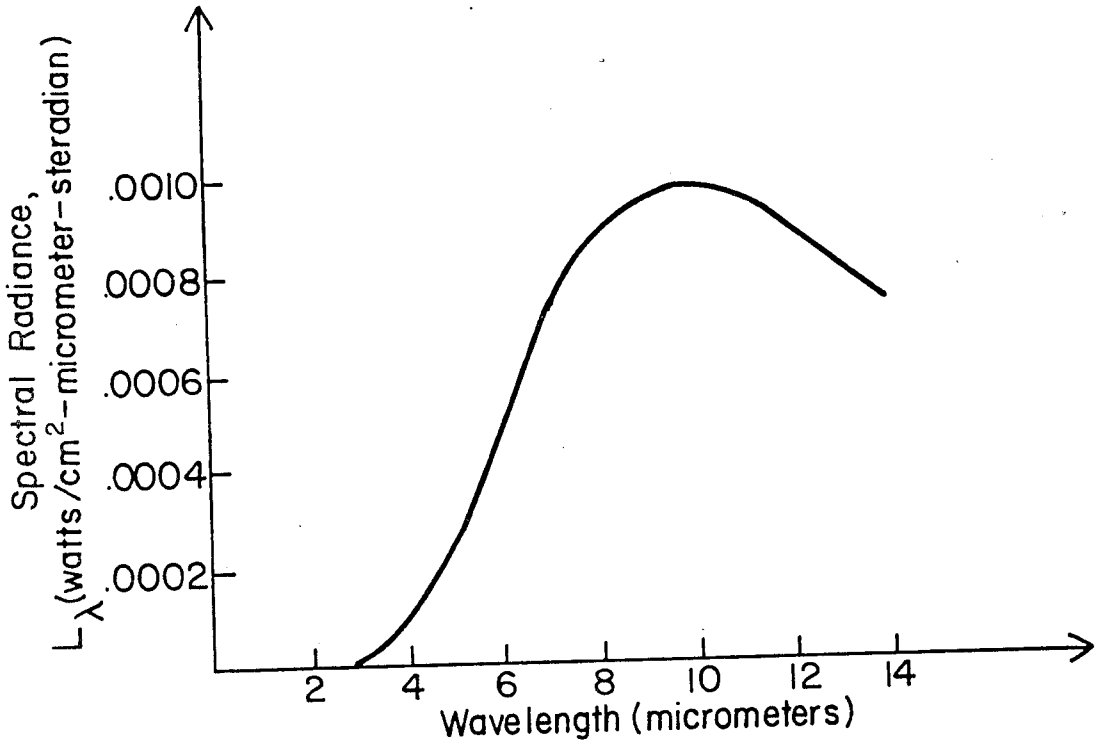

Figure 1.5. Spectral Radiance in the Emissive Region [9]

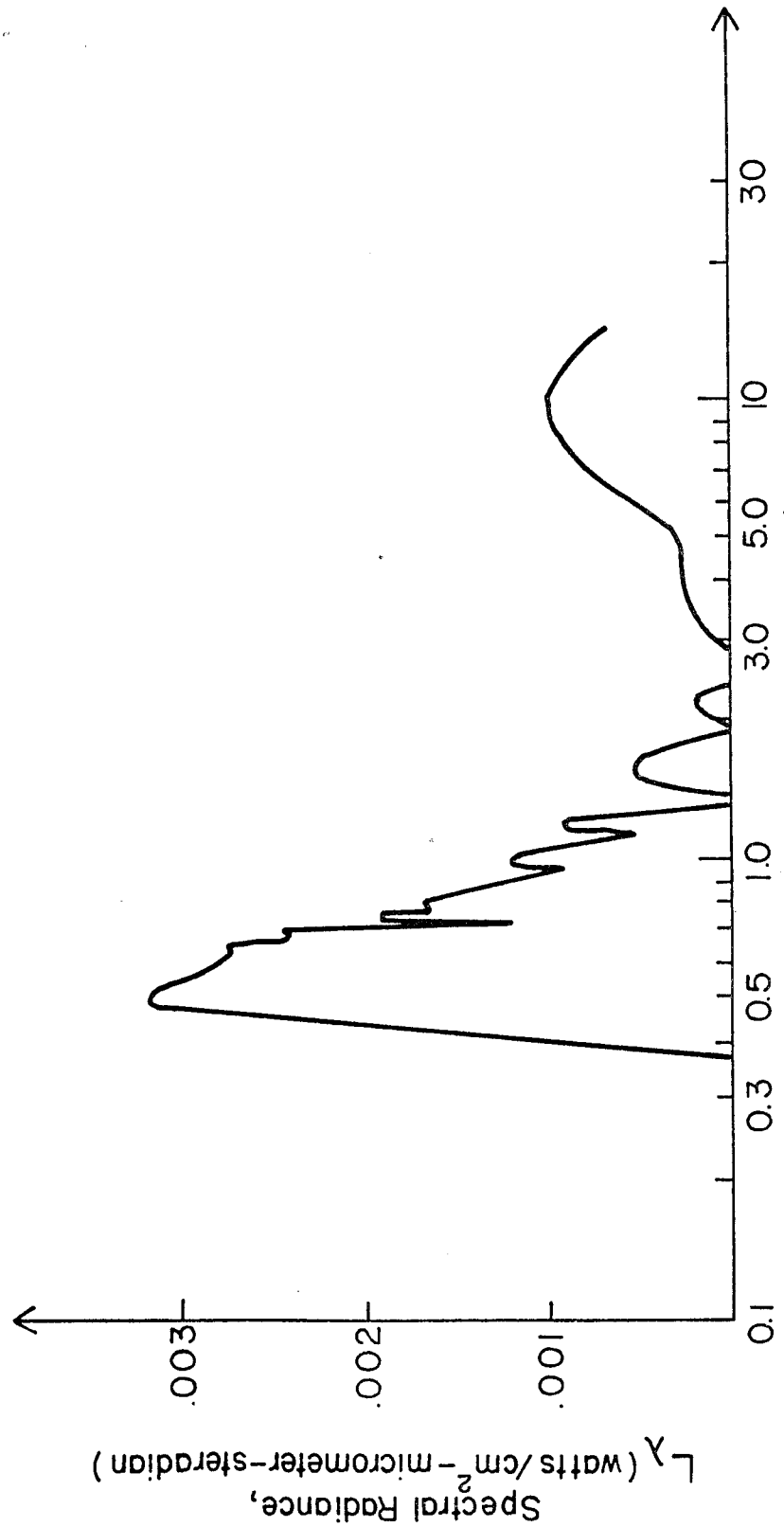

Figure 1.6. Total Spectral Radiance [9]

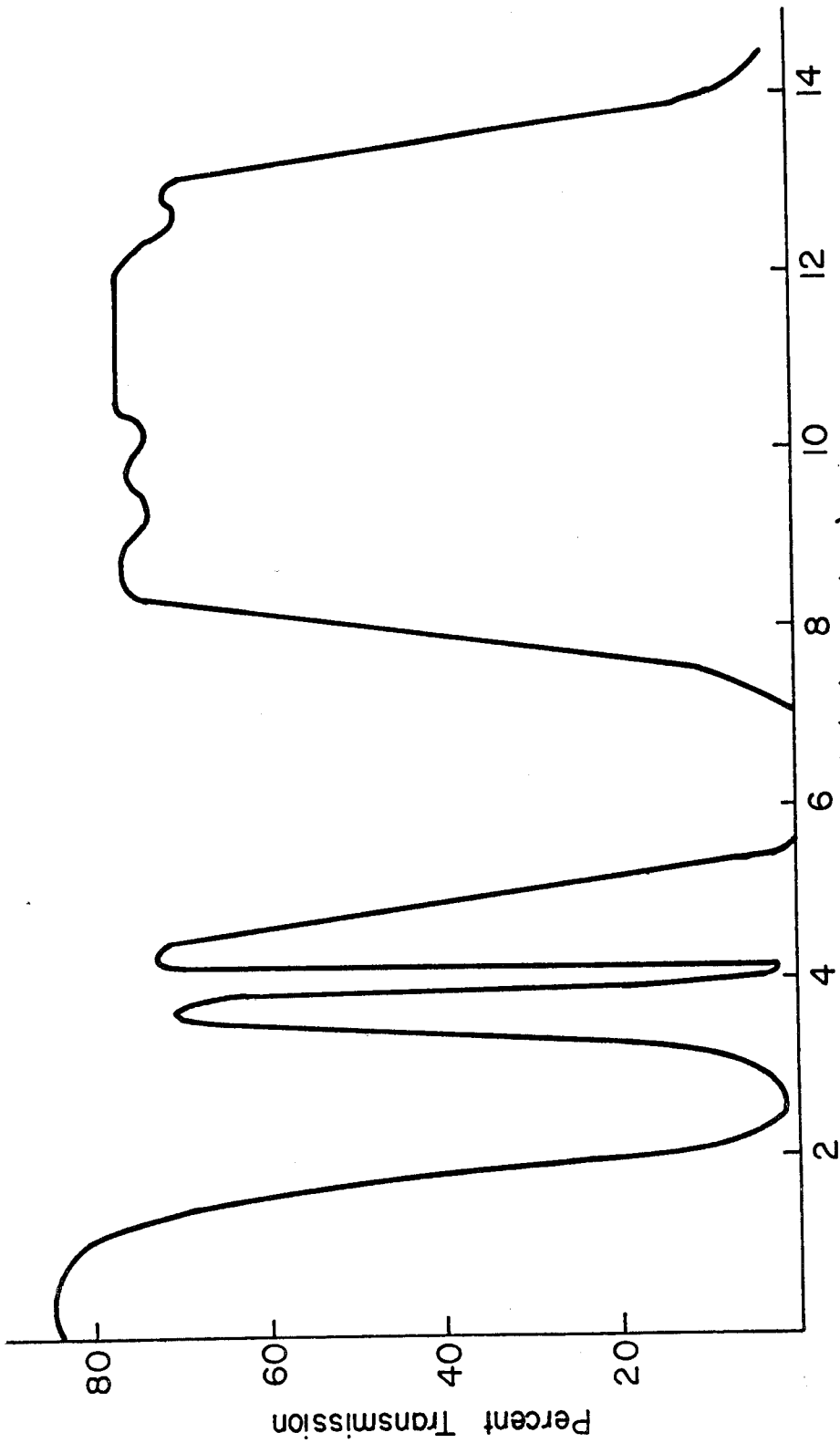

Figure 1.7. Atmospheric Transmission [11]

been utilized in MSS remote sensing systems. The most often used windows in remote sensing are numbers 1, 2, 3, 4, 5, 6, and 9 [11].

Table 1.1

Atmospheric Windows [11]

Window No.	Wavelength Limits
1	.40 to .72 μm
2	.72 to .94 μm
3	.94 to 1.13 μm
4	1.13 to 1.38 μm
5	1.38 to 1.90 μm
6	1.90 to 2.70 μm
7	2.70 to 4.30 μm
8	4.30 to 6.00 μm
9	6.00 to 15.00 μm
10	15.00 to 25.00 μm

If the atmospheric transmission is known for a spectral wavelength interval λ to $(\lambda + \Delta\lambda)$, the resultant power flow into the sensor may be given by [9]

$$P = \tau_a L_\lambda A \beta^2(\Delta\lambda) \tag{1.3}$$

in which P is the power in watts, τ_a the transmission of the atmosphere, and β the resolution angle of the system, defined as the angle from the sensor within which the electromagnetic energy is received at any instant, and A is the effective area of the receiving optics.

With these preliminary remarks in mind, attention is now directed to the multispectral scanner itself. In the following section a discussion is given of the manner in which these radiometric properties of matter may be utilized to record analogue data using the multispectral scanner, and how these analogue records may be processed to produce digital data arrays for analysis.

1.2 Digital Multispectral Scanning System

In this section, the steps taken to record the electromagnetic energy using a multispectral scanner will be discussed. The processing steps which take the data from electromagnetic waves, to analogue records from the MSS, and from these analogue records to digital data arrays will be discussed. The final form of data, the digital array is the form which is utilized at the Laboratory for Applications of Remote Sensing (LARS) to perform automated interpretation, and it was this data format which was used to investigate the geometric properties of the digital MSS system.

1.2.1 The Multispectral Scanner

Figure 1.8 depicts the scanning and data collection system for a typical multi-spectral scanning system. The system depicted is an aircraft system, in which a rotating mirror or prism scans the terrain in narrow strips or lines oriented normal to the direction of flight. Forward motion of the aircraft provides continuous coverage by assuring an advance for each line, allowing for some overlap between successive strips. The system utilized at LARS

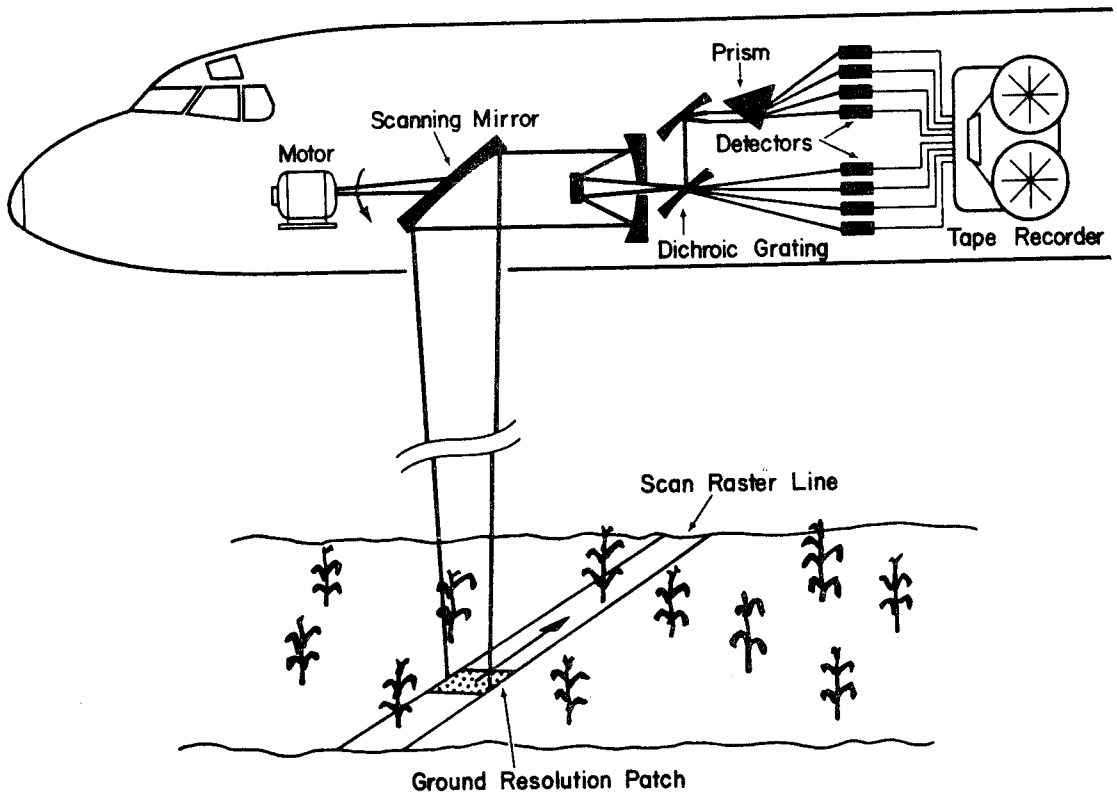

Figure 1.8. A Multispectral Scanner [1]

to generate basic data for digital processing is discussed further.

The electromagnetic energy incident upon the mirror or prism is optically focused upon a separating prism or diffraction grating which separates the incident energy into different wavelength bands. Each band is directed to an appropriate detector, and the signal generated is recorded on magnetic tape as an analogue signal, each spectral band representing a data "channel". The data is recorded on 14 track one inch magnetic tape as a series of continuous signals. The first track of tape contains a synchronizing signal to note the beginning and end of each scanner revolution. Also on this track is a signal from a roll stabilization gyro, which indicates the true roll of the aircraft during each scan line period. The remaining 13 tracks are data channels, which record calibration sources both internal and external to the aircraft, as well as recording the radiance from the ground scene of interest. Therefore, up to 13 channels in 13 spectral bands may be recorded simultaneously. The optical system shown in Figure 1.8 is of the converging optics type coupled with a rotating mirror-prism. Other optical configurations are available utilizing an oblique mirror or wedge, and converging optics [10, 11]. If digital analysis of MSS data is desired, these tapes are subject to digitization in an analogue to digital sampling procedure.

1.2.2 Advantages of Multispectral Recording

The MSS sensing system has several advantages over more conventional sensors such as photography. The data are recorded in a quantitative manner suitable for processing into numerical data. The recording and processing can be calibrated, resulting in high repeatability of decisions based upon statistical procedures. The possibility of detailed numerical analysis allows the discrimination of subtle differences within the data resulting in a high probability of isolating classes of interest through automated interpretation and classification. A class may be thought of as any physical division of interest to the investigator, which is believed to be spectrally separable from other classes. Examples of classes are wheat, corn, oats, and other crops which may be appropriate in an agricultural experiment utilizing airborne sensors. Another example of classes would be bare soil, green vegetation, and water, which may be appropriate for an investigation of a rural environment using spacecraft gathered data. Urban, suburban, and rural may define classes of interest for studies of urban areas using spacecraft data.

An illustrative example is cited by Holter [4], in which a comparison of the information available on black and white film, color film, and the multispectral system is made. For this example it is assumed that the electromagnetic spectrum is divided into 12 wavelength bands, and each band is assumed to have 10 levels of intensity, or density. Black and white photography senses instantaneously all of the bands in the photographic region of the electromagnetic spectrum. The maximum density would occur when

the maximum intensity is present in each band, and there will be 10 x 12, or 120 density values discernible below this value. Each of these values, however may occur from a different combination of bands, and the band combination causing this density cannot be discerned. Color film may be thought of as recording in 3 bands, representing the 3 emulsions used. If each emulsion is assumed sensitive to one third of the 12 spectral bands, then each emulsion could discern 40 densities, and the discernible number of states rises to approximately 6.4×10^4. A multispectral sensor, on the other hand, senses each band separately, and stores the data separately, so that the total number of states available from the multispectral sensor data which could be recognized is 10^{12}.

Although meaningful interpretation can and has been done by conventional interpretation methods utilizing multispectral images in order to make efficient use of all of the data available in this form, human decision making becomes too slow by several orders of magnitude. Further, the human interpreter finds it impossible to simultaneously discern differences in spectral tones, as displayed upon images, for more than a few (3) spectral bands. Such data may be analyzed with automated systems of interpretation, utilizing digital or analogue computing equipment. If the digital approach is chosen, the analogue flight record must be converted into data forms compatible with the digital computer, such as digital data tapes. If such a form is generated, and appropriate digital decision

algorithms are written, then computer aided analysis may be performed with speed and accuracy, and quantitative results obtained.

1.2.3 Generating Digital Data Arrays

In order to utilize digital data handling and interpretation of MSS data, a system for converting the analogue record to digital data format must be implemented. One such system, flown by the Environmental Research Institute of Michigan (ERIM) relies upon a roll gyro signal to establish the roll of the aircraft for each scan line. Figure 1.9 (adapted from [12]) depicts the manner in which the roll of the aircraft is monitored in flight and later utilized in analogue-digital (A-D) conversion to generate roll compensated data. As the scanning prism rotates, a magnet attached to the shaft passes a coil at the same point for each revolution. Referring to Figure 1.9a, as the magnet passes the coil, it generates a synchronizing pulse which is placed on the analogue record (Figure 1.9b), and simultaneously triggers a constant slope electronic ramp signal generator. When the signal generated is equal to that of the output signal from the roll gyro (Figure 1.9c), indicating the position of the aircraft roll with respect to nadir, a roll pulse is generated with respect to the synchronizing pulse upon the analogue record. Thus the magnitude of roll is recorded upon the analogue record for each scan line. These synchronizing and roll pulses are recorded upon the first track of the analogue recording tape within the aircraft.

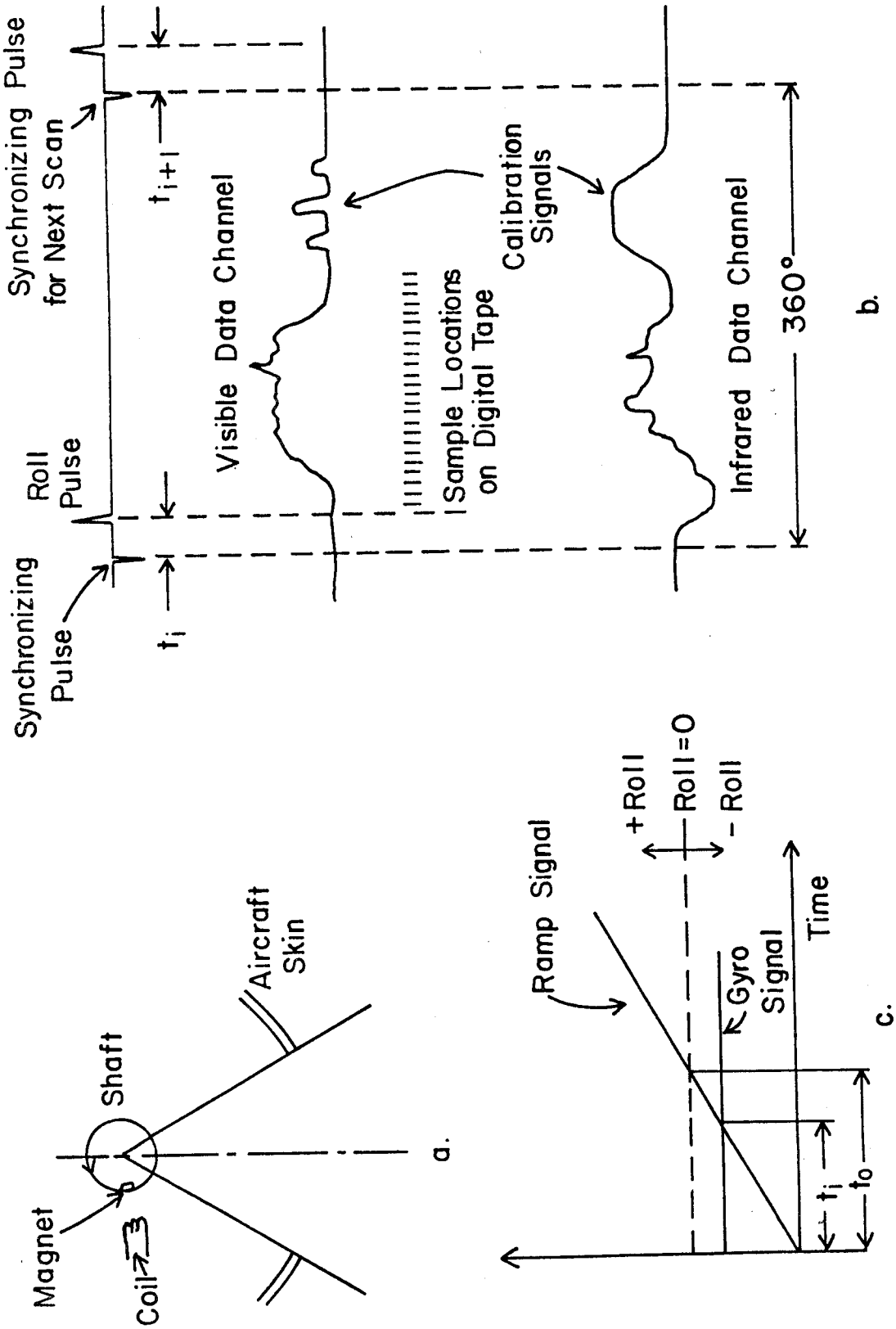

Figure 1.9. Digital Sampling of Analogue Data [12]

As the scan continues past the aircraft aperture, the spectral radiance is recorded across the ground scene on the remaining tracks of the tape for up to 13 data channels. As the rotation is continued, the sensor receives reference signals (from a light source, heat plates for the emissive regions of the infrared spectrum, and the sun). These reference values are used subsequently as calibration data. Figure 1.9b depicts the first track and two typical data channels.

Digital sampling is then done in the laboratory using analogue to digital (A-D) conversion equipment. The size of a data sample, and hence the angular interval of a digitized element in the along-scan direction is determined from the angular scan rate of the rotating prism, by selecting an appropriate sampling rate in the A-D converter. As an example, consider a data set in which the scene was scanned at a rate of 3000 revolutions per minute. The resulting period of rotation for the scanning prism, t_r, is then 1/50 sec., and is represented on the analogue record by the distance between sucessive synchronizing pulses, as shown in Figure 1.9b. If a nominal desired angular sampling interval γ, is desired, the number of samples between synchronizing pulses may be computed and a time interval of sampling computed, which may be dialed into the A-D converter.

For a nominal angular sample interval, or instantaneous field of view, of $\gamma = 6$ milliradians, the number of samples between synchronizing pulses (representing one revolution, or 2π radians) may be computed as

$$n = \frac{2\pi}{.006} \cong 1048 \text{ samples},$$

or, in terms of time interval of sampling in the A-D converter,

$$\Delta t = \frac{.006}{2\pi} (.02) = 1.9 \times 10^{-5} \text{ sec.}$$

In practice, the time interval of sampling is limited to stepped values, and hence the actual sampling resolution will be slightly different from the nominal value.

After the time interval for sampling is known, the actual sampling is done with respect to the roll pulse. Beginning at the roll pulse position, the analogue record for each channel is instantaneously sampled at the time intervals calculated, as shown in Figure 1.9b. Since the sampling begins at the roll pulse position for each scan line, any sample, say sample number 100, on each scan line is recorded on the digital tape such that it represents the same angle with respect to the nadir, resulting in roll stabilized data. The analogue data for each channel at every sample point is quantified on a scale ranging from 0 to 255, in order that it may be represented on the digital data tape (or in the digital computer) by a single byte (8 bits). A detailed explanation of the method in which the resulting data are stored on computer compatible tapes is given in reference [12].

For each resolution element, there is a position in a matrix representing the scan line number in one dimension, and the element number within that line in the other dimension. Associated with that position are several spectral values equal in number to the spectral bands, or channels, of the system. The data, then, may

be considered as a three dimensional matrix of spectral values of size i x j x n, where i is the number of scan lines in the flight, j is the number of elements within each scan line, and n is the number of data channels recorded. Subsequent automated classification and interpretation schemes then consider an n-dimensional vector for each element in the i x j positional array, as the data form.

In the following section, the use of the data arrays thus generated to form images is discussed. The use of computer aided analysis algorithms operating on the data within these arrays is also presented. The development and application of these computer aided analysis and classification procedures constitutes the major portion of the current research and development tasks performed at LARS.

1.3 Computer Aided Analysis Using Digital MSS Arrays

In the preceding section, the generation of digital MSS data arrays was discussed. In this section, the use of these arrays to extract meaningful information concerning resources at or near the Earth's surface will be presented.

1.3.1 Displays of MSS Data Arrays

Whether the arrays generated are to be utilized for interpretive purposes or to investigate geometry, it is convenient to be able to display the information visually. The task of machine aided interpretation utilizes the arrays directly, after preliminary decisions are made from displays of the data. An alternate method of considering the data format, which is of more interest from the

photogrammetric aspect, is to consider the data as an image. Under ideal conditions, the image formed by a display of the digitized spectral values may be seen to consist of two types of projections as will be discussed in a later section of this chapter. In the direction of flight, the data is recorded in a line-by-line fashion, resulting in an essentially orthographic projection. In the direction perpendicular to the direction of flight, the image is a perspective projection about the effective perspective center of the scanner.

If a display of this image is desired, the information stored on magnetic tape, must be processed to form a gray scale matrix. In the LARS system, the data analyst determines the number of gray scale levels desired (usually 10 to 12), and histograms are calculated for all spectral values within the area of interest.

These histograms are then divided into a number of bins equal to the number of gray scales desired. The abscissa is divided such that the same number of data array elements fall into each bin. Each interval along the x axis is then assigned a symbol or gray scale level. When the array is subsequently displayed, the result is that every symbol will occur with the same frequency within the display. The result is equally active gray scale levels over the image. Display of the image may be accomplished in two ways. The data tapes may be used to drive the scanning raster upon a television monitor, with the gray scale levels determining the voltage of the raster signal. This form of display utilizes the LARS Digital Video Display Unit, shown in Figure 1.10 [13], and henceforth referred to as the digital display unit. An alternate

Figure 1.10. Digital Display Monitor [13]

display form is a gray scale printout utilizing the line printer of the computer. Different gray scale values are represented by alphanumeric characters available on the line printer. Figure 1.11 [13] illustrates these two methods of display. The digital display unit is well suited to the display of gray tone imagery and allows great flexibility, through the use of an attached light pen, for purposes of interpretation. The line printer image form is useful for geometric studies, since it readily allows for the isolation of single element positions.

1.3.2 Computer Aided Analysis

As mentioned previously, the abundance of data generated by MSS systems require that interpretation be automated as fully as possible, to make maximum use of the unique properties of the multispectral approach. Computer aided analysis in this context, will denote the assignment of each element in the data array into one of a finite number of pre-assigned "classes" of interest, according to some decision rule. Different algorithms for this purpose abound in literature [14 through 19]. A brief introduction to the method used at LARS will be presented in this section. The method is based upon statistical pattern recognition techniques.

Figure 1.12 [14] depicts in a block diagram a general pattern recognition system. The receptor or sensor in this case would be the multispectral scanning apparatus. Data from this sensor may be represented as an n-dimensional vector for each element in the positional array, where n would be the number of spectral channels used.

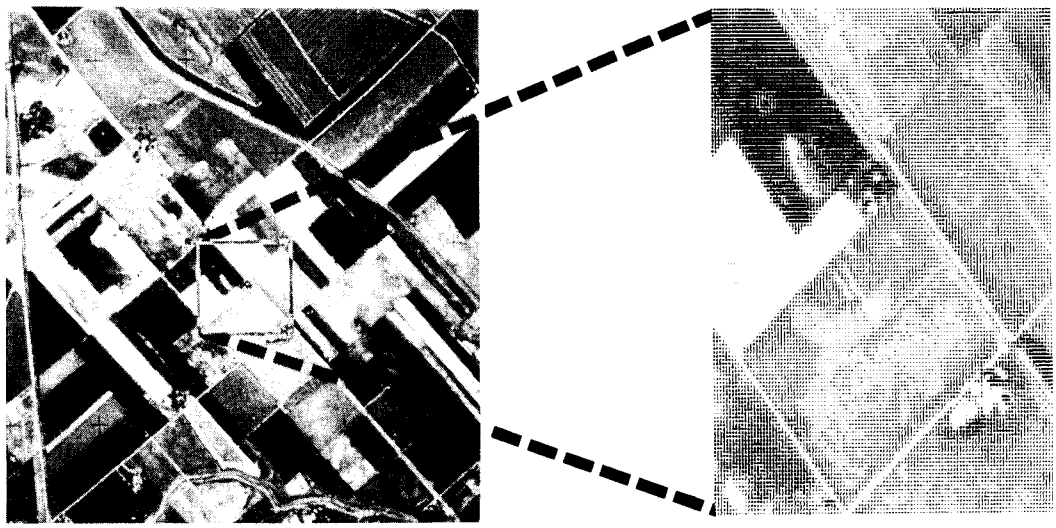

a. b.

Figure 1.11. Examples of Gray Scale Displays [13]

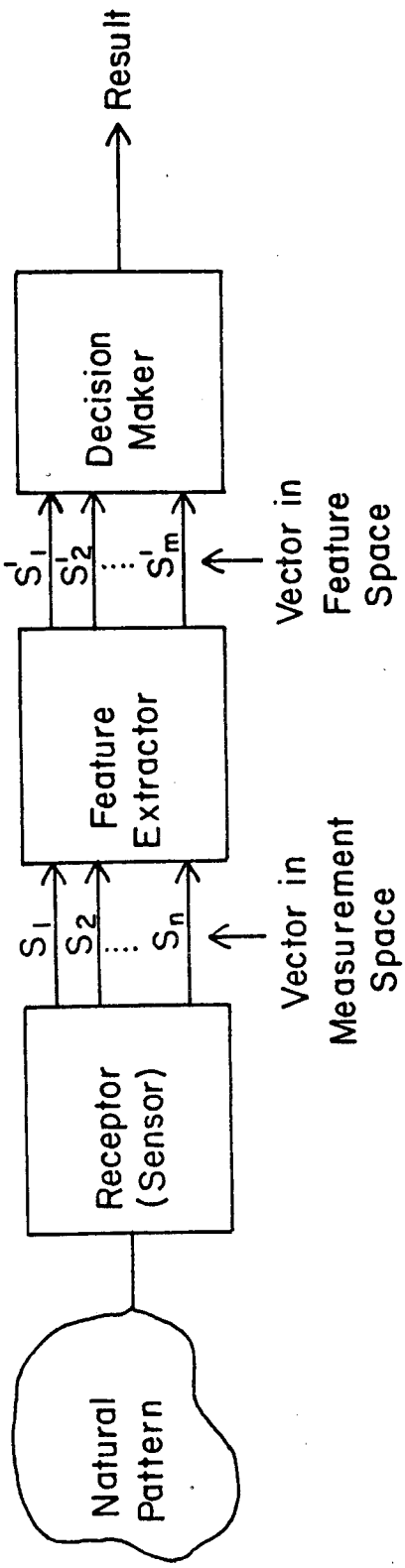

Figure 1.12. A Pattern Recognition System [14]

The purpose of the feature extractor is to generate a feature space vector containing maximal information for discrimination purposes. As an example which has been used in the LARS system, the data analyst selects the desired dimension of the feature space vectors to be used. The analyst may elect to perform classifications using four of the channels when originally a total of twelve channels were recorded. A statistical quantity called "divergence" between class pairs is computed for all possible groups of four channels included within the original twelve channels. This divergence is a measure of the spectral separability of the classes based upon each group of four channels. Based upon this quantity, one group of four channels would be selected to perform the classification. Usually the four channel combination chosen will be the set which has the greatest average divergence between pairs, although other selection criteria may be used. The net result of the feature extractor as used at LARS is to select some subset of dimension m from the original n channels of the measurement space vector ($m \leq n$). The feature extractor could, however, be a more complicated transformation. The measurement space vector would be

$$\underline{S} = \begin{bmatrix} s_1 \\ s_2 \\ \vdots \\ s_n \end{bmatrix} \tag{1.4}$$

and the feature space vector for analysis would be

$$\underline{S}' = \begin{bmatrix} s'_1 \\ s'_2 \\ \vdots \\ s'_m \end{bmatrix} \tag{1.5}$$

The decision maker is of course an important step in the classifying procedure, since it assigns each point in the data array to some particular class based upon a decision rule formulated from calculations made upon the feature space vector.

Each element and its associated m-dimensional vector represents a point in an m-dimensional feature space, and it is the location of points within this space which serves as a basis for classification. Figures 1.13 and 1.14 represent a two dimensional example, in which two wave length bands, λ_1, and λ_2 are the feature space coordinates. Figure 1.13 (course notes, EE 595, Purdue University) shows typical spectra of soil and vegetation. The spectra are assumed to be sampled as noted on the figure at wavelengths λ_1 and λ_2. The points in the two dimensional feature space (λ_1, λ_2) are then plotted in a two dimensional feature space as shown in Figure 1.14.

Natural phenomena, however, such as radiated and reflected electromagnetic energy from which spectral data are derived exhibit some inherent randomness. Spectra from two separate representatives

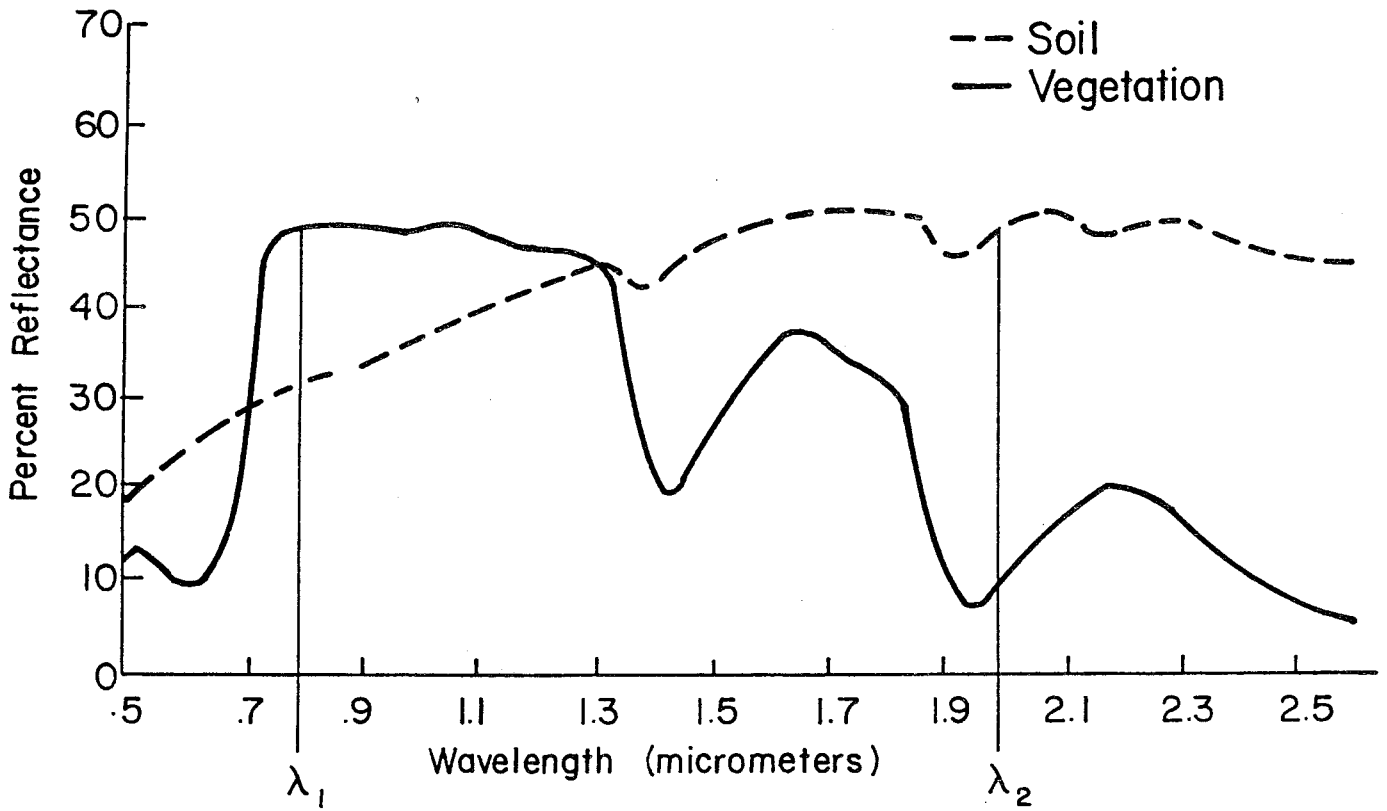

Figure 1.13. Spectral Reflectance for Vegetation and Soil
(From course notes, E.E. 595, Purdue University)

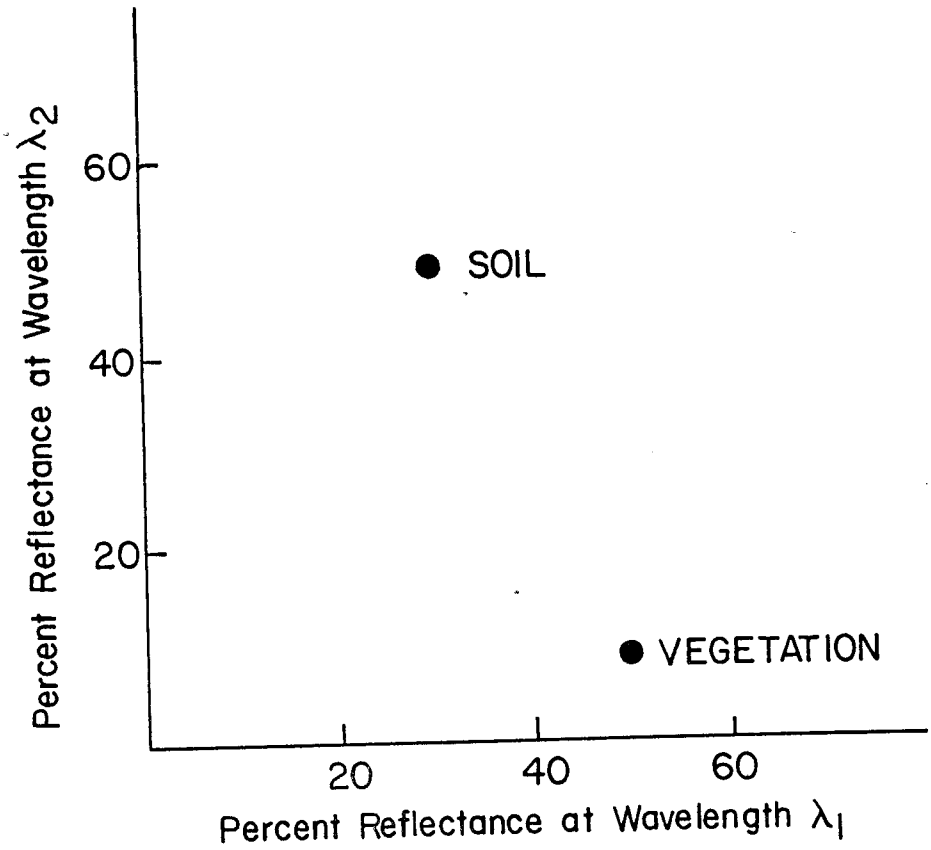

Figure 1.14. Representation of Two Classes in a Two Dimensional Feature Space [14]

of the same class would not be identical, and therefore the (λ_1, λ_2) measurements would not fall at the same point in the feature space. Instead, samples from different elements tend to fall in areas or "clouds" within the feature space. For example, Figure 1.15 depicts many observations from 3 classes plotted in the feature space. The decision making function of the classifier divides the feature space into a number of regions (the basis of which will be discussed subsequently) each representing a class of interest. The decision making algorithm examines each new data point to determine into which region it will fall, and classifies the point accordingly.

The classification problem then, becomes one of defining decision surfaces separating the appropriate regions, as shown in Figure 1.15. For the two dimensional feature space shown, the decision surfaces become lines. In order that the classifier may designate the decision surfaces before classification of unknown data points takes place, definition of these surfaces is done based upon "training samples", which may be generated from two different approaches, the data bank approach and the extrapolation approach [1].

In the data bank approach, an attempt is made to gather as many samples of spectral signatures as possible, in as many classes as may be useful to the data analyst. For any given problem a subset of classes present in the scene scanned would be chosen and decision surfaces calculated between these classes. Each incoming data point would then be placed into one of the regions defined by these classes. This method would have the advantage of requiring a minimum of a priori knowledge of the data to be classified, and the same

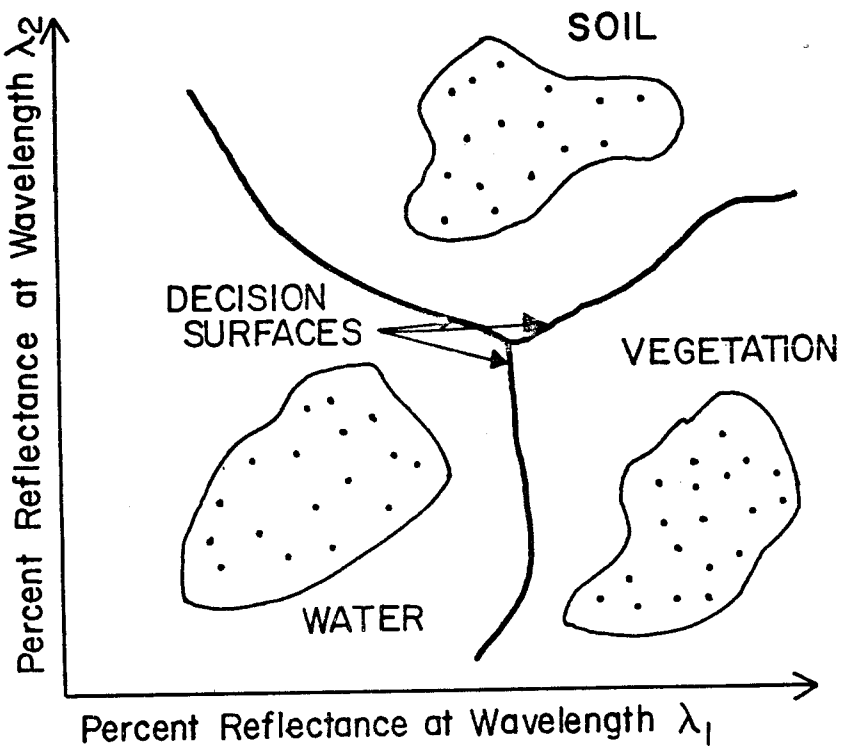

Figure 1.15. Classification Regions for Three Classes in a Two Dimensional Feature Space [14]

data bank of spectral signatures could be used to classify any number of new data sets.

This method has serious drawbacks, however, since the data bank of spectral signatures would have to be very large, and would have to include signatures gathered under many different conditions in order to account for natural statistical variations, such as temporal (time) variations, sun angle variations, variations in the atmosphere, seasonal variations, etc.

Using the extrapolation approach, however, these problems are circumvented to some extent. The training samples for this method are samples of known classification, drawn as a subset of the data to be classified, assuring that the training samples were gathered under the same conditions as the data to be classified. Decision boundaries are determined from these training samples, and the entire set of data is then classified accordingly. Thus, the classification is based upon an extrapolation of a few known points within the data set itself.

The method has the advantage that much less calibration is required of the sensor. However, it does require the acquisition of some a priori knowledge of the scene being scanned. This knowledge may be gained from ground observations in populated or accessable areas, limited photographic missions in inaccessable areas, or a combination of the two. It is this method which is primarily utilized at LARS.

The actual assignment of decision surfaces is the subject of continuing investigations. As a simple example, the centroid of each

class may be calculated, and the surface equidistant between centroids of adjacent classes used as the decision surface. In this case, the decision surfaces shown in Figure 1.15 would become straight line segments. At LARS, the decision surfaces are calculated to minimize the average expected loss of classification accuracy, as based upon some assumed loss function. The data in the spectral channels is assumed Gaussian in its randomness, and the resulting classification system is a maximum likelihood decision rule.

If the feature space is divided into regions as just described, every incoming point must be assigned to one of the designated classes. In virtually any scene, however, there are elements which do not belong reasonably to any of the finite number of classes designated. To avoid these gross misclassification errors, the concept of thresholding is used. If the probability of an element belonging to any of the designated classes is smaller than some preassigned threshold probability, then that element is assigned to none of the classes of interest but instead is placed in a null class which will represent "all others".

If training sample areas are difficult to delineate, another procedure called clustering, or unsupervised classification, may be used to supplement the above procedure. In using clustering, the analyst decides upon some number of groups into which he desires that the spectral data be divided. The clustering algorithm then performs this division, dividing the data into this number of groups, choosing those groups which are most separable based upon the spectral values stored in the data arrays. These groups are called "clusters".

After these groups have been isolated, however, the data analyst must determine whether each cluster represents a class in the physical sense, whether each cluster represents a single class or a combination of classes, and whether the classes isolated are of interest.

The above brief summary of data classification has used as an example the system utilized at LARS. The system is based upon spectral separability of data elements. It should be noted that other information may also be used for interpretation, such as spatial information, temporal (time) information, polarization, and combinations of these.

To date, all of the algorithms and procedures described have used as the basic data source the arrays directly as they have come from the A-D conversion. No attempt has been made to analyze the geometry of the data arrays. This analysis is desirable in order to be able to extract from digital MSS data arrays not only the interpretive information of "what" is included in the information, but also the metric information of "where" and the quantitative information of "how much". In the next section an introduction to the geometric distortions present in the data arrays will be given, to aid in understanding the types of geometric deformations to which the data arrays are subject.

1.4 Geometric Distortions in MSS Imagery

Investigations concerning MSS digital data arrays have previously dealt primarily with the automated interpretation phases of analysis through pattern recognition using statistical concepts. Geometry of the image has been either neglected entirely or subordinated to

the interpretation analysis. The MSS data, however, is subject to geometric distortions, which may be serious if it is desired to analyze the data to extract metric as well as qualitative information. It would be desirable to be able to obtain metric information from the data arrays. Positional information may then be associated with each properly classified element, and reliable information concerning areas may be obtained.

1.4.1 Ideal Geometry

Figures 1.16 and 1.17 illustrate geometry of a multispectral scanner under ideal conditions. The case illustrated represents the recording of the j-th element in an arbitrary scan line, i. In this case the following assumptions are made:

1.) The aircraft is flying perfectly straight, at a constant elevation above datum, and at a constant ground speed.

2.) The aircraft is subject to no angular exterior orientation perturbations. That is, there is assumed to be no roll (ω), pitch (ϕ), or yaw (κ) of the aircraft.

3.) Each scan line is assumed to be instantaneously recorded.

Under these conditions the resulting image is recorded as an orthographic projection in the direction of flight (X), and as a perspective projection in the direction normal to the direction of flight (Y).

In Figure 1.16, β represents the angular resolution of the beam in the down strip or X direction and will be the same as the physical resolution of the scanner. The angle γ represents the effective angular resolution in the along-scan or Y direction and

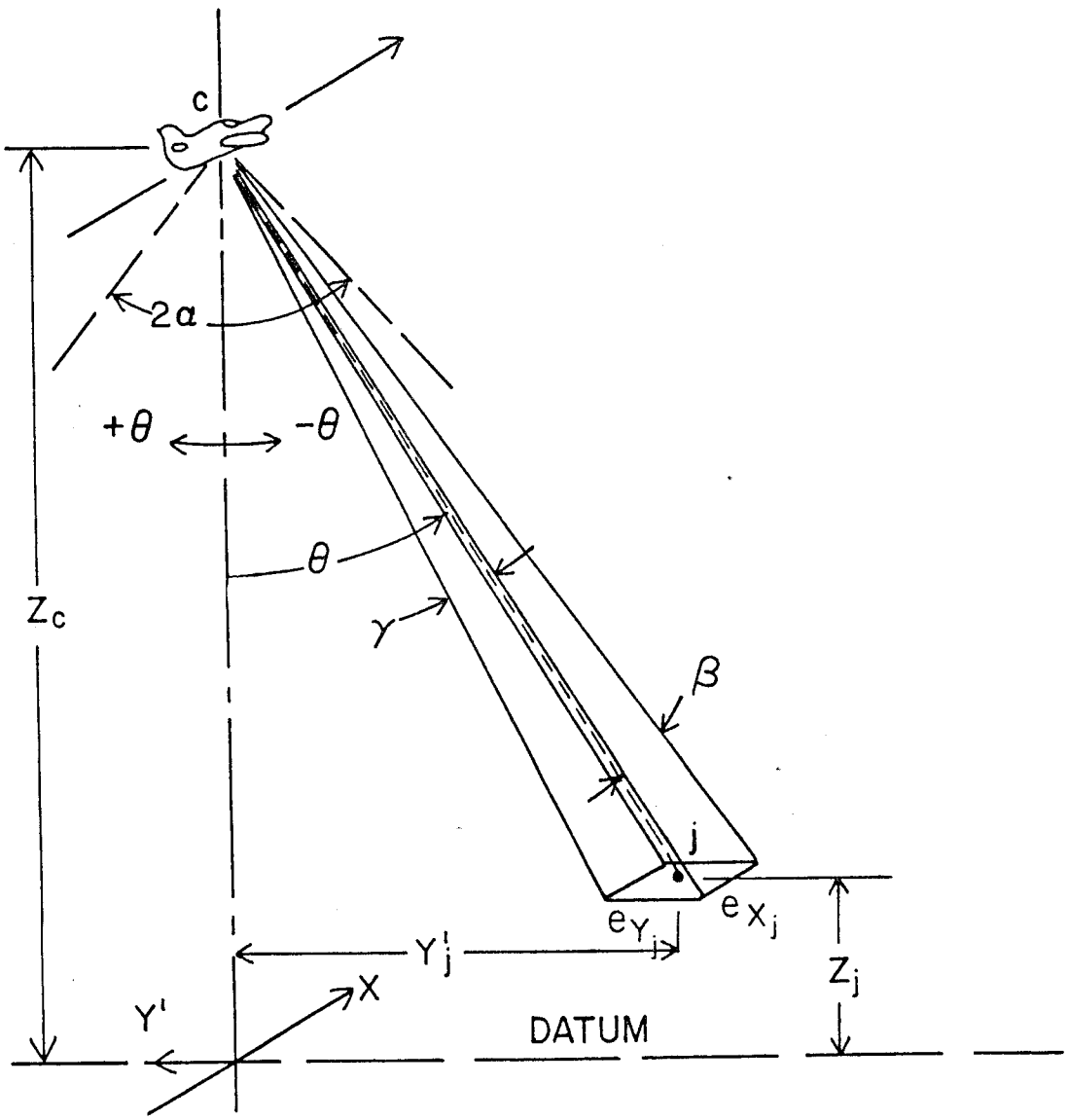

Figure 1.16. Geometric Parameters of Scanning

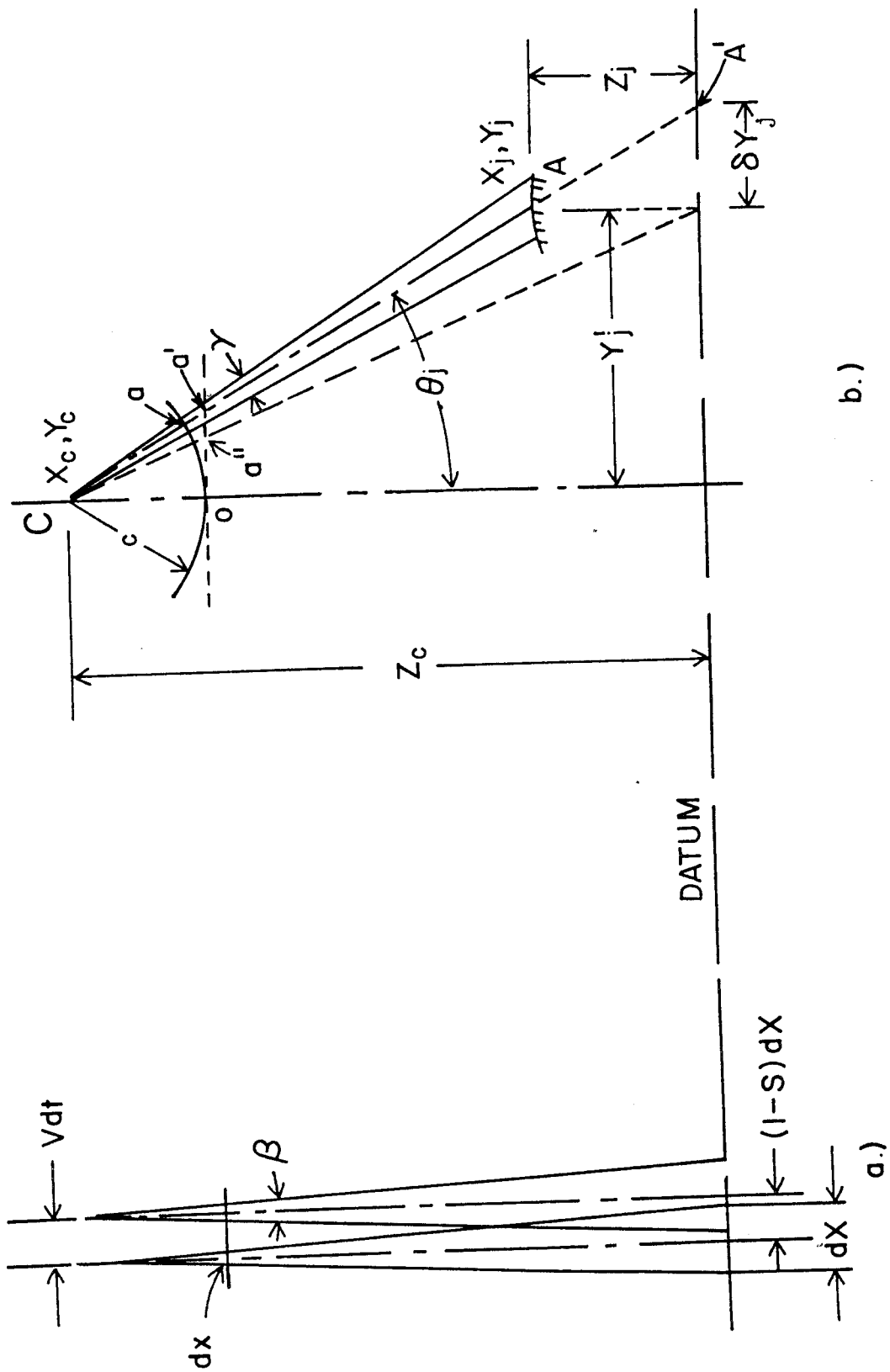

Figure 1.17. Ideal Geometry of the Multispectral Scanner

is determined during the analogue to digital conversion. This represents the effective instantaneous field of view (IFOV) of the sensor. The total angle scanned, called the total field of view (TFOV) is 2α. The effective aperture of the sensor is represented by the β by γ solid angle.

Figure 1.17a depicts the down strip or X direction. For this direction the X_j coordinate for the object point j is a function of time down the strip and may be written

$$X_j = X_c = X_o + \int_{T_o}^{T_i} V(t)dt \tag{1.6}$$

in which X_c is the X coordinate of the scanner at the instant of imaging point j on scan line i, X_j for point j, T_i is the time epoch at the instant of recording point j and is the same for all points on scan line i under the assumption that the scan line is instantaneously recorded, X_o is the X position of the first scan recorded and V is the aircraft velocity which is assumed constant for the ideal case. If the scanning rate is adjusted such that an overlap (overscan) will occur between scans at the nominal aircraft velocity, then the average advance for each scan line will be (1-S)dX, where S is some overlap factor, and dX is the scan width on the datum given by (see Figure 1.17)

$$dX = Z_c\beta \tag{1.7}$$

In this expression Z_c represents the altitude of the aircraft above datum when recording scan line i. Further, the image element size in the down strip direction is given by

$$dx = c\beta \tag{1.8}$$

in which c is an effective sensor constant, analogous to the recording barrel radius (camera focal length) in panoramic photography. Noting from Figure 1.17a that

$$V\,dt = (1-S)dX \tag{1.9}$$

and solving Equation (1.8) for β, the following expression results from substitution of the expression for β into Equation (1.7).

$$X_j = X_c = X_o + \int_o^x (1-S)\,\frac{Z_c}{c}\,dx' \tag{1.10}$$

For $T_o = 0$, the image strip coordinate is equal to zero, and at time $t = T_i$, $x' = x$, the image x coordinate of point j.

Applying the ideal assumptions mentioned above, in which aircraft velocity and flying height above datum are assumed constant down the flight line, the expression becomes

$$X_j = X_c = X_o + (1-S)\,\frac{Z_c}{c}\,x \tag{1.11}$$

In reality, of course, the aircraft velocity and flying height may be a function of time, and hence of the image x coordinates. If a polynomial form for these quantities is assumed, then a polynomial form of one degree higher will result for X_j after integration of

Equation (1.10). If a harmonic form is assumed, then a harmonic form will remain after integration.

In Figure 1.17b is shown the recording geometry in the direction perpendicular to the direction of flight. For this case, the ground coordinate Y_j is given by

$$Y_j = Y_c + Y'_j$$

or

$$Y_j = Y_c + (Z_c - Z) \tan\theta_j \tag{1.12}$$

in which Y_j is the ground coordinate of point j, Y_c is the Y coordinate of the sensor at the instant of recording j, Z is the elevation of the terrain (assumed level) in which Z_j in Figure 1.17b has been replaced by the constant elevation Z. The angle θ_j is the scan angle at the instant of recording given by

$$\theta_j = y_j/c \tag{1.13}$$

and y_j is the image position normal to the flight line axis and would be represented in digital recording by the column position with respect to the scan line center.

1.4.2 Variations from Ideal Geometry

This idealized geometry is obviously not realized in practice, since the ideal positions as given by the projection Equations (1.11, 1.12) are perturbed by the following geometric factors.

1.) The effects of changing ground resolution element size at different scan angles, and effectively recording on a cylindrical rather than plane surface, which causes a panoramic appearance. These are termed "scan angle effects".

2.) The effect of neglecting relief difference of object points above or below the assumed datum surface. This will be called "topographic effect".

3.) Removing the assumption of ideal flight conditions leads to "sensor exterior orientation effects".

4.) Relaxing the assumption that each scan line is instantaneously recorded, but in fact, requires some finite recording time, leads to "scan time effects".

1.4.2.1 Scan Angle Effects. Although each element along the scan in the image is displayed with equal width, significant distortions occur along each scan due to a changing ground size of resolutions elements. From Figure 1.16, the element size in the direction of flight, or X direction, is given by

$$e_{x_j} = \beta(Z_c - Z_j) \sec\theta_j \tag{1.14}$$

In the direction perpendicular to the direction of flight, or along-scan direction, the ground coordinate of the point j is given by

$$Y_j = Y_c + (Z_c - Z_j) \tan\theta_j \tag{1.15}$$

If the sampling angle, γ, (see Figure 1.16) is sufficiently small, as is usually the case, then it can be considered as a differential change in the scan angle θ_j, that is

$$\gamma \tilde{=} d\theta \tag{1.16}$$

Differentiating Equation (1.15) with respect to θ_j, the resulting expression is

$$dY_j = (Z_c - Z_j) \sec^2\theta_j \, d\theta$$

or

$$e_{Y_j} = \gamma(Z_c - Z_j) \sec^2\theta_j \qquad (1.17)$$

Figures 1.18 and 1.19 show plots of the ground resolution element size as a percentage of flying height above terrain in the X and Y directions, respectively. These plots show various values of the angular resolution. Most aircraft data handled by the LARS system is digitized in the γ = 3-6 mrad range in the Y direction. The angular resolution of the ERIM M-7 scanner, from which most present LARS aircraft digital data is derived is on the order of 2-3 mrad, representing β. The scan angle limits of the ERTS scanner is on the order of 5.75° either side of nadir.

As an example consider a typical aircraft flight as utilized by LARS, with nominal flying height above terrain of 5000 ft. (1.52 km), digitization parameter γ = 6 mrad, β = 2.5 mrad. Then the ground size of a resolution element would vary from 12.5 ft. x 30 ft. (3.81 m x 9.14 m) at nadir to 17.7 ft. x 60 ft. (5.39 m x 18.29 m) at a scan angle of 45°. As may be seen from Figures 1.18 and 1.19, the ground resolution element size increases very rapidly, particularly in the Y direction, for scan angles in excess of 45°, which would result in great image distortions. Therefore, most aircraft scanner data is collected within the range of $\alpha \leq \pm$ 40°. For small scan angles (e.g. ERTS, in which α < 6°) the effect is not as serious as for larger angles.

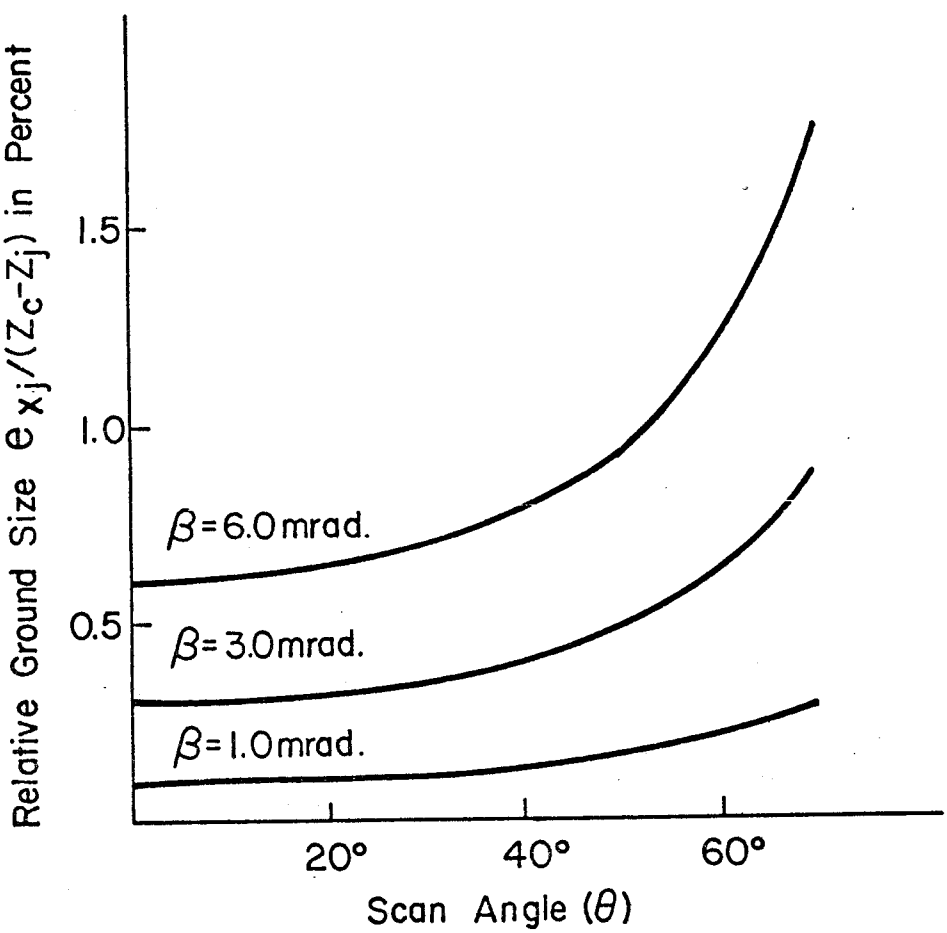

Figure 1.18. Resolution Element Ground Size in X Direction

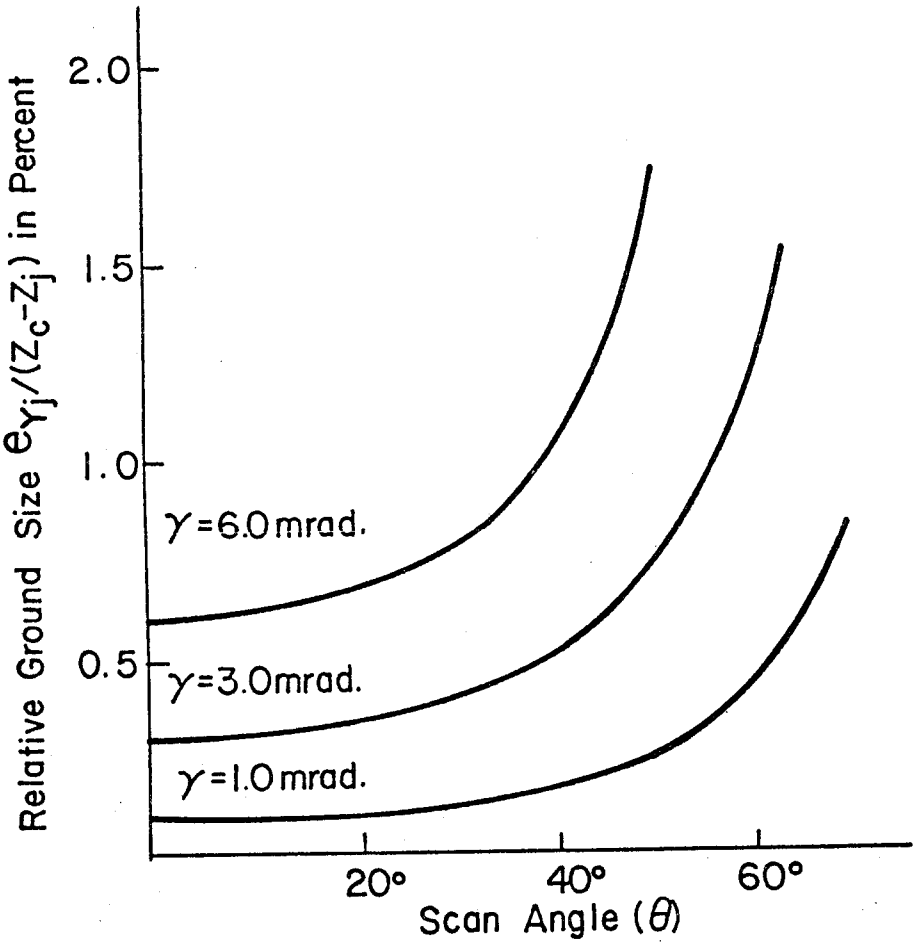

Figure 1.19. Resolution Element Ground Size in Y Direction

In addition to the distorting effect of changing ground resolution element size, there exists in each scan line a panoramic image displacement. This displacement is due to the fact that the data are effectively imaged upon a cylindrical surface, rather than a plane. From Figure 1.17b, this displacement may be seen to be the difference between some hypothetical image position, denoted a', and the actual image position a. The resultant image displacement is given by

$$\delta y = Oa' - Oa = c(\tan\theta_j - \theta_j) \tag{1.18}$$

Figure 1.20 shows graphically the magnitude of this displacement relative to the effective principal distance, c, for varying scan angles. It should be noted that this displacement increases very rapidly for scan angles in excess of 45°.

1.4.2.2 Topographic Effect. The neglect of terrain variation is not uncommon in the interpretive treatment of multispectral scanner data arrays. The resulting displacement may become appreciable at large scan angles. Referring to Figure 1.17b, if point A is imaged and assumed to be on some datum surface, while in fact it lies at some elevation Z_j above datum, the effect is to image the point as if its Y position was at A' on the datum. The effective ground displacement due to neglecting topography may be given by

$$\delta Y_j = Z_j \tan\theta_j \tag{1.19}$$

in which Z_j is the element elevation relative to datum, and δY_j is the resulting Y displacement at ground scale. The proper image

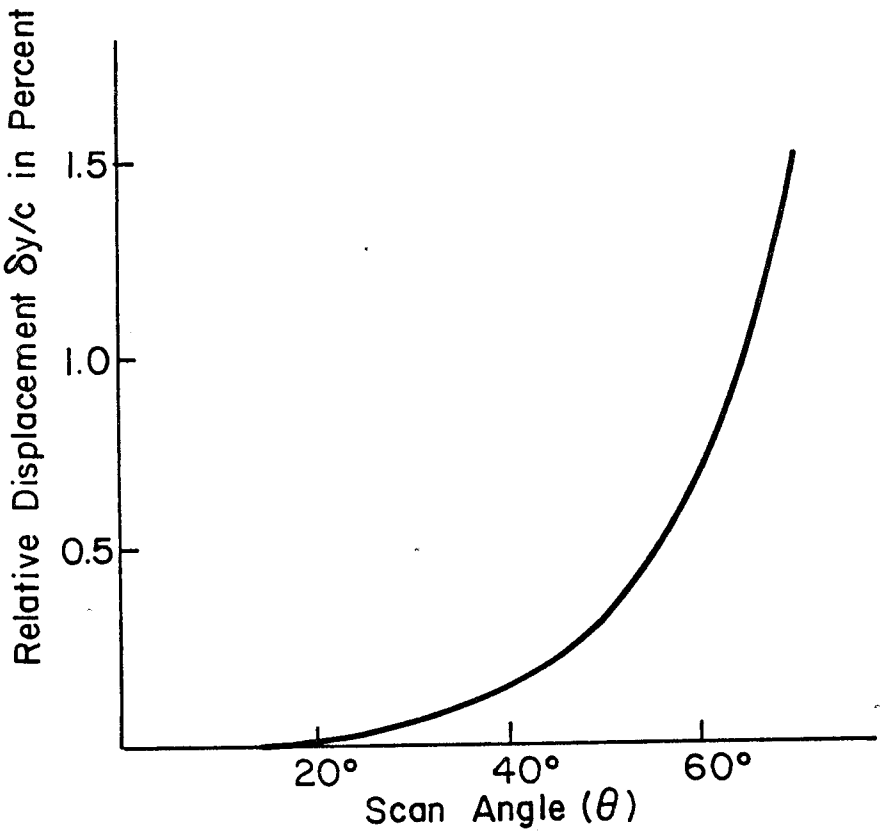

Figure 1.20. Panoramic Image Displacement as Given by Equation (1.18)

position for this element would then be at a", if the element is to retain its proper Y position, after reduction to the datum surface. This error, δY_j, will vary from zero at nadir to a value equal to Z_j at a 45° scan angle and would increase rapidly for scan angles greater than 45°. In order to alleviate this error, some method must be chosen to assign elevations to every element with an acceptable accuracy. This problem will be dealt with in greater detail in a later section. At this point it should be mentioned, however, that if multiple coverage of ground areas are available, for example from side lapping flight lines, the possibility exists to obtain these element elevations directly from the imagery, by forming intersections. However, if only singly scanned data are available, then some source external to the data arrays must be used to provide these element heights.

1.4.2.3 Exterior Orientation Effects. In addition to scan angle and topographic effects, a major source of error is that of sensor exterior orientation variations during scanning. In actuality, of course, an aircraft cannot be controlled such that its elevation and velocity remain constant, nor can it be constrained to lie on a perfectly straight flight path. In addition, an aircraft cannot be stabilized such that roll, pitch, and yaw are held negligible. Many scanning systems, however, are roll stabilized, such as the ERIM M-7 scanner which supplies the present bulk of aircraft data to LARS. For these systems, the ω term may be approximated by zero.

Figures 1.21 and 1.22 illustrate the resulting deformations which occur when the perfect orientation assumptions of Section 1.4.1

are not realized. Figure 1.21 illustrates the effect of two of the angular orientation elements and one of the positional elements. In Figure 1.21a, the effect of pitch (ϕ) variations down the strip is to cause the scanner to "gallop" in the X direction, alternately increasing and decreasing the nominal scan overlap value, S, described in Section 1.4.1. The effect of a change in flying altitude is to cause a spread of the sensed ground element in the direction normal to flight as may be seen from Figure 1.21b.

The yaw (κ) variation is due to the rotation of the scanner about a near vertical axis as it flies the strip. For example, in Figure 1.21c, assume a road is exactly perpendicular to the flight direction, but is imaged when the aircraft has a yaw. Then when the imagery is displayed, each line is displayed horizontally, and the x coordinates along the road will be displaced such that the road will no longer appear perpendicular to the flight line axis.

Figure 1.22 [20] shows the resultant ground coverage of a scanner under various perturbations in sensor exterior orientation elements. From Figure 1.22, an important aspect of scanned imagery becomes apparent. Because only two-dimensional information is available from the imagery, it becomes impossible to separate the effects of each orientation element variation. For example, considering 1.22a, a constant aircraft pitch in scanning several successive lines is impossible to distinquish from the effect which would be recorded if a constant X shift of the coordinate system was done. From 1.22i, it is not possible to distinguish between a linear rate of aircraft pitch, and a linear rate of change of aircraft velocity.

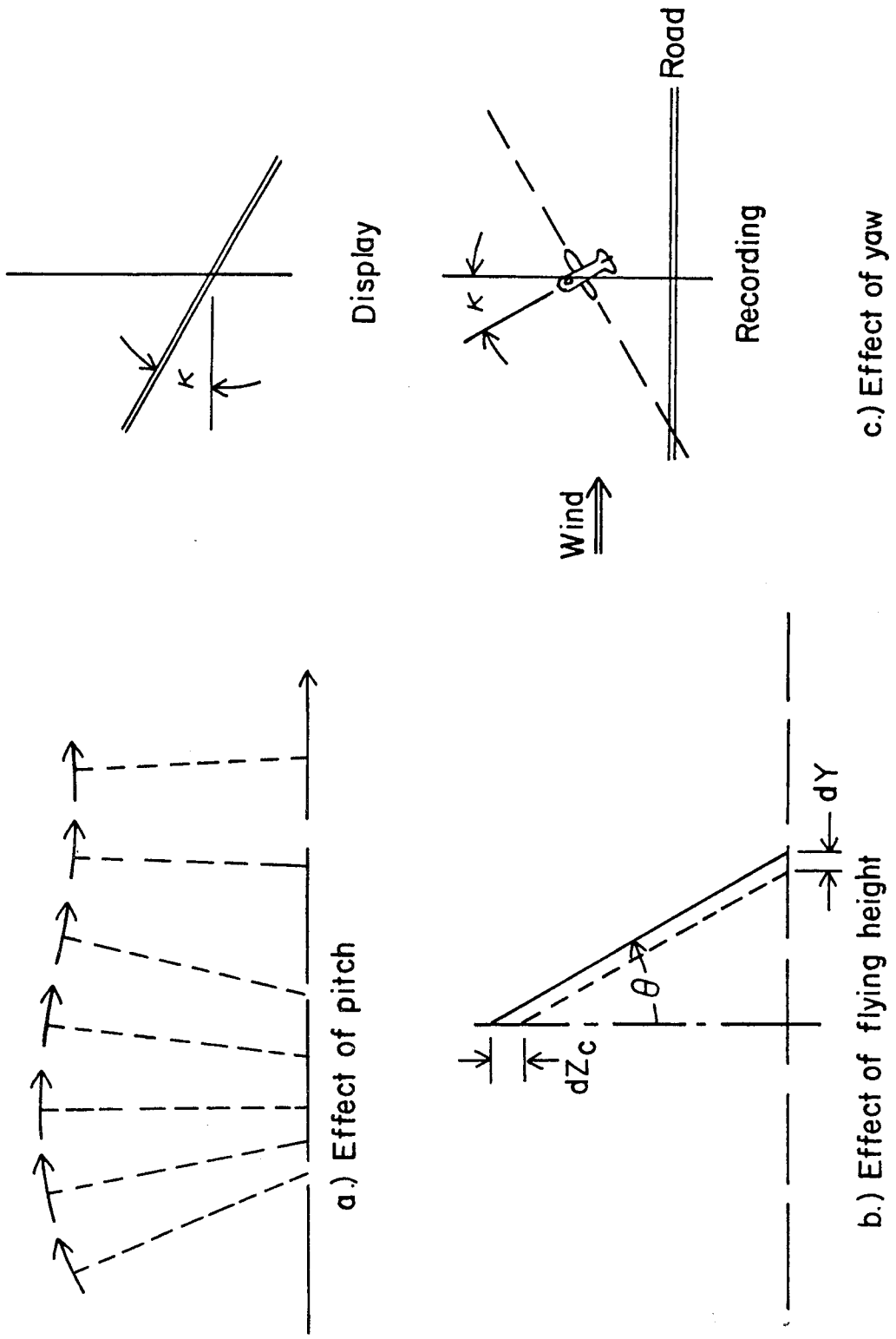

Figure 1.21. Effect of Some Aircraft Instabilities

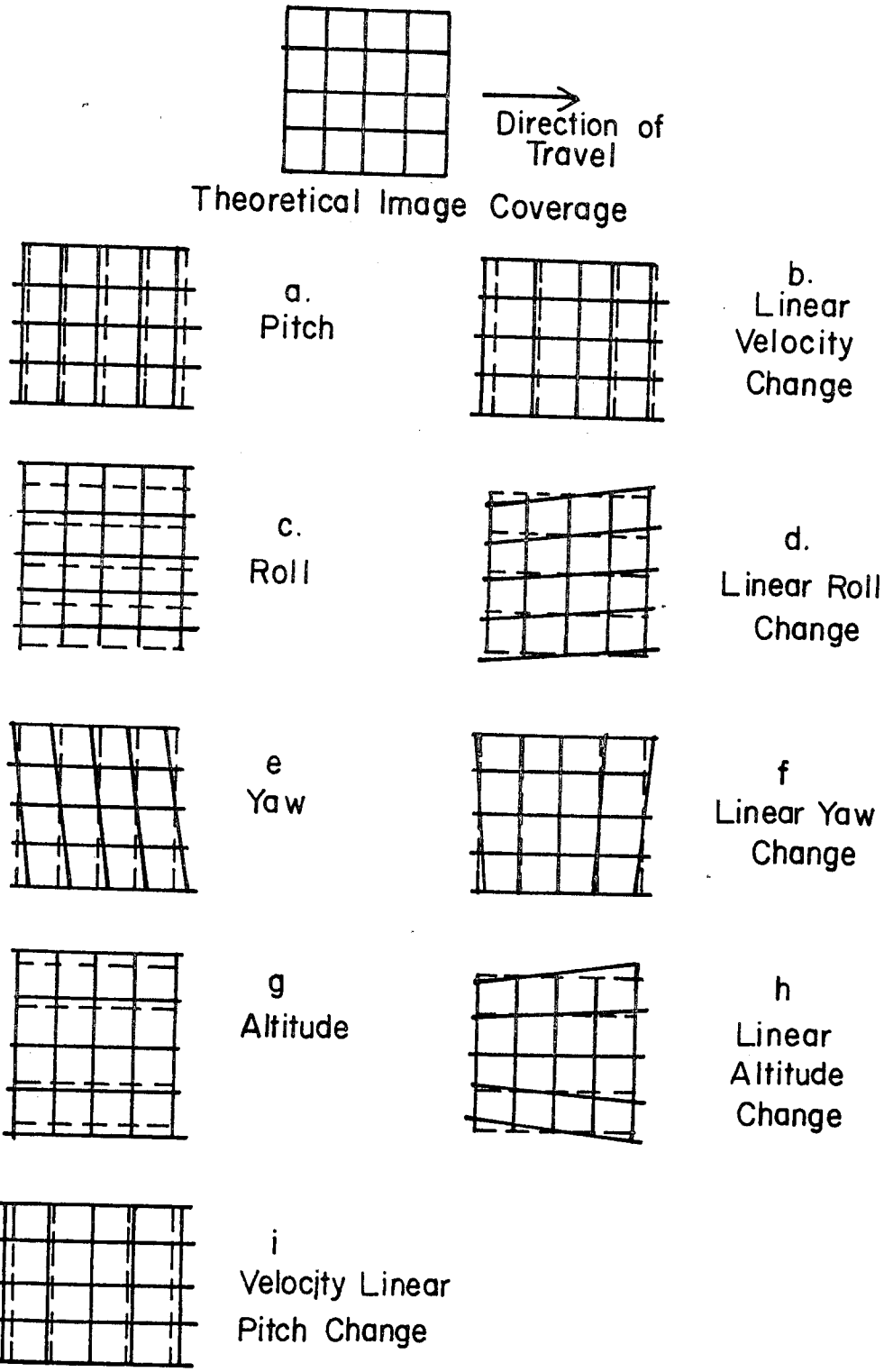

Figure 1.22. Resultant Earth Coverage of Scanner in the Presence of Different Vehicle Orientation Irregularities (Adapted from [20])

Thus, it would be unreasonable to expect the recovery of all orientation parameters from the imagery, especially if only singly scanned imagery is available. Kratky [21] also points out this inseparability of orientation elements based upon scanner imagery.

The variation in these elements of sensor exterior orientation down the flight line are in general stochastic in nature, or random time functions. The cumulative effect of these, however, may be considered deterministic or analytical, particularly for short sections of the flight line [22]. It may be possible then to approximate these variations within a short section using such functions as polynomials or harmonics [21, 22, 23].

Ideally, the mathematical functions expressing the behavior of exterior orientation elements should be in terms of time. However, time may not be recorded with sufficient accuracy to be relied upon for such analysis. Alternatively, if the concept of a constant effective speed of "film" travel (v) is utilized, then the x coordinate of the imagery may replace time in these functions. When the data is in the form of digital arrays, x may further be replaced by the scan line number as the independent variable,

$$x = v(T - T_o) \tag{1.20}$$

$$t = \frac{x}{v} \tag{1.21}$$

where $t = T - T_o$.

As an example, if Y_c is assumed to be approximated by a second order polynomial in time within a section of a flight line

$$Y_c = a'_o + a'_1 t + a'_2 t^2 \tag{1.22}$$

then the resulting polynomial form in terms of the image x coordinate would be

$$Y_c = a_o + a_1 x + a_2 x^2 \tag{1.23}$$

in which

$$\begin{aligned} a_o &= a'_o \\ a_1 &= a'_1/v \\ a_2 &= a'_2/v^2 \end{aligned} \tag{1.24}$$

Derenyi and Konecny [22, 24, 25] investigated the effect of differential changes in each of the exterior orientation elements on the ground coordinates. The equations utilized were based upon Hallert's differential formulas [26] modified for scanned imagery. The resulting form of the equations is

$$\begin{aligned} dX_j &= (Z_c - Z_j) \tan\theta_j \, d\kappa + (Z_c - Z_j) d\phi + dX_c \\ dY_j &= \tan\theta_j \, dZ_c - (Z_c - Z_j)(1 + \tan^2\theta_j) d\omega + dY_c \end{aligned} \tag{1.25}$$

For the present investigation, ground displacements were calculated for representative values of the orientation element differential changes for various combinations of flying height and scan angle. Figures 1.23, 1.24, 1.25, and 1.26 illustrate the ground displacements due to some of the terms in Equations 1.25. Figure 1.23 depicts

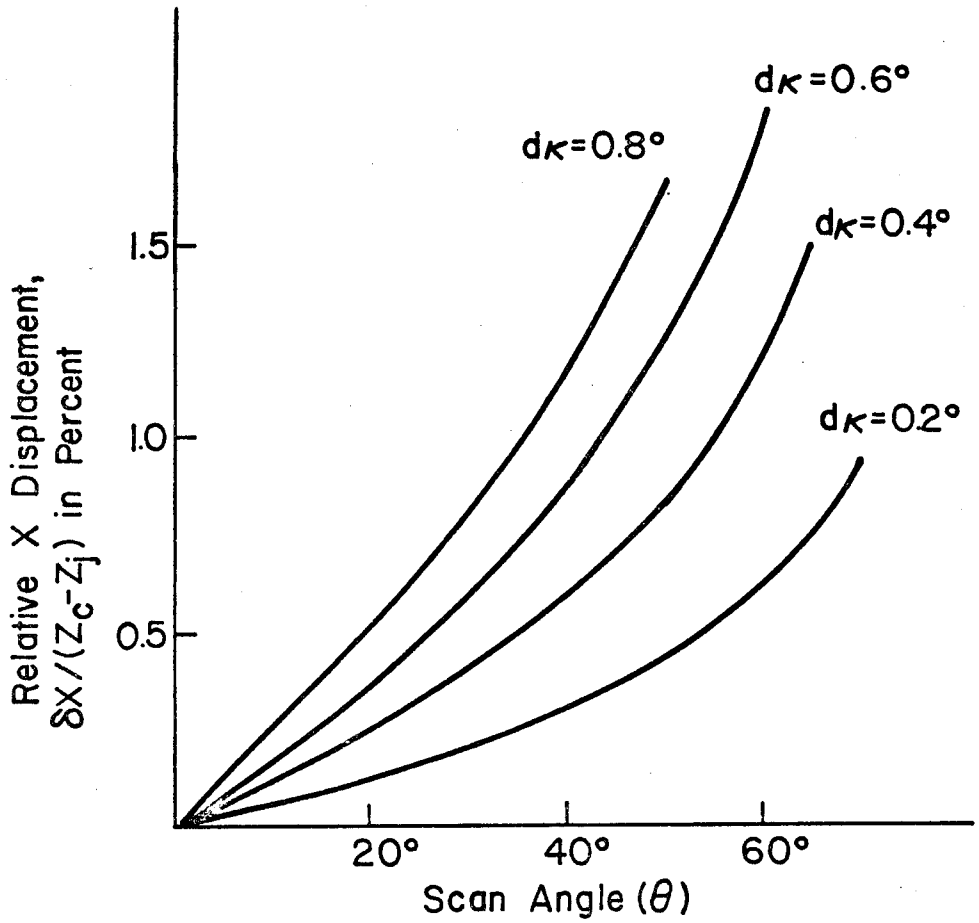

Figure 1.23. Ground Displacement in X Direction Due to Change in Yaw (dκ)

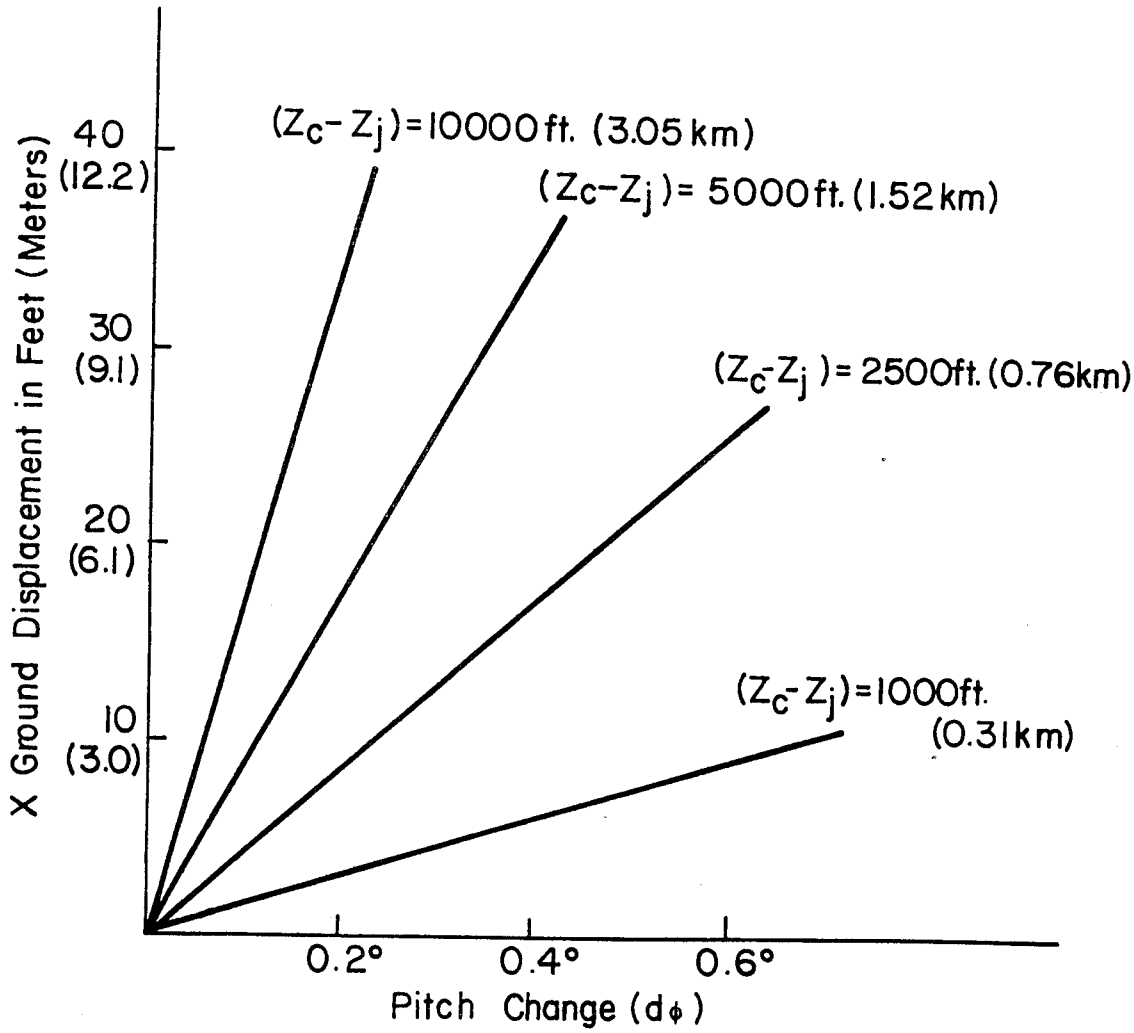

Figure 1.24. X Ground Displacement Due to Pitch Change ($d\phi$)

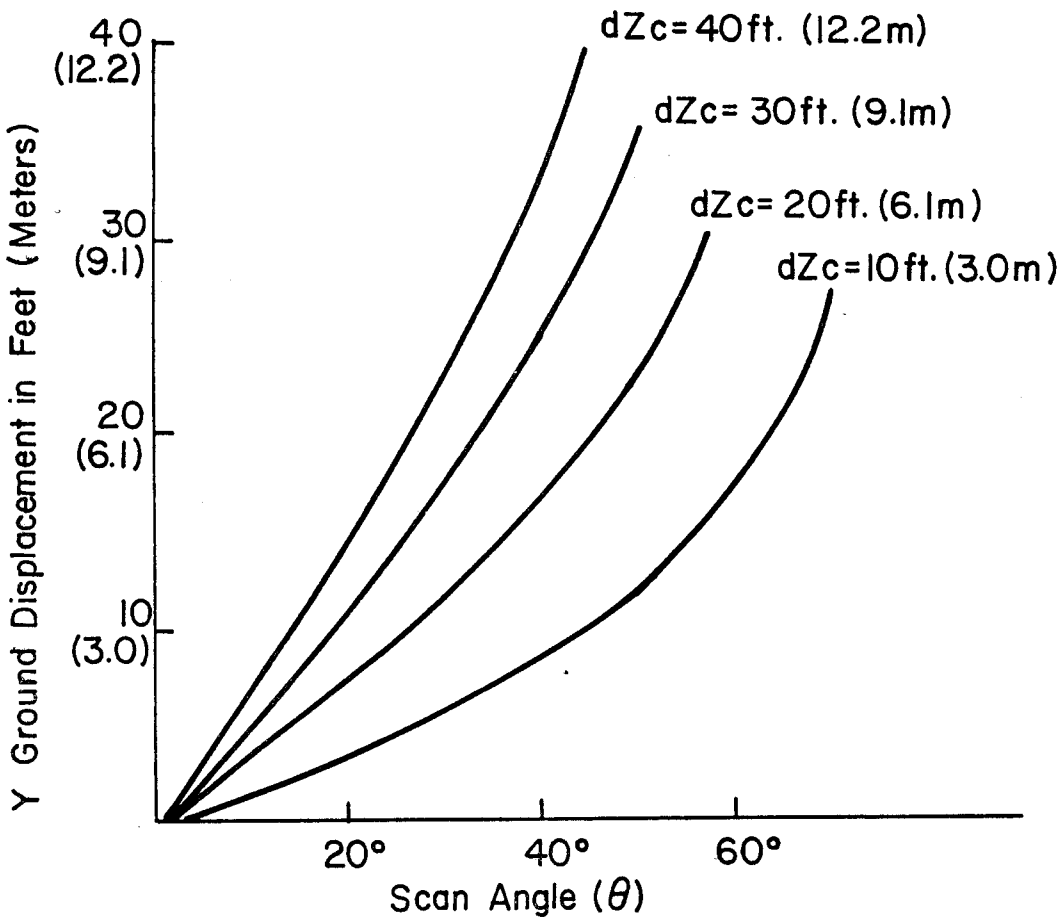

Figure 1.25. Y Ground Displacement Due to Flying Height Change (dZ_c)

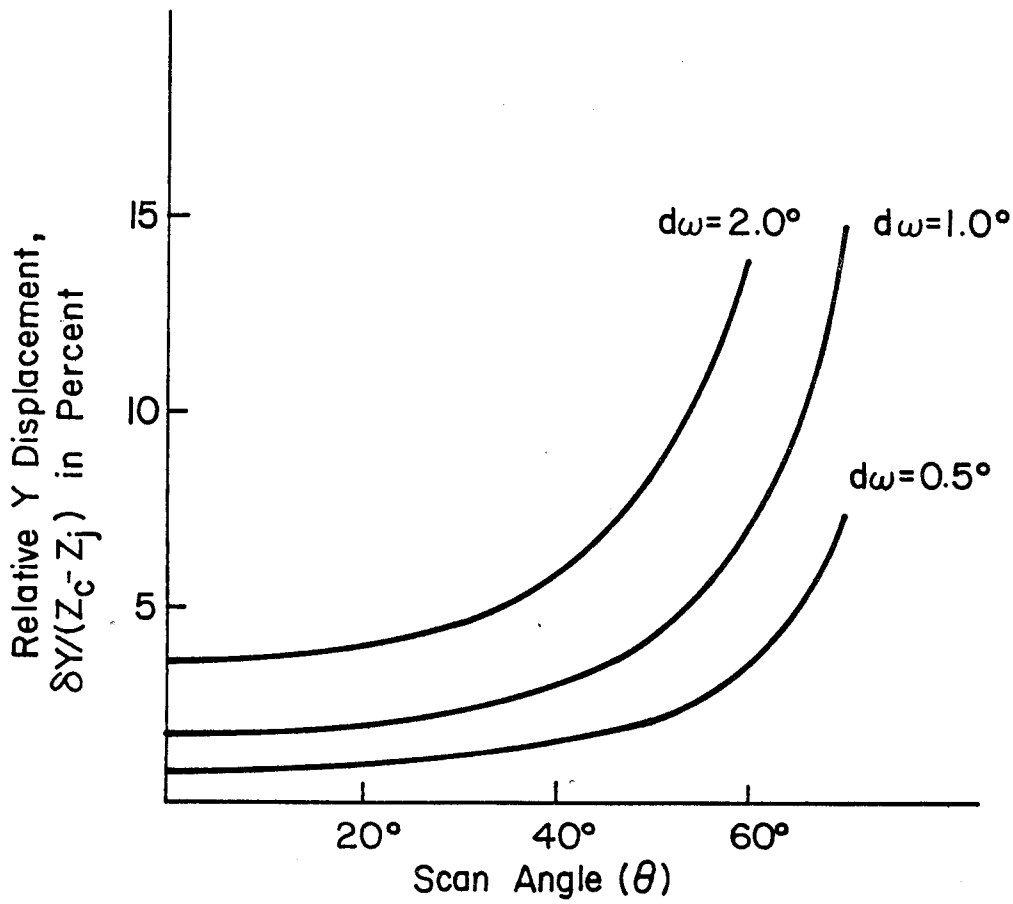

Figure 1.26. Ground Displacement in Y Direction Due to Change in Roll (dω)

the X ground displacement relative to flying height above terrain due to a differential change in yaw ($d\kappa$). Figure 1.24 depicts the absolute displacement at ground scale for various values of flying height due to a small change in pitch ($d\phi$). Figure 1.25 illustrates the resulting Y coordinate change as a function of scan angle, θ, for various values of differential changes in flying height (dZ_c). Figure 1.26 gives the Y displacement relative to flying height as a function of scan angle, due to changes in the roll angle ($d\omega$).

1.4.2.4 Scan Time Effect. If the assumption that each scan line is recorded instantaneously is relaxed, then the data would be recorded as shown in Figure 1.27, assuming aircraft velocity, V, to be constant during the very short time span of a single scan. The X_j coordinate of any point may then be written as

$$X_j = X_c + \frac{y_j}{2\pi c} t_r V \qquad (1.26)$$

in which y_j is the along-scan image distance to point j, or the column number for digitally recorded arrays. The t_r term is, as before, the period of revolution of the scanning mirror, and c is the sensor constant (see Figures 1.16, 1.17).

The period of revolution, t_r, is a well defined term for most scanning systems. However, the aircraft velocity V, is a function of time, and some difficulty may be encountered in accurately monitoring this velocity. It is possible, however, to include this scan time effect into the κ term of sensor exterior orientation as observed from Figure 1.27.

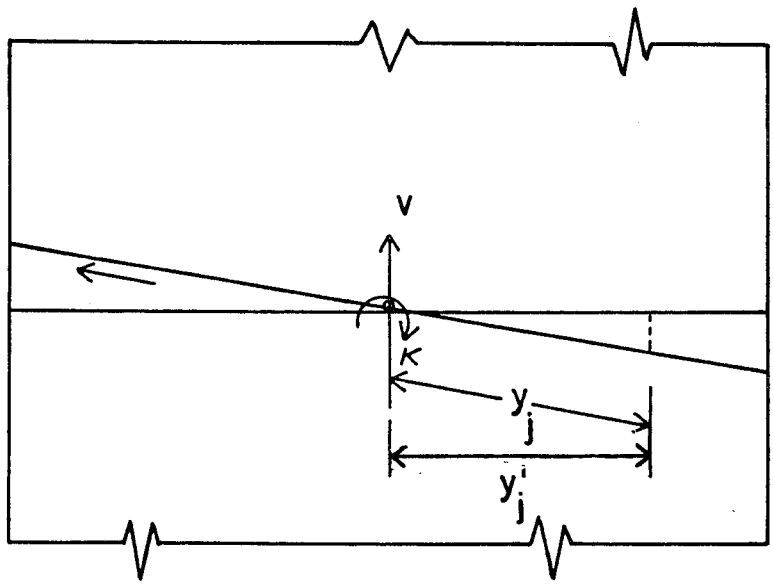

Figure 1.27. Equivalent Yaw Due to Scan Time Effect

1.5 Review of Previous Investigations

The imagery generated by an optical-mechanical scanner contains many of the features of imagery generated by more conventional strip and panoramic photography. Consequently, many of the geometric characteristics of the panoramic and strip imageries serve as a basis for analysis of scanned imageries, and the review will begin with a discussion of these more conventional sensing systems. This will be followed by a chronological review of previously published investigations of the geometric aspects of nonconventional sensors. These sensors include radar sensors such as Plan Position Indicator (PPI) and Side Looking Airborne Radar (SLAR), infrared line scanning systems (IRLS), and multispectral scanning systems (MSS). The last portion of the review deals with the recent advent of remote sensing from spacecraft, and the geometric peculiarities of such systems, particularly the simplifying assumptions which are possible due to the relatively high stability of such sensing platforms. Particular attention will be paid to the Earth Resources Technology Satellite (ERTS), which contains an MSS system. The inclusion of this sensing system led directly to several fruitful investigations of scanner geometry.

In the late 19th century an Italian named Porro developed a camera employing the panoramic principle. The instrument, fitted with a telescope and level, recorded photographs on a strip of sensitized paper held against the surface of an upright cylinder. Only fairly recently, however, have intensive efforts been directed toward the design, development, testing, and routine application

of panoramic cameras to aerial photography [27]. Continuous strip photography was first used in 1932, and was initially intended for low altitude, high speed reconnaissance.

Early papers by Katz [28, 29] presented methods by which object heights could be extracted from continuous strip imagery using parallax measurements made on the photograph. Wohl and Stickle [30] in 1959 derived data concerning traffic velocities and volumes based upon the geometry of the continuous strip camera. In an article published in 1962, Elms [31] proposed the possibility of using the convergent strip camera system as a mapping tool. In that article, the requisite equations for determination of ground elevations and distances were derived under the assumption of the aircraft flying straight and level. The effects of errors due to insufficient image motion compensation, aircraft velocity and position variations, and aircraft angular orientation variations were investigated and their effect upon the original equations was presented. The conclusion which Elms reached was that mapping was possible using imagery from a strip camera, although the use of conventional plotting systems as they then existed was precluded.

Ockert [32], in an article published in 1960, compared the frame and strip cameras for potential use in satellites. The conclusions he reached were that the frame camera, due to its highly refined and perfected geometry was preferable to the strip camera with its complex geometry. The problem of time dependent orientation parameters was recognized, with its attendant difficulties in performing radial and space triangulation based upon strip imagery.

In a paper published in 1961 [33] Abraham developed projection equations for frame, strip, and panoramic cameras, and used these equations to perform variance propagation investigations in an attempt to quantitatively evaluate the accuracies obtainable from the three camera types. After first formulating the projection equations of the frame camera, Abraham developed transformations for the panoramic and strip imageries to reduce measured coordinate values in these systems to equivalent frame camera coordinates. These transformations were introduced into the original projection equations to form projection equations for the panoramic and strip cameras. Variance propagation was carried out for a test case and numerical values computed. The results indicated that expected ground coordinate standard errors were about 10% greater for X coordinates obtained from panoramic images than those from frame photography, and about 15% greater for Y coordinates. The strip camera yielded expected errors about 14% in X and 23% in Y over those of the frame camera.

A two article series [34, 35] authored by Itek Laboratories and published in Photogrammetric Engineering in 1961-62 did much to acquaint the photogrammetric community with the advantages, disadvantages and geometric peculiarities of the various panoramic cameras. The first article, published in Dec. 1961, dealt with the advantages of the panoramic camera (high resolution coupled with wide angle coverage), its disadvantages (longer cycling times resulting in unsuitability for low altitude, high speed aerial photography), and the two basic physical configurations possible in panoramic camera (direct scanning or rotating prism). The second of the

articles dealt with the geometric properties of the images produced by panoramic photography. In particular, effects of cylindrical imaging (previously discussed in Section 1.4.2.1), the scan (sweep) positional effect due to camera motion during exposure, and the effect of image motion compensation were discussed.

Kawachi [36] in 1965 presented image displacement equations for image motion due to angular orientation instabilities of frame and panoramic cameras. Kawachi also presented plots of rates of change for the roll, pitch and yaw orientation elements for a typical reconnaissance aircraft. These plots indicated the stochastic nature of the orientation elements.

Gullicksen [37] in 1967 advocated the use of strip photography as a map substitute in order to eliminate the mosaicing necessary with frame photography. Equations for planimetric errors which resulted from the direct use of a strip photograph as a map substitute were presented, and a numerical example was computed.

An article by Gill [38] in 1964 presented parallax equations for convergent panoramic photographs, and related these to a relative orientation procedure by analytic means. The photographs were relatively oriented in segments or parts, in order that the method could be used in an analytical plotter with limited format size. A test grid was simulated and the procedure tested using the AP-II analytical plotter, with the results indicating the feasibility of analytic relative orientation of panoramic photography.

Hovey [39] in 1965, reiterated the advantages of panoramic photography, reviewed the image displacements inherent in the imagery,

and advocated greater use of panoramic imagery by the photogrammetric community.

Skiff [40] in 1967 published an article treating strip and panoramic photographs analytically. The article used tensor notation throughout. Collinearity equations were presented for frame, strip and panoramic photography, and the basic equations necessary for triangulation using two photos were obtained. Skiff included the concept of time varying orientation parameters, and assumed a linear time function for aircraft positional elements for the strip case, and a uniform angular velocity for the panoramic sweep. Derivatives of the resulting equations were presented for subsequent linearization. In concluding, Skiff suggested the use of a constant orientation assumption over a portion of the imagery.

In a very important paper [41] published in 1967, Case formulated analytic expressions for projection and collinearity equations associated with panoramic and strip photography. The basic principle advocated in this paper is the reduction of image coordinates from strip or panoramic photography to coordinates on an "equivalent frame photograph", through simple transforming equations. The resulting image coordinates, it was believed, could then be treated using existing programs for space resection, relative orientation, and block adjustment. This formulation differed from that of the earlier work of Abraham [33] dealing with the same concept, in that a unified matrix approach was utilized, rather than deriving each case separately from the geometry of the projection. Derenyi [22] points out that Case advocated the use of a constant orientation

assumption for short sections of the imagery. This paper used standard matrix notation and a photogrammetric approach, and served as a basis for further analytical formulations of the less conventional sensors, such as SLAR and optical-mechanical scanners.

A panoramic rectifier described by Wright [42] effectively projected a panoramic negative from a cylindrical surface having as its radius the principal distance of the imaging camera onto a tangent plane, forming a rectified image which would eliminate scan angle effects. Problems in lens design for this rectifier were presented in this paper.

Masry [23] in 1969 published an article treating convergent stereo strip photography in a rigorous analytical manner. The necessary coplanarity condition for relative orientation was presented, and it was noted that all exterior orientation elements of the strip camera were dynamic in nature, that is, stochastic functions of time. Masry proceeded to make the assumption that the angular orientation elements of roll, pitch, and yaw were constant during any short period, or piece of imagery. The positional elements of relative orientation X_c, Y_c, Z_c were assumed to have some general polynomial form for both sides of the stereo strip photography, resulting in a polynomial form for the base elements of relative orientation B_x, B_y, B_z. Relative orientation was presented by dividing the strip into sections of a length approximately equal to the image length covered by the parallax angle. Corresponding sections were relatively oriented using a successive procedure in which the orientation elements of the section just relatively oriented,

on one side of the film, were used as the elements of orientation for the opposite section on the other side of the film, since they were simultaneously recorded.

Masry then presented projection equations to form model coordinates if orientation parameters were assumed known, and test cases were run on both simulated and real imagery. Problems occurring were due primarily to the instability of the solution for orientation parameters and resulting model coordinates, caused mainly by small parallax angles in the convergent strip camera. Model coordinate errors were found to be largest in the Y direction (perpendicular to flight direction). Masry concluded that if monitoring of orientation elements were done, the model coordinate stability would naturally be greatly enhanced.

In 1971 Derenyi [22] completed a thesis relating to relative orientation of strip imagery. The dynamic nature of the imagery caused by continuously changing orientation parameters was recognized and described. Two basic schemes of relative orientation were presented to cope with this problem.

In the first of these, called the line-by-line method, two corresponding lines perpendicular to the flight direction were relatively oriented, and this procedure was repeated down the strip to form a series of line models. Intermediate values were obtained by interpolation by harmonics or polynomials. Since only three orientation parameters were recoverable by relatively orienting a line pair, an investigation was conducted into the effect of the omission of two orientation parameters upon the remaining three. The results,

as indicated by both theoretical error propagation studies and tests on real and simulated imagery, indicated that serious errors would be introduced unless the omitted parameters were monitored or stabilized to the same precision expected from the relative orientation itself.

In the second method investigated, termed the section-by-section method, portions of the strip were treated as a unit for the relative orientation procedure. In this method, some assumptions concerning the behavior of the exterior orientation elements over the section are necessary. Two assumptions were investigated in detail. In the first of these, the constant orientation assumption, the aircraft orientation parameters were assumed to remain fixed for each section pair to be relatively oriented. Error propagation studies by Derenyi indicated this method could result in serious errors due to the low attainable precision of the $d\phi$ term. Since Derenyi's analysis dealt primarily with convergent stereo systems, this low precision, coupled with a small parallax angle of convergence, would result in large expected errors of model point elevations formed by subsequent intersections. This problem could be alleviated by larger parallax angles, but if this is done, then longer sections are required, resulting in a loss of validity of the constant orientation assumption. An analysis was also carried out to assess the effect of this error, i.e. the assumption of constant orientation when, in fact, orientation is dynamic in nature. It was found that large errors in $d\phi$ and $d\kappa$ result from relatively small non-uniformities in orientation.
A further manifestation of the constant orientation assumption within

a section is also apparent. At section boundaries down the strip, discontinuities in orientation parameters, and hence, model coordinates, will appear.

As an attempt to partially overcome these problems, a changing orientation assumption, to be approximated by linear orientation changes within a section, was also investigated. It was found that significant improvement in accuracies resulted from this more realistic assumption, and the discontinuities at section boundaries disappeared.

As a further attempt to strengthen relative orientation procedures, Derenyi suggested a "triple channel recording" system, in which a convergent stereoscopic system would include not only fore and aft looking sensors, but also an additional vertical one. By this method, the three lines recorded could be treated much as lines from a single frame in a frame camera, and many of the techniques of frame photography could be employed. It was felt that use of this scheme would allow greater parallax angles, and hence help alleviate the low precision attainable in the $d\phi$ term, and subsequent model point elevations.

Derenyi also analyzed the sidelapping flight line configuration. As mentioned in Section 1.4.2.3, the inability to separate analytically between some orientation elements results in the possibility of recovering only two orientation elements, and then only by using the line-by-line approach. Derenyi draws the conclusion that this flight configuration was therefore unsuitable for relative orientation. It should be mentioned, however, that this means relative orientation in the strict photogrammetric sense, in which it is desired to recover

five orientation elements. While this is clearly impossible using sidelapping flight lines, it may be possible, after some type of relative or absolute orientation has been done, to obtain model elevations by intersection.

In fact, Leberl [6] in 1972 studied the propagation of error from orientation parameters to model coordinates for optical-mechanical scanners. His results indicated that, with regard to error propagation, the sidelapping of flight lines was the optimum scheme in order to minimize cofactors of the Z model coordinate, or elevations.

A recent use of panoramic photography of general interest was reported by Alderman [43], in which a convergent panoramic photography system was used in establishing control on the lunar surface. Operating from the Apollo 15 Scientific Instrument Module, an optical bar camera was used to generate overlapping panoramic photography. The resulting imagery was used to generate models by the process of relative orientation utilizing the constraints imposed by the orbit of the spacecraft. These were subsequently assembled into a strip using the method of Schut [44]. Subsequent transformation of the assembled strip to control points was then carried out. A linear rate of change for exterior orientation elements was assumed to accomodate the dynamic nature of the imagery.

With the advent of the concept of "remote sensing" in the general sense, beginning in the early 1960's, the photogrammetric community has been faced with problems of an unusual and challenging nature. The unconventional sensor types advocated for use, such as SLAR and MSS, although having unique data gathering capabilities such

as all weather operation and image forming capabilities outside the visible range of the spectrum, suffer from problems of reduced resolution and image distortion due to the dynamic mode of image formation.

The use of radar as a remote sensing system has been progressing for some time, beginning with the Plan Position Indicator (PPI) first developed around 1940, with Side Looking Airborne Radar (SLAR) coming into existance around the mid 1950's. Leberl [45] presents a detailed history and literature review on radar remote sensing systems.

Suits [46] reported in 1960 on the nature of infrared radiation as a source of imagery. Recording systems based upon both cameras and scanner-detector configurations were presented. Colwell [47] in 1963 published an article which did much to acquaint the photogrammetric community with the basic matter-energy relationships necessary for image formation by remote sensing. Leonardo [48] in 1964 published a further article dealing with general advantages and problems associated with remote sensing systems.

In an early paper, Harris and Woodbridge [49] presented the basic configuration for a thermal scanning system and the concepts of spectral radiance in the emissive region of the spectrum, as well as atmospheric transmission.

Suits [50] in 1966 advocated that security restrictions on infrared scanning devices be lifted, in order that the scientific community as a whole might benefit from this relatively new data gathering system. Suits reported on an anticipated reduction in

the classification of instruments, thus alerting the photogrammetric profession to its availability.

Other sources of general information on remote sensing and remote sensing systems may be found in references [4, 10, 11, 27, 51, 52], as well as the series of LARS annual reports [53-56], and the proceedings of symposia held at the University of Michigan [57].

In the mid 1960's, the airborne multispectral scanner was used at the Willow Run Laboratory of the University of Michigan (now Environmental Research Institute of Michigan). Since 1966 Purdue University's Laboratory for Applications of Remote Sensing has been formulating and developing a digital system of MSS data handling to perform automated interpretation based upon spectral differentiation by statistical and pattern recognition techniques [53, 54, 55, 56]. Recent papers by Wilson [58] and Lapides [59] have emphasized the utility of multispectral scanners and enumerated their unique advantages, as well as limitations associated with the data available from them. Carnes [60] reported on advances in auxiliarly equipment associated with such scanning systems.

Until recently, much effort has been spent on investigations into the radiometric and interpretative aspects of data gathering, data handling, and automated interpretation. The geometric aspects of the data arrays generated were ignored or sublimated to the more pressing problems of research into and development of the radiometric and interpretive aspects noted above. As the analysis of non-metric facets progressed, however, the problems of geometric factors in these scanning systems became more apparent and work in this area was begun.

In a series of two papers [24, 25] Derenyi and Konecny first applied a photogrammetric approach to the optical-mechanical scanning system. These papers dealt with the basic recording system, the scan angle effects of varying resolution size and panoramic displacement mentioned in Section 1.4.2.1, and the dynamic nature of scale factors involved in a scanning system. The study of exterior orientation effects was based upon a modification of Hallert's differential formulas. The effect of errors in determination of angular resolution size was also assessed. In the second of the papers, the authors presented a projection equation in matrix form which considered the dynamic nature of the imagery, accounting for the movement of the projection center during recording.

Konecny, in a series of papers, [7, 61, 62, 63] summarized the basic projective relationships associated with various remote sensing systems. These papers dealt with methods of approximate relative orientation and rectification of imageries recorded with dynamic systems and discussed accuracies which may be expected utilizing these systems. The latest paper [7] provides an excellent summary of most of the work done on geometry of non-conventional remote sensors to date.

A paper by Taylor [64] provides useful insight into rectification procedures for infrared line scanning sensors. Rectification equations are derived from basic projection equations by first assuming a perfect orientation case, and analyzing image displacements after subsequent perturbations in roll (ω), pitch (ϕ), and yaw (κ).

A series of papers [6, 45, 65, 66, 67, 68] written by Leberl treat geometric aspects of the two most popular non-conventional remote sensors, side looking airborne radar (SLAR) and the optical-mechanical scanner. Leberl was primarily interested in SLAR imagery, and his work culminated in a doctoral thesis [45] which is particularly notable for two reasons. The first of these is the extensive bibliography included on radar in general, and in particular, SLAR. The second notable point in this work is the introduction of interpolative techniques for the rectification or restitution of SLAR imagery. Using stochastic concepts, these interpolative techniques present a viable alternative to the projection equations for image rectification or restitution. These techniques may prove to be quite useful for the rectification of digital MSS data arrays, since they appear well suited to this digital data handling format (particularly when scanned terrain is relatively flat).

A paper by Markarian, et. al. [69] in 1971 presented a scheme of utilizing general polynomials for rectification of digitized imagery. The concept of treating the data as an uncorrected input array used to generate a rectified output array was utilized, and the principal of digitally "stepping" on the output array and placing gray scale values from computed positions in the distorted input array was advocated. Further, it was recommended that the "nearest neighbor" be used as the gray scale value from the input array, rather than to attempt interpolation of gray scale values.

Increasing interest in these geometric aspects of remote sensing systems is evidenced by the increase in literature in this area

very recently. Masry and Gibbons [70] reported on the use of the analytical plotter for rectification of scanned infrared imagery. Rectification of planimetry using the LR-2 line drawing rectifier, as reported by Forrest [71] handles either SLAR or scanned imagery.

In a paper by Bosman, et. al., [72] a programming system called KARIN is described for planimetric mapping from single or overlapping strips of remote sensing data such as SLAR or infrared line scanner (IRLS). Graham [73] and Yoritomo [74] described restitution schemes for radar imagery at this same meeting.

In the early 1970's the use of satellites and spacecraft as remote sensing platforms was realized. The culmination of this long awaited event came about with the launching of the ERTS-1 satellite on July 23, 1972, which contained both return beam vidicon (RBV) and multispectral scanner (MSS) imaging systems. Because of this event, considerable effort was expended prior to, and immediately after, the launch on geometric problems associated with the MSS. The Skylab manned orbiting Earth resources laboratory contains photographic and MSS imaging systems. The Skylab MSS is of the conical scanning type.

General information on the imaging of the Earth's surface from space, and the ERTS-1 and Skylab systems and their sensors in particular may be found in references [75, 76, 77, 78, 79, 80, 81, 82, 83]. In a very revealing paper, Forrest [75] explains the unique advantages of using satellite imagery, particularly from scanners, for cartographic use. Consideration was given to the scanner geometry and resolution, and the use of ground control points extracted from

existing maps was advocated to resect for sensor orientation elements for the precision required for mapping beyond that obtainable from satellite ephemeris data. Forrest points out the greater stability of orientation in spacecraft over that of airborne sensors. The conclusion was drawn that mapping from space images economically compares very favorably with that of conventional techniques, and this cost may be spread among users of the imagery outside of those with cartographic interests.

In two recent papers [81, 82], Doyle summarizes the types of sensors which have to date been used from spacecraft, and describes some of their uses. Processing of the data and imagery generated is also discussed.

The geometric problems associated with imaging with spacecraft mounted sensors have been addressed by several investigators. Although, as previously mentioned, spacecraft orientation instabilities are generally less pronounced in these systems than with airborne systems, these investigations yield valuable insight into possible analysis methods for airborne systems.

Colvocoresses [84] as early as 1970 published an article dealing with geometric errors to be expected in ERTS imagery. He analyzed image displacements for 5 possible sources: Earth curvature, atmospheric refraction, camera obliquity (or exterior orientation angular elements), terrain relief, and map projection error. The effect of atmospheric refraction was found to be negligible, and that due to terrain relief would be minimal except in extreme cases. Other errors were easily modeled except for the obliquity error.

Colvocoresses advocated not processing images in an element by element manner except for special purposes.

A series of papers by Kratky [21, 85, 86, 87] addressed these problems from the photogrammetric viewpoint. Of particular interest for this investigation is the formulation of functional forms to account for orientation instabilities of the scanning system. After presenting the basic projection and collinearity equations for the scanned imagery, the use of two alternate functional forms to approximate orientation variations with time is investigated. These are polynomial and harmonic functions. Kratky presents the equations in matrix form for resection to solve for the parameters of these functions, including explicit presentation of the coefficient matrix and constant vector for each of the functional forms considered, when substituted into the linearized collinearity equations. Because of the smaller and smoother orientation behavior of spacecraft systems over airborne systems, it was possible to incorporate small angle approximations into the analysis, yielding simplified equation forms. Kratky also points out the inability to distinguish between the correlated orientation elements ϕ and X_c, the pitch and sensor X position, using singly scanned imagery. Thus, it is indicated, resection for all orientation parameters is impossible. However, the remaining parameters may compensate for these neglected elements, and result in acceptable image positions after subsequent projection.

The geometric processing of ERTS imagery in the United States has been discussed by several investigators [20, 88, 89]. Forrest [20] describes the bulk image processing scheme (currently called "system

corrections"), as well as the more refined precision processing ("scene corrections") used on selected imagery as requested by the user. The bulk image processor transforms the scanned imagery to a central perspective projection. The purpose of this transformation is to generate a series of "frames" from sections of the imagery as they would appear if recorded by a frame camera. The element corrections are fully calculated for intersections of a nine by nine grid. These displacement values calculated incorporate corrections for Earth rotation, as well as roll, pitch, and yaw values, which are taken from satellite data. Image positions between these 9 by 9 array points are assigned by linear interpolation.

The precision processed (scene corrected) images are generated as a subset of the above bulk processed (system corrected) imagery, incorporating more sophisticated techniques for geometric improvement. The use of ground control points extracted from existing maps, and identifiable on the imagery are used to refine image position corrections. Forrest points out several advantages in the use of ground control points.

1.) The use of control points allows for obtaining the positional accuracy desired in the precision processed imagery.

2.) Failure of the attitude sensor (the sensing unit which monitors the angular orientation elements of the spacecraft sensor) will not jeopardize the possibility of geometric improvement of the imagery.

3.) The direct determination of sensor orientation elements by resection from these points serves as a check on the attitude sensor, and serves to refine the orientation element values used in the bulk processing.

4.) The use of redundant control points and least squares adjustment techniques allow the estimation of obtainable accuracies for orientation elements and indicate the positional accuracies of the control points used.

The resection equations used to correct the MSS imagery in precision processing solve for eight parameters. These parameters reflect the image displacements caused primarily by errors in pitch, roll, and yaw, and by rates of change of these orientation elements. Once again, due to the small, smooth nature of the spacecraft orientation variations, the use of polynomial functional forms may be used to represent these image displacements. The equations used are

$$\begin{aligned} \Delta x &= a_o + [1 + (x/H_s)^2] + a_1 x + a_2 y + a_3 xy \\ \Delta y &= b_o + [1 + (y/H_s)^2] + b_1 x + b_2 y + b_3 xy \end{aligned} \qquad (1.27)$$

in which Δx and Δy represent image shifts from the x and y positions recorded on the bulk processed imagery, H_s is the spacecraft altitude at image scale, and a_i, b_i are the eight parameters to be solved for in the spatial resection. It should be noted that terrain relief is neglected in these equations. Kratky [21] points out that the effect of terrain relief is less than the ground resolution size of an element unless terrain elevation differences on the order of 2600 ft. (800 m) are encountered within a single frame. Such

relief differences do exist in some ERTS frames, and the planimetric accuracy in such frames will suffer accordingly.

Since digital data handling techniques for MSS data have become operational at LARS and elsewhere, it is desirable to investigate the geometry of such imagery in greater detail. The geometry of the scanning system will be analyzed in this investigation, with particular emphasis to be placed upon techniques which are suited to the digital data handling approach. Existing published literature in this area has dealt with data from spacecraft platforms, in which simplifying assumptions may be made, or for digitized frame photography. The investigation in this thesis will attempt to deal with the more general problem of gathering MSS data from an airborne platform, for which the simplifying assumptions based upon platform stability do not in general hold. This combination of a general geometric analysis, valid for both airborne and spaceborne systems, coupled with the digital data analysis, it is felt, will provide a much needed work not present in existing literature. The chapter immediately succeeding this will therefore deal with the general geometric problems associated with the MSS scanning system, in order that the relationships obtained may be utilized for the analysis of specific areas of interest in MSS digital data systems.

2. GEOMETRIC ANALYSIS OF MSS DATA ARRAYS FROM SINGLY SCANNED AREAS

2.1 Remote Sensing as a Transformation

According to Mikhail and Baker [5], remote sensing may be thought of as a mapping of multidimensional object space onto another space, the sensor space, having the same or fewer dimensions. Such a mapping may be effected through a transformation taking a multidimensional object space vector into multidimensional sensor space vector to be stored for subsequent retrieval and analysis. This may be termed the "remote sensing transformation". The dimensions of each vector will depend upon the degree of simplification of the physical phenomena involved, and the characteristics of the sensor employed. Examples of information content which may be included in the object space vector are [5]: spectral radiance from each resolution element in a particular wavelength band, polarization of the radiant energy with respect to the object space coordinate system, and coherence, both spatial and temporal, of the radiant waves. Components of the sensor space vector may include: spectral irradiance incident on the sensor in each wavelength band considered, the direction of polarization (if retained) with respect to the sensor coordinate system, the degree to which coherence is attenuated, and frequency and phase shifts of the carrier or force field if active sensing systems are utilized.

An important characteristic of sensors with image forming capabilities is that geometric image positions can be generated from the sensor space vector record stored. In most non-mapping systems to date, this geometric image position is not considered the primary goal of the recording. However, the fact that it can be recovered affords a unique opportunity to the interpretive data analyst and photogrammetrist. This leads to a unified data analysis concept in which analysis of both the non-metric data for interpretation as well as the metric record inherent in the data becomes possible. As indicated in Chapter 1 in the review of previous investigations, a two step sequential procedure has been used for some scanning systems (notably spacecraft systems) in which scanned data has been processed for geometric restitution, with the resulting data then utilized for automated interpretation. However, the possibility of simultaneous digital analysis of both the interpretive and geometric aspects has not been greatly exploited to date. With the more traditional photographic sensors, the nature of the methods used for both interpretation and photogrammetry has largely precluded this unifying concept. The photo interpreter has used methods of visual inspection, relying on visual "keys" to arrive at decisions. The photogrammetrist has relied heavily upon accurate reconstruction of the geometry of the photograph to extract positional and metric information about the object space. An examination of the object and sensor space vectors for black and white frame photography may perhaps explain why these traditional fields of interpretation and photogrammetry remain separated. For each point imaged in the

photograph, the object space and sensor space vectors may be thought of as each having two parts. The first part will contain the non-metric information which may be sensed and recorded (such as spectral information, polarization, etc.), the second portion will contain geometric information. Consequently, the object space vector for each point may take the form:

$$\begin{bmatrix} S_1 \\ \vdots \\ S_n \\ \hline X \\ Y \\ Z \end{bmatrix}$$

$S_1 \ldots S_n$: spectral radiance from n wavelength bands within the photographic region

X, Y, Z: point position in object space

where consideration is given only to spectral values for the non-metric portion. The resulting sensor space vector is of the form

$$\begin{bmatrix} D \\ \hline x \\ y \end{bmatrix}$$

D: film density recorded for the point

x, y: point position in image space

These vectors are related through some physical-geometric transformation which transforms the (n + 3) dimensional vector for a point in object space into a 3-dimensional vector in the sensor space. The physical transformation takes the n spectral values emanating from the point into a single density value D. The geometric portion

of the transformation takes the object space position (X, Y, Z) into the two-dimensional image position (x, y). The parameters associated with this geometric transformation are well known in photogrammetry, and consist of sensor position (X_c, Y_c, Z_c), sensor attitude (ω, ϕ, κ), and internal sensor characteristics (x_o, y_o, f, particularly for frame photography).

The problem with this transformation in general, which led to the traditional separation of the fields of photo interpretation and photogrammetry, lies in the suitability of each part of the transformation for numeric analysis. Traditionally, the interpreter does not look only at a single point density value, but notes the density, texture, size, shape, shadow, tone, color, and pattern of objects before concluding their nature [90]. Recent attempts at automating this procedure, in which photographic densities are quantified and computations performed upon them are actually attempts to simulate these visual "keys".

The geometric portion of the transformation, however, lends itself quite well to both analog as well as analytical treatments. This characteristic has spawned the practices of photogrammetry.

However, with the advent of the unconventional sensors, particularly the multispectral scanners, the extensive volume of the data severely curtails the role of direct human interpretation. Furthermore, the availability of the acquired data in digital form makes it possible to apply efficient computational decision making techniques and automated interpretation, as briefly described in Section 1.3. For the MSS system, considering only spectral information

for the non-metric portions of the vectors, the total object space vector would be of the form

$$\begin{bmatrix} S_1 \\ \vdots \\ S_n \\ \hline \bar{X} \\ Y \\ Z \\ \hline \bar{T} \end{bmatrix}$$

spectral radiance reflected and emmitted in n wavelength bands

element position in object space

time

and the form of the resulting sensor space vector would be

$$\begin{bmatrix} S'_1 \\ \vdots \\ S'_m \\ \hline \bar{x} \\ y \end{bmatrix}$$

spectral irradiance recorded in m channels ($m \leq n$)

element position in image space

For the MSS transformation, the nature of the sensor makes it necessary to regard time as part of the object space vector, and the dynamic nature of the sensing process is reflected in the way in which the transformation parameters of the geometric portion are handled.

Because the sensor is recording continuously during the aircraft flight, the sensor position (X_c, Y_c, Z_c)as well as attitude (ω, ϕ, κ)

become continuous stochastic functions of time. Other parameters of transformation for the geometric portion are c, a sensor internal constant analagous to the principal distance of panoramic recording, and v, a rate of imaging recording surface advance (see Section 1.4.2). Because of the dynamic nature of the sensing process, geometric analysis becomes more involved and less precise. However, the main advantage of the system is the retention of the several spectral irradiance numbers for each element, which allows measurement and computation for interpretive purposes.

In summary then, the MSS sensor allows the retention of sufficient information to make feasible a simultaneous analysis of both the physical (non-metric) characteristics as well as the metric (geometric) aspects of the data recorded. This simultaneous analysis may be brought about by combining the automated classification techniques discussed briefly in Section 1.3 with the geometric analysis methods to be discussed in this thesis. Therefore, the opportunity is available for considering a unification of the activities of both interpretation and photogrammetry.

This has not as yet been effected, however, for two primary reasons:

1.) Historically, interpretation and photogrammetry have been considered separately. It was thus only natural to continue this trend even after these new sensors became available. Also, there exists a shortage of personnel who are adequately trained in both interpretive (particularly automated interpretation) and photogrammetric techniques.

2.) The concept of combining the two computationally oriented fields of automated interpretation and photogrammetry, while logical, is quite a complex problem. Perhaps correctly, researchers to date have concentrated on one or the other aspect, in order to simplify the problems confronted and gain new knowlege.

The work done in automated interpretation has largely ignored the geometric aspects of the data vectors. As more sophisticated classification algorithms became available, however, and as progress was made in automated interpretation, it has become apparent that the geometric aspects are gaining in importance. It is now becoming the task of the data analyst to raise not only the question of "what" (interpretation) but also of "where" and "how much" (geometry). This problem is well illustrated by the operational ERTS system, in which it was felt that, even for bulk (system corrected) images, some geometric analysis and preprocessing was necessary to efficiently utilize the data. It is therefore the objective of the work reported on herein to analyze in detail the geometric aspects of MSS digital data arrays in an attempt to provide answers to these queries. The subsequent section will introduce the basic transformation relationships which serve as the basis of analysis of MSS data from the geometric standpoint.

2.2 The MSS Geometric Transformation

Figure 2.1 represents the recording of one channel of data during the scanning process of the MSS, in which the data array is considered as an image. Each array position would then have an associated "picture element" or "pixel". The two dimensional matrix of numbers would then be equivalent to the size of the imagery record. The line number i would represent a single scan, and within each scan the value j would represent the element position. With these comments in mind, Figure 1.17 may be thought of as the recording of the j-th element along the i-th scan line. Each picture element is recorded at a particular instant of time, thus making time an important variable. Following are the basic variables for subsequent analysis. Many of these variables have been previously introduced, but are included here for ease of reference.

T_o	the epoch, or time instant, of beginning of recording (at zero x*-coordinate)
t_r	time period for one revolution of the scanner
T_{ij}	time instant of recording point j on scan line i
θ_j	instantaneous scan angle with respect to a scanning axis passing through the effective perspective center and the scan line center
2α	total scan angle (α on either side of scanning axis)
c	constant representing a "principal distance" or the equivalent of the radius of a cylindrical recording drum

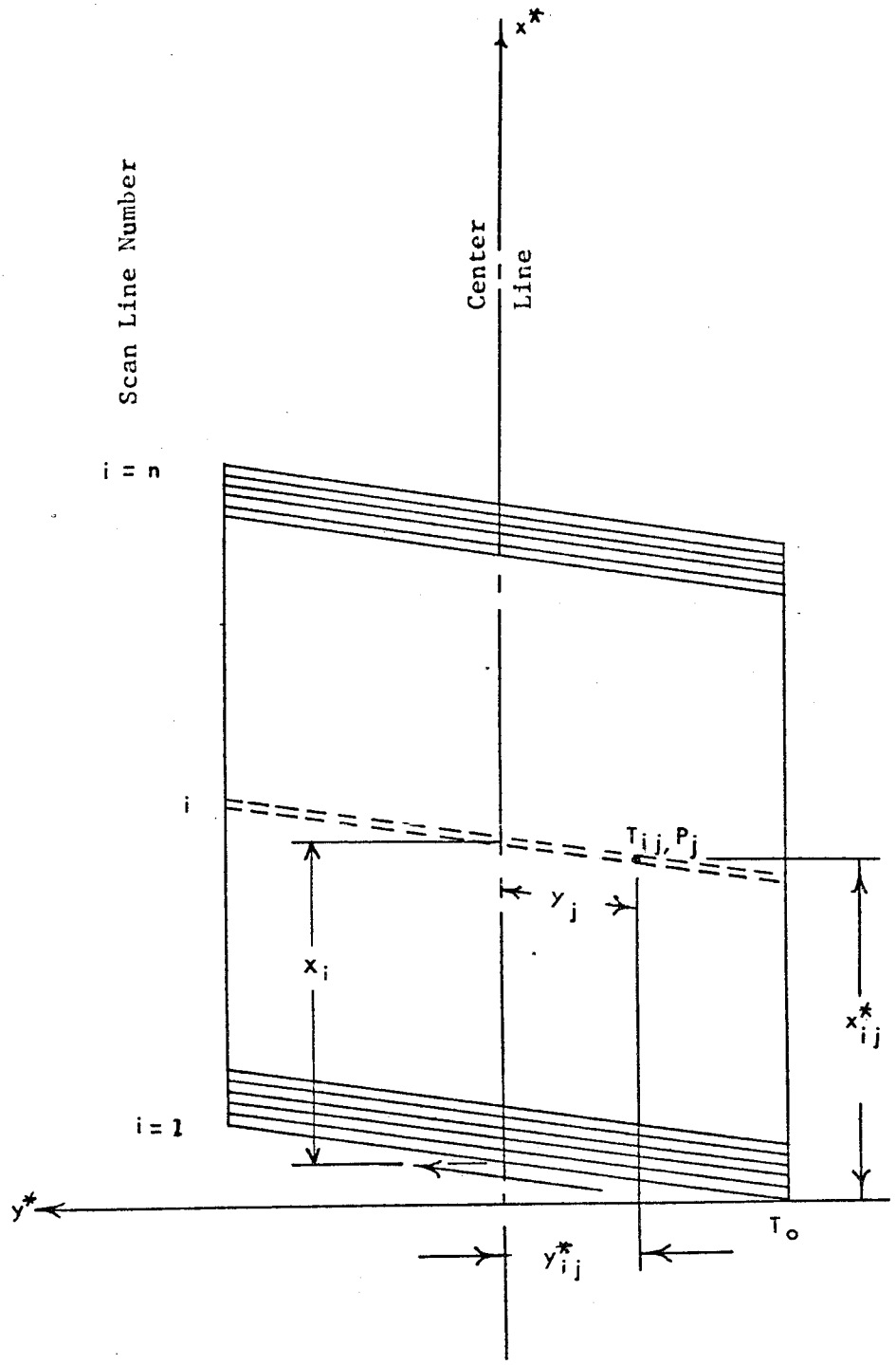

Figure 2.1. The MSS Image

v	speed representing "film" advance in case of pictorial recording, or its equivalent when recording in other modes (magnetic tape, etc.), taken as a constant
$(x^*, y^*)_{ij}$	cartesian coordinates of point P_{ij} (either image or its equivalent in digital recording) as shown in Figure 2.1
y_j	<u>distance along scan line</u> i from scan line center to P_{ij}
$\underline{M}_{ij}(t)$	instantaneous orientation matrix at T_{ij} (taking object system to sensor system)
x_i	distance along the image center line from the beginning of the recording, represented in digital recording by the scan line number i
k'_j, k_j	scale factors between object and sensor spaces for point j on scan line i, ($k_j = k'_j/\cos\theta_j$). k'_j is the actual scale factor of panoramic recording. Referring to Figure 1.17b, this scale factor would be represented by the ratio of lengths $\overline{Ca}$ and $\overline{CA}$. k_j is the scale factor for the equivalent frame photograph.
(X_c, Y_c, Z_c)	instantaneous position of exposure station at T_{ij}
$(X, Y, Z)_j$	object coordinates of any point j on scan line i

Using the above variables, several useful relationships may be derived. If, as is usually the case, the period of revolution of the scanner (t_r) is a well defined quantity, then the time of imaging each element within the array may be determined from its array position by the relationship

$$T_{ij} = T_o + (i-1)t_r + \frac{(\alpha + \theta_j)}{2\pi} t_r \qquad (2.1)$$

in which the substitution $\theta_j = y_j/c$ has been made.
The x* cartesian coordinate of the point may then be determined by introducing v defined above:

$$x^*_{ij} = v(T_{ij} - T_o) \qquad (2.2)$$

If the relationship of Equation (2.1) is introduced into this expression, the result becomes

$$x^*_{ij} = v\left[(i-1)t_r + \frac{(\alpha + \theta_j)}{2\pi} t_r \right] \qquad (2.3)$$

The y* cartesian coordinate may be determined using the Pythagorean Theorem from Figure 2.1.

$$y^{*2}_{ij} = y^2_j - \left[\frac{v\theta_j t_r}{2\pi}\right]^2 \qquad (2.4)$$

It may be seen from Figure 1.17b that in the y direction, imaging takes place from about a perspective center having object space coordinates (X_c, Y_c, Z_c) at the instant of imaging point P_j.

The vector between the perspective center and a point in the object space coordinate system may then be written

$$\vec{A} = \begin{bmatrix} X_j - X_c \\ Y_j - Y_c \\ Z_j - Z_c \end{bmatrix} \tag{2.5}$$

An image space coordinate system may be defined by a right hand system in which the xy plane is tangent to the effective panoramic cylinder at the scan line center with the y axis in the direction of a scan line. The z image axis would be perpendicular to the xy plane and complete the right hand system. The vector above may then be written in this coordinate system as

$$\vec{A} = \underline{M}_{ij}(t) \begin{bmatrix} X_j - X_c \\ Y_j - Y_c \\ Z_j - Z_c \end{bmatrix} \tag{2.6}$$

In the image system, the vector from the perspective center to the image position may be written

$$\vec{a} = \begin{bmatrix} 0 \\ c \sin \theta_j \\ -c \cos \theta_j \end{bmatrix} \tag{2.7}$$

The vector $\vec{A}$ would be represented in Figure 1.17b as the line segment $\overline{CA}$, and vector $\vec{a}$ would be represented by line segment $\overline{Ca}$.

Assuming no systematic effects, these vectors must be collinear. If vector $\vec{a}$ of (2.7) is multiplied by the proper scale factor, the resulting vector will be equal to that from Equation (2.6), leading to:

$$\frac{1}{k'_j}\begin{bmatrix} 0 \\ c \sin\theta_j \\ -c\cos\theta_j \end{bmatrix} = \underline{M}_{ij}(t)\begin{bmatrix} X_j - X_c \\ Y_j - Y_c \\ Z_j - Z_c \end{bmatrix} \qquad (2.8)$$

Combination of the expressions of (2.2) and (2.8) with $k'_{ij} = k_{ij}\cos\theta_j$ results in the following four dimensional metric MSS transformation for rectilinear scanning:

$$\begin{bmatrix} x^*_{ij} \\ 0 \\ c/k_j \tan\theta_j \\ -c/k_j \end{bmatrix} = \begin{bmatrix} v & \underline{0}_{1,3} \\ 0 & \underline{M}_{ij}(t)_{3,3} \end{bmatrix} \begin{bmatrix} T_{ij} - T_o \\ X_j - X_c \\ Y_j - Y_c \\ Z_j - Z_c \end{bmatrix} \qquad (2.9)$$

This general transformation may then be used in subsequent analyses to investigate the geometric characteristics of digital MSS data arrays.

When digital arrays are displayed, all elements in a single scan line i are displayed with a constant strip coordinate x_i. The data may then be analyzed as if all points in a single scan line were imaged instantaneously with some residual yaw, as explained in Section 1.4.2.4. The instant of recording would be assumed equal for all points j in a scan line i, i.e. $x^*_{ij} = x_i$ and $T_{ij} = T_i$ in

the first equation of (2.9). The image coordinates which would be measured from a digital array display would be the i, j array element positions, or x_i, y_j if the array is considered as an image.

It may be shown that the projection equations presented in Section 1.4.1, which were generated from the basic geometry of scanning under ideal conditions, may also be derived from this general transformation if appropriate assumptions are made. For example, the first equation of (2.9) yields directly the transformation from time to image x coordinate as given previously in Equation (1.20) Under the assumption of ideal orientation, the matrix $\underline{M}_{ij}(t)$ becomes identity. If this substitution is made, the second equation of (2.9) yields directly the relationship of Equation (1.11). Also under this assumption, if the last equation is solved for $-c/k_{ij}$, and the result is substituted into the third equation, the resulting expression will be identical to Equation (1.12).

The general transformation of Equation (2.9) may also be used to investigate the effect of small perturbations in orientation elements from the idealized case. Considering a single scan line, using $\theta_j = y_j/c$ and introducing

$$h_j = c/k_j \tag{2.10}$$

the three dimensional geometric MSS transformation, after inversion, may be written as

$$\begin{bmatrix} X_j - X_c \\ Y_j - Y_c \\ Z_j - Z_c \end{bmatrix} = \underline{M}^t{}_j \begin{bmatrix} 0 \\ h_j \tan \theta_j \\ -h_j \end{bmatrix} \qquad (2.11)$$

and rearranging,

$$\begin{bmatrix} X_j \\ Y_j \\ Z_j \end{bmatrix} = \begin{bmatrix} X_c \\ Y_c \\ Z_c \end{bmatrix} + \underline{M}^t{}_j \begin{bmatrix} 0 \\ h_j \tan \theta_j \\ -h_j \end{bmatrix} \qquad (2.12)$$

In order to investigate the effects of small changes in the orientation parameters X_c, Y_c, Z_c, ω, ϕ, κ, on the coordinates of an object point the total differential of (2.12) must be evaluated. In order to evaluate the total differential, the partial derivatives of the equation set must be evaluated for each of the six orientation elements. Considering the sequential set of angles (ω, ϕ, κ), according to Lucas [91]

$$\frac{\partial \underline{M}_j}{\partial \omega} = \underline{M}_j \begin{bmatrix} 0 & 0 & 0 \\ 0 & 0 & 1 \\ 0 & -1 & 0 \end{bmatrix}$$

$$\frac{\partial \underline{M}_j}{\partial \phi} = \underline{M}_j \begin{bmatrix} 0 & \sin \omega & -\cos \omega \\ -\sin \omega & 0 & 0 \\ \cos \omega & 0 & 0 \end{bmatrix}$$

$$\frac{\partial \underline{M}_j}{\partial \kappa} = \begin{bmatrix} 0 & 1 & 0 \\ -1 & 0 & 0 \\ 0 & 0 & 0 \end{bmatrix} \underline{M}_j \tag{2.13}$$

It is also necessary to evaluate the differential of the equations with respect to the parameter h_j, as it contains the scale factor k_j which is a variable for each point. Proceeding with the evaluation of this total differential:

$$\begin{aligned} \begin{bmatrix} dX \\ dY \\ dZ \end{bmatrix}_j &= \begin{bmatrix} dX \\ dY \\ dZ \end{bmatrix}_c + \underline{M}^t{}_j \begin{bmatrix} 0 \\ \tan\theta_j \\ -1 \end{bmatrix} dh_j \\ &+ \begin{bmatrix} 0 & 0 & 0 \\ 0 & 0 & -1 \\ 0 & 1 & 0 \end{bmatrix} \underline{M}^t{}_j \begin{bmatrix} 0 \\ h_j \tan\theta_j \\ -h_j \end{bmatrix} d\omega \\ &+ \begin{bmatrix} 0 & -\sin\omega & \cos\omega \\ \sin\omega & 0 & 0 \\ -\cos\omega & 0 & 0 \end{bmatrix} \underline{M}^t{}_j \begin{bmatrix} 0 \\ h_j \tan\theta_j \\ -h_j \end{bmatrix} d\phi \\ &+ \underline{M}^t{}_j \begin{bmatrix} 0 & -1 & 0 \\ 1 & 0 & 0 \\ 0 & 0 & 0 \end{bmatrix} \begin{bmatrix} 0 \\ h_j \tan\theta_j \\ -h_j \end{bmatrix} d\kappa \end{aligned} \tag{2.14}$$

It is now assumed that the changes in angular orientation elements take place from a perfect orientation position of $\omega = \phi = \kappa = 0$.

Then $\underline{M}_j = \underline{I}$, for which $h_j = Z_c - Z_j$ as may be seen from the last equation of (2.11) under this ideal orientation assumption, and the resulting equations become

$$\begin{bmatrix} dX \\ dY \\ dZ \end{bmatrix}_j = \begin{bmatrix} dX \\ dY \\ dZ \end{bmatrix}_c + \begin{bmatrix} 0 \\ \tan\theta_j \\ -1 \end{bmatrix} dh_j + \begin{bmatrix} 0 \\ h_j \\ h_j \tan\theta_j \end{bmatrix} d\omega + \begin{bmatrix} -h_j \\ 0 \\ 0 \end{bmatrix} d\phi + \begin{bmatrix} -h_j \tan\theta_j \\ 0 \\ 0 \end{bmatrix} d\kappa \tag{2.15}$$

It should be noted here that Equation (2.15) represents a projection from two-dimensional space in the sensor to three dimensional object space. It is not possible from single imagery to determine all three coordinates $(X, Y, Z)_j$, because the unknown scale factor k_j is implicit in h_j. Therefore, in order to derive the two possible coordinates it will be assumed that Z is constant for all j. Since Z is assumed constant, $dZ_j = 0$, and the last of the equations in (2.15) may be written explicitly as

$$0 = dZ_c - dh_j + h_j \tan\theta_j \, d\omega$$

Then

$$dh_j = dZ_c + h_j \tan\theta_j \, d\omega$$

Substituting this expression into the first and second equations of (2.15) results in

$$\begin{aligned} dX_j &= dX_c - h_j\, d\phi - h_j \tan\theta_j\, d\kappa \\ dY_j &= dY_c + \tan\theta_j\, dZ_c + h_j(1 + \tan^2\theta_j)\, d\omega \end{aligned} \tag{2.16}$$

Equations (2.16) may be seen to be termwise identical to those of Equations (1.25) in which $h_j = Z_c - Z$. The contradiction in signs for the $d\omega$, $d\phi$, and $d\kappa$ terms is due to the fact that Equations (1.25) were written as a special case of Hallert's original projection equations. Hallert, in his derivation [26], defined the positive sense of rotation for the angular elements in the opposite sense from that customarily used in the United States, and applied here.

2.3 Collinearity Equations for MSS

The collinearity condition introduced in Section 2.2 serves as the basis for collinearity equations. The collinearity equations for frame photography have been used extensively in the past as the basis of analytical photogrammetry [93, 94]. Similar equations for scanned imagery may be derived using Equations (2.9). Considering a single picture element the i, j subscripts may be dropped and the geometric portion of Equations (2.9) may be written as

$$\begin{bmatrix} 0 \\ c/k \tan\theta \\ -c/k \end{bmatrix} = \begin{bmatrix} m_{11} & m_{12} & m_{13} \\ m_{21} & m_{22} & m_{23} \\ m_{31} & m_{32} & m_{33} \end{bmatrix} \begin{bmatrix} X - X_c \\ Y - Y_c \\ Z - Z_c \end{bmatrix} \tag{2.17}$$

Performing the matrix multiplication, dividing the first two equations by the third, and rearranging yields

$$0 = \frac{m_{11}(X - X_c) + m_{12}(Y - Y_c) + m_{13}(Z - Z_c)}{m_{31}(X - X_c) + m_{32}(Y - Y_c) + m_{33}(Z - Z_c)}$$

$$0 = \tan\theta + \frac{m_{21}(X - X_c) + m_{22}(Y - Y_c) + m_{23}(Z - Z_c)}{m_{31}(X - X_c) + m_{32}(Y - Y_c) + m_{33}(Z - Z_c)} \qquad (2.18)$$

An alternate form may be derived using the transpose of (2.17),

$$0 = (X_c - X) + (Z - Z_c)\ \frac{m_{21}\tan\theta - m_{31}}{m_{23}\tan\theta - m_{33}}$$

$$0 = (Y_c - Y) + (Z - Z_c)\ \frac{m_{22}\tan\theta - m_{32}}{m_{23}\tan\theta - m_{33}} \qquad (2.19)$$

If, in these equations, an ideal orientation assumption is made in which $\underline{M}$ is taken equal to $\underline{I}$ then Equations (2.19) reduce to the same results given in Equations (1.11) and (1.12) in Section 1.4.1.

If six orientation elements were assumed unknown for each scan, it would be impossible to have a solution and derive metric information from MSS data arrays. Therefore, some type of functional behavior (polynomials, harmonics, etc.) must be assumed for those orientation elements. Once decided upon, object space control may be used to determine the coefficients of these functions (resection), then Equations (2.19) may be used to determine other object points (intersection). In practice, both operations are performed simultaneously.

2.4 Linearization of MSS Collinearity Equations

The equations represented by (2.18) and (2.19) are nonlinear in nature. In order to investigate image and object point coordinate deformations, and to perform space resection utilizing the method of least squares, it is desirable to generate linear approximations for them. The usual technique applied in photogrammetry utilizes a Taylor's series expansion about some approximations for the variables involved. The resulting linearized equations, as customarily written in adjustments, will be of the form

$$\underset{2,1}{F} = \underset{2,2}{A}\ \underset{2,1}{V} + \underset{2,q}{B}\ \underset{q,1}{\Delta} + \underset{2,1}{F^{\circ}} = \underset{2,1}{0} \qquad (2.20)$$

in which $\underline{A}$ represents the Jacobian matrix of the functions with respect to observed quantities, and $\underline{V}$ the vector of observational residuals. The $\underline{B}$ matrix in Equation (2.20) is the Jacobian of the functions with respect to the parameters of the transformation, and $\underline{\Delta}$ represents corrections to approximations for these parameters. The $\underline{F}^{\circ}$ vector in Equation (2.20) represents the numerical values of the functions evaluated at initial observation values and parameter approximations. The final estimates of the observations are given by

$$\underset{2,1}{L} = \underset{2,1}{L^{\circ}} + \underset{2,1}{V} \qquad (2.21)$$

in which $\underline{L}^{o}$ is a vector of a priori values of the observations. For the problem under consideration,

$$\underset{2,1}{\underline{L}} = \begin{bmatrix} x \\ y \end{bmatrix} \tag{2.22}$$

in which the image space coordinates for each point will be considered as observations. The final parameter estimates are

$$\underset{q,1}{\underline{X}} = \underset{q,1}{\underline{X}^{o}} + \underset{q,1}{\underline{\Delta}} \tag{2.23}$$

in which $\underline{X}^{o}$ is a vector of approximations and q is the total number of parameters. Of these q total parameters, 3 will represent the object space coordinates (X, Y, Z), and the remaining p = q - 3 parameters will represent those parameters necessary to the functions used to model the six exterior orientation elements.

Consider, first the linearization of the collinearity equations as given in Equations (2.18). The functions may be written in the short form

$$\begin{aligned} F_1 &= \frac{U}{W} = 0 \\ F_2 &= \tan y/c + \frac{V}{W} = 0 \end{aligned} \tag{2.24}$$

where

$$\begin{bmatrix} U \\ V \\ W \end{bmatrix} = \frac{M}{3,3} \begin{bmatrix} X - X_c \\ Y - Y_c \\ Z - Z_c \end{bmatrix} \tag{2.25}$$

The elements of exterior orientation are functions of time (and hence x), and may be written in functional form as

$$\begin{aligned} X_c &= X_c\,(\underline{P}_X,\ x) \\ Y_c &= Y_c\,(\underline{P}_Y,\ x) \\ Z_c &= Z_c\,(\underline{P}_Z,\ x) \\ \omega &= \omega\,(\underline{P}_\omega,\ x) \\ \phi &= \phi\,(\underline{P}_\phi,\ x) \\ \kappa &= \kappa\,(\underline{P}_\kappa,\ x) \end{aligned} \tag{2.26}$$

where $\underline{P}_X$, $\underline{P}_Y$, $\underline{P}_Z$, $\underline{P}_\omega$, $\underline{P}_\phi$, $\underline{P}_\kappa$ are vectors of the specific parameters in each of the given functions. If polynomial forms are assumed for these functions, these vectors, will contain the polynomial coefficients of the functions. For example, if it is assumed that the aircraft altitude Z_c is represented by the second order polynomial

$$Z_c = p_{0Z} + p_{1Z}\,x + p_{2Z}\,x^2$$

then the $\underline{P}_Z$ vector would be of order three and of the form

$$\underset{3,1}{P_Z} = \begin{bmatrix} p_{0Z} \\ p_{1Z} \\ p_{2Z} \end{bmatrix}$$

The linearized form of equations (2.24) may be written in matrix notation as

$$\underset{2,1}{F} = \underset{2,1}{F^o} + \underset{2,1}{A_1}\,\delta y + \underset{2,3}{\ddot{B}}\,\underset{3,1}{\ddot{\Delta}} + \underset{2,6}{\dot{B}_o}\,\underset{6,1}{\dot{\Delta}_o} = \underset{2,1}{0} \tag{2.27}$$

in which

$$\underset{3,1}{\ddot{\Delta}^t} = [\delta X\ \delta Y\ \delta Z] \tag{2.28}$$

$$\underset{6,1}{\dot{\Delta}^t_o} = [\delta X_c\ \delta Y_c\ \delta Z_c\ \delta\omega\ \delta\phi\ \delta\kappa] \tag{2.29}$$

and $\underset{}{A_1}$, $\underset{}{\ddot{B}}$ and $\underset{}{\dot{B}_o}$ are Jacobian matrices of the collinearity equations with respect to y, the (X, Y, Z) coordinates, and the exterior orientation elements respectively. The functional dependency of the $\underset{}{\dot{\Delta}_o}$ vector is now introduced, in linearized form:

$$\begin{aligned}
\delta X_c &= \underset{1,r}{C_X}\,\underset{r,1}{\dot{\Delta}_X} + d_X\,\delta x \\
\delta Y_c &= \underset{1,s}{C_Y}\,\underset{s,1}{\dot{\Delta}_Y} + d_Y\,\delta x \\
\delta Z_c &= \underset{1,t}{C_Z}\,\underset{t,1}{\dot{\Delta}_Z} + d_Z\,\delta x \\
\delta\omega &= \underset{1,f}{C_\omega}\,\underset{f,1}{\dot{\Delta}_\omega} + d_\omega\,\delta x \\
\delta\phi &= \underset{1,g}{C_\phi}\,\underset{g,1}{\dot{\Delta}_\phi} + d_\phi\,\delta x \\
\delta\kappa &= \underset{1,h}{C_\kappa}\,\underset{h,1}{\dot{\Delta}_\kappa} + d_\kappa\,\delta x
\end{aligned} \tag{2.30}$$

in which the $\underline{C}$ terms are Jacobian matrices of the functions assumed with respect to the parameters, the $\dot{\underline{\Delta}}$ vectors are corrections to the functional parameters, and the d terms are derivatives with respect to the observed quantity x. Using (2.30), equation (2.27) becomes

$$\underline{F} = \underline{F}^{o} + \underline{A}_{1}\,\delta y + \ddot{\underline{B}}\,\ddot{\underline{\Delta}} + \dot{\underline{B}}_{o} \begin{bmatrix} \underline{C}_{X} & & & \\ & \underline{C}_{Y} & & \\ & & \ddots & \\ & & & \underline{C}_{K} \end{bmatrix} \begin{bmatrix} \dot{\underline{\Delta}}_{X} \\ \dot{\underline{\Delta}}_{Y} \\ \vdots \\ \dot{\underline{\Delta}}_{K} \end{bmatrix} \tag{2.31}$$

$$+ \dot{\underline{B}}_{o} \begin{bmatrix} d_{X} \\ d_{Y} \\ \vdots \\ d_{K} \end{bmatrix} \delta x = \underline{0}$$

or

$$\underline{F} = \underline{F}^{o} + \dot{\underline{B}}_{o}\,\underline{D}\,\delta x + \underline{A}_{1}\,\delta y + \ddot{\underline{B}}\,\ddot{\underline{\Delta}} + \dot{\underline{B}}_{o}\,\underline{C}\,\dot{\underline{\Delta}} = \underline{0} \tag{2.32}$$

To get (2.32) in the conventional form of (2.20) then

$$\underset{2,2}{A} = \left[\underset{2,6}{(\dot{B}_o} \; \underset{6,1}{D}) \quad \underset{2,1}{A_1}\right]$$

$$\underset{2,p+3}{B} = \left[\underset{2,6}{(\dot{B}_o} \; \underset{6,p}{C}) \quad \underset{2,3}{\ddot{B}}\right] = \left[\underset{2,p}{\dot{B}} \; \underset{2,3}{\ddot{B}}\right]$$

$$\underset{1,2}{V^t} = [\delta x \; \delta y]$$

$$\underset{1,q}{\Delta^t} = \left[\underset{1,r}{\dot{\Delta}^t}X \; \underset{1,s}{\dot{\Delta}^t}Y \; \underset{1,t}{\dot{\Delta}^t}Z \; \underset{1,f}{\dot{\Delta}^t}\omega \; \underset{1,g}{\dot{\Delta}^t}\phi \; \underset{1,h}{\dot{\Delta}^t}\kappa \; \delta X \; \delta Y \; \delta Z\right]$$

$$= \left[\underset{1,p}{\dot{\Delta}^t} \; \underset{3,1}{\ddot{\Delta}^t}\right]$$

where $p = r + s + t + f + g + h$ = the total number of parameters in functions of the exterior orientation elements.

In order to evaluate the matrices in Equation (2.32), the following relationship for a quotient of two functions, may be utilized

$$\frac{\partial}{\partial p}\left[\frac{G}{H}\right] = \frac{H\frac{\partial G}{\partial p} - G\frac{\partial H}{\partial p}}{H^2} = \frac{1}{H}\left[\frac{\partial G}{\partial p} - \frac{G}{H}\frac{\partial H}{\partial p}\right] \tag{2.33}$$

Where p is any independent parameter.

Utilizing this relationship the Jacobian matrices may be evaluated:

$$\underset{2,6}{B_o} = \begin{bmatrix} \frac{\partial F_1}{\partial X_c} & \frac{\partial F_1}{\partial Y_c} & \frac{\partial F_1}{\partial Z} & \frac{\partial F_1}{\partial \omega} & \frac{\partial F_1}{\partial \phi} & \frac{\partial F_1}{\partial \kappa} \\ \frac{\partial F_2}{\partial X_c} & \frac{\partial F_2}{\partial Y_c} & \frac{\partial F_2}{\partial Z_c} & \frac{\partial F_2}{\partial \omega} & \frac{\partial F_2}{\partial \phi} & \frac{\partial F_2}{\partial \kappa} \end{bmatrix}$$

$$= \frac{1}{W} \left[\begin{array}{ccc|c} \left[-m_{11} + \frac{U}{W} m_{31}\right] & \left[-m_{12} + \frac{U}{W} m_{32}\right] & \left[-m_{13} + \frac{U}{W} m_{33}\right] & \\ \left[-m_{21} + \frac{V}{W} m_{31}\right] & \left[-m_{22} + \frac{V}{W} m_{32}\right] & \left[-m_{23} + \frac{V}{W} m_{33}\right] & \end{array}\right. \quad (2.34)$$

$$\left.\begin{array}{|l} [m_{12}(Z-Z_c) - m_{13}(Y-Y_c) - U/W\{m_{32}(Z-Z_c) - m_{33}(Y-Y_c)\}] \\ [m_{22}(Z-Z_c) - m_{23}(Y-Y_c) - V/W\{m_{32}(Z-Z_c) - m_{33}(Y-Y_c)\}] \end{array}\right|$$

$$\left.\begin{array}{|ll} [-W\cos\kappa - U/W\,(U\cos\kappa - V\sin\kappa)] & [V] \\ [\,W\sin\kappa - V/W\,(U\cos\kappa - V\sin\kappa)] & [-U] \end{array}\right]$$

$$\underset{2,1}{A_1} = \begin{bmatrix} \frac{\partial F_1}{\partial y} \\ \frac{\partial F_2}{\partial y} \end{bmatrix} = \begin{bmatrix} 0 \\ \frac{1}{c}\sec^2(y/c) \end{bmatrix} \quad (2.35)$$

$$\underset{2,3}{\ddot{B}} = \begin{bmatrix} \frac{\partial F_1}{\partial X_1} & \frac{\partial F_1}{\partial Y_1} & \frac{\partial F_1}{\partial Z_1} \\ \\ \frac{\partial F_2}{\partial X_2} & \frac{\partial F_2}{\partial Y_2} & \frac{\partial F_2}{\partial Z_2} \end{bmatrix} \tag{2.36}$$

$$= \frac{1}{W} \begin{bmatrix} (m_{11} - \frac{U}{W} m_{31}) & (m_{12} - \frac{U}{W} m_{32}) & (m_{13} - \frac{U}{W} m_{33}) \\ (m_{21} - \frac{V}{W} m_{31}) & (m_{22} - \frac{V}{W} m_{32}) & (m_{23} - \frac{V}{W} m_{33}) \end{bmatrix}$$

The $\underline{C}$, $\underline{D}$ matrices will depend upon the functional forms assumed to model the elements of exterior orientation. As an example, if second order polynomials are assumed for these functions, then

$$\underset{6,18}{C} = \begin{bmatrix} 1 & x & x^2 & 0 & 0 & 0 & \cdots & 0 \\ 0 & 0 & 0 & 1 & x & x^2 & & 0 \\ \vdots & & & & & & \ddots & \vdots \\ 0 & 0 & 0 & \cdots & & & 1 \; x \; x^2 & \end{bmatrix} \tag{2.37}$$

$$\underset{6,1}{D} = \begin{bmatrix} p_{1X} + 2p_{2X}\, x \\ p_{1Y} + 2p_{2Y}\, x \\ \vdots \\ p_{1K} + 2p_{2K}\, x \end{bmatrix} \tag{2.38}$$

Finally, the F^o matrix may be written as

$$\underset{2,1}{F^o} = \begin{bmatrix} \frac{U^o}{W^o} \\ \\ \tan(y^o/c) + \frac{V^o}{W^o} \end{bmatrix} \tag{2.39}$$

in which the "o" indicates the evaluation at the original observations and parameter approximations.

An alternate linearized form may be obtained from Equation (2.19):

$$\begin{aligned} F_1 &= (X_c - X) + (Z - Z_c)\frac{U'}{W'} = 0 \\ F_2 &= (Y_c - Y) + (Z - Z_c)\frac{V'}{W'} = 0 \end{aligned} \tag{2.40}$$

in which the auxiliaries U', V', W' are defined as

$$\begin{bmatrix} U' \\ V' \\ W' \end{bmatrix} = \underset{3,3}{M^t} \begin{bmatrix} 0 \\ \tan(y/c) \\ -1 \end{bmatrix}$$

For this case, the linearized equations may be written in the same form as Equation (2.32), and the Jacobian matrices may be evaluated as

$$\underset{2,6}{\dot{B}'_o} = \begin{bmatrix} \frac{\partial F_1}{\partial X_c} & \frac{\partial F_1}{\partial Y_c} & \frac{\partial F_1}{\partial Z_c} & \frac{\partial F_1}{\partial \omega} & \frac{\partial F_1}{\partial \phi} & \frac{\partial F_1}{\partial \kappa} \\ \\ \frac{\partial F_2}{\partial X_c} & \frac{\partial F}{\partial Y_c^2} & \frac{\partial F}{\partial Z_c^2} & \frac{\partial F_2}{\partial \omega} & \frac{\partial F}{\partial \phi^2} & \frac{\partial F_2}{\partial \kappa} \end{bmatrix}$$

$$= \left[\begin{array}{cccc:c} 1 & 0 & -\frac{U'}{W'} & -\frac{U'V'(Z - Z_c)}{W'^2} & \\ 0 & 1 & -\frac{V'}{W'} & -\left[1 + \frac{V'^2}{W'^2}\right](Z - Z_c) & \\ \hdashline & & & \frac{Z - Z_c}{W'}(-V' \sin\omega + W' \cos\omega + \frac{U'^2}{W'} \cos\omega) & \\ & & & \frac{Z - Z_c}{W'}(U' \sin\omega + \frac{V'U'}{W} \cos\omega) & \end{array}\right. \quad (2.41)$$

$$\left.\begin{array}{c} \tan(y/c)(-m_{11} + \frac{U'}{W'} m_{13}) \frac{Z - Z_c}{W'} \\ \\ \tan(y/c)(-m_{12} + \frac{V'}{W'} m_{13}) \frac{Z - Z_c}{W'} \end{array}\right]$$

$$\underset{2,1}{A'_1} = \begin{bmatrix} \frac{\partial F_1}{\partial y} \\ \\ \frac{\partial F_2}{\partial y} \end{bmatrix} = \frac{(Z - Z_c) \sec^2(y/c)}{cW'} \begin{bmatrix} m_{21} - \frac{U'}{W'} m_{23} \\ \\ m_{22} - \frac{V'}{W'} m_{23} \end{bmatrix} \quad (2.42)$$

$$\underset{\sim}{\ddot{B}'} = \begin{bmatrix} -1 & 0 & U'/W' \\ 0 & -1 & V'/W' \end{bmatrix} \quad (2.43)$$

And the $\underline{C}$, $\underline{D}$ matrices would be as previously defined. The $\underline{F}'^{o}$ vector is

$$\underset{2,1}{\underline{F}'^{o}} = \begin{bmatrix} (X_c^o - X^o) + (Z^o - Z^o_c)\,\dfrac{U'^o}{W'^o} \\ (Y^o_c - Y^o) + (Z^o - Z^o_c)\,\dfrac{V'^o}{W'^o} \end{bmatrix} \tag{2.44}$$

These linearized collinearity equations may also be used to derive the differential displacement equations (2.16). (see Appendix A).

It has been the purpose of this chapter to provide the derivation of the most general forms of analytic expressions which may be used to analyze the geometric aspects of MSS data recording. In the following chapter these general expressions will be used to generate algorithms for the purpose of restituting MSS data arrays. In addition, alternate restitution methods based upon stochastic concepts rather than the known geometric relationships will be introduced.

3. RESTITUTION OF MSS DATA ARRAYS FROM SINGLY SCANNED AREAS

The term "restitution", as used in this investigation, indicates the processing of MSS data arrays in an attempt to generate within the spectral arrays, element positions which will represent a planimetric orthographic projection. If a display of the arrays is done after such processing, the resulting image would appear as a map substitute, much like the more conventional orthophoto. The term "rectification" has also been used by other investigators to denote this process.

In this chapter, methods of restitution for MSS digital data arrays are presented, and the advantages and disadvantages of each method enumerated. In all of the discussion presented, it is assumed that only data from singly scanned areas are available. In the first section, procedures utilizing resampling algorithms are presented. These algorithms are useful as an initial step in order to simplify subsequent, more refined procedures. The second section deals with parametric methods using collinearity equations and polynomials which are derived from the linearized form of collinearity equations. Alternative methods based upon stochastic rather than deterministic concepts are presented in section three. These methods are denoted as nonparametric methods. Section four contains a discussion of the problem of assigning element elevations. These elevations may

be utilized in the parametric methods of restitution. Finally, special techniques useful for restitution of MSS digital data, as opposed to continuously recorded data, are presented in section five.

3.1 Resampling Algorithm

Under the assumption of ideal orientation of the sensor, the data generated by the MSS in the direction of flight, or X direction, represents an orthographic projection with no further processing. Further processing would be required, however, in the direction perpendicular to flight, along each scan line, to remove the scan angle effects and topographic relief displacement. This may be accomplished using resampling algorithms which operate on a single scan line at a time. The purpose of such algorithms are to digitally resample each data array line such that each element in the resampled line contains spectral values representing ground elements having equal dimensions in the Y direction on a datum. After applying such algorithms, the resulting arrays may still be in error due to the following:

1.) The use of such processing is based upon the assumption of perfect orientation, and the effects of changes with respect to time in the orientation elements X_c, Y_c, Z_c, ω, ϕ, κ are neglected, which may result in appreciable image position errors.

2.) A lack of perfect synchronization between the aircraft velocity and angular scanning velocity, as well as the

difference between the angular resolution size in the x and y directions (β and γ, see Figure 1.16), results in a differential scale in the x and y directions after processing.

Nevertheless, these resampling algorithms have several advantages:

1.) They are computationally efficient. The processing of one scan line at a time requires only a small image point buffer within the computer, and the computing time for such algorithms is relatively small.

2.) The algorithms result in the correction of image displacements due to panoramic recording. The arrays resulting after processing "look better" upon display, and may thus be useful for interpretation and identification of control points.

3.) These algorithms may be useful as an initial step in processing. Subsequent more refined algorithms for further geometric processing may therefore be simplified. For example, the piecewise polynomial to be discussed in Section 3.2.2 will contain fewer terms if the arrays are first processed in this manner. Some of the nonparametric techniques to be discussed in Section 3.3 require that the arrays be first transformed to a trend surface, and the resampling algorithms accomplish this.

This section is devoted to the derivation of resampling algorithms. The derivations consider two cases, the first of which deals with

the correction of scan angle effects only, under the assumption that the object space points have a constant elevation, and the second deals with a generalization to include topographic relief displacements.

3.1.1 Resampling to Correct Scan Angle Effects [95]

The purpose of this algorithm is to resample the data so that, after resampling, every sample element in the data array represents an element with equal dimension in the Y, or along scan, direction. That is, every scan line after resampling contains the same number of elements as before resampling, but object space elements are equally spaced along the datum. The algorithm developed by Phillips [95] at LARS is presented here.

Figures 3.1a and 3.1b represent the geometry of this resampling procedure, with 3.1b being an enlarged view in the vicinity of the sensor. Referring to these figures, the following parameters may be defined:

- h - flying height above datum defined as before by $h = (Z_c - Z)$, where Z is the elevation (assumed constant) of the datum surface
- W - length of the scan line in object space
- N - total number of samples per scan, constrained to remain the same before and after resampling
- n - number of samples to right of nadir (if symmetric scanning is employed, as is usual, then $n = N/2$ and $n\gamma = \alpha$)
- j - sample number after resampling

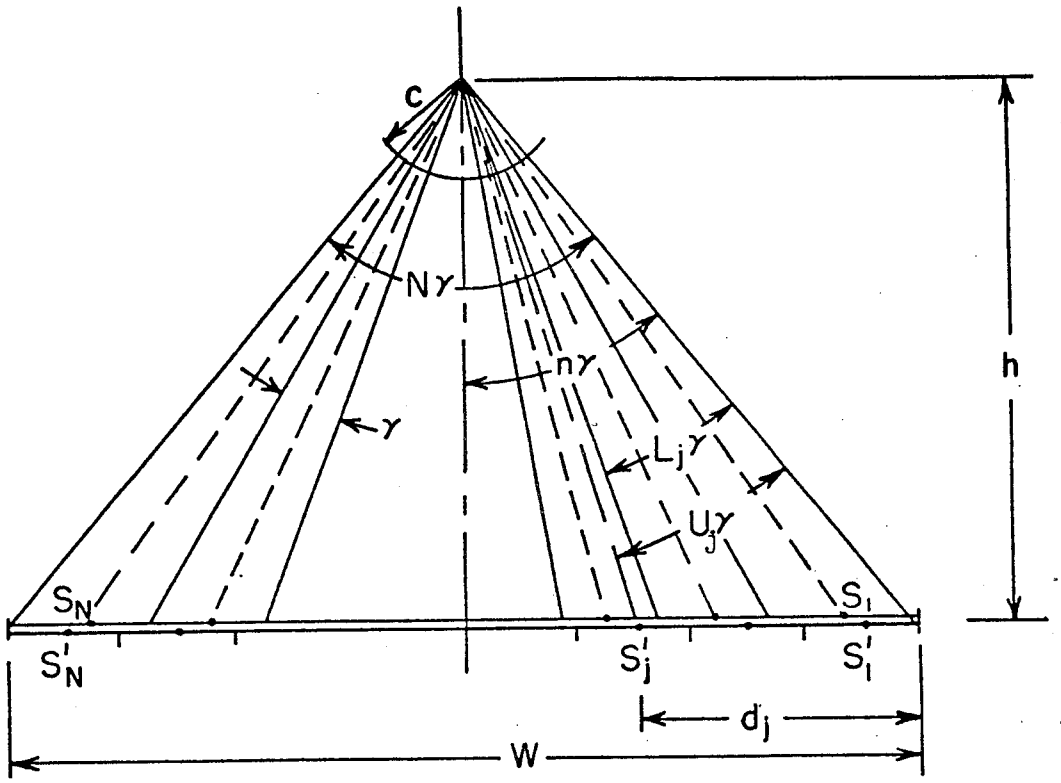

a.

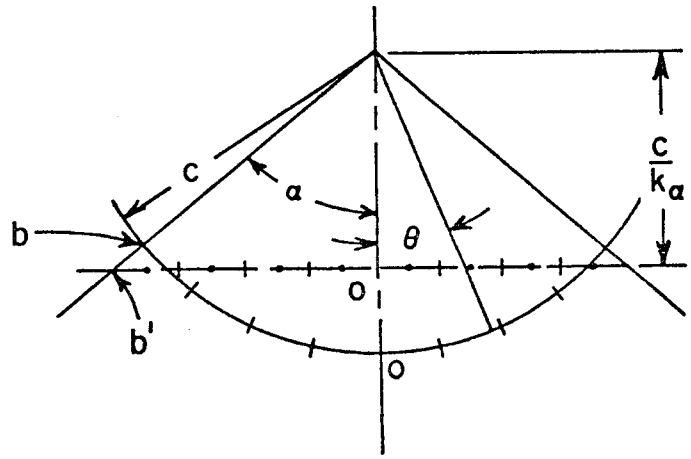

b.

Figure 3.1. Resampling to Correct Scan Angle Effects

S'_j - spectral value to be placed in the j-th position by resampling

U_j - sample number in the same line in the array before resampling corresponding to the j-th resampled position, to be solved for by the resampling algorithm

L_j - integer portion of U_j

C_j - fractional portion of U_j

S_{L_j} - spectral value stored in position L_j in the array before resampling

d_j - distance along datum from beginning point of sampling to position j in the resampled array

The variables θ, γ, α, and sensor constant c are as described in Section 1.4.

With the above variables, several relationships may be written. The scan line length is given by

$$W = h \tan(n\gamma) + h \tan(N\gamma - n\gamma) \tag{3.1}$$

After resampling, every sample along the datum has the same dimension in the Y direction along the scan, defined by

$$Y = W/N \tag{3.2}$$

From Figure 3.1a, the distance d_j may be written, in terms of sample widths as

$$d_j = j(W/N) - (1/2)(W/N) = \frac{(2j - 1)}{2} W/N \tag{3.3}$$

This distance may also be written in terms of sample angle (γ) as

$$d_j = h \tan(n\gamma) + h \tan(U_j\gamma - n\gamma) \tag{3.4}$$

Equating the right hand sides of (3.3) and (3.4), and solving for U_j yields

$$U_j = \frac{n\gamma + \tan^{-1}\left[\frac{W}{hN}\left[\frac{2j-1}{2}\right] - \tan n\gamma\right]}{\gamma} \tag{3.5}$$

If Equation (3.1) is substituted into (3.5), the final expression is

$$U_j = n + \frac{1}{\gamma}\tan^{-1}\left[(\tan n\gamma + \tan(N\gamma - n\gamma))^{\frac{(2j-1)}{2N}} - \tan n\gamma\right] \tag{3.6}$$

Figures 3.2 and 3.3 depict this relationship in graphical form. Figure 3.2 shows a plot of U_j versus j for a real data case, with $\gamma \cong 6$ mrad, and N = 222. Figure 3.3 represents the image displacement $U_j - j$ versus j. The slight lack of symmetry in this example is due to the fact that, for this particular flight, $n \neq N/2$.

If the quantities $S'_1, S'_2, \ldots S'_j, \ldots S'_N$ (see Figure 3.1a) represent the spectral values to be stored after resampling, a linear interpolation scheme may be used to assign the S'_j values. If the quantity U_j computed above is considered to be composed of an integer part L_j and a fractional part C_j such that

$$U_j = L_j + C_j \tag{3.7}$$

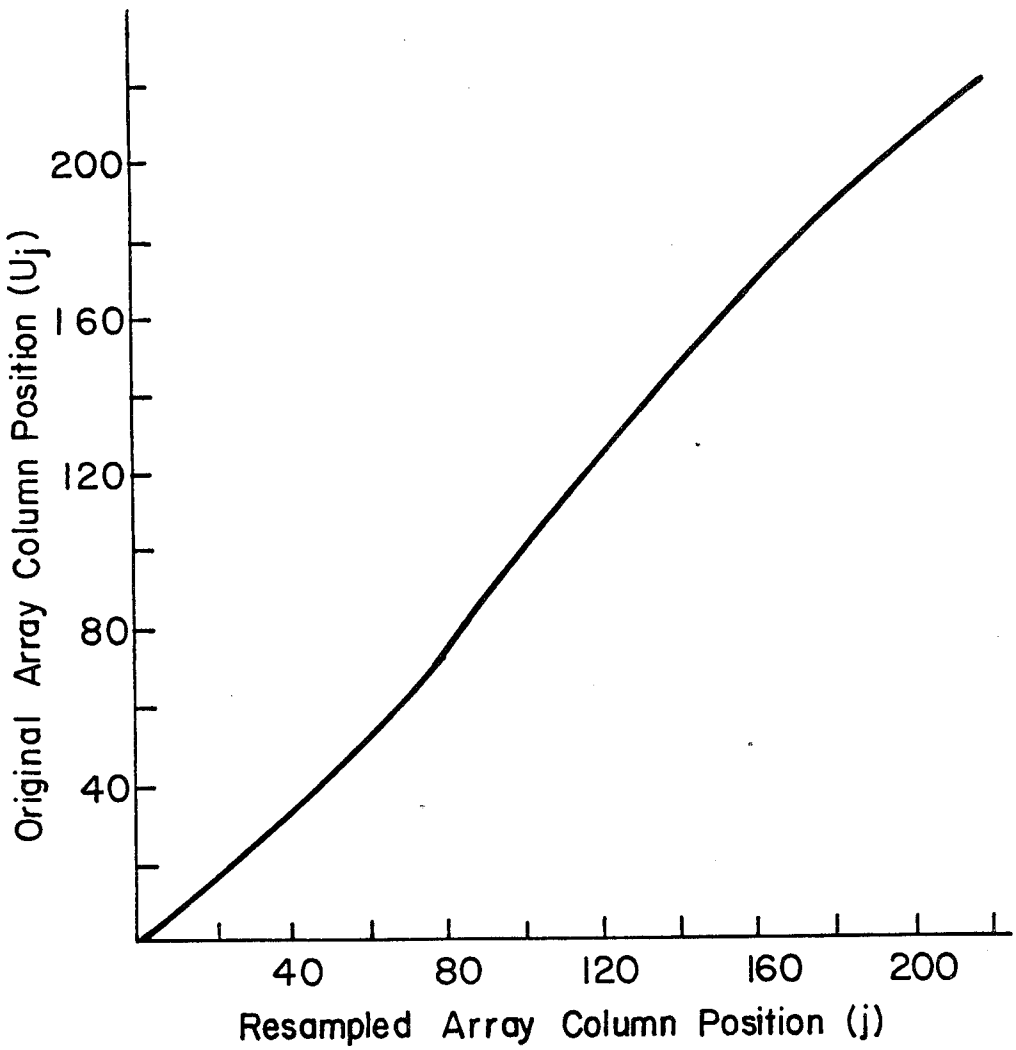

Figure 3.2. Resampled Array Column Positions

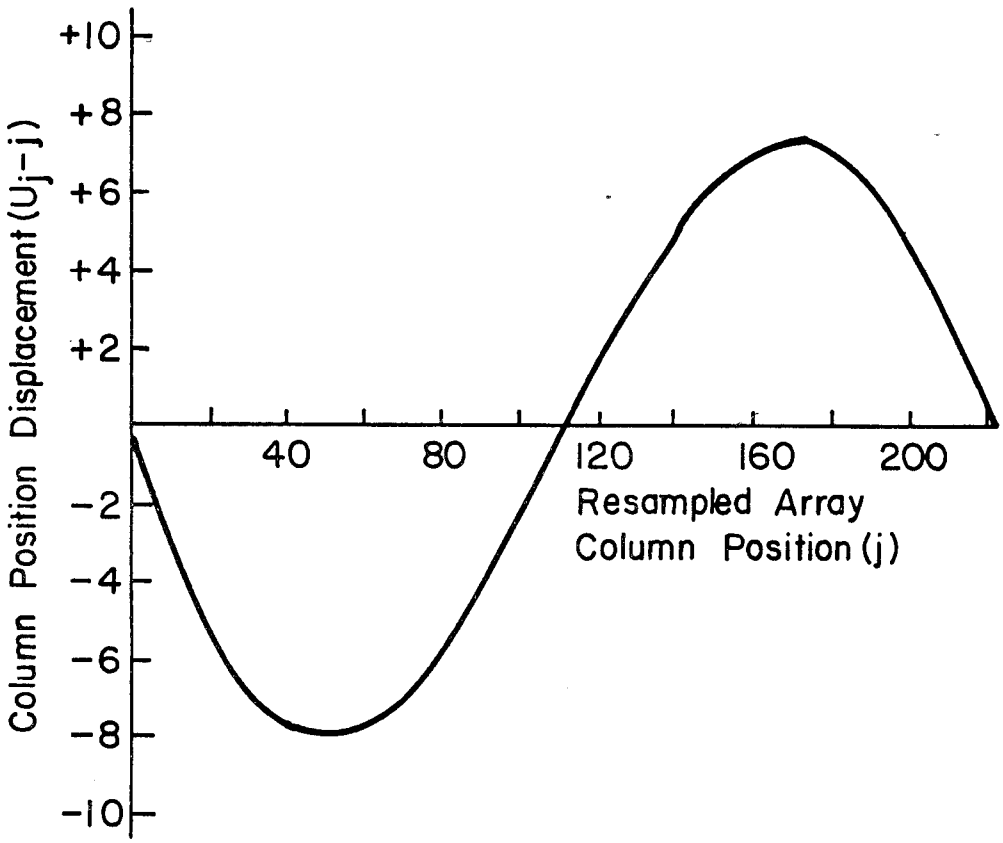

Figure 3.3. Column Position Displacement Due to Resampling

then the S'_j values may be interpolated from the spectral values originally stored in the array before resampling. The spectral value assigned to the j-th position would then be

$$S'_j = S_{L_j} + C_j (S_{L_j+1} - S_{L_j}) \tag{3.8}$$

Alternatively, if a nearest neighbor approximation is to be used, as advocated by Markarian, et. al. [65], the resulting function would be

$$S'_j = \begin{cases} S_{L_j} & C_j \leq 0.5 \\ S_{L_j+1} & C_j > 0.5 \end{cases} \tag{3.9}$$

Resampling in this manner results in the removal of the panoramic distortion within the data arrays. This processing differs from the usual reduction of panoramic image coordinates to a plane "equivalent frame photograph" position as presented by Case [41]. The effective plane photograph position by Case would by $y'_j = c \tan \theta_j$, in which the panoramic image position is projected to a plane tangent to the cylindrical recording surface. The result of resampling is to project the panoramic image onto a plane at some effective principal distance c'. The case under consideration is illustrated in Figure 3.1b, for the symmetric case (n = N/2). Since the total number of samples is constrained to remain the same, and each sample will be displayed with the same dimension before and after resampling, the distance Ob before resampling and O'b' after resampling must be the same. This is equivalent to imaging on a plane, indicated

by the dashed line in Figure 3.1b, lying at some equivalent principal distance from the perspective center and given by

$$c' = \frac{c}{k_\alpha} \tag{3.10}$$

where k_α is a function of the number of samples along the line and the angular resolution (γ).

From Figure 3.1b

$$O'b' = Ob$$

hence

$$(c/k_\alpha) \tan\alpha = c\alpha \tag{3.11}$$

for symmetric scanning of α on either side of the scanning axis. The above equation may be solved for k_α

$$k_\alpha = \frac{\tan\alpha}{\alpha} \tag{3.12}$$

and subsequent image positions on the resampling plane are given by

$$y' = c' \tan(U_j\gamma - \alpha) = c' \tan\theta_j \tag{3.13}$$

A simplified example may be illustrative. Consider the case of symmetric scanning, in which $n = N/2$ and $n\gamma = \alpha$. For this case, the resampling algorithm may be written

$$U_j = n + \frac{1}{\gamma} \tan^{-1}\left[\frac{2j - 1}{N} \tan n\gamma - \tan n\gamma\right]$$

or

$$U_j = n + \frac{1}{\gamma} \tan^{-1} \left[\frac{2j - 1}{N} \tan \gamma - \tan \gamma \right]$$

If it is assumed for this simplified example that the total number of samples per line is eight (N = 8), and that the angular sampling interval (γ) is 0.1 radian, then the total scanning angle on either side of the scanning axis (α) will be 0.4 radian. Referring to Figure 3.1b, to determine the spectral values to be placed in the third sample position in the resampled line (j = 3),

$$U_3 = 4 + \frac{1}{0.1} \tan^{-1} \left[\frac{(2)(3) - (1)}{8} \tan 0.4 - \tan 0.4 \right]$$

or

$$U_3 = 2.26$$

This represents the sample position along the line in the uncorrected array which would be used to assign spectral values to the j = 3 sample position in the resampled array. If the linear interpolation method is used, then

$$L_3 = 2$$

$$C_3 = 0.26$$

and the spectral value assigned would be given by

$$S'_3 = S_2 + 0.26(S_3 - S_2)$$

If, on the other hand, the nearest neighbor method is applied, then the spectral value assigned to this resampled position for each channel would be given by

$$S'_3 = S_2$$

3.1.2 Resampling to Include Topographic Displacement [96]

The algorithm given by Equation (3.6) is valid only for the case in which element elevations are assumed constant, i.e. $Z_j = Z$ for all j. A generalization of this algorithm was developed by Trinder [96] and corrects simultaneously for scan angle effects and image displacement due to terrain relief. The result to follow is a slight modification to that algorithm.

Figure 3.4 shows the geometry of this resampling. The illustration is similar to that of Figure 3.1a except that the actual topographic surface has replaced the assumed flat plane representing the terrain. It is assumed that an elevation value, Z_{L_j}, is available for each element in the uncorrected array. With this assumption, the variables given in the preceding derivation are used except that a flying height above terrain may now be defined for each element as

$$h_{L_j} = Z_c - Z_{L_j}$$

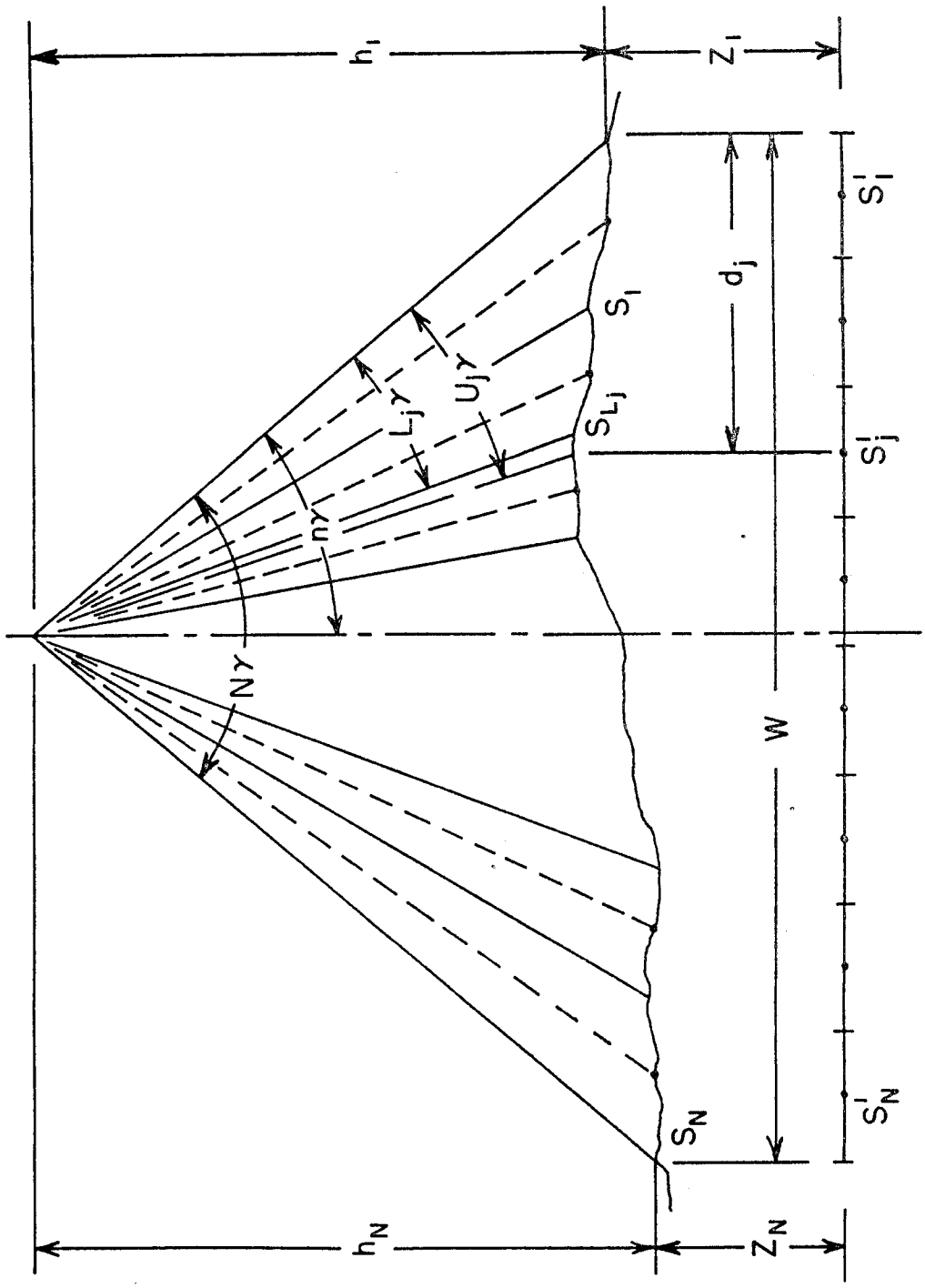

Figure 3.4. Resampling to Include Topographic Relief Effects

The derivation proceeds in a manner similar to that given for the preceding case, and the resulting algorithm may be given by (See Appendix B)

$$U_j = n + \frac{1}{\gamma}\tan^{-1}\left\{\frac{1}{h_{L_j}}\left[\frac{2j-1}{2N}\,h_N\tan(N\gamma - n\gamma) + \frac{2j-1}{2N}\tan(n\gamma) - h_1\tan(n\gamma)\right]\right\} \tag{3.14}$$

The spectral values may be assigned after resampling using either of the two methods cited in the preceding section, i.e., by linear interpolation of spectral values from the uncorrected arrays, or by a nearest neighbor approximation.

3.2 Parametric Methods of Restitution

In this section, methods of restitution based upon the MSS collinearity equations and piecewise polynomials are discussed. These methods are called "parametric methods", since an attempt is made in them to estimate scanning parameters. In both of these methods, an attempt is made to estimate the parameters of functions assumed to represent the behaviour of the scanner orientation elements.

3.2.1 Restitution by MSS Collinearity Equations

Probably the most logical mathematical technique to generate restituted arrays of singly scanned data is the direct use of the MSS collinearity equations as given in Equations (2.19). These equations represent most closely the actual physical situation as it occurs during recording. After the assumption of appropriate functions to represent the behavior of the exterior orientation

elements, a solution may be obtained using sufficient object space control points to apply least squares. For this purpose, the expanded linearized form of the collinearity equations, as presented in Equation (2.32), may be utilized. An iterative technique employing successive relinearizations about updated estimates from each preceding iteration is utilized. The final result is the determination of other points at any desired scale, as a restituted array for each channel representing a single wavelength band. The method is subject to several limiting factors.

1.) Functional forms, such as polynomials or harmonics, representing exterior orientation variations must be assumed. If the actual stochastic variation of these elements is not reasonably approximated by these functional forms, serious errors may result. To partially overcome this difficulty the flight line may be divided into sections, each having a separate set of coefficients.

2.) If the flight line is treated in sections, it is necessary to introduce constraining conditions at the section interfaces. This insures obtaining the same results for each element along an interface from either side of the interface. (Thus the least squares solution must consider the problem of parameter constraints.) This problem is addressed in more detail in Section 3.2.3.

3.) Some exterior orientation elements are highly correlated, and therefore recovery of all such elements may not be

possible using singly scanned data arrays. A previous example demonstrated this correlation for the ϕ and X_c terms. Under the conditions of flat terrain it is not possible, using singly scanned arrays, to differentiate between the effect of a $\delta\phi$ change and a δX_c change. This result was verified in real data tests using arrays obtained over terrain having relief differences of up to 300 feet (90 m). Referring to Figure 1.21a as a first approximation, the change in X object space coordinate may be given as

$$\delta X = (Z_c - Z)\phi$$

But the effect of this change may not be distinguished from the effect of a δX_c change. Thus, if functional forms are assumed for the X_c, Z_c terms, the ϕ term may not be recovered. Konecny [7] and Derenyi [22] note this problem and suggest that recording of selected exterior orientation parameters to sufficient accuracy represents a possible, although expensive, solution. Kratky [21] notes the problem as well, but suggests that acceptable restitution of the image may be accomplished even though absolute values of the elements will be in doubt.

4.) If topographic relief displacement is to be compensated for during restitution, some method of assigning an elevation to each data array element must be devised. Since only singly scanned data arrays are being considered, the source

of such elevation information must be external to the data arrays themselves, such as existing topographic maps. The problem is further complicated in that these element elevations must be assigned prior to processing for restitution, i.e., they must be assigned to the uncorrected arrays with acceptable accuracy. This problem is dealt with in Section 3.4.

In summary, although the direct use of the MSS collinearity equations is accompanied by some problems which must be considered, these equations represent the best obtainable mathematical model for scanned imagery, and must be considered as the basic restitution method on which other approximations are based. In the next section, the use of polynomials derived from the linearized collinearity equations is investigated as a restitution method.

3.2.2 Use of Piecewise Polynomials

Since the recovery of absolute orientation parameters, based upon the MSS collinearity equations and availability of control, is not possible for each individual scan line, the use of such collinearity equations requires an approximation. It may be reasonably argued therefore that a restitution based upon another mathematical model could result in final element positions having positional accuracies approaching those obtainable using collinearity. One such possibility is the use of piecewise polynomials. Using appropriate simplifying assumptions, these polynomials may be derived

directly from the more rigorous collinearity equations and thus represent a logical step in a search for an alternative mathematical model.

Two cases may be derived. In the first case, it is assumed that the data are panoramically recorded. In the second case, the data are assumed to be resampled such that they are effectively recorded upon a planar surface (i.e. an attempt has been made at eliminating the panoramic effect).

3.2.2.1 Polynomials for Panoramic Recording. For this case, Equations (2.16) may be utilized directly. The object space coordinates are given by combining the ideal positions from Equations (1.11) and (1.12), and the differential changes from Equations (2.16). If $h = Z_c - Z$, and both Z_c and Z are assumed constant, then h is a constant, and the transformation from the two dimensional image space into an object space which has been approximated as two dimensional may be written

$$\begin{aligned} X &= X_c + \delta X_c - h\delta\phi - h \tan\theta\, \delta\kappa \\ Y &= Y_c + \delta Y_c + h \tan\theta + \tan\theta\, \delta Z_c + h(1 + \tan^2\theta)\delta\omega \end{aligned} \tag{3.15}$$

Any number of polynomial forms may be defined, depending upon the functions selected to represent the variation of exterior orientation elements within a section. As a first example the assumption is made that the change in each orientation element (i.e., δX_c, δY_c, etc.) varies as a linear function of x within each section, or

$$
\begin{aligned}
\delta X_c &= A_X + B_X\, x \\
\delta Y_c &= A_Y + B_Y\, x \\
\delta Z_c &= A_Z + B_Z\, x \\
\delta\omega &= A_\omega + B_\omega\, x \\
\delta\phi &= A_\phi + B_\phi\, x \\
\delta\kappa &= A_\kappa + B_\kappa\, x
\end{aligned}
\tag{3.16}
$$

These relationships may be substituted directly into Equations (3.15) with the results, after regrouping, of

$$
\begin{aligned}
X &= (X_c + A_X - hA_\phi) + (B_X - hB_\phi)x - hA_\kappa \tan\theta - hB_\kappa x \tan\theta \\
Y &= (Y_c + A_Y + hA_\omega) + (B_Y + hB_\omega)x + (h + A_Z)\tan\theta \\
&\quad + B_Z\, x \tan\theta + hA_\omega \tan^2\theta + hB_\omega x \tan^2\theta
\end{aligned}
$$

If the first two terms of the series expansion are taken for $\tan\theta (\tan\theta \tilde{=} \theta + \frac{1}{3}\theta^3)$, and using $\theta = y/c$ (c is the effective panoramic recording radius), the resulting polynomials are

$$
\begin{aligned}
X &= A_1 + A_2x + A_3y + (A_3/3c^2)y^3 + A_4xy + (A_4/3c^2)xy^3 \\
Y &= B_1 + B_2x + B_3y + (B_3/3c^2)y^3 + B_4xy + (B_4/3c^2)xy^3 \\
&\quad + B_5y^2 + (2B_5/3c^2)y^4 + (B_5/9c^4)y^6 + B_6xy^2 \\
&\quad + (2B_6/3c^2)xy^4 + (B_6/9c^4)xy^6
\end{aligned}
\tag{3.17}
$$

in which

$$A_1 = X_c + A_X - hA_\phi \qquad B_1 = Y_c + A_Y + hA_\omega$$
$$A_2 = B_X - hB_\phi \qquad B_2 = B_Y + hB_\omega$$
$$A_3 = -hA_\kappa/c \qquad B_3 = (h + A_Z)/c$$
$$A_4 = -hB_\kappa/c \qquad B_4 = B_Z/c$$
$$B_5 = hA_\omega/c^2$$
$$B_6 = hB_\omega/c^2$$

The last six terms of the second equation of (3.17) will be zero if the system is roll stabilized (i.e. $\omega = 0$). Note that the original 12 parameters of Equations (3.16) have been consolidated to only 10 parameters, since the parameters for the δX_c and $\delta\phi$ terms always appear together, and therefore cannot be distinguished using singly scanned imagery of flat terrain. These parameters are A_i ($i = 1, 4$) and B_j ($j = 1, 6$).

If the exterior orientation variations within a section are assumed as second order polynomials of the form

$$\begin{aligned}
\delta X_c &= A_X + B_X x + C_X x^2 \\
\delta Y_c &= A_Y + B_Y x + C_Y x^2 \\
\delta Z_c &= A_Z + B_Z x + C_Z x^2 \\
\delta\omega &= A_\omega + B_\omega x + C_\omega x^2 \\
\delta\phi &= A_\phi + B_\phi x + C_\phi x^2 \\
\delta\kappa &= A_\kappa + B_\kappa x + C_\kappa x^2
\end{aligned} \qquad (3.18)$$

and these relationships are substituted directly into (3.15), the resulting polynomials are

$$
\begin{aligned}
X &= A_1 + A_2x + A_3x^2 + A_4y + (A_4/3c^2)y^3 + A_5xy \\
&\quad + (A_5/3c^2)xy^3 + A_6x^2y + (A_6/3c^2)x^2y^3 \\
Y &= B_1 + B_2x + B_3x^2 + B_4y + (B_4/3c^2)y^3 + B_5xy \\
&\quad + (B_5/3c^2)xy^3 + B_6x^2y + (B_6/3c^2)x^2y^3 + B_7y^2 \\
&\quad + (2B_7/3c^2)y^4 + (B_7/9c^4)y^6 + B_8xy^2 + (2B_8/3c^2)xy^4 \\
&\quad + (B_8/9c^4)xy^6 + B_9x^2y^2 + (2B_9/3c^2)x^2y^4 + (B_9/9c^4)x^2y^6
\end{aligned}
\tag{3.19}
$$

in which

$$
\begin{aligned}
A_1 &= X_c + A_X - hA_\phi & B_1 &= Y_c + A_Y + hA_\omega \\
A_2 &= B_X - hB_\phi & B_2 &= B_Y + hB_\omega \\
A_3 &= C_X - hC_\phi & B_3 &= C_Y + hC_\omega \\
A_4 &= -hA_\kappa/c & B_4 &= (h + A_Z)/c \\
A_5 &= -hB_\kappa/c & B_5 &= B_Z/c \\
A_6 &= -hC_\kappa/c & B_6 &= C_Z/c \\
 & & B_7 &= hA_\omega/c^2 \\
 & & B_8 &= hB_\omega/c^2 \\
 & & B_9 &= hC_\omega/c^2
\end{aligned}
$$

The last nine terms of the second equation of (3.19) will be zero if the system is roll stabilized ($\omega = 0$), since these coefficients are dependent upon ω only. The original 18 parameters in Equations (3.18) have been reduced to only 15 in (3.19) because

of the inability to separate parameters for δX_c and $\delta\phi$ using singly scanned data from flat terrain. The parameters are A_i $(i = 1, 6)$ and B_j $(j = 1, 9)$.

In both of these examples it has been assumed that all orientation elements were modeled using the same order polynomial. This need not necessarily be the case, since different order polynomials may be used. (e.g. $X_c = A_X + B_X x + C_X x^2 + D_X x^3$, $Y_c = A_Y + B_Y x + C_Y x^2$, $Z_c = A_Z + B_Z x$, $\delta\kappa = A_\kappa$).

These polynomials represent a transformation from a 2 dimensional image space into a 2 dimensional object space. The object space is actually 3 dimensional, and the assumption has been made that h is constant in order to perform this transformation. This assumption may be relaxed if Z coordinates have been assigned to the data arrays prior to processing. In this case, h is no longer a fixed constant, but instead, $h = Z_c - Z$ may be used in Equations (3.15), where Z denotes the elevation assigned to each point, and Z_c is the constant nominal flying altitude taken from the flight log. For linear functions, the polynomials when Z is included take the form

$$\begin{aligned} X = {} & A_1 + A_2x + A_3y + (A_3/3c^2)y^3 + A_4xy + (A_4/3c^2)xy^3 \\ & - Z[- A_5 - A_6x + (A_3/Zc)y + (A_3/3c^2Zc)y^3 \\ & + (A_4/Zc)xy + (A_4/3c^2Zc)xy^3] \\ Y = {} & B_1 + B_2x + B_3y + (B_3/3c^2)y^3 + B_4xy + (B_4/3c^2)xy^3 \\ & + B_5y^2 + (2B_5/3c^2)y^4 + (B_5/9c^4)y^6 + B_6xy^2 \\ & + (2B_6/3c^2)xy^4 + (B_6/9c^4)xy^6 - Z[(B_5c^2/Zc) + (B_5/Zc)y^2 \\ & + (2B_5/3c^2Zc)y^4 + (B_5/9c^4Zc)y^6 + (B_6c^2/Zc)x + (B_6/Zc)xy^2 \\ & + (2B_6/3c^2Zc)xy^4 + (B_6/9c^4Zc)xy^6 + (1/c)y + (1/3c^3)y^3] \end{aligned} \tag{3.20}$$

in which

$$
\begin{aligned}
A_1 &= X_c + A_X - Z_c A_\phi & B_1 &= Y_c + A_Y + Z_c A_\omega \\
A_2 &= B_X - Z_c B_\phi & B_2 &= B_Y + Z_c B_\omega \\
A_3 &= -Z_c A_\kappa / c & B_3 &= (Z_c + A_Z)/c \\
A_4 &= -Z_c B_\kappa / c & B_4 &= B_Z / c \\
A_5 &= A_\phi & B_5 &= Z_c A_\omega / c^2 \\
A_6 &= B_\phi & B_6 &= Z_c B_\omega / c^2
\end{aligned}
$$

The B_5, B_6 coefficients will become zero if the system is roll stabilized ($\omega = 0$) and the corresponding terms in Equations (3.20) will drop from the second expression. Similar expressions, with a corresponding increase in the number of terms within the polynomials may be derived under the assumption of second order polynomial variations for exterior orientation elements within sections. Again polynomials of different order could be assumed for the different orientation elements.

Other investigators, notably Kratky [21], have considered the possibility of approximating the behaviour of orientation elements within a section by harmonic functions. In this case, functions may be written for exterior orientation elements of the form

$$
\begin{aligned}
\delta X_c &= A_X \sin C_X x + B_X \cos C_X x \\
\delta Y_c &= A_Y \sin C_Y x + B_Y \cos C_Y x \\
\delta Z_c &= A_Z \sin C_Z x + B_Z \cos C_Z x \\
\delta\omega &= A_\omega \sin C_\omega x + B_\omega \cos C_\omega x \\
\delta\phi &= A_\phi \sin C_\phi x + B_\phi \cos C_\phi x \\
\delta\kappa &= A_\kappa \sin C_\kappa x + B_\kappa \cos C_\kappa x
\end{aligned}
\qquad (3.21)
$$

These expressions may be substituted into Equations (3.15), which results in a complicated harmonic equation set. Kratky, in a subsequent communication with this investigator, indicated that use of these harmonics was troublesome. It was found that, unless very close estimates of the parameters in these functions were known, it was difficult to obtain convergence for the parameters using least squares.

3.2.2.2 Polynomials for Equivalent Rectilinear Recording. The polynomials in Section 3.2.2.1 may be simplified if resampling is first done using the resampling algorithms presented in Section 3.1. The resulting data arrays will represent the data form as if the arrays had been recorded on a planar surface at an effective principal distance of c', as presented in Section 3.1.1. The algorithm of Equation (3.6) is first considered, in which the j term would correspond to the y' parameter of Equation (3.13), and U_j would represent the corresponding position in the arrays before resampling and hence define the scanning angle θ. Since the y' and θ values are taken with respect to the scan line center,

$$\theta = (U_j - n)\gamma \tag{3.22}$$

$$y' = \frac{W}{N}(j - n - 1/2) \tag{3.23}$$

If the assumption is made that symmetric scanning is employed, in which n = N/2, and that resampling takes place upon a planar surface

at an effective principal distance of $c' = c/k\alpha$ as shown in Figure 3.1b, the scan line length is given by

$$W = 2c' \tan n\gamma \tag{3.24}$$

The resampling algorithm for symmetric scanning is given by

$$U_j = n + 1/\gamma \tan^{-1} \left[\frac{(2j - 1)}{N} \tan n\gamma - \tan n\gamma \right]$$

Substituting this expression for U_j into Equation (3.22) yields

$$\theta = \tan^{-1} \left[\frac{(2j - 1)}{N} \tan n\gamma - \tan n\gamma \right] \tag{3.25}$$

Solving Equation (3.23) for j and substituting the result into (3.25), yields

$$\theta = \tan^{-1} \left[\left(\frac{2y'}{W} + 1 \right) \tan n\gamma - \tan n\gamma \right]$$

or

$$\theta = \tan^{-1} \left(\frac{2y'}{W} \tan n\gamma \right) \tag{3.26}$$

Taking the tangent of both sides of (3.26) and substituting the expression for W from (3.24) results in

$$\tan\theta = \frac{y'}{c'} \tag{3.27}$$

If (3.27) is used in Equations (3.15) the resulting differential equations become

$$\begin{aligned} X &= X_c + \delta X_c - h\delta\phi - (h/c')y'\,\delta\kappa \\ Y &= Y_c + \delta Y_c + (h/c')y' + (y'/c')\delta Z_c + h[1 + (y'/c')^2]\delta\omega \end{aligned} \tag{3.28}$$

Assuming h is constant, in order to accomplish a transformation from two dimensional image space into a two dimensional object space, and that linear functions are used for the orientation element variations, as given in (3.16), the resulting polynomials for this case are

$$\begin{aligned} X &= A_1 + A_2\,x + A_3\,y' + A_4\,xy' \\ Y &= B_1 + B_2\,x + B_3\,y' + B_4\,xy' + B_5\,y'^2 + B_6\,xy'^2 \end{aligned} \tag{3.29}$$

in which

$$\begin{aligned} A_1 &= X_c + A_X - h\,A_\phi & B_1 &= Y_c + A_Y + h\,A_\omega \\ A_2 &= B_X - h\,B_\phi & B_2 &= B_Y + h\,B_\omega \\ A_3 &= -h\,A_\kappa/c' & B_3 &= (h + A_Z)/c' \\ A_4 &= -h\,B_\kappa/c' & B_4 &= B_Z/c' \\ & & B_5 &= h\,A_\omega/c'^2 \\ & & B_6 &= h\,B_\omega/c'^2 \end{aligned}$$

If the scanner used is roll stabilized, the last two terms of the second equation of (3.29) will disappear. As mentioned before, the parameters associated with the $\delta\phi$ and δX_c functions always appear together combined in the A_1, A_2 polynomial coefficients, and hence the effects of the δX_c and $\delta\phi$ terms are not separable, resulting

in the reduction of the original 12 parameters to 10 for flat terrain. These parameters are A_i ($i = 1, 4$) and B_j ($j = 1, 6$).

Note that the formulation of polynomials utilizing the resampling algorithm does not reduce the number of parameters. The parameters within these polynomials are dependent only upon the functions assumed for the elements of exterior orientation, and hence are unaffected by resampling. The effect of resampling is to reduce the number of terms within the polynomials by making unnecessary an expansion to approximate the trigonometric function within Equation (3.15).

Assuming second order polynomials to represent orientation variations within sections as given in Equations (3.18) results in

$$\begin{aligned} X &= A_1 + A_2\, x + A_3\, x^2 + A_4\, y' + A_5\, xy' + A_6\, x^2y' \\ Y &= B_1 + B_2\, x + B_3\, x^2 + B_4\, y' + B_5\, xy' + B_6\, x^2y' \\ &\quad + B_7\, y'^2 + B_8\, xy'^2 + B_9\, x^2y'^2 \end{aligned} \tag{3.30}$$

in which

$$\begin{aligned} A_1 &= X_c + A_X - h\, A_\phi & B_1 &= Y_c + A_Y + h\, A_\omega \\ A_2 &= B_X - h\, B_\phi & B_2 &= B_Y + h\, B_\omega \\ A_3 &= C_X - h\, C_\phi & B_3 &= C_Y + h\, C_\omega \\ A_4 &= -h\, A_\kappa/c' & B_4 &= (h + A_Z)/c' \\ A_5 &= -h\, B_\kappa/c' & B_5 &= B_Z/c' \\ A_6 &= -h\, C_\kappa/c' & B_6 &= C_Z/c' \\ & & B_7 &= h\, A_\omega/c' \\ & & B_8 &= h\, B_\omega/c'^2 \\ & & B_9 &= h\, C_\omega/c'^2 \end{aligned}$$

Similar to the presentation in Section 3.2.2.1, the effects of topography may be included within these polynomials by relaxing the assumption of constant h and including the element elevations assigned ($h = Z_c - Z$) for each element. Under the assumption that orientation element variations are linear, the resulting polynomials become

$$\begin{aligned} X &= A_1 + A_2\, x + A_3\, y' + A_4\, xy' - Z[-A_5 - A_6\, x \\ &\quad + (A_3/Z_c)y' + (A_4/Z_c)xy'] \\ Y &= B_1 + B_2\, x + B_3\, y' + B_4\, xy' + B_5\, y'^2 + B_6\, xy'^2 \\ &\quad - Z[(B_5\, c'^2/Z_c) + (B_5/Z_c)y'^2 + (B_6\, c'^2/Z_c)x \\ &\quad + (B_6/Z_c)xy'^2 + (1/c')y'] \end{aligned} \tag{3.31}$$

in which

$$\begin{aligned} A_1 &= X_c + A_X - Z_c\, A_\phi & B_1 &= Y_c + A_Y + Z_c\, A_\omega \\ A_2 &= B_X - Z_c\, B_\phi & B_2 &= B_Y + Z_c\, B_\omega \\ A_3 &= -Z_c\, A_\kappa/c' & B_3 &= (Z_c + A_Z)/c' \\ A_4 &= -Z_c\, B_\kappa/c' & B_4 &= B_Z/c' \\ A_5 &= A_\phi & B_5 &= Z_c\, A_\omega/c'^2 \\ A_6 &= B_\phi & B_6 &= Z_c\, B_\omega/c'^2 \end{aligned}$$

and the B_5, B_6 coefficients will become zero if the system is roll stabilized ($\omega = 0$).

If second order variations in orientation elements are assumed, the resulting polynomial functions become

$$\begin{aligned} X &= A_1 + A_2\, x + A_3\, x^2 + A_4\, y' + A_5\, xy' + A_6\, x^2y' \\ &\quad - Z[-A_7 - A_8\, x - A_9\, x^2 + (A_4/Z_c)y' + (A_5/Z_c)xy' \\ &\quad + (A_6/Z_c)x^2y'] \end{aligned}$$

$$Y = B_1 + B_2 x + B_3 x^2 + B_4 y' + B_5 xy' + B_6 x^2y' + B_7 y'^2 + B_8 xy'^2 + B_9 x^2y'^2 - Z[(B_7 c'^2/Z_c) + (B_7/Z_c)y'^2 + (B_8 c'^2/Z_c)x + (B_8/Z_c)xy'^2 + (B_9 c'^2/Z_c)x^2 + (B_9/Z_c)x^2y'^2 + (1/c')y'] \quad (3.32)$$

in which

$$A_1 = X_c + A_X - Z_c A_\phi \qquad B_1 = Y_c + A_Y + Z_c A_\omega$$

$$A_2 = B_X - Z_c B_\phi \qquad B_2 = B_Y + Z_c B_\omega$$

$$A_3 = C_X - Z_c C_\phi \qquad B_3 = C_Y + Z_c C_\omega$$

$$A_4 = - Z_c A_\kappa/c' \qquad B_4 = (Z_c + A_Z)/c'$$

$$A_5 = - Z_c B_\kappa/c' \qquad B_5 = B_Z/c'$$

$$A_6 = - Z_c C_\kappa/c' \qquad B_6 = C_Z/c'$$

$$A_7 = A_\phi \qquad B_7 = Z_c A_\omega/c'^2$$

$$A_8 = B_\phi \qquad B_8 = Z_c B_\omega/c'^2$$

$$A_9 = C_\phi \qquad B_9 = Z_c C_\omega/c'^2$$

and the B_7, B_8, B_9 coefficients become zero if $\omega = 0$.

3.2.3 Constraints at Section Boundaries

It has been stated previously that if a restitution is to be attempted using the collinearity or polynomial models, it is desirable to treat the flight line in sections. Dividing the flight line into sections allows the use of simpler functional assumptions for the exterior orientation elements to approximate their actual stochastic behavior with acceptable accuracy. If the entire flight line is treated as one unit, the functional behaviour assumed for the exterior orientation elements must be correspondingly more complex to yield comparable results. On the other hand, if the flight line is treated

in sections, control points within each section may be used to determine functional parameters which are valid only within that section. This is desirable in an element by element restitution, since fewer terms must be evaluated within the computer for each element than if more complicated functional forms were assumed in treating the entire flight line as a unit.

Treatment of the flight line in sections, however, introduces some problems. If each section is treated entirely independently, with an independent set of parameters, then restituted X, Y coordinate discontinuities will occur at the section boundaries. To avoid these discontinuities, introduction of constraints at section boundaries is necessary.

In using collinearity equations or polynomials, the arrays are segmented along lines of constant x coordinate, i.e., constant data array line number. The joining conditions consist of the requirement that restituted positions along the line have the same values after transformation by either of the two possible collinearity or polynomial functions. Other constraints may also be considered in which, not only positions, but derivatives of first, second, or greater order may also be constrained to be equal along these section borders and thus a smoothing of the imagery across section boundaries may be introduced. These, however, are unduly complex and for this investigation, only the simplest case of constraints on coordinate position along the interface are considered. This problem may be efficiently treated if the concept of parameter con-

straints is applied at the time of estimating the parameters by least squares. In this case the linearized model may be written

$$\begin{aligned} \underline{A}\,\underline{V} + \underline{\ddot{B}}\,\underline{\Delta} + \underline{\dot{B}}\,\underline{\dot{\Delta}} + \underline{F}^{\circ} &= \underline{0} \\ \underline{\dot{C}}\,\underline{\dot{\Delta}} + \underline{G}^{\circ} &= \underline{0} \end{aligned} \tag{3.33}$$

in which linearized constraint equations are used to augment the original linearized condition equations.

If, for example, the polynomial forms given by Equations (3.20) are considered as a mathematical model, the constraint equations along the interface between one section, u, and the succeeding section, v = u + 1 may be determined as follows.

Considering the first equation of (3.20) and equating X coordinates from sections u and v yields

$$\begin{aligned} &\{A_1 + A_2\,x + A_3\,y + (A_3/3c^2)y^3 + A_4\,xy + (A_4/3c^2)xy^3 \\ &\quad - Z[-A_5 - A_6\,x + (A_3/Z_c)y + (A_3/3c^2Z_c)y^3 \\ &\quad + (A_4/Z_c)xy + (A_4/3c^2Z_c)xy^3]\} \\ &= \{A_1 + A_2\,x + A_3\,y + (A_3/3c^2)y^3 + A_4\,xy + (A_4/3c^2)xy^3 \\ &\quad - Z[-A_5 - A_6\,x + (A_3/Z_c)y + (A_3/3c^2Z_c)y^3 \\ &\quad + (A_4/Z_c)xy + (A_4/3c^2Z_c)xy^3]\}_v \end{aligned}$$

Equating the constant terms and the coefficients of the y and Z terms respectively yields

$$\begin{aligned}(A_1 + A_2\,x)_u &= (A_1 + A_2\,x)_v \\ (A_3 + A_4\,x)_u &= (A_3 + A_4\,x)_v \\ (A_5 + A_6\,x)_u &= (A_5 + A_6\,x)_v\end{aligned} \tag{3.34}$$

Equating the coefficients of y^3, yZ, and y^3Z yields the following additional equations.

$$\begin{aligned}[(A_3/3c^2) + (A_4/3c^2)x]_u &= [(A_3/3c^2) + (A_4/3c^2)x]_v \\ [A_3/Z_c) + (A_4/Z_c)]_u &= [(A_3/Z_c) + (A_4/Z_c)x]_v \\ [A_3/3c^2Z_c) + (A_4/3c^2Z_c)x]_u &= [(A_3/3c^2Z_c) + (A_4/3c^2Z_c)x]_v\end{aligned} \tag{3.35}$$

Since the c and Z_c terms are treated as known constants for each flight line, it may be seen that Equations 3.35 are redundant since each of them can be reduced to the second equation of (3.34).

The remaining condition equations at each section boundary may be determined using the second equation of (3.20), and enforcing the constraint condition of equal Y coordinate along the boundary. The condition equations which result by equating the constant terms, the coefficients of y, and the coefficients of y^2 in this constraint are as follows.

$$\begin{aligned}(B_1 + B_2\,x)_u &= (B_1 + B_2\,x)_v \\ (B_3 + B_4\,x)_u &= (B_3 + B_4\,x)_v \\ (B_5 + B_6\,x)_u &= (B_5 + B_6\,x)_v\end{aligned} \tag{3.36}$$

The additional constraint equations which may be formed by equating y^3, y^4, y^6, Z, Zy^2, Zy^4, Zy and Zy^3 coefficients, respectively, are

$$
\begin{aligned}
[(B_3/3c^2) + (B_4/3c^2)x]_u &= [(B_3/3c^2) + (B_4/3c^2)x]_v \\
[(2B_5/3c^2) + (2B_6/3c^2)x]_u &= [(2B_5/3c^2) + (2B_6/3c^2)x]_v \\
[(B_5/9c^4) + (B_6/9c^4)x]_u &= [B_5/9c^4) + (B_6/9c^4)x]_v \\
[(B_5c^2/Z_c) + (B_6c^2/Z_c)x]_u &= [(B_5c^2/Z_c) + (B_6c^2/Z_c)x]_v \\
[(B_5/Z_c) + (B_6/Z_c)x]_u &= [(B_5/Z_c) + (B_6/Z_c)x]_v \\
[(2B_5/3c^2Z_c) + (2B_6/3c^2Z_c)x]_u &= [(2B_5/3c^2Z_c) + (2B_6/3c^2Z_c)x]_v \\
[(B_5/9c^4Z_c) + (B_6/9c^4Z_c)x]_u &= [(B_5/9c^4Z_c) + (B_6/9c^4Z_c)x]_v \\
1/c &= 1/c \\
1/3c^3 &= 1/3c^3
\end{aligned}
\tag{3.37}
$$

All of these equations are either identities, or may be reduced to one of the equations of (3.36) and are thus not independent. The final set of six independent equations necessary to enforce the constraint condition at section boundaries when utilizing the method of piecewise polynomials may be written by combining Equations (3.34) and (3.36) as follows

$$
\begin{aligned}
(A_1 + A_2\,x)_u &= (A_1 + A_2\,x)_v \\
(A_3 + A_4\,x)_u &= (A_3 + A_4\,x)_v \\
(A_5 + A_6\,x)_u &= (A_5 + A_6\,x)_v \\
(B_1 + B_2\,x)_u &= (B_1 + B_2\,x)_v \\
(B_3 + B_4\,x)_u &= (B_3 + B_4\,x)_v \\
(B_5 + B_6\,x)_u &= (B_5 + B_6\,x)_v
\end{aligned}
\tag{3.38}
$$

The x image coordinate value in these equations represents the constant image x value at the boundary. Thus these equations contain only parameters and may be linearized and used to augment the linearized condition equations during the process of least squares adjustment. If higher order polynomials are assumed for the elements of exterior orientation, the number of constraint equations will remain the same. However, each constraint will contain higher order terms in x.

If the collinearity equations are utilized the necessary constraints may be written quite simply by enforcing the conditions that, along the boundary between sections, the values of the exterior orientation elements must be the same whether computed using the parameters from section u or those associated with section v.

$$\begin{aligned} X_{cu} &= X_{cv} \\ Y_{cu} &= Y_{cv} \\ Z_{cu} &= Z_{cv} \\ \omega_u &= \omega_v \\ \phi_u &= \phi_v \\ \kappa_u &= \kappa_v \end{aligned} \tag{3.39}$$

For example, if linear variations are assumed for these elements within each section, the necessary constraint equations are

$$
\begin{aligned}
(A_X + B_X\, x)_u &= (A_X + B_X\, x)_v \\
(A_Y + B_Y\, x)_u &= (A_Y + B_Y\, x)_v \\
(A_Z + B_Z\, x)_u &= (A_Z + B_Z\, x)_v \\
(A_\omega + B_\omega\, x)_u &= (A_\omega + B_\omega\, x)_v \\
(A_\phi + B_\phi\, x)_u &= (A_\phi + B_\phi\, x)_v \\
(A_\kappa + B_\kappa\, x)_u &= (A_\kappa + B_\kappa\, x)_v
\end{aligned}
$$

It is noted that the number of equations is the same as in the piecewise polynomial formulation, since the piecewise polynomials simply represent a different parameterization based upon a linearized form of the same collinearity equations.

3.3 Nonparametric Techniques

The preceding parametric methods of restitution attempt to estimate the coefficients of polynomials used to approximate the stochastic variation of scanner exterior orientation elements. Completely different techniques for restitution of remote sensing imagery have been applied by Leberl [45, 68], which may be termed "nonparametric" or "stochastic". The methods outlined by Leberl are in turn based upon earlier work by Pinkwart [97] and Schatz [98]. In this case, the difference in coordinate values in the x and y directions between uncorrected and restituted arrays is assumed to be a realization of a two dimensional stochastic field and attempts are made to obtain estimates for these differences by nonparametric

interpolative methods. No effort is made with these methods to estimate parameters associated with orientation. An estimate is made of the correlated portion of these coordinate differences, under the assumption that the mathematical model governing these correlated effects (often improperly called "systematic" effects) is not known.

The use of these methods assumes that a data array is a realization of a stationary random function, i.e., a random function for which the associated probability distribution functions remain unchanged with a shift along the independent variable axis or axes. Further, the property of ergodicity is assumed for the data array, which allows the use of values at different points in a field from only one of its realizations instead of many values at one point, which would require many realizations of the random field. References [109] and [114] may be consulted for a detailed discussion of stationary random functions and ergodicity.

In addition, for certain of the nonparametric techniques to be discussed, particularly the linear ones, it is desirable to assume that the data array is isotropic. That is, that the correlated x and y mismatches between uncorrected and restituted data arrays are independent of coordinate direction, and dependent only upon distance between points. Thus, the field is assumed to be point symmetric. This assumption is definitely not valid for uncorrected MSS digital data arrays, and preprocessing is necessary in order to make this assumption applicable.

3.3.1 Arithmetic Mean [45, 98]

In this method, estimates of mismatch in the x and y directions are computed for each data array element based upon a known vector of such differences for a control point set. The control point vector of differences is defined as

$$\begin{aligned} s_{xi} &= x_i - X_i \\ s_{yi} &= y_i - Y_i \end{aligned} \tag{3.40}$$

for i = 1,...n control points, where x_i, y_i represent the uncorrected image coordinate values for the i-th control point, taken from a gray scale display of the array, and X_i, Y_i are the corresponding object space coordinates of the same control point, after a conformal similarity transformation to the image coordinate system. Estimates of the x, y differences for an arbitrary element within the array are defined by a simple weighted arithmetic mean of the form

$$\begin{aligned} \hat{s}_x &= \frac{\sum_{i=1}^{n} w_i \, s_{xi}}{\sum_{i=1}^{n} w_i} \\ \hat{s}_y &= \frac{\sum_{i=1}^{n} w_i \, s_{yi}}{\sum_{i=1}^{n} w_i} \end{aligned} \tag{3.41}$$

in which the w_i terms are weighting factors assumed to be dependent only upon the distance within the array between the element in

question and the control point being considered. Empirical weighting functions are then assumed [45, 98] of the form

$$w_i = \frac{1}{d_i}^m$$

or

$$w_i = \frac{1}{1 + d_i}^m \qquad (3.42)$$

in which

$$d_i = \sqrt{(x - x_i)^2 + (y - y_i)^2}$$

is the distance considered. The choice of the power m to be used is relatively arbitrary, depending upon the desired amount of correlation between widely separated points. If it is desired that correlation between points decrease rapidly, a choice of m = 3 is suitable, in that correlation will drop off rapidly with distance, and only a nominal amount of computation is required.

If this technique is applied directly using uncorrected data arrays and object space control which has been scaled to the image, the results will be acceptable in the x direction, but serious errors will remain in the y coordinate direction. The reasons for this are two-fold.

1.) The arithmetic mean is a linear algorithm, both in x and y. While linearity of the data arrays can be well approximated over limited areas in the x direction, the recording of the data arrays in the y direction is panoramic in nature and hence non-linear.

2.) Due to the nature of scanning, the y direction in most instances will not have the same scale within the data arrays as in the x direction. (Scales in the x and y direction will be the same only if the β and γ sample angles are the same, and the period of rotation of the scanning prism is perfectly coordinated with the aircraft velocity.) Thus the data arrays, or images have differential scale values in the x and y directions.

In order to effectively utilize the method of the arithmetic mean, then, it is desirable to pre-process the data arrays in a simple manner to circumvent the problems outlined above. To handle the first problem, each element y coordinate, or column number, would be processed using the resampling algorithm of Equation (3.13), in order to remove panoramic displacements. To resolve the second problem, these resulting column values would then be scaled to the object space control Y values, to remove differential scale.

Thus, the processing of the data arrays by arithmetic mean would more realistically be defined by

$$\begin{aligned} s_{xi} &= x_i - X_i \\ s'_{yi} &= y'_i - Y_i \end{aligned} \tag{3.43}$$

in which y'_i represents the image y coordinate values after pre-processing.

3.3.2 Moving Averages [45, 98]

The method of moving averages represents a generalization which allows greater flexability in the point mismatch estimate computations than does the arithmetic mean. In using the method, the x, y mismatches are to be estimated using polynomials or other types of functions. The most commonly used examples are the linear (affine) case

$$\begin{aligned} \hat{s}_x &= a_o + a_1 x + a_2 y \\ \hat{s}_y &= b_o + b_1 x + b_2 y \end{aligned} \tag{3.44}$$

or the second order polynomial case

$$\begin{aligned} \hat{s}_x &= a_o + a_1 x + a_2 y + a_3 xy + a_4 x^2 + a_5 y^2 \\ \hat{s}_y &= b_o + b_1 x + b_2 y + b_3 xy + b_4 x^2 + b_5 y^2 \end{aligned} \tag{3.45}$$

The a_i, b_i coefficients of these functions are computed by weighted least squares utilizing the n reference points at which the x, y mismatches are known. The weight for each reference point is assigned as a function of the distance from the element where the estimate is being computed to the control (reference) point, such as the expressions of (3.42). For each point to be interpolated, a new set of the a_i, b_i coefficients must be computed using weighted least squares.

As an example, consider the affine case of Equations (3.44). Condition equations would be written for the control points where

x, y mismatch values are known. Considering the interpolation for the x coordinate, linear condition equations may be written of the form

$$\underset{n,1}{V_x} + \begin{bmatrix} 1 & x_1 & y_1 \\ 1 & x_2 & y_2 \\ & \vdots & \\ 1 & x_n & y_n \end{bmatrix} \begin{bmatrix} a_o \\ a_1 \\ a_2 \end{bmatrix} = \begin{bmatrix} s_{x1} \\ s_{x2} \\ \vdots \\ s_{xn} \end{bmatrix}$$

and the parameters (a_o, a_1, a_2) may be determined by weighted least squares using the method of indirect observations ($\underline{V} + \underline{B}\,\underline{\Delta} = \underline{F}^o$). The weight matrix may be taken as

$$\underset{n,n}{\underline{W}} = \underline{W}_x = \underline{W}_y = \begin{bmatrix} w_1 & & & & \\ & w_2 & & & \\ & & \ddots & & \\ & & & & w_n \end{bmatrix}$$

An identical analysis and least squares solution technique may be used for the y coordinates to solve for the (b_o, b_1, b_2) parameters. Having obtained a_i, b_i, Equation (3.44) is then used to compute $\hat{s}_x$, $\hat{s}_y$. The entire procedure is repeated for every point to be interpolated.

Note that as each x, y position is interpolated, the d_i terms of Equation (3.42) will vary, hence the w_i terms will also vary. Therefore, a different coefficient set (a_i, b_i) must be evaluated for every point during a restitution, and the method may become computationally time consuming.

An advantage of the method lies in the fact that it will ordinarily require no pre-processing of the data arrays, as is necessary when using the arithmetic mean. The "systematic" effects of panoramic displacement and differential x, y scales are adequately incorporated within the estimating expressions. Such processing however, may allow the use of simpler functional forms to model the displacements in lieu of more complicated functions.

It may be shown that the arithmetic mean method of the preceding Section (3.3.1) is a special case of the method of moving averages. In this instance, only the constant terms are used to estimate the mismatch at the point being interpolated, or

$$\begin{aligned} \hat{s}_x &= a_o \\ \hat{s}_y &= b_o \end{aligned} \tag{3.46}$$

For this case, the linear condition equations become for the x coordinate

$$\underset{n,1}{V_X} + \begin{bmatrix} 1 \\ 1 \\ \vdots \\ 1 \end{bmatrix} a_o = \begin{bmatrix} s_{x1} \\ s_{x2} \\ \vdots \\ s_{xn} \end{bmatrix}$$

from which, using the same diagonal weight matrix $\underline{W}_X$ above, the parameter estimate becomes

$$a_o = \frac{\sum_{i=1}^{n} w_i \, s_{xi}}{\sum_{i=1}^{n} w_i}$$

Performing the same for y, leads to results identical to those of Equation (3.41).

3.3.3 Meshwise Linear Transformation [45, 98]

For this method, the control point set is first connected into a mesh. A commonly used mesh consists of a set of contiguous triangles. For each element to be transformed, this set of triangles is searched to determine the one in which the element being considered lies. Once this is determined, the transformation is accomplished by a linear affine transformation of the form given in (3.44), in which the coefficients are determined uniquely from the three control points forming the triangle in which the element is found to lie. Three equation pairs of the form of (3.44) are written at the triangle vertices where coordinate displacements are known, and these are solved uniquely for the 6 coefficients (a_i, b_i) required.

The method requires no pre-processing of the data, as the affine transformation allows for differential scale values in the x and y direction, and accomodates the panoramic effect by defining "secant planes" in the y direction. The method is computationally efficient in that only three points in the neighborhood of the element being transformed are used to uniquely define the coefficients, utilizing explicit formulas rather than least squares. The method gives

identical results along the boundary between adjacent triangles when utilizing the parameters associated with either triangle.

A variation of this method is termed overdetermined meshwise linear transformation. In this case, the control point field is used to define quadrangles, rather than a triangular mesh. For each quadrangle it is possible to define four possible triangles using three of the four possible points each time. Any element within a quadrangle will fall in two of these four triangles. The transformation outlined above may be performed on the element for each of these two triangles, and the final estimates of mismatch will be taken as the average of these two, or may be determined by the method of least squares.

The method, however, suffers from serious drawbacks. The foremost of these is that it may not allow the transformation of all elements within the data array. In order that all elements within the data array may fall in one of the triangular meshes defined by the control points, it is necessary that, as a minimum, four of the control points fall at the extreme corners of the flight line. A control point, however, must be identifiable both on a map sheet (if maps are being used for planimetric object space control) and on a display of the data arrays. Clearly it is impossible that such points would fall at the flight line corners for every data array. Thus, the definable mesh using identifiable control points will not cover all of the flight line. This would make it necessary, if using a meshwise linear transformation, to define some element transformations by extrapolation utilizing the

parameters of Equation (3.44), which in turn are based upon only 3 control points. Such extrapolation is dangerous and may lead to gross errors, depending on the distance from the nearest control.

A lesser, but still serious disadvantage of the method lies in the amount of human intervention necessary. The restitution of MSS digital data arrays, by whatever method, must be basically a computer oriented procedure to be compatible with automated interpretation when the two fields are finally combined. The necessity of defining triangular meshes by hand, which is necessary when using meshwise linear transformation, largely defeats the automated aspects so desirable in such arrays.

3.3.4 Linear Least Squares Interpolation and Filtering

Probably the most sophisticated of the nonparametric methods is that of linear least squares interpolation and filtering. The reader is referred to [99] for a detailed explanation of the method by Kraus and Mikhail. Basically, the method defines the x and y mismatch estimates in terms of observed mismatch values at the n control points and covariance matrices, written in the form

$$\underset{2,1}{\begin{bmatrix} \hat{s}_x \\ \hat{s}_y \end{bmatrix}} = \underset{2,2n}{\underline{c}^t} \quad \underset{2n,2n}{\underline{C}^{-1}} \quad \underset{2n,1}{\underline{\ell}} \tag{3.47}$$

The vector $\underline{\ell}$ of observed mismatches at control points, is considered to be composed of correlated random components, $\underline{s}$, and uncorrelated random components, $\underline{r}$.

$$\underline{\ell} = \underline{s} + \underline{r} \tag{3.48}$$

The $\underline{C}$ matrix is the autocovariance matrix for the n control points used,

$$\underset{2n,2n}{\underline{C}} = \begin{bmatrix} \underset{n,n}{\underline{C}_{xx}} & \underset{n,n}{\underline{C}_{xy}} \\ \underset{n,n}{\underline{C}_{yx}} & \underset{n,n}{\underline{C}_{yy}} \end{bmatrix} \tag{3.49}$$

and the $\underline{c}$ matrix is the cross-covariance matrix of the element being transformed with respect to the control points,

$$\underset{2n,2}{\underline{c}} = \begin{bmatrix} \underset{n,1}{\underline{c}_{xx}} & \underset{n,1}{\underline{c}_{xy}} \\ \underset{n,1}{\underline{c}_{yx}} & \underset{n,1}{\underline{c}_{yy}} \end{bmatrix} \tag{3.50}$$

The elements of both of these matrices are computed from covariance functions which are determined by a priori knowledge, or may be obtained from the control point data if a general form is assumed for the function, as described by Kraus and Mikhail [99]. If an isotropic field is assumed, then distances between points may be taken as the independent variable for generating the covariance functions. If this assumption is to be approximately valid, the data arrays must be pre-processed as described in Section 3.3.1, using the resampling algorithm of Equation (3.13) to reduce panoramic distortion, and scaled in the y direction.

A more serious assumption associated with the method is stationarity. The method is predicated upon the fact that the random function

being considered for the field is stationary. If a non-stationary process is modeled as if it were stationary, then the computed sample covariance will not fit reasonably to an allowable covariance function form. One of the characteristics for an auto-covariance function associated with a stationary process is that its largest magnitude is at the origin. Thus, if sample auto-covariance values computed from the control point data increase in magnitude with increasing distance, this is evidence that the process is not stationary, and that one of the basic assumptions of the method of linear least squares interpolation is not being fulfilled.

If this result is found within MSS data after pre-processing, it is possible to apply linear least squares only if stationarity is assumed for the stochastic field within a limited region about the point being interpolated. Therefore sample covariance points may be calculated only within a limited region, and allowable covariance functional forms fit to these points. The net result of this technique is that reference points beyond some critical radius about the point being interpolated are assumed to have insignificant correlation with the point, and thus do not contribute appreciably to the filtering and interpolation process.

The theory of linear least squares interpolation and prediction has been used with success in geodesy, and its application in this field has been documented by Moritz [100, 101]. In the latter paper, Moritz presents a generalization of the concept, in which correlation among points to be interpolated is considered. Leberl [45], however,

points out that work by Wolf [102] has shown that the inclusion of correlation between points to be interpolated leads to an over-constrained situation, and thus the independent interpolation of points as represented by Equation (3.47) represents the most feasible method of applying linear least squares.

3.4 Assignment of Element Elevations

Element elevations must be pre-assigned to the uncorrected data arrays if the resampling algorithm of Section 3.1.2 is to be used, or if analysis or restitution is to be attempted using collinearity (Section 3.2.1) or the more general polynomials (Section 3.2.2). The purpose of this section is to investigate methods by which this may be accomplished, and the problems associated with such methods.

Element elevations may be derived from the MSS data itself only if the object space has been scanned more than once, as will be the case if overlapping strips of data are available. Most present data pertain to singly scanned areas, as were the data available for this investigation. Therefore, elevations must be obtained from sources external to the MSS data. Possible sources for these data are existing topographic maps, such as the 1:24000 scale topographic maps of the U. S. Geological Survey which were utilized for this investigation. For compatability with the MSS digital data, height information must be processed into a digital terrain model (DTM). The DTM is a numeric representation of a topographic surface, in which elevations are given at discrete, closely spaced, X-Y point positions over the area being considered.

The DTM may be of two types.

1.) Random, in which the planimetric point positions at which elevation values are known have a more or less random pattern over the area considered. This type of DTM would result, for example, if the digitization of a contour map was carried out by following selected contours, sampling X-Y point positions at intervals along each contour.

2.) Uniform pattern, such as a grid, in which the DTM is represented by closely spaced planimetric point positions arranged in a regular grid over the area. This type of DTM would result, for example, if the contour map were digitized by taking profiles at equally spaced intervals over the area. Then point elevations would be sampled at equally spaced intervals along each profile.

In some cases, the DTM may be constructed from the random contour following method, and pre-processed into the patterned form.

3.4.1 Accuracy Restrictions

At this point a method must be found to reliably assign an appropriate elevation to every data array element. A seeming paradox exists, since the DTM is essentially in an orthographic system, having been generated from map data. At the time when element elevations must be assigned, the MSS data arrays have all of the image displacements and distortions due to scan angle, topographic, and exterior orientation effects. However, the two data sets must be superimposed such that "acceptably accurate" element elevations may be obtained for the MSS data from the DTM. For purposes of

this investigation, elevations were assumed to be "acceptably accurate" if the planimetric error due to height assignment would be less than a single resolution element.

The solution to the problem of superimposing the two data sets lies in the nature of the MSS arrays themselves. Since the data arrays can resolve only to the value, e_Y, given in Equation (1.17), it is only necessary to assign element elevations with an accuracy yielding a planimetric error of a magnitude equal to or less than e_Y, after subsequent processing. Recalling (1.17), the resolution in Y is

$$e_{Y_j} = \gamma(Z_c - Z_j) \sec^2\theta$$

Using Equation (1.19), the allowable height assignment tolerance Z_e, is obtained as

$$\begin{aligned} Z_e &= e_{Y_j}/\tan\theta \\ &= \gamma(Z_c - Z_j) \sec^2\theta/\tan\theta \\ &= \gamma(Z_c - Z_j)/\sin\theta\cos\theta \\ &= 2\gamma(Z_c - Z_j)/\sin 2\theta \end{aligned} \qquad (3.51)$$

Figure 3.5 shows graphically the magnitude of this allowable height assignment tolerance for various values of angular resolution, γ. Using Equation (3.51) at nadir, the allowable tolerance is infinite since a change in elevation has no effect on the image y position. The value of Z_e decreases to a minimum at 45°, where planimetric displacement becomes equal to height assignment tolerance. The

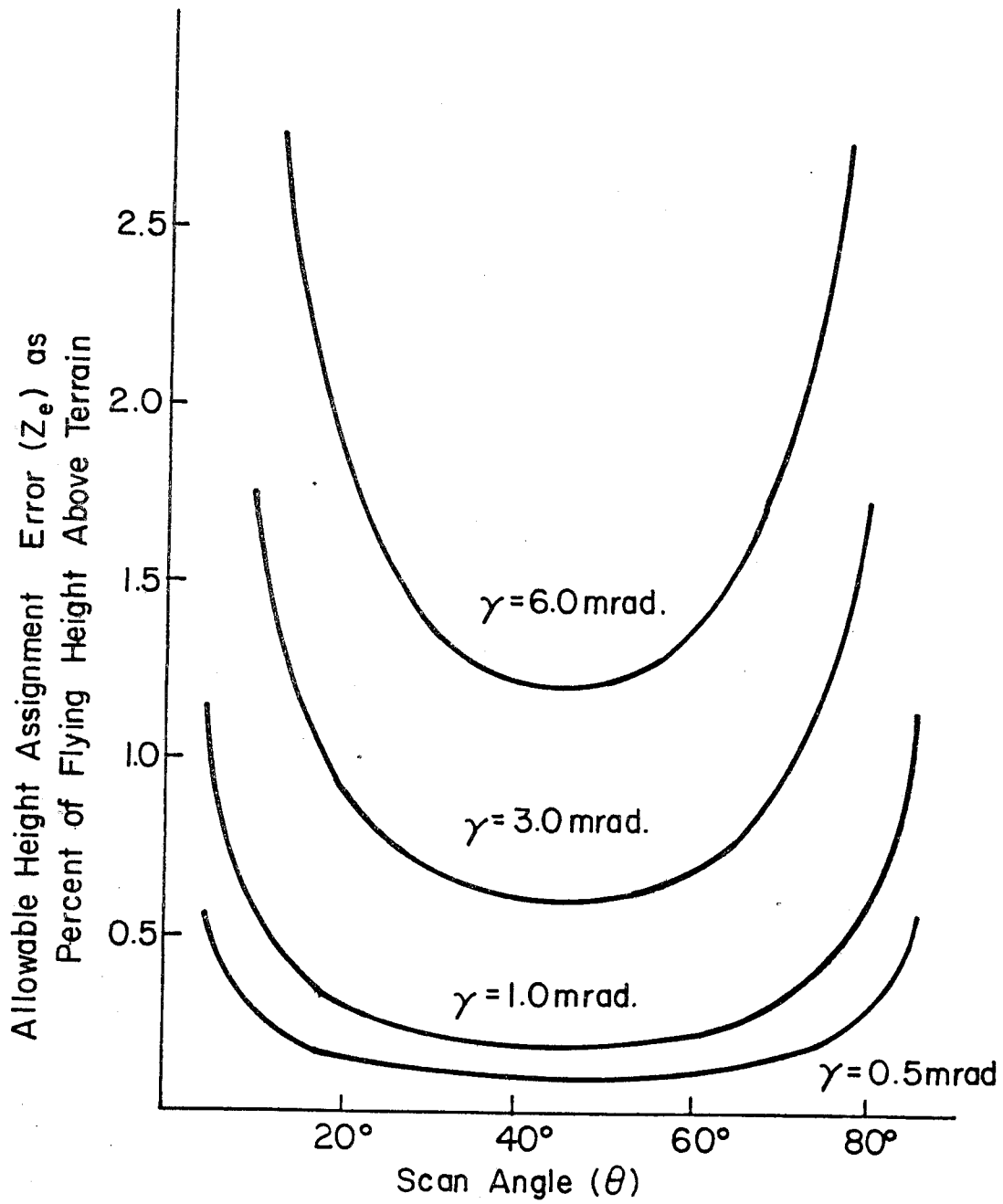

Figure 3.5. Allowable Height Assignment Error

allowable value then increases for scan angles beyond 45°, since the ground size of a resolution element increases rapidly beyond this point. Such high values of scanning angle are rarely used in practice at the present time.

To superimpose the two data sets within this tolerance, it is necessary to find a transformation which will yield a height assignment error of less than that given by Equation (3.51). To do this, ground slopes must be considered. In Figure 3.6, the term δY represents the planimetric displacement in Y resulting from some transformation used to superimpose the MSS data upon the DTM for height assignment purposes. The e_Y value is the size of the element at the given scan angle θ. The resulting elevation tolerance is given by

$$Z_e = \lambda(\delta Y) \tag{3.52}$$

in which λ is the ground slope in the vicinity. If the expression for allowable height assignment tolerance ($e_Y/\tan\theta$) from Equation (3.51) is substituted for Z_e into this expression and the resulting equation is solved for δY, then

$$\delta Y = \frac{e_Y}{\lambda \tan\theta} \tag{3.53}$$

which represents the allowable planimetric tolerence which may be acceptable in an approximate transformation for height assignment purposes, and still result in less than a one resolution element planimetric error after subsequent processing, utilizing for example

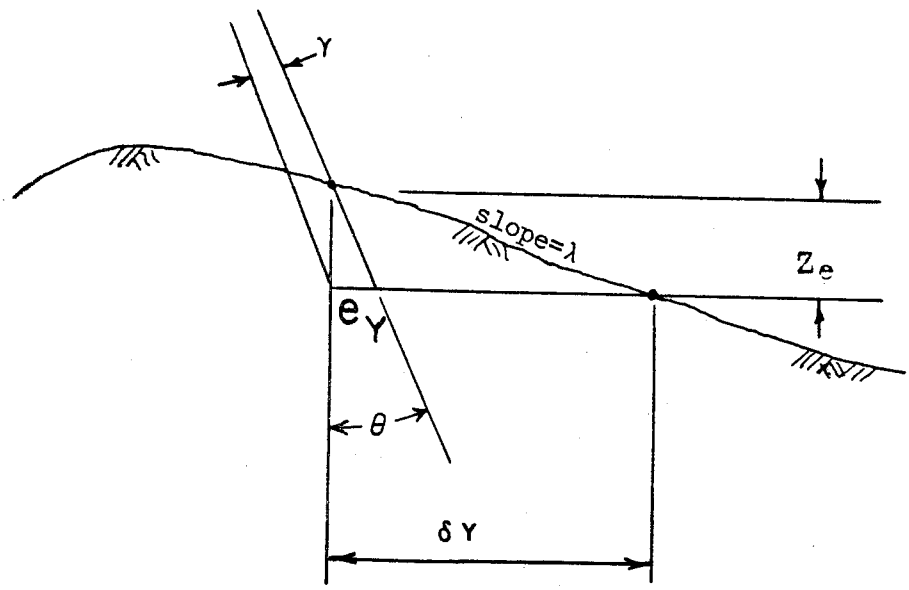

Figure 3.6. Y Displacement Due to Ground Slope

the methods of Section 3.2. In reality, ground slopes rarely exceed 0.5 and scan angles (θ) normally do not exceed 40°. Thus a transformation yielding errors on the order of 3 resolution elements may be appropriate for this step of height assignment. This value is necessary only near the flight line edges, and even larger tolerances would be acceptable near the flight line center.

A simple transformation which may be used for this step in the processing is the well known affine transformation. If this transformation is utilized within sections down the flight strips, the resulting planimetric error is found to be within acceptable limits. No constraints are necessary at section boundaries, since the transformation is used only internally within a program to approximately fit the data arrays to selected control points within the DTM. Coordinates of the control points required for this transformation may be taken from the same map source used to generate the DTM. The transformation is used only to assign element elevations, and no actual horizontal restitution of the MSS array positions would be done at this time. The more sophisticated approaches given in Section 3.2 would be utilized for the actual transformation of elements into a restituted array.

3.4.2 Contour-Scan Intersections

This method of element elevation assignment seems to be the simplest conceptual procedure if the DTM available is of the random type generated by the contour following procedure. The DTM data, if stored according to contours, may be used directly in the form

generated by the digitizing equipment. For this type of DTM, as mentioned previously, contours may be sampled in a digitizer at random intervals along their length.

Each scan line may be transformed according to the affine transformation described in Section 3.4.1. The parameters of this affine transformation are estimated using the method of least squares, based upon ground control points. At this stage, the contours and the transformed scan lines will be superimposed approximately in a near-orthographic system. For each scan line thus transformed, all contours in the vicinity are searched digitally until an intersection of the contour and the scan line is detected. At this point, that position along the scan line is assigned the elevation of the contour. The tracing of the contour is then continued to determine if any further intersections occur with this same scan line. All contours in the area are traced in this manner until all intersections are found for this scan line. The intersection points are then re-sorted so that they are in order along the scan, and elements which are intermediate between intersection points are assigned elevations by linear interpolation between these known elevations. This process is repeated until every scan in the flight line has been processed. The resulting element elevations are stored on the original MSS data tape as an extra channel of data, in the same format as that given in Section 1.2.3.

The advantages of the method are:

1.) Relatively efficient computation: Only straight line equations are used throughout for finding contour-scan

intersection points and for interpolating element elevations between these intersections.

2.) Small storage requirements: At any time, the computer is required to store only the positional data for a single scan line and a single contour.

The major disadvantage of the method is the determination of the element elevations near the beginning and end of each scan. Contour-scan intersections will obviously occur exactly at the scan line ends only by chance, and with virtually zero probability. Thus, some method must be devised for assigning those elevations near scan line ends before the first intersection point and beyond the last. Extrapolation may be dangerous. An attempt must be made to interpolate these end points between contours, and a complex decision procedure is necessary to determine the contour pair between which an end point lies.

3.4.3 Polyconic and Polynomial Surface Approximations

A different approach to the problem of element elevation assignment is to attempt to adequately model by analytic expressions the topographic surface in the region of each element, based upon some subset of the digitized sample points. One example of a mathematical modeling technique is the multiquadric analysis advocated by Hardy [103, 104]. The latter reference contains an excellent summary and introduction to the method.

The general form of the mathematical model which Hardy advocates is

$$\sum_{k=1}^{n} C_k[q(x_k, y_k, x, y)] = z \qquad (3.54)$$

in which x_k, y_k, (k=1,...n) are the coordinates of the sample points be being considered in the vicinity of the element position x, y after its approximate transformation by the affine transformation, and z is the estimated element elevation associated with the point. The C_k terms are coefficients to be multiplied by each of the quadric surface equations assumed. The C_k coefficients are estimated only once, and retain the same value over the section being considered regardless of the (x, y) location of the point being interpolated. The z elevation is a function of x and y resulting from a summation of a series of quadric surfaces having axes of symmetry at the x_k, y_k sample points. According to Hardy, the most often utilized forms of the quadric surfaces chosen are those of a cone, in which

$$q(x_k, y_k, x, y) = [(x_k - x)^2 + (y_k - y)^2]^{1/2} \qquad (3.55)$$

of a hyperboloid, in which,

$$q(x_k, y_k, x, y) = [(x_k - x)^2 + (y_k - y)^2 + C]^{1/2} \qquad (3.56)$$

of a paraboloid, in which,

$$q(x_k, y_k, x, y) = [(x_k - x)^2 + (y_k - y)^2]^a; \; a \leq 1/2 \qquad (3.57)$$

and an inverse hyperboloid, in which

$$q(x_k, y_k, x, y) = [(x_k - x)^2 + (y_k - y)^2 + C]^{-1/2} \tag{3.58}$$

Thus, when given a set of n sample points such as would be generated, for example, in contour digitization, at every sample point an equation could be written of the form

$$\sum_{k=1}^{n} C_k[q(x_k, y_k, x_m, y_m)] = z_m \tag{3.59}$$

in which m is the sample point being considered. There would be n such equations generated, assuming it is desired to have a quadric axis at each sample point. Using the matrix notation of Hardy

$$\underset{n,n}{A} \quad \underset{n,1}{C} = \underset{n,1}{Z} \tag{3.60}$$

the coefficient vector desired, $\underline{C}$, could be solved for by

$$\underset{n,1}{C} = \underset{n,n}{A^{-1}} \quad \underset{n,1}{Z} \tag{3.61}$$

and elevations for elements could then be calculated from Equation (3.54).

The system has many advantages, one of which is that it allows nonlinear modeling of the topography, which is obviously not possible with the linear interpolation scheme of the contour-scan intersection method. It also allows the computation of element elevations near scan line ends with more reliability than with contour-scan intersections.

However, if a large data set of points is available in the DTM, then the matrix $\underline{A}$ in Equations (3.60) and (3.61) will become very large. The computing time necessary to solve (3.60) for the coefficients will be quite large, and the time necessary to compute each element elevation will also become excessive, as the summation of n polynomials to be evaluated must be performed. In cases of this nature, Leberl [45] suggests using a relatively small subset of the total sample points available, such that

$$d_k \leq d$$

where d defines some convenient "circle of influence" for each element, and d_k is the distance from the element being considered to each sample point.

$$d_k = \sqrt{(x_k - x)^2 + (y_k - y)^2}$$

Another possible compromise to cut computing time would be to use a larger subset of the sample points (and hence larger $\underline{A}$ and $\underline{C}$ matrices), but evaluate the multiquadric function of Equation (3.54) only at selected element locations along each scan line, for example, every fifth element. Then points intermediate between these could be assigned elevations by linear interpolation.

A recent paper by Jancaitis and Junkins [105] presents a polynomial procedure for modeling the topographic surface, with new polynomial coefficients being computed as the vicinity being considered is varied. In this method, the area is divided into a number of

small square areas to form a lattice. Within each square, the topographic surface is to be represented by a polynomial of the form

$$z = \sum_{ij} C_{ij} x^i y^j \qquad (3.62)$$

in which the coefficient subscripts correspond uniquely to the exponents i, j of the x, y arguments.

The coefficients of this polynomial, which ordinarily is chosen to contain 12 terms, are determined by matching the estimated elevations and slopes in the x and y directions of the four corner points for each square incremental area, thus enforcing continuity in elevation and slope at the boundaries between adjacent squares.

These estimated elevations and slopes at each corner or lattice point are obtained by fitting a plane at each lattice point to some subset of the sample points determined during digitization, in the immediate vicinity of the lattice point.

After the preliminary affine transformation of each element, these transformed coordinates are utilized directly in Equation (3.62) to obtain an estimate of the elevation for that element.

3.4.4 Other Interpolative Methods

The methods of Section 3.3 may also be utilized to estimate elevations of elements within the MSS data arrays. In this case, the interpolation becomes a one-dimensional case, in which the reference point set would be represented by the digitized values of the DTM.

The methods which may be applied may be taken directly from Section 3.3. For the arithmetic mean, for example, the estimate for elevation of an element would be given by

$$\hat{z} = \frac{\sum_{k=1}^{n} w_k z_k}{\sum_{k=1}^{n} w_k}$$

in which the z_k values are the elevations at the sample points of the DTM, $\hat{z}$ is the estimated elevation of the point being considered, and, the weighting factor w_k for each sample point may be evaluated by either

$$w_k = \frac{1}{d^m_k} \qquad \text{or} \qquad w_k = \frac{1}{1 + d^m_k}$$

in which

$$d_k = \sqrt{(x - x_k)^2 + (y - y_k)^2}$$

where x, y is the approximate orthographic element position after the affine transformation, and x_k, y_k is the digitized position of the point at which z_k has been sampled.

The DTM will generally contain a very great number of sample points. To obtain reasonable computing times it will normally be required that only points within some circle of influence will be considered, such that

$$d_k \leq d$$

The same procedure as that outlined in Section 3.3.2 may be used for a moving average interpolation, which will allow a non-linear interpolation. The estimate will, of course, be only a one dimensional estimate in z. The use of the meshwise linear transformation is hardly practical for estimation of element elevations, in that it requires the determination of a unique set of contiguous triangular meshes in order to implement the method. With the very large data set of points generated in digitizing the DTM, the number of triangles becomes excessive.

The use of linear least squares interpolation to estimate element elevations requires first the reduction to a reference, or trend surface. Leberl [45] points out that meaningful correlations between terrain points exist even over sizeable distances (30 km). He recommends the use of the method of moving averages to first estimate the trend surface, and subsequent utilization of the linear least squares in an attempt to refine the element elevation estimate. Since, as was shown in Section 3.4.1, the final positional accuracy is relatively insensitive to small errors in element elevations, it is doubtful that the increase in element elevation accuracy is worth the increased computing time necessary to implement the method of linear least squares interpolation.

All of the above discussion has been concerned with general mathematical models which may be used for analysis or restitution of MSS data. In the following section, the unique problems associated with restituting MSS data stored in digital form are discussed.

3.5 Direct and Inverse Restitution Techniques

The restitution equations described in Sections 3.2 and 3.3 were based upon the premise that a transformation was being used from the uncorrected data array (or image) into the orthographic object space. These equation forms and relationships are most convenient if estimation of the parameters of imaging is being attempted, and may be used with efficiency for restituting conventional recording media, such as photographic imaging. The use of such relationships may be termed a "direct" approach to restitution, since projective relationships are used to project directly from uncorrected x, y image positions to restituted X, Y positions (by analogue or analytical means).

Because of the nature of digital MSS data, however, further considerations are necessary in attempting to apply this approach to such a digital data form. The digital data is stored in a line by line fashion, and within each line, spectral value locations are limited to integer positions, both in the uncorrected image array, and the restituted output array resulting from such processing. If the direct technique were used, then restitution would be accomplished by measuring x, y uncorrected image coordinates and projecting to restituted X, Y positions using, for example, the collinearity equations of (2.19) or one of the piecewise polynomial formulations. This leads to two problems.

1.) The resulting X, Y position pairs will be randomly generated. This means that a large number of the coordinate pairs

must be stored in an output buffer. A continuous sorting must be implemented to arrange these pairs into positions along array lines to be stored in a restituted output array.

2.) Unique X, Y pairs may not be generated for output. The X, Y pairs thus generated must be in integer form in order to occupy locations within the output array. The same integer position within the output array may result from two or more x, y positions in the uncorrected input array, and thus result in a multiplicity of spectral combinations which could be assigned to it. Further, there will be positions within the output array which would have no spectral values assigned because for some X, Y output array positions, there may be no x, y pair which would map into these positions through the projective expressions, since the X, Y values are limited to integer values. Spectral values for such "holes" may be assigned by interpolating spectral values from surrounding output buffer positions.

The advantage of this method is that use of the direct projective restituting relationships (collinearity or polynomial) requires no iterative procedure. The element elevation values assigned are associated with the x, y uncorrected image positions. Hence, for each element to be projected, x, y and object space Z coordinates are known, along with the parameters of projection. The X, Y restituted position may be calculated with a single application of the restituting relationships.

An alternate restitution technique is to "step" along positions in the restituted output array as the independent variables (X, Y) as advocated by Markarian, et. al. [69], and compute the associated x, y position for each restituted array position. The spectral values in this position are then assigned to the restituted array position. For purposes of this discussion, such an approach will be called the "inverse" restitution technique.

This procedure circumvents the storage and sorting of an output buffer within the computer, and assures that each point within the output array will have assigned to it a spectral value for each channel.

However, this approach also has two major drawbacks associated with the data processing.

1.) Since X, Y values are assigned as the independent variables, then x, y uncorrected array positions are randomly generated, thus necessitating the storage of a large number of these values in a buffer during restitution. After the computation of the x, y position for each associated X, Y output location, this buffer must be searched for the nearest integer array position to the desired x, y image position, and the associated spectral values stored in the restituted output array position. This input buffer, however, is somewhat easier to handle than an output buffer, since it is in array form, containing integer array positions in a line by line arrangement.

2.) Perhaps more serious is the requirement of an iterative computational procedure. This may not apply for those based upon the greatest simplifying assumptions, such as the assumption of flat terrain and constant or linearly varying exterior orientation elements. The following analysis explains the procedure.

For this purpose, the inverse form of the MSS collinearity equations (2.18) are considered. Capitalizing on the fact that the left hand side of the first equation of (2.18) is zero, these equations may be written as (dropping the j subscripts)

$$\begin{aligned} 0 &= m_{11}(X - X_c) + m_{12}(Y - Y_c) + m_{13}(Z - Z_c) \\ \tan(y/c) &= \frac{-[m_{21}(X - X_c) + m_{22}(Y - Y_c) + m_{23}(Z - Z_c)]}{m_{31}(X - X_c) + m_{32}(Y - Y_c) + m_{33}(Z - Z_c)} \end{aligned} \tag{3.63}$$

Note that in the first equation of (3.63), the only variables are X, Y, Z, and x, which is included in the functions assumed for exterior orientation elements. Assuming for the present that Z has a constant value (perfectly flat terrain) then if X, Y are treated as independent variables, and if the parameters associated with the X_c, Y_c, Z_c positional orientation elements and the ω, ϕ, κ angular orientation elements are known from a previous space resection, then the first equation of (3.63) may be solved for x. This solution may be direct if fairly simple functional forms have been assumed for orientation elements, or iterative if more complex functional forms have been assumed. The value obtained for x may be substituted directly into the second equation of (3.63) to then solve for the y image coordinate.

If for this case the assumption of constant Z is relaxed, an iterative technique is required. If element elevations have been assigned to the data arrays before processing is begun, then they are associated with the x, y uncorrected image positions not the X, Y coordinate values used as the independent variables. An iterative technique would then be employed in which a Z value would be estimated (perhaps as an average elevation) and equations (3.63) would be solved for new x, y values. The element elevation stored in this location would then be taken as an updated value of Z, and new x, y values computed. This process would be repeated until no meaningful difference in the x, y values is noted. This is the technique to be utilized if a restitution based directly upon collinearity is to be employed.

If a polynomial approximation is to be used for an element by element transformation using this inverse technique, the problem becomes more complex. It is, in general, not possible to write a linearized transformation equation which may be solved explicitly for x, y image coordinates if X, Y object space coordinates are designated as independent variables, since the orientation elements of scanning are given as functions of the x image coordinates.

If an element by element restitution is to be attempted by the inverse technique utilizing polynomial approximations, it is suggested that the polynomials of Section 3.2.2 be utilized in an iterative manner.

This choice between the direct and inverse methods of final transformation of elements is necessary only with the direct collinearity and polynomial formulations. The resampling algorithms of Section 3.1 are already in the inverse form, in which the restituted array position, j, is used as the independent variable, and the corresponding position, U_j, in the original uncorrected array is computed in order to assign spectral values within the restituted array.

The inverse technique is easily incorporated within the nonparametric methods. These techniques are not based upon analytic forms of modeling the transformation, but are based upon stochastic concepts in which an attempt is made to estimate the correlated components of a stochastic field without defining an analytic form. The mismatch estimates resulting from these methods may be applied to the X, Y positions to estimate the x, y uncorrected image position in order to assign spectral values.

In summary, if direct restitution is attempted using projective collinearity or polynomial forms, one is confronted with problems of output buffer storage and sorting in generating restituted arrays, and the problem of assigning spectral values to the X, Y restituted position for which there are no associated x, y image positions based upon the direct projective relationships. On the other hand, if inverse relationships are used, the storage and sorting procedures are simplified, but the actual transformation calculations require an iterative procedure. For this investigation, no attempt was made to assess the relative efficiency of the direct approach with

respect to the inverse technique. The restitutions performed in this study utilized the inverse approach, in order that modifications of software routines already available at LARS could be used. It is left to future investigation to examine the direct technique.

3.6 Concluding Remarks

This chapter has served to introduce possible methods of restitution for singly scanned MSS digital data arrays, and some of the problems associated with such restitution methods. The resampling algorithms first presented are useful in many cases as a first step in the restitution process. The pre-processing of the data using these algorithms is useful in simplifying subsequent parametric algorithms, or in approximating isotropy for some of the nonparametric methods.

The parametric methods of restitution utilizing MSS collinearity equations or piecewise polynomials represent perhaps the most intuitively obvious methods of restitution, since they are based directly upon the known relationships of the MSS transformation. If these methods are to be used to obtain the best possible accuracy, then Z coordinate information must be introduced into the data arrays from some source.

The nonparametric methods included represent an entirely different approach to the problem of restitution. These algorithms assume that no analytical form is known for a mathematical model. An attempt is made to estimate the correlated effects within the data arrays, based upon stochastic concepts.

The unique nature of the digital data form requires that special data handling techniques be utilized for an efficient element by element restitution. A choice is necessary between a direct approach utilizing the direct projective relationships relating the image and object space element locations, and an inverse approach based upon the imaging form of these relationships. The direct approach has the drawbacks of requiring the storage of a random output buffer coupled with sorting and interpolation requirements, but has the advantage that the direct projective relationships may be used and require only a single application for each element being transformed. The inverse approach results in simpler storage and searching procedures, but requires an iterative procedure for the element by element calculations required in the restitution.

In the following chapter an operational procedure is presented to collect many of the concepts discussed previously into a logical sequence for analysis and restitution of digital data arrays. This procedure is used to test the methods of restitution on existing MSS digital data arrays, and the accuracies obtained from these methods are compared.

4. NUMERICAL RESULTS

4.1 The Data Arrays

The methods of analysis and restitution presented in the preceding chapter were tested on two flight line arrays of actual data available at LARS. Both were flown during the corn blight watch experiment administered by LARS during the summer of 1971 [106, 107]. The University of Michigan scanner was used at a nominal altitude of 5000 ft. (1524 m) above sea level and digitization performed with a nominal angular resolution of 6 milliradians.

The first of these flights, number 208, was located in northwestern Indiana near the city of Lafayette. Figure 4.1 depicts a grey scale display of this array from the line printer. The display is of channel 6, which represents the spectral band between the wavelengths of 0.58 and 0.65 micrometers. Figure 4.2 portrays this same flight line, also from channel 6, as an image taken from the digital display monitor. These images are at an approximate scale of 1:58000. This array contains 1591 lines and 222 columns, and represents a ground area approximately eight miles (13 km) long and one mile (1.6 km) wide. Since it was desired to utilize existing U. S. Geological Survey maps as a source of specific point positions, as well as terrain elevations, it was necessary to locate array positions on the line printer display which were also identifiable

Upper half

Lower half

Figure 4.1. Line Printer Display of Unprocessed Array for Flight 208

Figure 4.2. Digital Display of Unprocessed Array for Flight 208

on the map sheet. This flight line was well suited for this purpose. Terrain variation within the flight line was quite small, on the order of 50 ft. (15 m), ranging from an elevation of approximately 700 ft. (213 m) to approximately 750 ft. (229 m) above mean sea level. A large proportion of the area within the flight line was under cultivation, with no forest cover. The area contained numerous fence, road, and stream intersections which could be easily located on both the line printer display and the map sheet. These array positions were determinable on the line printer display to within one or two resolution elements. After extracting these array positions, the corresponding points were marked on the map sheet for later coordinate digitization.

All points thus located on both the digital array and the map sheet are referred to in this section as reference points. From this set of reference points, a subset of control points was chosen. These control points served as the basic data source from which parameter estimates or nonparametric algorithms were calculated in the analysis methods to be discussed. The points in the remaining subset of reference points are referred to as check points, and are used to assess the accuracy obtained in the subsequent analysis methods. A total of one hundred such reference points were located within the flight line. Of these, thirty nine were used as the actual control points to determine the parameters for the various analysis methods, and sixty one were withheld as check points to investigate the results which were obtained. A mistake in digitizing

one of the check points was subsequently discovered, and the tests performed used only sixty check points.

The second flight line chosen, flight number 218, is located in west central Indiana near the city of Bloomington. Figure 4.3 shows a line printer display of this flight line, and Figure 4.4 depicts the same flight line from the digital display monitor. As before, the images shown are for channel 6 representing the spectral wavelength band from 0.58 to 0.65 micrometers. These images are at an approximate scale of 1:54000. This array contains 1439 lines and 222 columns, and represents a ground area approximately seven miles (11 km) in length, with a width of approximately one mile (1.6 km). Total terrain elevation variation within the flight line is on the order of 300 ft. (91 m), ranging from a low elevation of approximately 550 ft. (167 m) to a high of about 850 ft. (259 m) above mean sea level. Most of the area is wooded such that a tree canopy obscures much of the ground. The area contains fewer roads and fences than the flight line previously discussed, with far fewer recognizable intersections and easily identifiable array positions. For these reasons greater difficulty was encountered in reliably locating reference points within the array. Thirty three points were finally assigned over the entire flight line, of which twenty four were utilized as control to determine the parameters of the analysis, and nine were withheld as test points. However, because of discovery of a mistake in digitization of one of the control points, a set of only 32 was used (23 control, 9 check) in performing the tests of analysis methods discussed below.

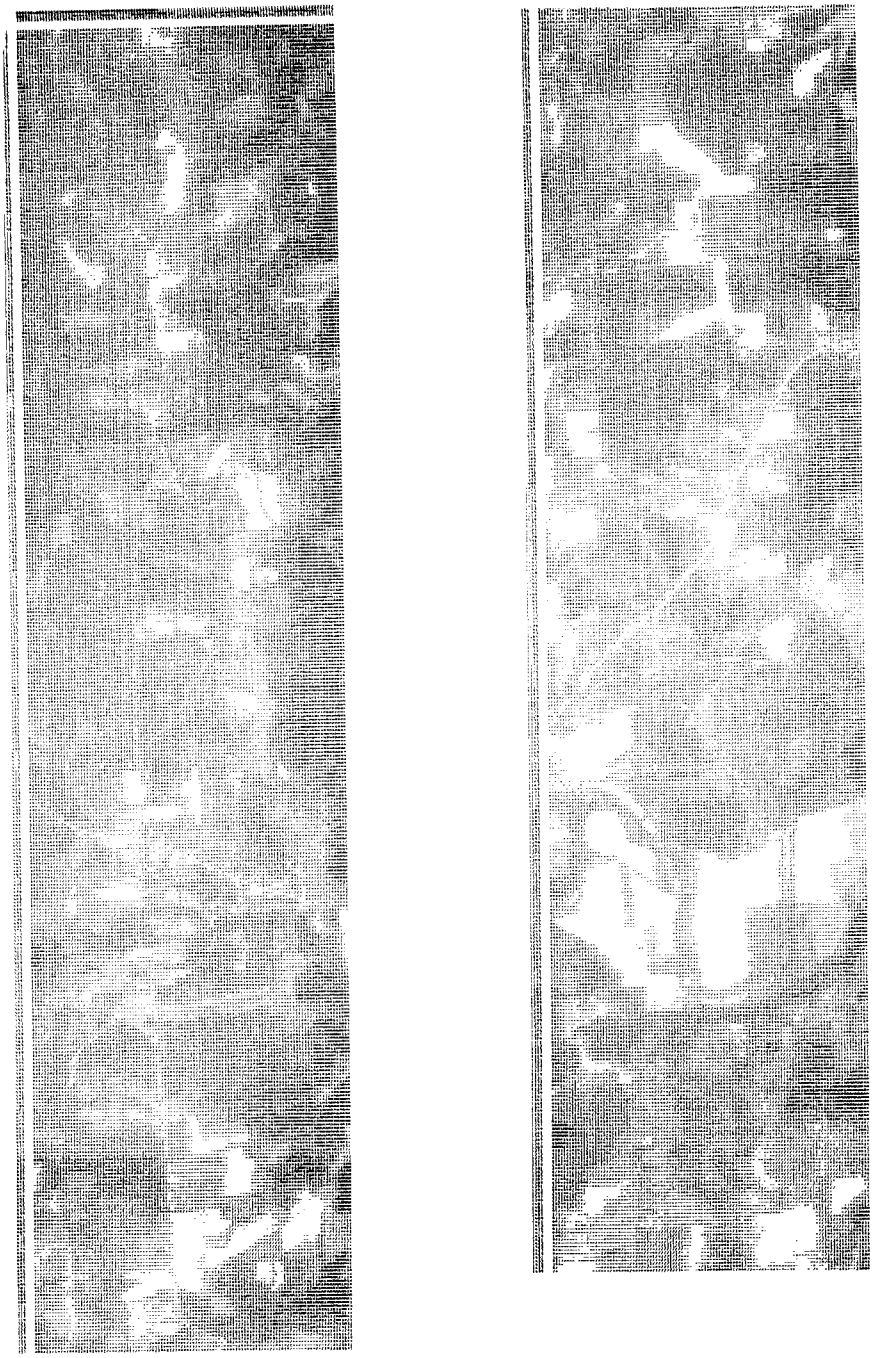

Upper half

Lower half

Figure 4.3. Line Printer Display of Unprocessed Array for Flight 218

Figure 4.4. Digital Display of Unprocessed Array for Flight 218

Uncertainties of 3 or 4 resolution elements were not unusual in assigning array positions to these 32 points.

In order to illustrate the geometric distortions inherent in data arrays obtained by multispectral scanners, planimetry was traced from the map sheets for both flight lines for comparison purposes. Figure 4.5 shows some of the planimetric features of flight 208 near the top of the flight line, and Figure 4.6 portrays planimetry from flight 218, near the bottom of the flight line. In these figures, a heavy solid line is used to denote roads, a lighter solid line is used to represent streams or ditches, and a light broken line represents fences. A comparison of these figures with those of Figures 4.2 and 4.4 will illustrate the deformations in the imagery which are perceivable to the human eye. The most readily apparent deformation is that due to the scan angle effects, and the different scales in the x and y directions. For example, the triangular area (arrow A in Figures 4.2 and 4.5) near the top of flight 208 formed by the intersecting roads and the stream cutting across them has been visibly deformed, showing a widening at the top and a resultant lessening of the inclination with which the stream cuts across the flight line in this area. Another good example of these deformations is found near the bottom of flight 208. Here an interstate highway cuts diagonally across the flight line (arrow B, Figure 4.2). Careful visual study reveals image deformation displacing the originally straight alignment of the roadway into a curved alignment. Also apparent, particularly on the display for flight 208 (Figure 4.2), is the perturbation due to changes in Y_c, the sensor Y position,

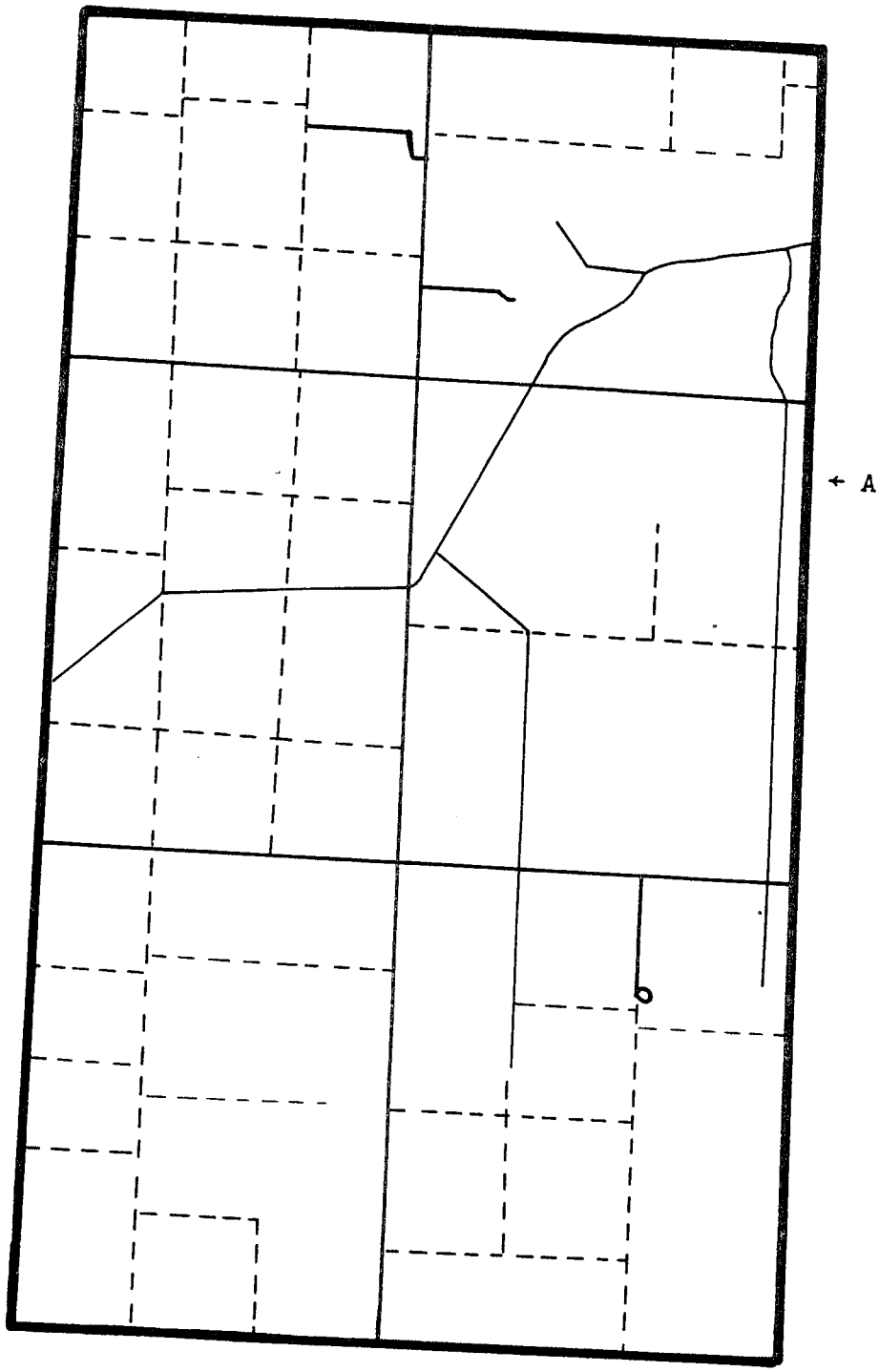

Figure 4.5. Partial Planimetric Map Near Top of Flight 208

Figure 4.6. Partial Planimetric Map Near Bottom of Flight 218

as evidenced by the departure of the central roadway from the straight alignment shown on the map sheet. Upon close inspection of the display for flight 208 (Figure 4.2), the effects of scan time and/or κ rotation down the flight line, is evidenced by the rotation of the cross roads and field boundaries. Scan angle deformation is also apparent in flight 218, near the river bend area. The river bend itself shows a visible spread due to these effects (arrow A, Figures 4.4 and 4.6). Also the road running diagonally across the flight line above the river upon close inspection shows a reduction in the inclination (arrow B, Figures 4.4 and 4.6).

4.2 Flow Chart for MSS Digital Data Analysis

Figure 4.7 illustrates the system for analysis of digital MSS data arrays which was used in this investigation. The flow chart shown displays a method of integrating the principles and mathematical techniques discussed in the previous chapter into a coherent and organized system for the analysis and restitution of digitally recorded multispectral scanner arrays. Referring to Figure 4.7, the first step in the procedure, after the desired control points have been chosen, is the digitization of map data for the control point coordinates, and contour information for subsequent assignment of element elevations. For this investigation, the digitization was carried out on a LARR-V cartesian coordinate digitizer at Purdue University. In the following, the coordinate axes of the digitizing equipment will be denoted U-V to differentiate them from the object space X-Y system, or the image x-y system.

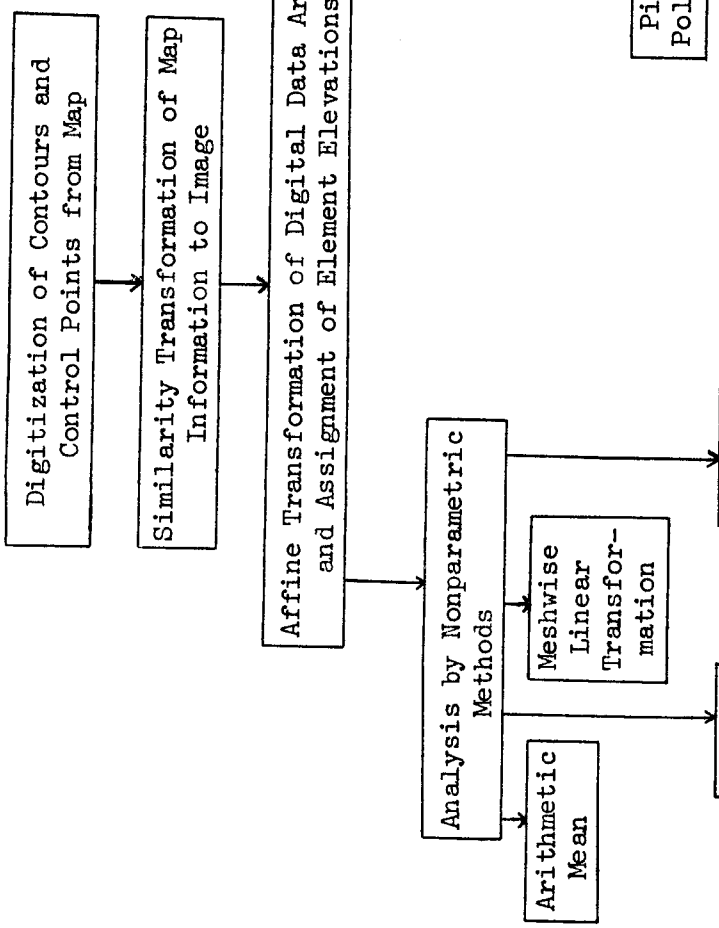

Figure 4.7. System for Analysis of MSS Digital Data Arrays

In Figure 4.8 is shown the operation of this digitization equipment. The material from which U-V coordinate values are to be digitized (in this case, the map sheet) is fastened upon a large flat bed. Points are located by the operator with a cursor operating along perpendicular U-V axes. The U-V coordinates under the cursor are instantaneously displayed upon a console shown in Figure 4.8 directly behind the operator. The U-V coordinate values of a point may be automatically recorded upon punched cards using the keypunch shown in the lower right foreground of Figure 4.8. This keypunch is interfaced with the digitizer, and the operator activates a relay when he is over a point for which he wants the U-V coordinate value recorded on cards.

For this investigation, the following steps were followed in the digitization of the map information.

1.) The map sheet was fastened upon the flat bed. An attempt was made to approximately align the direction of the flight line with the U axis of the digitizer.

2.) Universal Transverse Mercator (UTM) grid marks on the map edges were digitized, first along the map edge aligning more nearly to the digitizer U axis, then along the other edge. These 1000 m (3281 ft.) intervals could then be used to define an absolute scale to transform data arrays to ground system coordinates after the analysis and/or restitution has been accomplished.

3.) All reference point U-V coordinates were digitized in the order of their numbering.

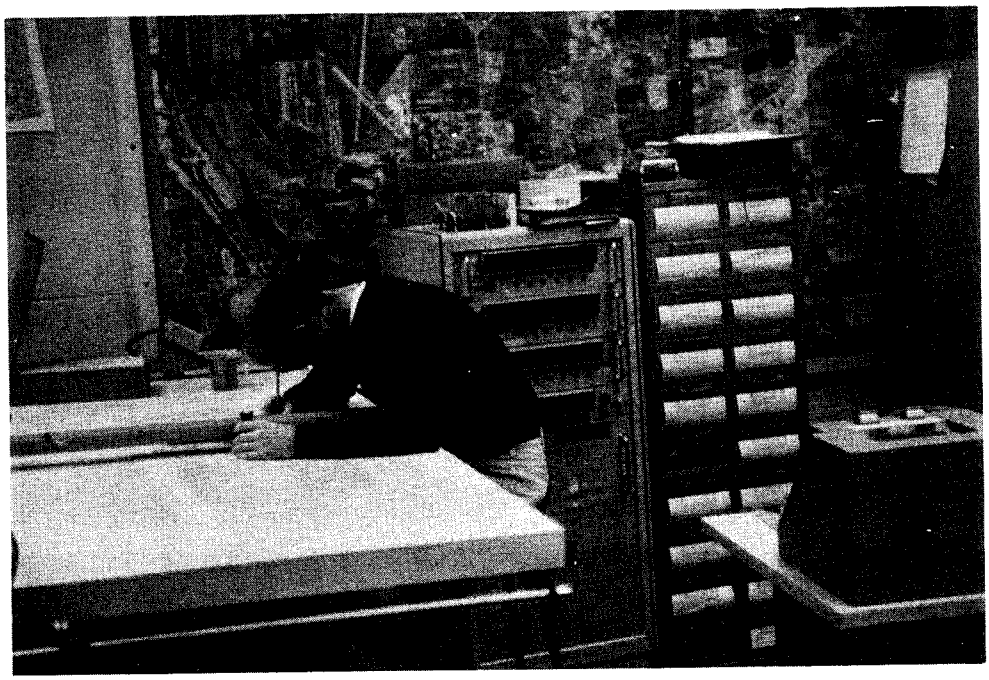

Figure 4.8. Digitization of Map Information

4.) Contour information was digitized. The method used was the contour following mode, in which selected contours were followed and U-V coordinates were digitized at random sample intervals along each contour. These values were recorded directly upon punched cards. Each card was formatted to record first a count index, representing the total number of contour points recorded previously for the contour being followed. Next, the elevation of the contour was recorded, followed by 8 values of U-V coordinates of 8 of the sample points digitized along the contour. Using this format, a total of about 1000 cards resulted for flight 208, and approximately 3000 cards were required for the more rugged terrain of flight 218.

After digitization of the map data, this information was transformed from the U-V digitizer system into a cartesian coordinate system at the image, or array scale. The transformation used to generate these scaled control and contour X-Y points was the well known conformal similarity transformation. The equations of the transformation are of the form

$$\begin{aligned} X &= \lambda(U \cos \phi + V \sin \phi) + X_o \\ Y &= \lambda(-U \sin \phi + V \cos \phi) + Y_o \end{aligned} \qquad (4.1)$$

in which X_o, Y_o are translations, ϕ is the rotation between the two systems, and λ is a scale factor. These four parameters were determined using least squares techniques, to bring the digitized map data to the same approximate scale and orientation as the digital

data arrays. All coordinates of the digitized map data were then transformed using Equation (4.1), and all subsequent steps were performed at image scale. Table 4.1 shows the values of the reference point positions for flight 208 after their transformation to image scale, and the line-column array positions for the corresponding points within the data array. Table 4.2 shows the reference point coordinates for flight 218. After these preliminary steps, the elements of the arrays, were transformed to the scaled control values using an affine transformation, and elevations were assigned to each element. Geometric analysis and restitution was then performed using the methods described in Sections 3.1 - 3.3. These steps in the flow chart are explained in more detail in the following sections.

4.3 Results of Elevation Assignment Algorithms

In Section 3.4, several possible methods of assigning elevations to elements within the data arrays were presented. Two of the possible methods were tested in this investigation. For flight 208, having flat terrain and hence relatively few digitized contour points, both the contour-scan and arithmetic mean nonparametric methods were attempted. For flight 218, having more rugged terrain and many more digitized contour points, only the contour-scan intersection method was done, for reasons which will be discussed subsequently.

As pointed out in Section 3.4.1, the affine transformation was used within the element elevation assignment program, to approximately

Table 4.1

Reference Point Coordinates for Flight 208

Control Points

Point Number	Transformed Map Position X	Transformed Map Position Y	Array Position Line (x)	Array Position Col (y)
3	209.3	47.1	215	26
7	210.8	164.6	208	187
8	352.9	47.0	356	29
11	442.1	47.6	447	27
13	559.6	47.9	564	26
15	593.9	105.9	595	104
17	677.4	106.0	679	103
18	612.3	194.2	611	218
20	793.6	106.7	798	105
22	903.7	49.6	909	27
24	908.8	164.9	907	186
25	964.6	106.7	965	106
28	1024.1	164.2	1024	185
29	1136.1	51.4	1139	31
30	1141.1	164.9	1138	187
31	1253.6	50.8	1254	30
34	1316.1	166.7	1310	189
38	1490.6	167.1	1479	194
40	34.7	104.6	30	97
43	57.9	192.6	45	215
44	91.8	46.9	93	21
47	152.2	104.9	153	105
54	325.4	104.8	324	107
55	325.7	164.0	321	188
63	443.3	104.6	447	104
64	444.0	193.9	443	218
66	499.0	105.2	502	103
68	502.3	193.6	501	218
71	624.1	46.7	630	26
72	727.7	164.9	726	186
74	734.5	47.4	741	27
75	846.8	48.6	854	27
77	850.9	164.3	852	187
83	1048.5	106.4	1051	105
89	1308.3	108.3	1305	107
92	1428.6	21.1	1426	1
94	1488.9	110.1	1482	116
97	1571.7	48.0	1568	33
100	1571.4	166.8	1565	195

Table 4.1, cont.

Check Points

Point Number	Transformed Map Position X	Y	Array Position Line (x)	Col (y)
1	92.5	105.2	90	102
2	179.7	47.1	185	26
4	209.7	75.0	212	62
5	210.5	105.4	212	105
6	92.9	132.6	88	141
9	353.7	69.1	355	64
10	354.5	105.3	355	106
12	443.6	165.2	443	186
14	560.4	105.8	564	104
16	677.1	47.3	681	26
19	792.4	48.4	801	28
21	795.2	164.2	795	185
23	905.8	106.6	908	105
26	1022.0	106.4	1024	106
27	1023.3	136.0	1024	148
32	1311.9	50.5	1310	30
33	1314.0	108.3	1309	107
35	1370.7	50.2	1370	27
36	1486.9	50.9	1484	33
37	1492.6	50.4	1490	33
39	1490.2	138.3	1482	157
41	35.9	162.9	28	179
42	63.5	75.5	62	58
45	122.2	77.0	122	64
46	123.0	104.8	121	105
48	152.6	134.0	149	148
49	180.5	74.9	184	62
50	181.3	104.9	182	106
51	210.4	134.2	210	148
52	268.7	164.3	263	189
53	325.0	46.9	326	29
56	384.9	164.6	384	188
57	404.6	46.7	410	27
58	397.2	164.6	396	187
59	412.9	47.1	418	27
60	412.9	75.0	418	62
61	414.0	164.7	415	187
62	442.5	75.0	447	60
65	453.9	104.7	457	104
67	500.7	134.8	503	146
69	530.8	105.3	535	104

Table 4.1, cont.

Check Points

Point Number	Transformed Map Position X	Y	Array Position Line (x)	Col (y)
73	764.5	105.4	764	104
76	848.8	106.0	851	105
78	879.2	134.8	880	148
79	879.6	164.4	879	186
80	936.3	106.2	936	106
81	1020.3	78.5	1025	64
82	1029.6	78.6	1032	65
84	1110.7	135.7	1110	149
85	1137.8	77.9	1138	65
86	1194.9	49.8	1198	29
87	1197.4	107.6	1198	107
88	1256.1	112.6	1253	117
90	1315.3	136.6	1310	150
91	1344.4	136.7	1339	150
93	1429.4	49.9	1425	31
95	1545.5	78.8	1541	71
96	1546.4	110.2	1538	120
98	1571.6	78.9	1566	74
99	1571.5	110.2	1566	120

Note: Check point 70 was omitted after a mistake in digitization for this point was discovered.

Table 4.2.

Reference Point Coordinates for Flight 218

Control Points

Point Number	Transformed Map Position X	Y	Array Position Line (x)	Col (y)
1	5.4	88.5	9	91
3	115.7	166.7	117	178
4	132.6	86.3	137	86
6	269.5	124.0	265	130
7	313.7	138.7	310	146
9	441.3	51.6	445	36
11	483.8	183.8	485	190
12	492.9	127.8	495	128
13	529.3	93.8	532	85
14	588.1	37.2	589	26
16	690.0	42.2	695	26
17	688.0	103.7	692	100
19	871.2	124.2	877	124
20	928.1	212.1	922	219
22	993.3	130.1	994	136
23	999.5	61.5	1001	52
24	1101.7	122.9	1099	131
25	1116.1	16.2	1122	12
28	1174.9	126.7	1171	134
29	1324.6	33.8	1325	24
30	1296.5	206.2	1289	213
32	1407.4	66.6	1409	57
33	1362.0	177.7	1358	189

Check Points

2	66.1	113.0	63	117
5	257.6	108.1	256	109
8	436.8	172.8	437	182
10	446.6	76.5	449	65
15	627.5	99.4	627	94
18	747.7	120.7	748	121
21	985.8	133.9	986	142
27	1121.3	106.8	1120	110
31	1367.5	64.5	1372	56

Note: Control point 26 was omitted after a mistake in digitization for this point was discovered.

transform the data arrays into the conformal system of the scaled control points. Parameters for this transformation were determined by least squares methods utilizing as input the scaled control point coordinates and the data array positions for the control points, as given in Tables 4.1 and 4.2. The flight lines were divided into sections, and an independent determination of the affine parameters was determined within each flight line section for the affine equations of the form

$$\begin{aligned} X &= A_o + A_1 x + A_2 y \\ Y &= B_o + B_1 x + B_2 y \end{aligned} \qquad (4.2)$$

Table 4.3 portrays the results of this least squares fit for flight 208. In this instance, the flight line was divided into five sections. Table 4.4 depicts the results of the analysis for flight 218, in which the flight line was segmented into four sections. The resulting standard deviations and variances are given in terms of array elements. The average ground size of such an element for the arrays tested is about 40 ft. diameter. This unit is often called a remote sensing unit, and is abbreviated rsu. Therefore, the statistical quantities given in such units reflect the accuracies of analysis methods in terms of the resolving power of the system, rather than absolute distances.

The pooled variance in these tables was computed as the summation for all sections divided by the summation of the degrees of freedom for all sections.

Table 4.3

Statistics from Affine Transformation for Flight 208

Section Number	1	2	3	4	5	Pooled*
Degrees of Freedom	14	14	12	12	16	68
A posteriori Estimate of Variance (rsu^2)	3.71	2.14	2.84	0.38	1.81	2.20
A posteriori Estimate of Standard Deviation (rsu)	1.93	1.46	1.69	0.61	1.34	1.48

Table 4.4

Statistics from Affine Transformation for Flight 218

Section Number	1	2	3	4	Pooled*
Degrees of Freedom	8	12	12	16	48
A posteriori Estimate of Variance (rsu^2)	5.91	7.18	10.35	12.26	9.45
A posteriori Estimate of Standard Deviation (rsu)	2.43	2.68	3.22	3.50	3.07

$$* \text{ pooled } \sigma^2 = \frac{\sum_{i=1}^{k} (\text{d.o.f.})_i \, (\sigma_i^2)}{\sum_{i=1}^{k} (\text{d.o.f.})_i} \quad \text{where k is number of sections}$$

The parameters thus generated were used within the element elevation assignment program to approximately fit the data arrays to the scaled control points. To test the suitability of this transformation, the analysis described in Section 3.4.1 must be performed. Ground slopes within flight 208 were very small, rarely exceeding 0.1, and the resultant allowable error for the affine transformation from Equation (3.53) is on the order of 12 resolution elements, even near the strip edges where the total scan angle approaches 38.5°. Clearly, the a posteriori reference standard deviations obtained from the adjustment yield values well within this limit. For flight line 218, ground slopes were much steeper, approaching 0.5 in some places within the flight line. Assuming the worst case, in which the maximum slope of 0.5 occurs at the maximum scan angle of 38.5°, the allowable error is 2.5 resolution elements. The resultant a posteriori pooled reference standard deviation for this flight line was 3.07 resolution elements. This means that after element elevations were assigned, and subsequent analysis was done, some of the residual error within flight line 218 would possibly be due to topographic relief effects because of errors in assignment of element elevations. These values however, represent the worst case. Over most of the flight line, allowable planimetric error would be larger than the 2.5 resolution elements given, and resulting relief displacement errors would be reduced. For scan angles less than 26.5° for example, the allowable planimetric error would be greater than 4 resolution elements.

In Figures 4.9 and 4.10 are shown typical profiles from each of the two flight lines from which an indication of the reliability of the height assignment algorithms may be gained. In Figure 4.9 is depicted a typical profile across the flight line for data array line 763 of flight 208. In this figure, the solid line represents a reference ground profile taken from the map sheet. The circle-dash combination represents the profile obtained by the contour-scan intersection method of element elevation assignment, and the dashed line represents the profile resulting from element elevation assignment using the arithmetic mean method. It should be noted that the elevations from the map are also subject to some error. The National Map Accuracy Standards for vertical map information state that 90% of the elevations interpolated from map contours shall be correct within 1/2 contour interval. For the relatively flat terrain in this flight line, the contour interval was 5 ft. (1.52 m) resulting in a 90% error of 2.5 ft. (0.76 m) and an approximate standard deviation of only 1.5 ft. (0.46 m) due to the map. It may be seen in Figure 4.9 that the profile from the map in almost all cases differs from that obtained by either of the elevation assignment methods by less than ten feet (3.05 m). In Figure 4.10, a similar portrayal of a typical scan line for flight 218 is shown. For this flight line, the map contour interval was 10 ft. (3.05 m) and elevation errors for points taken from the map were therefore 5 ft. (1.52 m) at the 90% level, for an approximate standard deviation of 3 ft. (0.92 m). Mismatches of up to 40 ft. (12.2 m) between the map profile

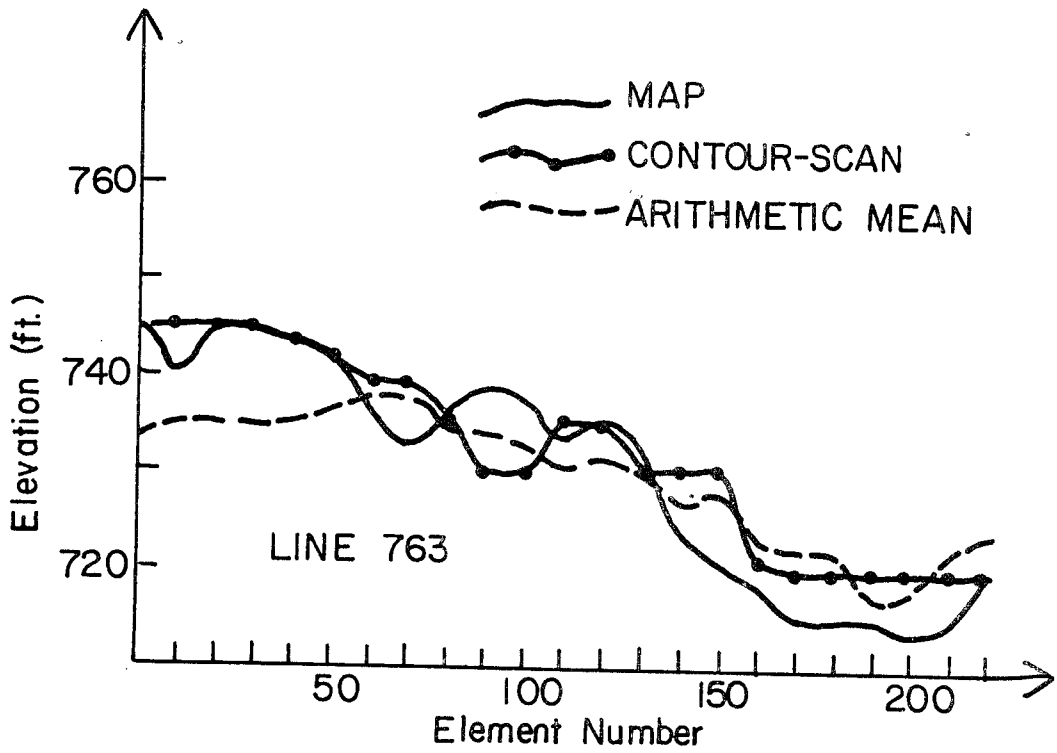

Figure 4.9. Typical Profile for Flight 208

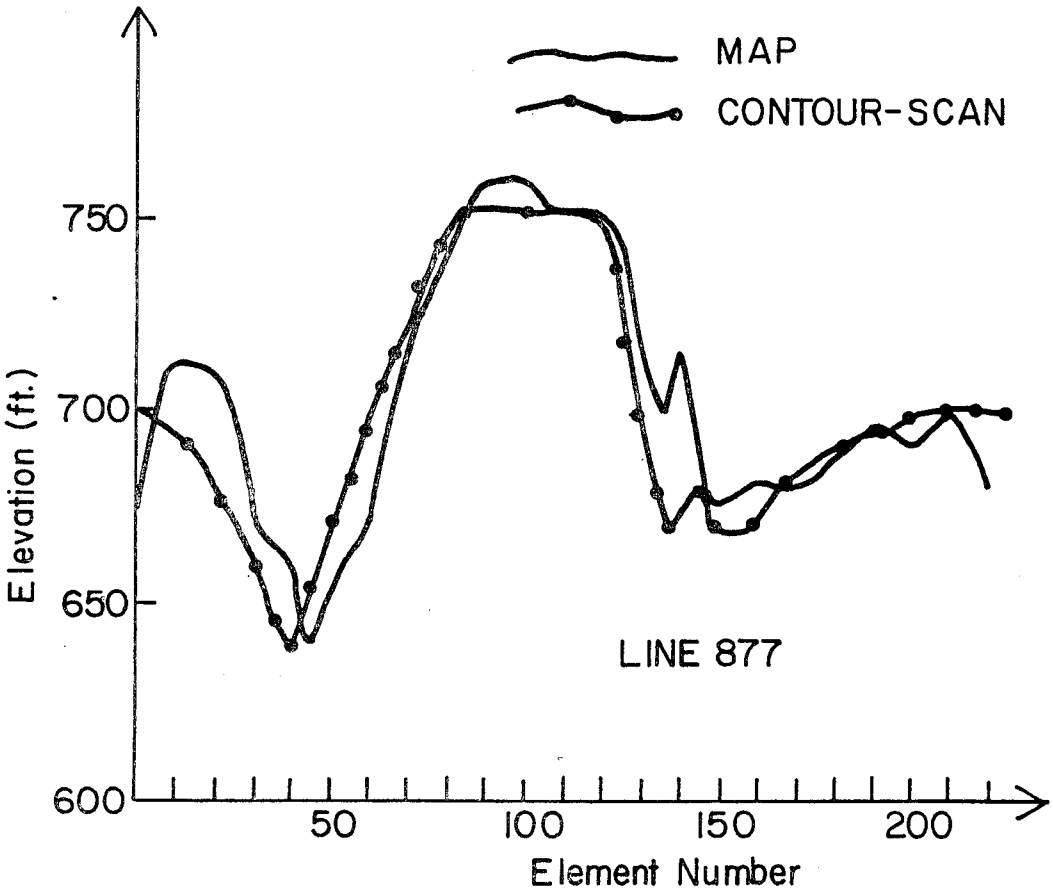

Figure 4.10. Typical Profile for Flight 218

and that obtained by element elevation assignment are seen to exist for short sections along the scan line. As will be shown subsequently, the allowable elevation assignment error for these flight lines is on the order of 60 feet. Thus, the maximum elevation assignment errors for these sample profiles (10 feet and 40 feet for flights 208 and 218, respectively) would result in planimetric errors of less than one resolution element.

A statistical test was performed to evaluate the sufficiency of the element elevations assigned. For this test, the elevations assigned to the reference point array locations by the element elevation assignment programs were compared with elevations for the corresponding points taken from the map sheet. The differences between elevations assigned from the programs and those taken from the map sheet were used as the data upon which to perform the statistical analyses. Table 4.5 gives the data generated for the control points of flight 208. In each case, the column noted as "Difference" shows the value obtained by subtracting the value taken from the map sheet from that assigned by the elevation assignment algorithm noted. Table 4.6 gives the same information for flight 218.

In order to evaluate the results of a statistical analysis, it is important to state the objectives and the desired results of such an analysis. First, it would be desired that the mean of the elevation differences be statistically near zero, in order that it may be stated that, on the average, the height assignment algorithms are assigning correct elevations. In addition it is desired that the variance, and the resulting standard deviation, be such

Table 4.5

Elevation Information for Flight 208

Control Point Number	A. Elevation from Map, in ft. (m)	B. Elevation Assigned by Contour-Scan, in ft. (m)	C. Difference, B-A in ft. (m)	D. Elevation Assigned by Arithmetic Mean, in ft. (m)	E. Difference, D-A in ft. (m)
3	695 (211.8)	695 (211.8)	0 (0)	696 (212.1)	1 (0.3)
7	705 (214.9)	705 (214.9)	0 (0)	705 (214.9)	0 (0)
8	709 (216.1)	710 (216.4)	1 (0.3)	710 (216.4)	1 (0.3)
11	708 (215.8)*	710 (216.4)	-2 (0.6)	710 (216.4)	2 (0.6)
13	706 (215.2)	709 (216.1)	3 (0.9)	710 (216.4)	4 (1.2)
15	685 (208.8)	695 (211.8)	10 (3.0)	696 (212.1)	11 (3.3)
17	704 (214.6)	705 (214.9)	1 (0.3)	704 (214.6)	0 (0)
18	719 (219.2)	720 (219.5)	1 (0.3)	715 (217.9)	-4 (-1.2)
20	715 (217.9)*	720 (219.5)	5 (1.5)	719 (219.2)	4 (1.2)
22	723 (220.4)	720 (219.5)	-3 (-0.9)	717 (218.5)	-6 (-1.8)
24	715 (217.9)*	715 (217.9)	0 (0)	715 (217.9)	0 (0)
25	718 (218.8)*	715 (217.9)	-3 (-0.9)	715 (217.9)	-3 (-0.9)
28	722 (220.1)	720 (219.5)	-2 (-0.6)	718 (218.8)	-4 (-1.2)
29	715 (217.9)	715 (217.9)	0 (0)	715 (217.9)	0 (0)
30	710 (216.4)*	720 (219.5)	10 (3.0)	710 (216.4)	0 (0)
31	721 (219.8)	724 (220.7)	3 (-0.9)	722 (220.1)	1 (0.3)
34	731 (222.8)	720 (219.5)	-11 (-3.3)	721 (219.8)	-10 (3.0)
38	700 (213.4)*	711 (216.7)	11 (3.3)	713 (217.3)	3 (-0.9)
40	751 (228.9)	755 (230.1)	4 (1.2)	751 (228.9)	0 (0)
43	751 (228.9)	746 (227.4)	-5 (1.5)	753 (229.5)	2 (0.6)
44	741 (225.9)	745 (227.1)	4 (1.2)	731 (222.8)	-10 (3.0)
47	743 (226.5)	740 (225.6)	-3 (-0.9)	744 (226.8)	1 (0.3)
54	745 (227.1)	745 (227.1)	0 (0)	744 (226.8)	-1 (-0.3)
55	741 (225.9)	740 (225.6)	-1 (-0.3)	743 (226.5)	2 (0.6)
63	733 (223.4)	731 (222.8)	-2 (-0.6)	732 (223.1)	-1 (-0.3)
64	729 (222.2)*	730 (222.5)	-2 (-0.6)	727 (221.6)	-2 (-0.6)

Table 4.5, cont.

Control Point Number	A. Elevation from Map, in ft. (m)	B. Elevation Assigned by Contour-Scan, in ft. (m)	C. Difference, B-A in ft. (m)	D. Elevation Assigned by Arithmetic Mean, in ft. (m)	E. Difference, D-A in ft. (m)
66	730 (222.5)	730 (222.5)	0 (0)	730 (222.5)	0 (0)
68	725 (221.0)	730 (222.5)	5 (1.5)	725 (221.0)	0 (0)
71	731 (222.8)	730 (222.5)	-1 (-0.3)	730 (222.5)	-1 (-0.3)
72	723 (220.4)	730 (222.5)	7 (2.1)	726 (221.3)	3 (-0.9)
74	731 (222.8)	725 (221.0)	-5 (-1.5)	730 (222.5)	-1 (-0.3)
75	729 (222.2)	725 (221.0)	-4 (-1.2)	728 (221.9)	-1 (-0.3)
77	727 (221.6)	725 (221.0)	-2 (-0.6)	725 (221.0)	-2 (-0.6)
83	730 (222.5)*	725 (221.0)	-5 (-1.5)	730 (222.5)	0 (0)
89	732 (223.1)	730 (222.5)	-2 (-0.6)	730 (222.5)	2 (0.4)
92	740 (225.6)*	740 (225.6)	0 (0)	740 (225.6)	0 (0)
94	741 (225.9)	740 (225.6)	-1 (-0.3)	740 (225.6)	1 (0.3)
97	729 (222.2)	735 (224.0)	6 (1.8)	731 (222.8)	2 (0.6)
100	731 (222.8)*	736 (224.3)	5 (1.5)	731 (222.8)	0 (0)

* These values were noted on the map as spot elevations. Other values were obtained by interpolating between contours on the map.

Resulting Statistics

	Data Set C	Data Set E
Degrees of freedom	38	38
Mean, in ft. (m)	+0.56 (+.17)	-0.15 (-0.4)
Variance	20.73	12.77

Table 4.6

Elevation Information for Flight 218

Control Point Number	A. Elevation from Map, in ft. (m)	B. Elevation Assigned by Contour-Scan, in ft. (m)	C. Difference B-A in ft. (m)
1	595 (181.4)	599 (182.6)	4 (1.2)
3	559 (170.4)	625 (190.5)	66 (20.1)
4	587 (178.9)	609 (185.6)	22 (6.7)
6	615 (187.4)	599 (182.6)	-16 (-4.9)
7	580 (176.8)	599 (182.6)	19 (5.8)
9	705 (214.9)*	699 (213.1)	-6 (-1.8)
11	561 (171.0)*	574 (175.0)	13 (4.0)
12	587 (178.9)	599 (182.6)	12 (3.7)
13	673 (205.1)*	663 (202.1)	-10 (-3.0)
14	593 (180.7)*	614 (187.1)	21 (6.4)
16	715 (217.9)	690 (210.3)	-25 (-7.6)
17	725 (221.0)	687 (209.4)	-38 (-11.6)
19	759 (231.3)	748 (228.0)	-11 (-3.4)
20	660 (201.2)	649 (197.8)	-11 (-3.4)
22	650 (198.1)	649 (197.8)	-1 (-0.3)
23	581 (177.1)	599 (182.6)	18 (5.5)
24	580 (176.8)	574 (174.9)	-6 (-1.8)
25	543 (165.5)	550 (167.6)	7 (2.1)
28	633 (192.9)	625 (190.5)	-8 (-2.4)
29	725 (221.0)	717 (218.5)	-8 (-2.4)
30	632 (199.6)	550 (167.6)	-82 (-25.0)
32	552 (168.2)	576 (175.6)	24 (7.3)
33	613 (186.8)*	549 (167.3)	-64 (-19.5)

* These values were noted on the map as spot elevations. Other values were obtained by interpolating between contours on the map.

Resulting Statistics

	Data Set C
Degrees of freedom	22
Mean, in ft. (m)	-3.48 (-1.06)
Variance	924.1

that the great majority of the data array positions would be within the allowable height assignment error as derived in Section 3.4.1. Referring to Figure 3.5 and Equation (3.51), it may be seen that the minimum value of this allowable error would occur near the flight line edge, at a scan angle of 38.6°. At this scan angle, with a flying height of 5000 ft. (1.52 km), the ground size of a resolution element in the Y direction is approximately 50 ft. (14.9 m) and the resulting allowable height assignment error is approximately 61 ft. (18.8 m). At a scan angle of 20°, the resulting ground size of a resolution element is 34 ft. (10.4 m) and the resulting allowable height assignment error is 93 ft. (28.5 m). Thus, it may be seen that 60 ft. would represent a conservative value, the square of which yields a variance against which to test the results from the height assignment algorithms.

A complete statistical analysis of flight 208 was not performed. A cursory inspection of the differences between the assigned element elevations and those from the map sheet (data sets C and E, Table 4.5) reveals that no value in the data even approaches the minimum acceptable value of 60 feet. Hence for this flight line the elevations may be assumed to be assigned with suitable accuracy, using either the contour-scan or arithmetic mean method. Due to its computational efficiency, the contour-scan method was utilized in subsequent analysis and restitution computations when element elevations were required.

For flight 218, the data from which statistical quantities were computed for testing were the differences between the elevations

assigned and those taken from the map (data set C, Table 4.6). As a first step, the data were tested for normality, in order that subsequent tests upon the mean and the variance would be valid. The Shapiro-Wilk test for small samples was used [108]. In this test a statistic, denoted w, is computed and compared with tabular values published in that reference in order to test the hypothesis that the data are normally distributed against the alternative that the data are not normally distributed. When the computed w from the data is below the appropriate tabulated value, then non-normality of the data is indicated. The value of w calculated from the data of flight 218 was 0.925. The value of w is computed as

$$w = \frac{b^2}{s.s.}$$

in which s.s. represents the sum of squares of the data values. The quantity b is calculated by first ordering the data in ascending order (d_1, d_2, . . . d_n where d_1 is the smallest value and d_n the largest data value). If n is an even integer, then a parameter k is defined such that n = 2k and b is computed with

$$b = \sum_{i=1}^{k} a_{n-i+1} (d_{n-i+1} - d_i)$$

where the a values are coefficients tabulated in the reference. If n is an odd integer then the central data value is omitted from the set and k is defined such that n = 2k + 1 and the expression for b becomes

$$b = a_n(d_n - d_1) + \ldots + a_{k+2}(d_{k+2} - d_k)$$

where the value of d_{k+1}, the sample median, does not enter the computation of b. The tabular values for the appropriate data sample size (23) is 0.914 for an α level of 0.05 and 0.928 for an α level of 0.10. The hypothesis that the data are normal may then be accepted at an α level of 0.05.

Next, the mean value of these data was computed and tested. The null hypothesis formulated was that the mean was equal to zero, versus the alternate hypothesis of a non-zero mean. The hypothesis was tested at an α level of 0.05. A t statistic was calculated from the data and found to be -0.549. The tabulated value for $t_{.975,22}$ was found to be 2.074. Thus, for a two-sided test, the null hypothesis would be rejected only if the t value calculated was greater than 2.074 or less than -2.074, and the hypothesis of zero mean was accepted.

The final test was performed upon the variance. This represents an important step, since it is here that the adequacy of the height assignment is determined. For this step, the sample variance of 924.1 calculated from the data was compared with the allowable height assignment variance assumed as 3600 (from the allowable height assignment error of 60 feet). It was assumed that the degrees of freedom associated with the allowable height assignment error is infinite. The null hypothesis was formulated that the variance calculated from the data was less than or equal to 3600, versus the alternative that this variance is larger than 3600. The hypothesis may then be tested using a χ^2 statistic, or an F statistic having infinite degrees of freedom in the denominator. A χ^2 statistic was calculated

from the data and found to be 5.65. The test was performed at an α level of 0.05, for which the tabulated value of $\chi^2_{.95,22}$ was found to be 33.9. The null hypothesis would be rejected only if the χ^2 value calculated from the data was greater than the value tabulated, and the hypothesis was accepted.

The net result of this test is that the elevation data assigned to the element array positions may reasonably be assumed to lie within 60 ft. of the true value. The resulting planimetric error due to elevation assignment errors will then be less than one resolution element. With this knowledge, attention is directed in the next section to the problem of testing the various methods of analysis and restitution previously presented.

4.4 Comparison of Analysis Methods

The purpose of this section is to systematically test the analysis and restitution methods presented in Chapter 3, when operating upon the actual data arrays chosen. For each method, the assumptions made for each analysis will be presented, numerical data resulting from the analysis will be given, and meaningful differences in the results under different assumptions will be pointed out.

4.4.1 Collinearity Equations

In testing this method a two step procedure was carried out in which control points from the map and the corresponding array positions were used to estimate parameters of the exterior orientation, followed by computation of coordinates of check points withheld from the adjustment. This results in two useful statistics.

1.) The a posteriori reference variance which is computed from the adjustment itself.

2.) A "positional check variance", based upon the variances in the X and Y directions computed from the check points.

For this purpose the square of the circular standard error as defined in [113] was used. A conservative estimate for this value c, is given in this reference as $c = 0.5(\sigma_x + \sigma_y)$. These quantities were assigned n - 1 degrees of freedom, where n is the number of check points, and were statistically tested for significant differences, in order to ascertain which of the assumed functional forms produced better results.

For each flight line, several cases with the following functional assumptions were performed, and the results from each were compared.

Case C1: For this case, the functional forms for the exterior orientation parameters were of the form

$$\begin{aligned} X_c &= A_X + B_X x \\ Y_c &= A_Y + B_Y x \\ Z_c &= A_Z + B_Z x \\ \kappa &= A_\kappa + B_\kappa x \\ \phi &= 0 \\ \omega &= 0 \end{aligned} \qquad (4.3)$$

In which the recoverable orientation elements are assumed as linear functions of x within a flight line section.

Case C2: For this case, functional forms are assumed to be

$$\begin{aligned} X_c &= A_X + B_X\, x + C_X\, x^2 \\ Y_c &= A_Y + B_Y\, x + C_Y\, x^2 \\ Z_c &= A_Z + B_Z\, x + C_Z\, x^2 \\ \kappa &= A_\kappa + B_\kappa\, x + C_\kappa\, x^2 \\ \phi &= 0 \\ \omega &= 0 \end{aligned} \tag{4.4}$$

These polynomials were used to investigate the usefulness of non-linear variations of orientation elements within a flight line section.

Case C3: For this case, an attempt was made to assume polynomial forms which would correct for non-linear effects within a section, and retain computational efficiency for the later element by element transformation of the arrays. The functional forms assigned here were:

$$\begin{aligned} X_c &= A_X + B_X\, x + C_X\, x^2 \\ Y_c &= A_Y + B_Y\, x + C_Y\, x^2 \\ Z_c &= A_Z + B_Z\, x \\ \kappa &= A_\kappa \\ \phi &= 0 \\ \omega &= 0 \end{aligned} \tag{4.5}$$

Using these polynomials, the intent was to model the non-linear effects within each section using non-linear functions which affect most directly the element positions, i.e. X_c, Y_c. The κ term is modeled as a constant within each section in order to avoid the

re-evaluation of trigonometric functions for each scan line. Note here that only a linear form was assumed to model the flying altitude. Experience gained during the investigation showed that the addition of an x^2 term in the polynomial used to model this element produced negligible improvement over the case using the functional form shown.

Case C4: In this case the following polynomial forms were assumed:

$$\begin{aligned} X_c &= A_X + B_X\, x + C_X\, x^2 \\ Y_c &= A_Y + B_Y\, x + C_Y\, x^2 \\ Z_c &= A_Z + B_Z\, x \\ \kappa &= A_\kappa + B_\kappa\, x \\ \phi &= 0 \\ \omega &= 0 \end{aligned} \tag{4.6}$$

The purpose here was to test if a significant difference could be detected by linear modeling of the κ term over the computationally more efficient model in which κ is assumed constant for the flight line (Case C3).

For each of the cases given above, three different procedures were used. The adjustment and checking was done first treating the entire flight line as a unit. That is, it was assumed that a single set of parameters was valid for the entire length of the flight line. Then the flight line was treated in two sections, in which a separate set of parameters was solved for in each section. For this mode, the flight line was divided into sections each about half the length of the flight line. As a third case, the flight

line was segmented into thirds and separate parameter sets computed for each of the three sections. For the instances in which the flight line was divided into sections, the constraints of Equation set (3.39) were enforced at the section boundaries.

A summary of the results for flight 208 is shown in Table 4.7. For each case, the total number of parameters is given, and the number of degrees of freedom for the adjustment. The reference variance resulting from the adjustment is next shown. This reference variance is a unitless quantity which, when multiplied by the assumed a priori variances of the observations will result in a posteriori estimates of these variances, as indicated by the least squares adjustment. For flight line 208, the a priori estimates of variance assumed were 1.0 for the scaled control points from the map, and 2.25 for the corresponding array positions taken from the line printer display. Table 4.8 shows the corresponding information for flight 218. For this flight line, the a priori estimates of variance on the control points were 1.0 for the scaled X-Y map coordinates and 6.25 for the corresponding x-y array positions.

The units for the standard deviations are in terms of elements within the data arrays, or remote sensing units (rsu). The estimates of standard deviation taken for the digitized map control points were based upon the National Map Accuracy Standards. The standards state that 90% of all "well defined" points plotted fall within 1/50 in. (0.5 mm) of their true position. Assuming equal errors in X and Y, the component 90% error estimates would be $E_X = E_Y = E/\sqrt{2}$ where E_X, E_Y are the 90% errors in X and Y, and E is the positional

Table 4.7

Statistics from Collinearity Analysis of Flight 208
(60 Check Points)

		Number of Sections		
		1	2	3
Case C1:	Number of Parameters	8	16	24
	Degrees of Freedom	70	66	62
	Reference Variance	2.58	1.14	0.96
	Check Variance x in rsu^2(d.o.f. = 59)	9.10	3.05	2.40
	Check Variance y in rsu^2(d.o.f. = 59)	4.55	4.04	3.41
	Positional Check Variance in rsu^2	6.63	3.53	2.88
Case C2:	Number of Parameters	12	24	36
	Degrees of Freedom	66	58	50
	Reference Variance	1.10	0.78	0.59
	Check Variance x in rsu^2(d.o.f. = 59)	2.48	2.27	2.03
	Check Variance y in rsu^2(d.o.f. = 59)	4.13	2.81	1.86
	Positional Check Variance in rsu^2	3.25	2.53	1.94
Case C3:	Number of Parameters	9	18	27
	Degrees of Freedom	69	64	59
	Reference Variance	1.14	0.86	0.65
	Check Variance x in rsu^2(d.o.f. = 59)	2.63	2.53	2.21
	Check Variance y in rsu^2(d.o.f. = 59)	4.05	2.81	1.90
	Positional Check Variance in rsu^2	3.29	2.67	2.06
Case C4:	Number of Parameters	10	20	30
	Degrees of Freedom	68	62	56
	Reference Variance	1.10	0.81	0.57
	Check Variance x in rsu^2(d.o.f. = 59)	2.56	2.45	2.08
	Check Variance y in rsu^2(d.o.f. = 59)	4.06	2.82	1.91
	Positional Check Variance in rsu^2	3.27	2.64	1.99

Table 4.8

Statistics from Collinearity Analysis of Flight 218
(9 Check Points Only)

		Number of Sections		
		1	2	3
Case C1:	Number of Parameters	8	16	24
	Degrees of Freedom	38	34	30
	Reference Variance	1.39	0.98	0.87
	Check Variance x in rsu^2(d.o.f. = 8)	7.30	6.59	7.30
	Check Variance y in rsu^2(d.o.f. = 8)	4.80	3.31	1.89
	Positional Check Variance in rsu^2	5.98	4.81	4.15
Case C2:	Number of Parameters	12	24	36
	Degrees of Freedom	34	26	18
	Reference Variance	1.08	0.70	0.48
	Check Variance x in rsu^2(d.o.f. = 8)	6.69.	15.51	17.86
	Check Variance y in rsu^2(d.o.f. = 8)	3.64	1.63	0.94
	Positional Check Variance in rsu^2	5.04	6.80	6.75
Case C3:	Number of Parameters	9	18	27
	Degrees of Freedom	37	32	27
	Reference Variance	1.04	0.79	0.71
	Check Variance x in rsu^2(d.o.f. = 8)	7.55	9.92	8.69
	Check Variance y in rsu^2(d.o.f. = 8)	3.78	1.91	1.35
	Positional Check Variance in rsu^2	5.50	5.13	4.22
Case C4:	Number of Parameters	10	20	30
	Degrees of Freedom	36	30	24
	Reference Variance	1.06	0.78	0.65
	Check Variance x in rsu^2(d.o.f. = 8)	6.74	9.12	9.44
	Check Variance y in rsu^2(d.o.f. = 8)	3.78	1.91	1.34
	Positional Check Variance in rsu^2	5.15	4.84	4.47

error given by the accuracy standards. The resulting standard deviation estimates in X and Y then become approximately .008 in. (0.2 mm) each. The resulting ground scale distance when these numbers are divided by the 1:24000 scale of the U.S.G.S. 7 1/2 minute quadrangle maps used is about 10 ft. (3.1 m). This is on the order of one half the ground size of a data array element at nadir. However, many of the map points digitized were not "well defined", as described in the accuracy standards. A value of 1 rsu was therefore assigned for the a priori estimates of standard deviation for map coordinates. The a priori standard deviation for corresponding data array positions were based upon the difficulty found in assigning these positions within the data arrays. Thus, for flight 208, standard deviation estimate of 1.5 rsu (variance 2.25) was chosen, and for the more difficult flight 218, a standard deviation of 2.5 rsu (variance 6.25) was chosen.

In order to compare the accuracies obtained for the cases tested, tables of F statistics were computed based upon the a posteriori reference variances obtained from the adjustments, and the resulting positional check variances. These F statistics were computed as ratios of resulting variances between the various cases. Table 4.9 shows the resulting F statistics formed by the quotient of the a posteriori reference variances for the various cases tested for flight 208. As an example the value 2.26 in the second row, first column of Table 4.9 represents the ratio of the a posteriori reference variance of 2.58 obtained in Case C1 treating the entire flight line as a unit, divided by the a posteriori reference variance of 1.14

Table 4.9

Tabulation of F Statistics for Flight 208 Formed from Reference Variances from Collinearity Analysis

		Case C1			Case C2			Case C3			Case C4		
		Number of Sections											
		1	2	3	1	2	3	1	2	3	1	2	3
Case C1	1	1.00											
	2	2.26*	1.00										
	3	2.69*	1.19	1.00									
Case C2	1	2.34*	1.04	1.14	1.00								
	2	3.31*	1.46	1.23	1.41	1.00							
	3	4.37*	1.93*	1.63*	1.86*	1.32	1.00						
Case C3	1	2.26*	1.00	1.19	1.04	1.46	1.93*	1.00					
	2	3.00*	1.32	1.12	1.28	1.10	1.46	1.32	1.00				
	3	3.97*	1.75*	1.48	1.69*	1.20	1.10	1.75*	1.32	1.00			
Case C4	1	2.34*	1.04	1.14	1.00	1.41	1.86*	1.04	1.28	1.69*	1.00		
	2	3.18*	1.41	1.18	1.36	1.04	1.37	1.41	1.06	1.25	1.36	1.00	
	3	4.52*	2.00*	1.68*	1.93*	1.37	1.03	2.00*	1.51	1.14	1.93*	1.42	1.00

* Denotes values which are statistically significant at an α level of .05.

obtained for the same functional assumptions (Case C1) but dividing the flight line into two approximately equal sections. The asterisk opposite this value indicates a significant difference between these variances. Therefore, significant improvement is noted for this data array if linear assumptions are made for the functions of exterior orientation and the flight line is divided into two sections over the case in which linear functions are assumed and the flight line is treated as a single unit. Table 4.10 tabulates the F statistics resulting between cases tested if the positional check variances are used to form the values. Tables 4.11 and 4.12 show the resulting F statistics obtained in this manner for flight 218.

Based upon the information in these tables, several facts may be pointed out.

1.) In general, in order to discern statistically significant improvement over the linear assumptions of case C1, a combination of higher order assumptions was necessary, coupled with a division of the flight line into three sections.

2.) In general, no significant difference was noted between Case C2 and Case C3. This suggests that the computationally efficient model of Case C3 is adequate for non-linear effects. For the arrays tested then, modeling of Z_c and κ by second order functions resulted in no statistical improvement over modeling Z_c as a linear function and κ as a constant value.

3.) No statistically significant difference was noted between Case C3 and Case C4, suggesting that for the arrays tested,

Table 4.10

Tabulation of F Statistics for Flight 208
Formed from Positional Check Variances from Collinearity Analysis

		Case C1			Case C2			Case C3			Case C4		
		Number of Sections											
		1	2	3	1	2	3	1	2	3	1	2	3
Case C1	1	1.00											
	2	1.88*	1.00										
	3	2.36*	1.22	1.00									
Case C2	1	2.04*	1.08	1.13	1.00								
	2	2.62	1.39	1.14	1.28	1.00							
	3	3.41*	1.81*	1.48	1.67*	1.30	1.00						
Case C3	1	2.06*	1.07	1.15	1.02	1.30	1.70*	1.00					
	2	2.48*	1.32	1.08	1.22	1.05	1.37	1.23	1.00				
	3	3.23*	1.72*	1.40	1.59*	1.23	1.06	1.60*	1.30	1.00			
Case C4	1	2.03*	1.08	1.13	1.00	1.29	1.68*	1.01	1.22	1.59*	1.00		
	2	2.52*	1.34	1.10	1.24	1.04	1.35	1.25	1.01	1.28	1.25	1.00	
	3	3.32*	1.77*	1.45	1.63*	1.27	1.03	1.65*	1.34	1.03	1.64*	1.33	1.00

Number of Sections

* Denotes values which are statistically significant at an α level of .05.

Table 4.11

Tabulation of F Statistics for Flight 218 Formed from Reference Variances from Collinearity Analysis

		Case C1			Case C2			Case C3			Case C4		
		Number of Sections											
		1	2	3	1	2	3	1	2	3	1	2	3
Case C1	1	1.00											
	2	1.42	1.00										
	3	1.60	1.12	1.00									
Case C2	1	1.29	1.10	1.24	1.00								
	2	1.98*	1.40	1.24	1.54	1.00							
	3	2.89*	2.04	1.81	2.25*	1.46	1.00						
Case C3	1	1.34	1.06	1.19	1.04	1.49	2.17	1.00					
	2	1.76*	1.24	1.10	1.37	1.13	1.64	1.32	1.00				
	3	1.96*	1.38	1.22	1.52	1.01	1.48	1.46	1.11	1.00			
Case C4	1	1.31	1.08	1.22	1.02	1.51	2.21*	1.02	1.34	1.49	1.00		
	2	1.78	1.26	1.11	1.38	1.11	1.62	1.33	1.01	1.10	1.36	1.00	
	3	2.14*	1.51	1.34	1.66	1.08	1.35	1.60	1.22	1.09	1.63	1.20	1.00

* Denotes values which are statistically significant at an α level of .05.

Table 4.12

Tabulation of F Statistics for Flight 218
Formed from Positional Check Variances from Collinearity Analysis

		Case C1			Case C2			Case C3			Case C4		
	Number of Sections	1	2	3	1	2	3	1	2	3	1	2	3
Case C1	1	1.00											
	2	1.24	1.00										
	3	1.44	1.16	1.00									
Case C2	1	1.19	1.05	1.22	1.00								
	2	1.14	1.41	1.64	1.35	1.00							
	3	1.13	1.40	1.62	1.34	1.01	1.00						
Case C3	1	1.09	1.14	1.32	1.09	1.24	1.23	1.00					
	2	1.17	1.07	1.24	1.02	1.32	1.31	1.07	1.00				
	3	1.42	1.14	1.02	1.20	1.61	1.60	1.30	1.22	1.00			
Case C4	1	1.16	1.07	1.24	1.02	1.32	1.31	1.07	1.00	1.22	1.00		
	2	1.24	1.01	1.17	1.04	1.40	1.39	1.14	1.06	1.15	1.06	1.00	
	3	1.34	1.08	1.08	1.13	1.52	1.51	1.23	1.15	1.06	1.15	1.08	1.00

assuming κ to be a constant throughout the flight line is practical.

4.) For flight 208, having small terrain elevation differences and a large number of control points, Tables 4.9 and 4.10 reveal a statistically significant improvement in the three section breakdown as compared with treating the entire flight line as a single section regardless of the analytical model. This suggests that, for flights having sufficient control and low terrain relief differences, adequate segmenting of the flight line should take precedence over the use of more complicated analytical models.

5.) As shown in Table 4.12, no significant differences between the various cases were obtained based upon the check variances for flight 218. This was expected since the degrees of freedom for these variances was quite small (8).

6.) Examination of Table 4.8 points out a danger associated with modeling the exterior orientation elements using a large number of parameters. For this flight line (218) having relatively few control points, it may be seen that when the higher order assumptions are made to model exterior orientation elements, combined with segmenting the flight line, the positional check variance actually increases over those cases having fewer parameters. This indicates that unless many control points are available, the more highly non-linear interpolations may be misleading and dangerous. Although these combinations result in lower reference

variances from the adjustment, the actual measure of the validity of the interpolation, the positional check variance, increases, due mainly to the relatively small degrees of freedom.

In summary, the analysis of the data from the two flight lines tested suggests that linear modeling of exterior orientation elements (Case C1) coupled with segmentation of the flight line represents a modeling method which avoids the problems discussed in 6. above. However, the functional forms of Case C3 are recommended. This combination of polynomials represents a computationally efficient method of accounting for non-linear behaviour in the data, and suitably avoids the problems of overparameterization discussed in 5. above. This case also results in less computation than for Case C1, since the trigonometric functions in the collinearity need be evaluated only once for each flight line section. It should be emphasized that the conclusions drawn and recommendations made are valid only for the two flight lines tested. Additional testing of arrays generated under varying conditions is necessary before firm conclusions may be drawn for digital MSS arrays in general.

Similar to the collinearity, the piecewise polynomial formulation represents another "parametric" method suggested for use in restituting MSS digital data arrays. In the next section, test cases for this method and results of their application to the data arrays chosen will be presented.

4.4.2 Piecewise Polynomials

To test the suitability of the use of piecewise polynomials in analysis and restitution of digital MSS data arrays, the polynomial forms of Section 3.2.2 were used. The data arrays were not resampled, but were used directly as they came from the digitizing equipment. As with the collinearity formulation, each polynomial form chosen was tested as the mathematical model, treating the entire flight line as one unit, in two approximately equal sections, and in three approximately equal sections. The constraints of Equations (3.38) were invoked at section interfaces. The arrays were roll stabilized, so that $\omega = 0$ was assumed, and the effect of ϕ was assumed incorporated within the X_c variation.

As previously mentioned in Section 3.2.3, the formulation of piecewise polynomials will yield results identical to the collinearity equations if the trigonometric series for tan θ is taken to a sufficient number of terms, and if the coefficients of the polynomials are estimated using the same least squares models as was used to estimate the parameters of the collinearity equations.

As a test of this supposition, the case was investigated in which the orientation elements were assumed to be approximated by second order polynomials for the entire length of flight line 218. This would represent Case C2, with the flight line as a single unit, in the previous section. Polynomials were generated similar to those of (3.20) except that tan θ was represented using additional terms in the series expansion beyond the first two represented in

(3.20). This formulation was programmed using the least squares model of combined observations and parameters. The a priori estimates of variance for the x, y, X, Y observed quantities were assigned the same values as were assumed for the collinearity formulation. The coefficients of the polynomials were then estimated using successive relinearizations in an iterative least squares solution. The results obtained were a reference variance of 1.08 and a positional check variance of 5.04. These values are identical to those obtained for the corresponding collinearity analysis, as may be seen in Table 4.8. In fact, the results were identical in all respects to those from the collinearity analysis. Thus, if sufficient terms are taken in expanding tan θ, and if the same rigorous least squares procedure is used to estimate coefficients, the results of a piecewise polynomial formulation will be identical to those using the collinearity equations.

However, the polynomials in Section 3.2.2.1 were derived assuming only the first two terms in the series expansion of tan θ. Further, it is customary when utilizing polynomials to solve for the coefficients by least squares using the method of indirect observations (multiple regression). This approximation requires no iterative procedure.

The estimates of the polynomial coefficients result from a single solution of the linearized equations ($\underline{V} + \underline{B\Delta} = F^{\circ}$) and the observations are assumed to have identity weight matrix. These approximations were made for the same test case from flight 218 and resulted in a positional check variance of 5.83 and an a posteriori reference variance from the adjustment of 7.78.

The positional check variance for the more rigorous adjustment was 5.04. The reference variance resulting from the more rigorous adjustment was 1.08, which when multiplied by the a priori variance estimate of 6.25 assumed for positions in the data array, yields a value of 6.75. The differences between these variances from the more approximate procedure (5.83 and 7.78) and the rigorous procedure (5.04 and 6.75) are not statistically significant at an α level of 0.05. It may reasonably be assumed then that the approximate procedure is suitable for use with piecewise polynomials. In the subsequent tests, the approximate polynomials of Section 3.2.2.1 were used, and coefficients were estimated using the least squares model of indirect observations.

The polynomial forms chosen to be tested were the following:

Case P1: The polynomials for this case were of the form:

$$\begin{aligned} X &= A_1 + A_2\, x + A_3\, y + A_4\, xy + (A_3/3c^2)y^3 + (A_4/3c^2)xy^3 \\ Y &= B_1 + B_2\, x + B_3\, y + B_4\, xy + (B_3/3c^2)y + (B_4/3c^2)xy^3 \end{aligned} \qquad (4.7)$$

which represents one of the simplest polynomial forms possible. In this case orientation element variations are assumed linear, and the first two terms of the trigonometric series expansion are used to approximate the scan angle. Topographic effects are neglected in this formulation.

Case P2: For this case, the polynomials used were:

$$
\begin{aligned}
X &= A_1 + A_2\,x + A_3\,y + A_4\,xy + (A_3/3c^2)y^3 + (A_4/3c^2)xy^3 \\
&\quad - Z[(A_3/Z_c)y + (A_3/3c^2Z_c)y^3 + (A_4/Z_c)xy + (A_4/3c^2Z_c)xy^3] \\
Y &= B_1 + B_2\,x + B_3\,y + B_4\,xy + (B_3/3c^2)y^3 + (B_4/3c^2)xy^3 \\
&\quad - Z[(1/c)y + (1/3c^3)y^3]
\end{aligned}
\tag{4.8}
$$

This formulation represents linear modeling of exterior orientation variation, but includes the effect of topographic elevations. It is equivalent to Case C1 of the collinearity formulation, in that the same assumptions concerning exterior orientation variations were made.

Case P3: The polynomials

$$
\begin{aligned}
X &= A_1 + A_2\,x + A_3\,x^2 + A_4\,y + A_5\,xy + A_6\,x^2y \\
&\quad + (A_4/3c^2)y^3 + (A_5/3c^2)xy^3 + (A_6/3c^2)x^2y^3 \\
Y &= B_1 + B_2\,x + B_3\,x^2 + B_4\,y + B_5\,xy + B_6\,x^2y \\
&\quad + (B_4/3c^2)y^3 + (B_5/3c^2)xy^3 + (B_6/3c^2)x^2y^3
\end{aligned}
\tag{4.9}
$$

were used. This formulation represents the assumption of second order polynomials for the variations of all of the elements of exterior orientation, in which terrain elevations are neglected.

Case P4: The polynomials used for this case are:

$$
\begin{aligned}
X = {} & A_1 + A_2 x + A_3 x^2 + A_4 y + A_5 xy + A_6 x^2y \\
& + (A_4/3c^2)y^3 + (A_5/3c^2)xy^3 + (A_6/3c^2)x^2y^3 \\
& - Z[(A_4/Z_c)y + (A_4/3c^2Z_c)y^3 + (A_5/Z_c)xy \\
& + (A_5/3c^2Z_c)xy^3 + (A_6/Z_c)x^2y + (A_63c^2Z_c)x^2y^3] \\
Y = {} & B_1 + B_2 x + B_3 x^2 + B_4 y + B_5 xy + B_6 x^2y \\
& + (B_4/3c^2)y^3 + (B_5/3c^2)xy^3 + (B_6/3c^2)x^2y^3 \\
& - Z[(1/c)y + (1/c^3)y^3]
\end{aligned}
\qquad (4.10)
$$

This form of the polynomials assumes second order variations of orientation elements and attempts to include topographic effects. It represents the same assumptions concerning exterior orientation behaviour as were made for the collinearity model in Case C2.

Table 4.13 summarizes the results of the analysis for flight 208. Table 4.14 depicts a tabulation of F statistics for this flight line formed from the reference variances from least squares analysis, and Table 4.15 is a tabulation of F statistics for this flight based upon check variances computed using check points withheld from the adjustment.

It may be seen from these tabulations that for this flight over flat terrain, the inclusion of elevation data had virtually no effect upon the accuracy obtained, as would be expected. For the lower order polynomials of Case P1 and Case P2, statistically significant improvement was noted in dividing the strip into 2 sections over that of treating the flight line as a unit, and little further improvement was noted for these lower order polynomials in going

Table 4.13

Statistics from Piecewise Polynomial Analysis of Flight 208
(60 Check Points)

		Number of Sections		
		1	2	3
Case P1:	Number of Parameters	8	16	24
	Degrees of Freedom	70	66	62
	Reference Variance	7.91	3.29	2.87
	Check variance x in rsu^2(d.o.f. = 59)	9.10	3.06	2.42
	Check variance y in rsu^2(d.o.f. = 59)	4.54	3.96	3.39
	Positional Check Variance in rsu^2	6.62	3.50	2.89
Case P2:	Number of Parameters	8	16	24
	Degrees of Freedom	70	66	62
	Reference Variance	7.92	3.29	2.86
	Check Variance x in rsu^2(d.o.f. = 59)	9.10	3.06	2.42
	Check Variance y in rsu^2(d.o.f. = 59)	4.57	4.01	3.41
	Positional Check Variance in rsu^2	6.64	3.52	2.89
Case P3:	Number of Parameters	12	24	36
	Degrees of Freedom	66	58	50
	Reference Variance	3.16	2.41	1.82
	Check Variance x in rsu^2(d.o.f. = 59)	2.49	2.28	2.01
	Check Variance y in rsu^2(d.o.f. = 59)	4.05	2.84	1.88
	Positional Check Variance in rsu^2	3.22	2.56	1.95
Case P4:	Number of Parameters	12	24	36
	Degrees of Freedom	66	58	50
	Reference Variance	3.16	2.40	1.83
	Check Variance x in rsu^2(d.o.f. = 59)	2.49	2.28	2.01
	Check Variance y in rsu^2(d.o.f. = 59)	4.09	2.86	1.92
	Positional Check Variance in rsu^2	3.24	2.57	1.96

Table 4.14

Tabulation of F Statistics for Flight 208
Formed from Reference Variance from Piecewise Polynomial Analysis

		Case P1			Case P2			Case P3			Case P4		
		Number of Sections											
		1	2	3	1	2	3	1	2	3	1	2	3
Case P1	1	1.00											
	2	2.40*	1.00										
	3	2.76*	1.15	1.00									
Case P2	1	1.00	2.40*	2.76*	1.00								
	2	2.40*	1.00	1.15	2.41*	1.00							
	3	2.76*	1.15	1.00	2.77*	.115	1.00						
Case P3	1	2.50*	1.04	1.10	2.51*	1.04	1.10	1.00					
	2	3.28*	1.36	1.19	3.29*	1.36	1.18	1.31	1.00				
	3	4.35*	1.81*	1.57*	4.35*	1.81*	1.57*	1.74*	1.32	1.00			
Case P4	1	2.50*	1.04	1.10	2.51*	1.04	1.10	1.00	1.31	1.74*	1.00		
	2	3.30*	1.37	1.20	3.30*	1.37	1.19	1.32	1.00	1.32	1.32	1.00	
	3	4.32*	1.80*	1.57*	4.33*	1.80*	1.56	1.73*	1.32	1.00	1.73*	1.31	1.00

Number of Sections

* Denotes values which are statistically significant at an α level of .05.

Table 4.15

Tabulation of F Statistics for Flight 208
Formed from Positional Check Variances from Piecewise Polynomial Analysis

		Case P1			Case P2			Case P3			Case P4		
		Number of Sections											
		1	2	3	1	2	3	1	2	3	1	2	3
Case P1	1	1.00											
	2	1.89*	1.00										
	3	2.30*	1.21	1.00									
Case P2	1	1.00	1.89*	2.30*	1.00								
	2	1.88*	1.01	1.22	1.88*	1.00							
	3	2.29*	1.20	1.01	2.30*	1.21	1.00						
Case P3	1	2.05*	1.09	1.11	2.05*	1.09	1.11	1.00					
	2	2.60*	1.37	1.13	2.60*	1.38	1.14	1.26	1.00				
	3	3.41*	1.80*	1.48	3.42*	1.81*	1.49	1.65*	1.31	1.00			
Case P4	1	2.04*	1.08	1.12	2.04*	1.09	1.11	1.01	1.27	1.66*	1.00		
	2	2.59*	1.36	1.12	2.59*	1.37	1.13	1.25	1.00	1.32	1.26	1.00	
	3	3.37*	1.79*	1.47	3.37*	1.80*	1.48	1.64*	1.31	1.00	1.65*	1.31	1.00

Number of Sections

* Denotes values which are statistically significant at an α level of .05.

from 2 to 3 sections. For the higher order polynomials, it was in general necessary to segment the flight into 3 sections before significant improvements could be discriminated over treatment as a single unit. In most cases, significant improvement was noted in going from the lower order polynomials of Case P1 and Case P2 to the higher order polynomials of Case P3 and Case P4 for the same number of sections.

Table 4.16 summarizes the results of the polynomial analysis for flight 218. Tables 4.17 and 4.18 depict tabulations of F statistics formed from the reference variances and check variances, respectively. Although improvements in the reference variances were generally noted when elevation information was included for this flight over moderate terrain relief, such improvements were not found to be statistically significant. Segmenting of the strip had no significant effect upon the accuracies obtained for the lower order polynomials. The only generally apparent statistically significant improvement in the reference variances appears to be in going from the lower order polynomial cases to the higher order Case P4 combined with segmenting the flight line into 3 sections. No significant differences were detected for flight 218 based upon the check variances, as may be expected due to the small degrees of freedom associated with these (8). Note that for this analysis, as with the collinearity model, the assumption of a large number of parameters could be dangerous, as indicated by the increase in the check variances. Thus, although the points included in the adjustment were fit quite

Table 4.16

Statistics from Piecewise Polynomial Analysis of Flight 218
(9 Check Points Only)

		Number of Sections		
		1	2	3
Case P1:	Number of Parameters	8	16	24
	Degrees of Freedom	38	34	30
	Reference Variance	10.20	7.94	6.80
	Check Variance x in rsu^2(d.o.f. = 8)	7.20	6.61	7.33
	Check Variance y in rsu^2(d.o.f. = 8)	5.67	4.74	1.84
	Positional Check Variance in rsu^2	6.40	5.64	4.13
Case P2:	Number of Parameters	8	16	24
	Degrees of Freedom	38	34	30
	Reference Variance	9.11	7.02	6.33
	Check Variance x in rsu^2(d.o.f. = 8)	7.19	6.58	7.26
	Check Variance y in rsu^2(d.o.f. = 8)	4.96	4.72	2.36
	Positional Check Variance in rsu^2	6.02	5.61	4.47
Case P3:	Number of Parameters	12	24	36
	Degrees of Freedom	34	26	18
	Reference Variance	8.88	5.52	4.19
	Check Variance x in rsu^2(d.o.f. = 8)	6.67	14.96	17.71
	Check Variance y in rsu^2(d.o.f. = 8)	4.91	2.02	1.32
	Positional Check Variance in rsu^2	5.76	6.99	7.17
Case P4:	Number of Parameters	12	24	36
	Degrees of Freedom	34	26	18
	Reference Variance	7.78	5.07	3.56
	Check Variance x in rsu^2(d.o.f. = 8)	6.64	14.88	17.69
	Check Variance y in rsu^2(d.o.f. = 8)	5.02	2.13	1.40
	Positional Check Variance in rsu^2	5.81	7.07	7.26

Table 4.17

Tabulation of F Statistics for Flight 218
Formed from Reference Variance from Piecewise Polynomial Analysis

		Case P1			Case P2			Case P3			Case P4		
		Number of Sections											
		1	2	3	1	2	3	1	2	3	1	2	3
Case P1	1	1.00											
	2	1.28	1.00										
	3	1.50	1.17	1.00									
Case P2	1	1.12	1.14	1.34	1.00								
	2	1.45	1.13	1.03	1.30	1.00							
	3	1.61	1.25	1.07	1.44	1.11	1.00						
Case P3	1	1.15	1.12	1.30	1.03	1.26	1.40	1.00					
	2	1.85*	1.44	1.23	1.65	1.27	1.15	1.61	1.00				
	3	2.43*	1.89	1.62	2.17*	1.68	1.51	2.12*	1.32	1.00			
Case P4	1	1.31	1.02	1.14	1.17	1.11	1.23	1.14	1.41	1.86	1.00		
	2	2.01*	1.56	1.34	1.80	1.38	1.25	1.75	1.09	1.21	1.53	1.00	
	3	2.86*	2.23*	1.91	2.56*	1.97	1.78	2.49*	1.55	1.17	2.18*	1.42	1.00

* Denotes values which are statistically significant at an α level of .05.

Table 4.18

Tabulation of F Statistics for Flight 218
Formed from Positional Check Variances from Piecewise Polynomial Analysis

		Case P1			Case P2			Case P3			Case P4		
		Number of Sections											
		1	2	3	1	2	3	1	2	3	1	2	3
Case P1	1	1.00											
	2	1.13	1.00										
	3	1.55	1.37	1.00									
Case P2	1	1.07	1.06	1.46	1.00								
	2	1.14	1.01	1.36	1.07	1.00							
	3	1.43	1.26	1.09	1.35	1.25	1.00						
Case P3	1	1.11	1.02	1.39	1.04	1.03	1.29	1.00					
	2	1.09	1.24	1.69	1.16	1.25	1.56	1.21	1.00				
	3	1.12	1.27	1.74	1.19	1.28	1.60	1.25	1.02	1.00			
Case P4	1	1.10	1.03	1.41	1.03	1.04	1.30	1.01	1.21	1.24	1.00		
	2	1.10	1.25	1.71	1.17	1.26	1.58	1.23	1.01	1.02	1.22	1.00	
	3	1.13	1.29	1.76	1.21	1.29	1.62	1.26	1.04	1.00	1.25	1.02	1.00

closely as shown by the lower reference variances, the true test of the fit, as given by the check variances computed from points withheld from the adjustment, deteriorated.

The value in including Z coordinate elevations is doubtful for this test array over moderate terrain relief. For this test, no significant improvement was gained in doing so, indicating that terrain relief effects are relatively small for this array, and such effects are at least partially compensated for in estimating the parameters of exterior orientation. However, a test with many more check points should be carried out before a more concrete assertion can be made regarding the inclusion of point elevations in the polynomials.

4.4.3 Nonparametric Methods

The four nonparametric methods of MSS digital data array analysis and restitution which were attempted for testing are:

1. Arithmetic mean
2. Moving average
3. Meshwise linear transformation
4. Linear least squares filtering

The first three of the above represent algorithms which may be applied to MSS digital data arrays in a fairly straightforward manner. The linear least squares filtering is highly dependent upon the validity of assumption of some statistical properties concerning the data arrays. Considerable difficulty was experienced in applying this method to the data arrays available for testing.

In implementing the arithmetic mean algorithm, the data arrays were first preprocessed using the resampling algorithm of

Equation (3.13), followed by approximate scaling in the y direction, in order to approximately equalize scales in the x and y directions. A weighting function was then chosen using only separation distance between points as the independent variable. For the flight lines tested, the weighting function was assumed to be of the form

$$w_i = \frac{1}{d_i^3} \tag{4.11}$$

For the test of the moving average algorithm, no preprocessing of the data was done. The weighting function of (4.11) was also used for this method, and the non-linear form of Equation (3.45) was utilized.

The meshwise linear transformation was also tested on both flight lines. No preprocessing of the data is required for this method, and no weighting function need be defined. The control points were connected into a triangular mesh, and each check point was transformed according to the unique parameters of an affine transformation defined by the coordinates of the three control points forming the triangle within which the check point lies.

Attempts were also made to analyze the applicability of the linear least squares filtering method as a restitution technique. The results of these attempts, however, were disappointing. Successful application of the method depends upon the data having specific statistical properties. The property of ergodicity must be assumed, which in turn depends upon stationarity of the data. In addition, isotropy of the two dimensional data field must be assumed [99].

The resampling algorithm of Equation (3.13), followed by approximate y direction scaling was used to preprocess the flight lines in an attempt to satisfy the isotropic requirement. Sample covariance points were then computed from the data sets using the method presented in [99]. Results of these steps for flight 208 are represented by Figure 4.11. From these plots, it is apparent that the data set cannot be considered to satisfy the statistical requisites over the entire length of the flight line, since no logical fit to these sample covariance points may be obtained using an allowable autocovariance functional form. Yaglom [109] and Bendat and Piersall [114] enumerate the characteristics of an autocovariance function as follows:

$$C(0) > 0$$

$$C(-\tau) = C(\tau)$$

$$C(\tau) \leq C(0)$$

in which C represents the value of the autocovariance function and τ represents the independent variable. The cross-covariance function need only satisfy the condition $C_{xy}(\tau) = C_{xy}(-\tau)$ [114]. It may be seen from the figure that no function having the properties described above may reasonably be fitted to these points. Similar results were obtained for flight 218.

In an attempt to alleviate these problems, covariance functions were calculated based only upon sample covariance points within limited regions, limiting the distance to less than 500 elements. Within these regions it was attempted to fit Gaussian functional

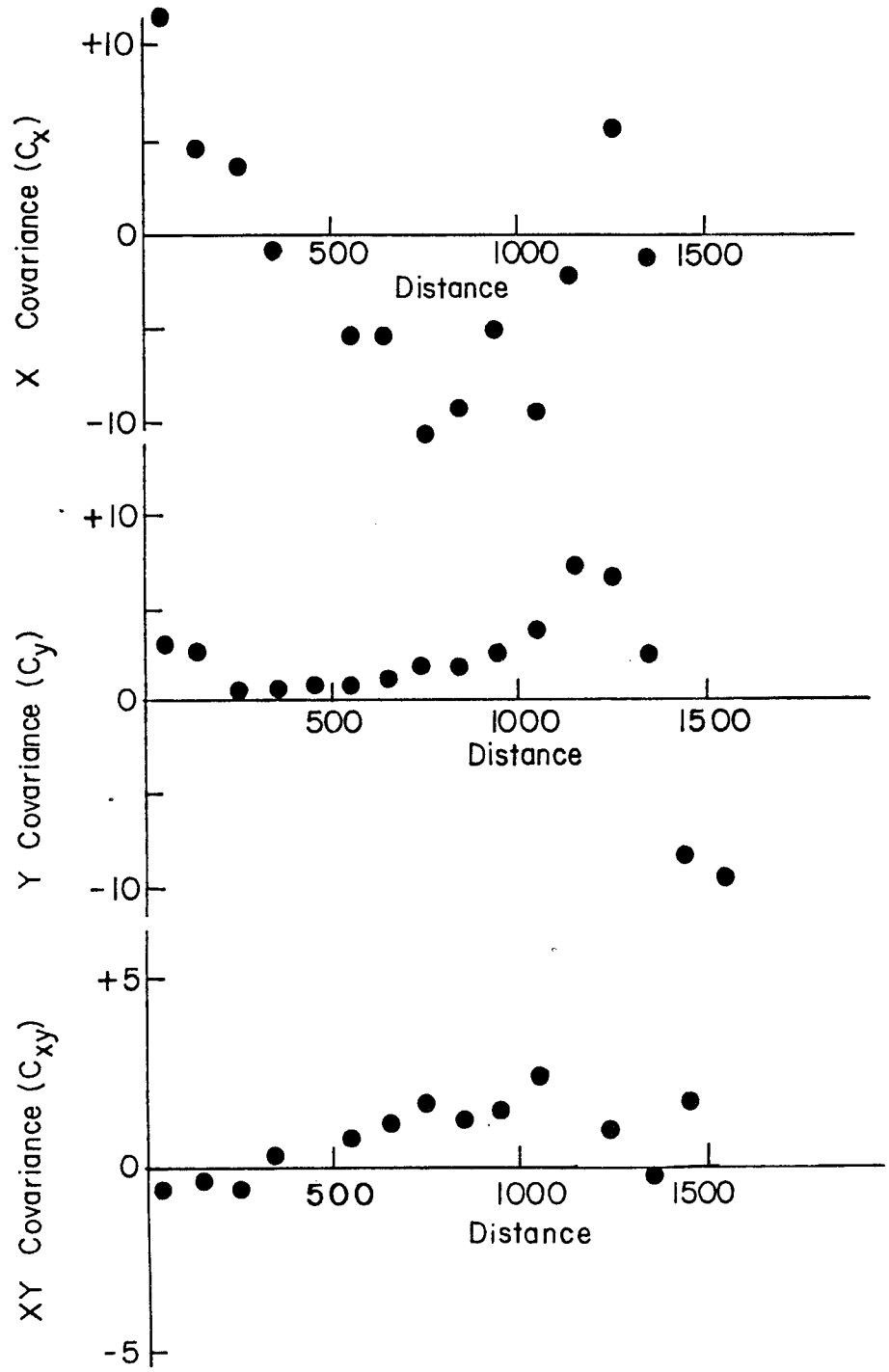

Figure 4.11. Sample Covariance Points for Flight 208

forms, as suggested by Kraus and Mikhail [99], to sample covariance points. The Gaussian type covariance function may be written in the form:

$$C(d) = C(0)\, e^{-kd^2} \tag{4.12}$$

in which the C(0) and k parameters are estimated by a least squares fit of the function to the sample covariance points.

After these covariance functions were determined, they were used to calculate the elements within the $\underline{C}$ matrix of Equation (3.49), as well as the $\underline{c}$ matrix. Each element of the sub-matrices $\underline{C}_x$, $\underline{C}_y$, $\underline{C}_{xy}$, $\underline{C}_{yx}$ in Equation (3.49) are computed from the appropriate covariance function. For the present investigation, two cases were considered. In the first, three separate covariance functions were determined for calculation of the terms in the $\underline{C}_x$, $\underline{C}_y$ and $\underline{C}_{xy}$ sub-matrices by a least squares fitting to the sample covariance points. For this case it was assumed $\underline{C}_{xy} = \underline{C}_{yx}$. In the second case, it was assumed that $\underline{C}_{xy} = \underline{C}_{yx} = 0$. This represents the case for which independent interpolation and filtering are done in the x and y directions.

If interpolation only is to be done, the diagonal elements of the $\underline{C}$ matrix will contain values C(0) from the appropriate auto-covariance functions. However, if estimates of random components $\hat{r}$ at the reference points are to be filtered, in addition to interpolation of the s components, the diagonal terms of the $\underline{C}$ matrix are replaced by variance terms V_x, V_y computed from the data set.

For the x variance terms, for example, the variance is computed by

$$V_x = \sum_{i=1}^{n} \ell^2_{xi}$$

in which $\ell_{xi} = X_i - x_i$ for n control points. It was this technique which was attempted in this investigation. Hence, simultaneous interpolation and filtering was attempted.

For the data sets available for testing, however, the results obtained using this linear least squares procedure were highly erratic. Combinations of covariance functions which appeared to yield acceptable results on one flight line yielded very large positional check variances on the other. A preliminary supposition is that the data sets, even after the preprocessing steps described above, do not adhere to the requisite statistical properties necessary for the successful application of the linear least squares algorithm.

Because of this unpredictability of results from the linear least squares procedure, this technique is not included in the tabulated results to be presented. In Table 4.19 the resulting statistics obtained from the processing of the data arrays for flight 208 by nonparametric interpolative methods are shown. The statistics shown are based upon check variances formed by applying the non-parametric methods to the check points as based upon the control points available within the strip. Sixty such check points were available for flight 208. In Table 4.20 a similar tabulation is shown for flight 218. Only nine check points were available for this

Table 4.19

Statistics from Analysis of Flight 208
by Nonparametric Interpolative Methods
(60 Check Points)

Arithmetic Mean	
Degrees of Freedom (x and y)	59
Check Variance, x, in rsu^2	2.44
Check Variance, y, in rsu^2	1.51
Positional Check Variance	1.86
Moving Average	
Degrees of Freedom (x and y)	59
Check Variance, x, in rsu^2	1.75
Check Variance, y, in rsu^2	4.16
Positional Check Variance	2.79
Meshwise Linear Transformation	
Degrees of Freedom (x and y)	59
Check Variance, x, in rsu^2	1.82
Check Variance, y, in rsu^2	5.09
Positional Check Variance	3.26

Table 4.20

Statistics from Analysis of Flight 218
by Nonparametric Interpolative Methods
(9 Check Points)

Arithmetic Mean	
Degrees of Freedom (x and y)	8
Check Variance, x, in rsu^2	10.69
Check Variance, y, in rsu^2	2.32
Positional Check Variance	5.76
Moving Average	
Degrees of Freedom (x and y)	8
Check Variance, x, in rsu^2	7.49
Check Variance, y, in rsu^2	3.82
Positional Check Variance	5.52
Meshwise Linear Transformation	
Degrees of Freedom (x and y)	8
Check Variance, x, in rsu^2	6.25
Check Variance, y, in rsu^2	5.86
Positional Check Variance	6.05

flight line, and the resulting degrees of freedom (8) for the x and y coordinate values, respectively, is quite small. Table 4.21 is a tabulation of the F statistics computed from the positional check variances for flight 208. Of interest here is the fact that the simplest interpolative method, that of the arithmetic mean, shows a significant reduction of variance over the meshwise linear transformation method. No other statistically significant differences were noted for this flight line. Table 4.22 shows a similar tabulation for flight 218. As might be expected, no significant differences between the interpolative methods were detected for the small degrees of freedom available. The inference to be drawn from these tables is that if restitution is to be done for the arrays tested using a nonparametric method, the choice of the simple arithmetic mean represents a logical and computationally efficient choice, well suited to automated restitution as a portion of automated interpretation. General conclusions should not be drawn, however, based upon such limited tests. Further investigations utilizing data arrays generated under a variety of conditions must be performed before a definitive statement may be made.

4.4.4 Summary of Results

The results of the tests performed on the data arrays chosen indicate that the nonparametric methods, particularly the arithmetic mean algorithm, represent <u>perhaps</u> the optimum method for restitution of MSS digital data arrays. For flight 208, each of the check variances from the collinearity and piecewise polynomial analysis were

Table 4.21

Tabulation of F Statistics for Flight 208
Formed from Positional Check Variances from Nonparametric Methods

	Arithmetic Mean	Moving Average	Meshwise Linear Transformation
Arithmetic Mean	1.00		
Moving Average	1.50	1.00	
Meshwise Linear Transformation	1.75*	1.17	1.00

* Denotes values which are statistically significant at an α level of .05.

Table 4.22

Tabulation of F Statistics for Flight 218
Formed from Positional Check Variances from Nonparametric Methods

	Arithmetic Mean	Moving Average	Meshwise Linear Transformation
Arithmetic Mean	1.00		
Moving Average	1.04	1.00	
Meshwise Linear Transformation	1.05	1.10	1.00

compared using the F statistic to that obtained by the arithmetic mean algorithm. It was found that, for the collinearity analysis, only the higher order polynomial assumptions, coupled with dividing the flight line into sections could compare favorably. In all cases of linear orientation variation assumption the check variances from the collinearity analysis were significantly higher than that obtained from the arithmetic mean analysis, at an α level of .05. Similar results were obtained when a comparison of the results of the polynomial analysis with that of the nonparametric methods was done. For flight 208, only the higher order polynomials coupled with dividing the flight line into three sections could compare favorably with any of the nonparametric methods. The nonparametric methods in general produced statistically better results than those from the lower order polynomials.

For flight 218, a comparison of the check variances obtained from the collinearity analysis and those from the nonparametric methods was also done. No statistically significant differences were found. A comparison of check variances from the polynomial analysis with those from the nonparametric methods also revealed no significant differences. These results are noteworthy, because in using the nonparametric methods no attempt was made to account for displacements due to topography. This would indicate that for arrays obtained by scanning areas of moderate terrain relief (e.g. flight 218) that errors due to relief displacement are small compared to those due to other sources (orientation, scan time, etc.), or that the nonparametric algorithms at least partially account for

the topographic effects or a combination of these factors. Therefore the nonparametric methods (particularly the relatively simple arithmetic mean algorithm) were shown to represent an effective method for use in the restitution of such arrays, at least for the arrays tested, although no general conclusions should be drawn from such limited tests.

4.5 Final Transformation of Flight Lines

A final transformation of the test flight lines was attempted utilizing the collinearity method of restitution. The method used was as described in Section 3.5. After estimating the parameters of the model, the restituted X_j, Y_j coordinate values were assigned as the independent variables in the transformation equations. An iterative procedure was utilized in which Z_j was first estimated, the collinearity equation for the coordinates in the direction of flight was then solved explicitly for x_j, the uncorrected array position, and this value was utilized in the second collinearity equation to solve for y_j, the along scan array position in the uncorrected array. These values were used to locate an updated value for the Z_j term, and the process was repeated until no change in the resulting array position was found. The spectral values in the x_j, y_j uncorrected array position were then assigned to the X_j, Y_j restituted array position after iterative transformation. This procedure was repeated for each data array element. The program utilized was a modification of Anuta's OVERLA program [110], which was originally written to superimpose different arrays of data containing essentially the same ground area.

Digital displays of the restituted arrays were then generated to assess qualitatively the results. In Figure 4.12 is shown the digital display of channel 6 for flight line 208 after restitution, which may be compared directly to Figure 4.2, the digital display of the unprocessed array. A careful study of these images reveals that improvements in the geometric characteristics of the array have been obtained. The narrowing of the flight line results from a correction of the scan angle effects and the differential scale in the x and y directions. The triangular area near the top of the flight line (arrow A, Figure 4.12) has been visibly restored to a configuration more closely matching the shape it should have as illustrated in the map planimetry of Figure 4.5. The alignment of the interstate highway cutting diagonally across the bottom half of the flight line (arrow B, Figure 4.12) has been visibly straightened, as has the alignment of the central roadway running down the flight line. Cross roads appear more nearly perpendicular to this central roadway, indicating that the scan time effects and the effects of aircraft yaw were compensated for.

The restituted array from channel 6 for flight line 218 is shown in Figure 4.13. The river bend (arrow A, Figure 4.13) in this display is seen to reflect more closely the map planimetry illustrated in Figure 4.6 than in the unprocessed array of Figure 4.4. The inclination of the roadway (arrow B, Figure 4.13) in this area also has been restituted into an alignment more closely matching that shown in Figure 4.6.

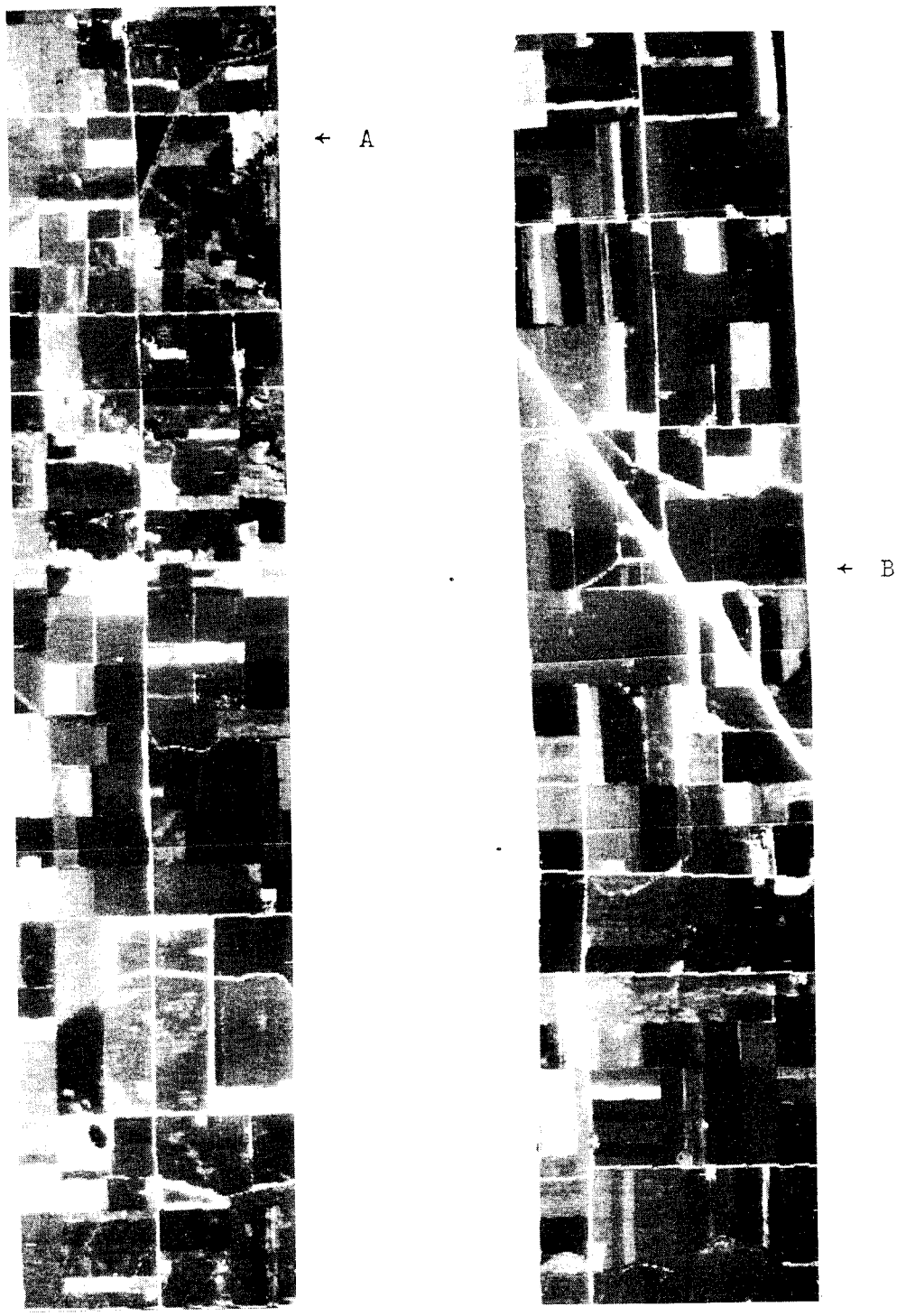

Figure 4.12. Digital Display of Processed Array for Flight 208

Figure 4.13. Digital Display of Processed Array for Flight 218

These displays illustrate the feasibility of algorithms to restitute the originally deformed data arrays into array systems displayable in an orthographic projection system. These restituted data arrays may be used to extract metric as well as interpretive information, and may serve as a basic data source for the existing automated interpretation algorithms, reflecting more closely the geometry of the area sensed as it actually appears in the ground system.

5. CONCLUSIONS AND RECOMMENDATIONS

The scope of the investigation has encompassed the analysis of the geometric aspects of recording multispectral scanner (MSS) data in a digital manner. An introduction to the digital techniques of utilizing MSS data has been presented, and the geometric distortions present in such arrays were described. The basic transformation equations for recording MSS data were given and specific expressions were derived from these for analysis and restitution of the data arrays. Nonparametric techniques of restitution were also utilized as an alternative to the parametric methods based upon the transformation relationships. Testing of both methods of analysis and restitution on actual digital data arrays was attempted. The numerical results obtained were for the case of singly scanned flight lines only, since no overlapping flight lines were available for testing in this investigation.

5.1 Conclusions

The investigation conducted supports the following conclusions:

1.) Significant geometric distortions are present in unprocessed MSS digital data arrays, and must be considered in order to reliably obtain reliable metric information for surveys of resources at

the Earth's surface. The major causes of these geometric perturbations present within the arrays are:

a.) changing ground resolution size at different scan angles and image position displacement due to panoramic recording

b.) terrain relief displacements due to topographic relief differences within the area scanned

c.) perturbations caused by the continuous changes in sensor exterior orientation elements during recording of the data

d.) effective image displacements due to forward motion of the sensor during the short time interval required to record a single scan line.

Two types of investigations were carried out for data arrays containing such geometric displacements. The problem of analysis was considered, in which it is desired to investigate the causes of the geometric displacements, and determine the resulting magnitudes and directions of the errors within the data arrays due to each cause. Subsequently, the problem of restitution of the data arrays was considered, in which it is desired to correct the geometric errors within the arrays using any convenient method, without necessarily isolating and investigating the individual causes of the errors.

2.) The MSS collinearity equations derived from the geometric portion of the more general MSS transformation provide a suitable mathematical model for both analysis and restitution of MSS data. These expressions represent the actual geometric relationships between ground points and image array positions at the moment of recording. Therefore they represent the most obvious mathematical

model, and serve as the basis of other approximate methods of analysis and restitution.

3.) The collinearity equations may be used with ground control points to perform space resection in order to obtain estimates for the elements of exterior orientation of the sensor during recording of the data. However there are some severe limitations on such resections. The most serious is that, since the multispectral scanner records continuously, each scan line has different exterior orientation elements than any other scan line. To solve for a separate set of exterior orientation elements for every scan line is impossible. Therefore, some assumption must be made concerning the variation of each exterior orientation element as the sensor progresses down the flight line. If a functional form is assumed for each of these orientation elements, the parameters of these functions will be determined by a space resection. If the actual stochastic variations of the exterior orientation elements are not reasonably approximated by the functional forms assumed, then the collinearity formulation and methods based upon the collinearity formulation lose their advantage, and other methods of analysis may compete favorably with the collinearity formulation as a mathematical model. It was found in this investigation that the assumption of polynomial functional forms for the orientation elements provided adequate accuracies and reasonable computational efficiency for the data arrays tested.

4.) If space resection is performed utilizing ground control points based upon the MSS collinearity equations for a singly scanned flight line, not all of the elements of exterior orientation for the

sensor can be recovered. A constant pitch (ϕ) of the sensor is not distinguishable from a constant X translation of the sensor perspective center (X_c). Likewise, a constant rate of change of pitch is not distinguishable from a constant aircraft velocity. Similar dependencies are found if higher order terms are attempted to simultaneously model the pitch and X translation of the sensor. Therefore not all of the elements of exterior orientation are recoverable.

5.) Significant improvements in the results of restitution using collinearity equations may be realized by breaking the flight line into sections. For the flight lines tested, sections of 800 lines or less were used. Control points within each section can then be used to define independent parameter sets for that section by space resection. Discontinuities in the restituted array positions at section boundaries may be avoided by utilizing parameter constraints during the least squares estimation of the exterior orientation parameters. This problem of discontinuities at section boundaries will be discussed further in a later conclusion.

6.) If restitution of MSS digital data arrays is to be attempted using the collinearity equations, then terrain height information may be introduced into the uncorrected data arrays in some manner, in order that relief displacements may be removed during the restitution procedure. One possible source of this information (used for this investigation) is the U.S. Geological Survey 7 1/2 minute quadrangle topographic map sheets. If these or other topographic map data are used as a source of elevation information, the data contained

on the map must be transformed into a digital data format in some manner. This digitized data must be superimposed upon the uncorrected digital MSS arrays such that an elevation is assigned to each element within the MSS digital data array with sufficient accuracy to allow restitution of the arrays to a precision within the size of the resolution of the data.

7.) Piecewise polynomial forms for restitution of MSS digital data arrays may be derived from the collinearity equations. These polynomials may be formulated to account for various assumptions concerning exterior orientation element variations, and for relief displacements within the arrays. These polynomial formulations require that a series expansion be used to approximate the trigonometric functions resulting from scan angle variations. If sufficient terms are taken in the series approximations, and if the proper rigorous least squares procedure is used, the results obtained are identical to the results using the collinearity formulations. If only a few terms are carried for the series expansion, and a simpler least squares procedure is used, the results from these polynomial models are in general, inferior to the results from collinearity analysis. The difference, however, was found not to be statistically significant.

8.) Both the collinearity and piecewise polynomial formulations were found to be relatively insensitive to moderate errors in assignment of element elevations to the uncorrected data arrays. The derivation of an allowable height assignment error formula revealed that an element elevation error of 1.2% of the flying height above terrain

would result in an error in position of less than the ground resolution size of an element for arrays digitized at 6 milliradians, at the extreme case of a scan angle of 45° from the vertical. In conducting tests on real data having flat and moderate terrain relief, it was found that the resulting positional error was affected to a greater degree by the assumption of functional forms for exterior orientation elements than by the inclusion of element elevation information within the expressions utilized.

9.) The assignment of elevations to element positions within the uncorrected arrays to the required accuracy was found to be relatively insensitive to the approximate planimetric transformation used to transform the original array positions to the coordinate system based upon digitized control points. An affine transformation, applied to sections of the flight line was found adequate for this purpose. Tests of real data arrays revealed that assignment of element elevations utilizing the affine transformation resulted in element elevation errors less than the theoretical allowable height assignment error.

10.) The assignment of element elevations by digitally searching for contour-scan line intersections followed by linear interpolation for elements between these intersection points was found to result in acceptable values for element elevations for the purposes of restitution. A more general interpolative technique (arithmetic mean) was attempted and found to result in much greater computation time with no significant improvement in accuracy.

11.) The use of MSS data in digital array form allows for two alternative transformation procedures for restitution. In the first instance, the more conventional procedure of utilizing image coordinates, or, for MSS digital data, array positions as independent variables is pursued. These are utilized in the restitution functions to generate restituted arrays having improved geometrical properties. This method has the advantage that the projective relationships may be used directly and requires no iterative steps in restitution. However, the method requires a large output buffer, interpolation of spectral density data, and may result in multiple assignments of spectral values to a single element location.

The second possible method utilizes the output array positions as independent variables and involves a solution of the restitution equations for the corresponding uncorrected data array positions. An input buffer is required in this case, and an iterative procedure is necessary, since elevation data are associated with the uncorrected array positions.

12.) If discontinuities are to be eliminated at section boundaries, constraints may be enforced to accomplish this. If the flight line is divided along lines of constant x image coordinate, the general constraint to be enforced is that the restituted X, Y position computed for every element along this boundary must be the same when computed using the parameters for the section on either side of the boundary. This results in six constraint equations whether utilizing the collinearity or piecewise polynomial formulations.

13.) The nonparametric methods introduced appear to be quite promising as an alternative to restitution of MSS digital data arrays using collinearity equations or piecewise polynomials. These nonparametric interpolative methods have some advantages over the more conventional methods of restitution which make them appear to be well suited for application to digital MSS data arrays.

a.) The accuracy of restitution using these nonparametric methods, as indicated by tests on real data arrays having flat and moderate terrain relief, was comparable to the restitution accuracy achieved by the more conventional methods utilizing collinearity equations or piecewise polynomials..

b.) The problem of assignment of element elevations may be avoided. The treatment of the geometric displacements as a realization of a two dimensional stochastic field from which trend has been reasonably removed, appears to have at least partially corrected for relief displacements within the interpolative algorithms themselves, without the need for assignment of element elevations for every data array position.

c.) Some of the nonparametric algorithms, notably the arithmetic mean algorithm, are quite simple and relatively fast computationally, resulting in efficiency in transforming large numbers of array point positions.

d.) There is no problem of breaking the flight line into sections, and hence no problem of removing discontinuities at section boundaries. The nonparametric algorithms are continuous throughout the flight line.

The primary disadvantage of the nonparametric interpolative methods is that some of them depend upon certain assumptions (isotropy, stationarity, ergodicity) of the stochastic field. MSS digital data arrays must be preprocessed in some manner to approximate isotropy. Serious doubts were raised during the investigation as to whether the digital MSS arrays obtained from aircraft, may be considered stationary, even over limited areas. For most of these nonparametric methods, however, the results of restitution were found to be acceptable even though the assumptions were not fully realized.

14.) For the arithmetic mean algorithm, it was found that a simple resampling algorithm, followed by approximate scaling in the direction normal to flight could be used to acceptably approximate isotropy.

15.) Of the nonparametric algorithms, the arithmetic mean algorithm appeared to be most promising for the data arrays tested. The method is simple, fast, and the resulting accuracy of restitution is comparable or superior to any of the other nonparametric methods or the parametric methods (collinearity equations and piecewise polynomials). The lone disadvantage of the method is that it requires pre-processing of each array position as discussed in conclusion 14.

16.) The moving average interpolative algorithm appears to be able to compete with that of the arithmetic mean. The ability of this algorithm to include non linear effects allows for the omission of pre-processing of the data arrays. However, for each element calculated during restitution using this method, a unique parameter

set must be evaluated by least squares techniques, resulting in an algorithm which is slower than that of the arithmetic mean, with no statistically significant improvement in accuracy of the restitution for the arrays tested.

17.) The meshwise linear transformation does not appear promising as a nonparametric algorithm for restitution of MSS digital data arrays. The method is predicated upon the fact that each element to be transformed lies within a triangle whose vertices represent control points which are identifiable both upon a map sheet and within the uncorrected data arrays. Such a condition cannot be fulfilled for every data array element within a flight line. A further disadvantage of the method is that a large amount of human intervention is required, in order to define a unique mesh of contiguous triangles formed from the control points. Therefore the method does not appear well suited to an automated technique combining the interpretive and geometric analysis of the data arrays.

18.) The results obtained in attempting to utilize the method of linear least squares interpolation and filtering were highly erratic. The method is highly dependent upon the fulfillment of the assumptions concerning stationarity, ergodicity, and isotropy of the stochastic field. The preliminary supposition as of this time is that one or more of these assumptions were not fulfilled for the data arrays tested.

5.2 Recommendations

The following suggestions are offered for further research and development efforts in the field of MSS digital data array utilization bases upon the experience of this investigation.

1.) An attempt should be made to implement a unified approach to amalgamate the classically separated activities of interpretation and mensuration. The digital method of analysis of MSS data arrays appears ideally suited to this purpose. The inclusion of the analysis and restitution methods presented in this thesis with existing automated interpretation techniques would result in the ability to extract quantitative information in addition to the qualitative information presently being generated, thus increasing the information obtainable from the MSS data concerning Earth resources.

2.) An investigation should be carried out concerning the applicability of functional forms other than polynomials to approximate the stochastic variation of exterior orientation parameters within sections of the flight line. Functional forms such as harmonics, although difficult to deal with, may result in greater accuracy of restitution.

3.) An investigation of the actual variation of exterior orientation elements with time should be carried out. Ideally, this would be accomplished by fully monitoring all sensor exterior orientation elements within an accuracy obtainable by resection. However, this would be quite expensive and is unlikely. Alternatively, the monitoring or stabilization of one additional exterior orientation element (in addition to the roll, ω) such as the pitch (ϕ) term could

be attempted. If this monitoring were combined with a flight over an area having very dense control, such that a resection for the remaining parameters could be carried out at very frequent intervals down the flight line, then a reliable estimate of the actual exterior orientation elements could be obtained. It would then be possible to state with more confidence the actual errors resulting from the omission of one of the exterior orientation elements within a section.

4.) It would be most useful to generate some experimental data arrays which include an accurate recording of time. In this way, the functions assumed for variation of exterior orientation elements could be formulated directly as time functions, and the suitability of utilizing the image x coordinate as a measure of time could be tested.

5.) Analysis and restitution methods should be tested on simulated data, having known stochastic characteristics. This would allow for controlled experimentation and reveal insights into the behaviour of real data arrays.

6.) All of the methods of restitution presented in this investigation should be tested on data arrays generated by flights over ground areas having more extreme relief differences. Of particular interest would be the applicability of the nonparametric algorithms to such data, since the algorithms presented do not consider terrain elevations.

7.) An investigation of the use of generalized nonparametric algorithms should be pursued, in which Z coordinate information is included.

8.) An investigation should be carried out concerning the effect upon accuracy of the control point distribution within a flight line. This should include studies of how the number and configuration of control points available affects accuracy. Results may then indicate the minimum number of control points which must by available in order to produce restituted data arrays of a certain accuracy requirement, and indicate the optimum configuration of such control points within the flight line area.

9.) Attempts should be made to utilize sources of planimetric control points other than maps. One possibility in this area is obtaining metric photography of the area as a control source. Aerial triangulation utilizing such photography could then be performed to define X-Y-Z ground control point coordinates. If such photography were available and was digitized, investigations to further improve accuracies could be carried out. Digital correlation computation could be investigated as a method of reducing the a priori variance of assigning array positions to control points. Digital correlators using digitized metric photography and the MSS data arrays should be developed in order to assign these control point array positions with greater reliability than is possible using subjective human decisions.

Another method of control which should be considered is direct targeting. In this manner, ground control point coordinates could be determined by direct measurement. This would call for an investigation of suitable target forms for multispectral scanners. Special targets would have to be designed for multispectral scanners, which would be discernable in several spectral bands.

10.) A further investigation should be conducted into methods of assigning elevations to data array positions. The nonparametric algorithms and mathematical modeling methods should be emphasized in this investigation, in order to see if better accuracies can be obtained, particularly for ground areas with extreme relief differences.

11.) Further investigations should be conducted concerning the applicability of the linear least squares interpolation technique for restitution of MSS digital data arrays. These investigations should include statistical testing of MSS digital data to ascertain whether the properties of stationarity, isotropy, and ergodicity may properly be assumed for such data. If so, further investigations may be conducted concerning pre-processing algorithms and covariance functions which may be useful in applying the linear least squares method to MSS digital data arrays.

12.) A systems analysis should be attempted to try to determine the most effective restitution method. In this investigation, accuracy of restitution has been the primary criteria for comparison. This should be supplemented by an economic analysis to determine the most efficient of the methods in terms of the total computing time involved as well as the human intervention necessary.

13.) Algorithms should be developed to determine quantitative information during the process of automated interpretation and restitution. Of particular interest would be algorithms to determine areas on the Earth's surface, in order that a processing system would result in both classifications and estimations of areas containing classes of interest.

14.) Investigations should be carried out on the usefulness of multi-scanned data arrays, particularly sidelapping flight lines. It is necessary that some data arrays be generated utilizing data from sidelapping flight lines, in order to assess the usefulness of such data. If this data were to become available, it would be possible to perform tests to determine whether this method could compete favorably with map contour digitization as a source of element elevation information, in terms of accuracy and cost.

As with most research efforts, the investigations carried out point to new problems and possibilities associated with the utilization of MSS data arrays. There is certainly no lack of possible research topics to be considered within this relatively young technology. As further research is carried forth, new paths of inquiry will doubtless become apparent.

BIBLIOGRAPHY

BIBLIOGRAPHY

1. Landgrebe, D., "Systems Approach to the Use of Remote Sensing", Course Notes: "Remote Sensing Technology and Applications", LARS, Purdue University, July 31 - Aug. 11, 1972.

2. Konecny, G., "Metric Problems in Remote Sensing", Paper presented to the Symposium of Commission IV, ISP, Delft, Netherlands, Sept., 1970.

3. Granicher, J., "Some Fundamentals of Remote Sensing", Unpublished paper presented to the CE 603, Advanced Photogrammetry class at Purdue University, May, 1971.

4. Committee on Remote Sensing for Agricultural Purposes, National Research Council, "Remote Sensing with Spectial Reference to Agriculture and Forestry", National Academy of Sciences, Washington, D.C., 1970.

5. Mikhail, E., and Baker, J., "Geometric Aspects in Digital Analysis of Multi-Spectral Scanner MSS) Data", Presented to the ASP Spring Meeting, Washington, D.C., Mar., 1973.

6. Leberl, F., "On Model Formation with Remote Sensing Imagery", Osterreichische Zeitschrift fur Vermessungswesen, 1972/2.

7. Konecny, G., "Geometrical Aspects of Remote Sensing", Invited paper, Commission IV, International Congress of Photogrammetry, Ottawa, 1972.

8. Hempenius, S., "Image Formation Technique for Remote Sensing from a Moving Platform", ITC Series A, No. 46, and ITC Series B, No. 53, Delft, 1969.

9. Holmes, R., and MacDonald, R., "The Physical Basis of System Design for Remote Sensing in Agriculture", Proc. of the IEEE, Vol. 5, No. 4.

10. Texas Instruments Incorporated, "Infrared System Design Considerations, SP14-GP68, May, 1968.

11. Silva, L., "Radiation and Instrumentation in Remote Sensing", Course Notes: "Remote Sensing Technology and Applications", LARS, Purdue University, July 31 - Aug. 11, 1972.

12. Simmons, W., "Multispectral Data Pre-processing", Unpublished LARS document.

13. Hoffer, R., Anuta, P., and Phillips, T., "Application of ADP Techniques to Multiband and Multiemulsion Digitized Photography", Photogrammetric Engineering, Vol. XXXVII, No. 10, Oct., 1972.

14. Swain, P., "Pattern Recognition: A Basis for Remote Sensing Data Analysis", LARS Information Note 111572.

15. Nilsson, N., "Learning Machines", McGraw-Hill, New York, 1965.

16. Nagy, G., "State of the Art in Pattern Recognition", Proc. of the IEEE, Vol. 56, No. 5.

17. Landgrebe, D., et. al., "Automatic Identification and Classification of Wheat by Remote Sensing", LARS Info. Note 21567.

18. Haralick, R., and Kelly, G., "Pattern Recognition with Measurement Space and Spatial Clustering for Multiple Images", Proc. of the IEEE, Vol. 57, No. 4.

19. Wacker, A., and Landgrebe, D., "Boundaries in Multispectral Imagery by Clustering", IEEE Symposium on Adaptive Processes (9th) Decision and Control.

20. Forrest, R., "Geometric Processing of ERTS Images", Paper presented to the Fall ASP-ACSM Convention, Sept. 7-11, 1971.

21. Kratky, V., "Precision Processing of ERTS Imagery", Proceedings of the Fall ASP-ACSM Convention, Sept. 7-11, 1971.

22. Derenyi, E., "An Exploratory Investigation Concerning the Relative Orientation of Continuous Strip Imagery", Tech. Report #8, Dept. of Survey Engineering, University of New Brunswick, Fredricton, N. B., Canada, 1971.

23. Masry, S., "Analytical Treatment of Stereo Strip Photos", Photogrammetric Engineering, Vol. XXXV, No. 12, Dec., 1969.

24. Derenyi, E., and Konecny, G., "Geometry of Infrared Imagery", Canadian Surveyor, Vol. XXVIII, No. 4, Sept., 1964.

25. Derenyi, E., and Konecny, G., "Geometry of Infrared Imagery", Photogrammetric Engineering, Vol. XXXII, No. 5, Sept., 1966.

26. Hallert, B., "Photogrammetry", McGraw-Hill Book Co. Inc. New York, 1960.

27. American Society of Photogrammetry, "Manual of Photogrammetry", Third Edition, Falls Curch, Va., 1966.

28. Katz, A., "A Problem at Inch'on", Photogrammetric Engineering, Vol. XVII, No. 1, Mar., 1951.

29. Katz, A., "Height Measurements with the Stereoscopic Continuous Strip Camera", Photogrammetric Engineering, Vol. XVIII, No. 1, Mar., 1952.

30. Wohl, M., and Stickle, S., "Continuous Strip Photography - An Approach to Traffic Studies", Photogrammetric Engineering, Vol. XXV, No. 3, 1959.

31. Elms, D. G., "Mapping with a Strip Camera", Photogrammetric Engineering, Vol. XXVIII, No. 4, Sept., 1962.

32. Ockert, D., "Sattelite Photography with Strip and Frame Camera", Photogrammetric Engineering, Vol. XXVI, No. 4, 1960.

33. Abraham, V., "Relative Geometric Strength of Frame, Strip, and Panoramic Cameras", Photogrammetric Engineering, Vol. XXVII, No. 5, Dec., 1961.

34. Itek Laboratories, "Panoramic Progress - Part I", Photogrammetric Engineering, Vol. XXVII, No. 5, Dec., 1961.

35. Itek Laboratories, "Panoramic Progress - Part II", Photogrammetric Engineering, Vol. XXVIII, No. 1, Mar., 1962.

36. Kawachi, D., "Image Motion Due to Camera Rotation", Photogrammetric Engineering, Vol. XXXI, No. 5, Sept., 1965.

37. Gullickson, S., "Continuous Strip Photography", Photogrammetric Engineering, Vol. XXXIII, No. 3, Mar., 1967.

38. Gill, C., "Relative Orientation of Sequented Panoramic Grid Models on the AP-II", Photogrammetric Engineering, Vol. XXX, No. 6, Nov., 1964.

39. Hovey, S., "Panoramic Possibilities and Problems", Photogrammetric Engineering, Vol. XXXI, No. 4, July, 1965.

40. Skiff, E., "Analytic Treatment of Strip and Pan Photos", Photogrammetric Engineering, Vol. XXXIII, No. 11, Nov., 1967.

41. Case, J., "The Analytical Reduction of Panoramic and Strip Photography", Photogrammetria, 1967.

42. Wright, R., "A Panoramic Rectifier for Tactical Field Use", Photogrammetric Engineering, Vol. XXXIV, No. 3, Mar., 1968.

43. Alderman, P., "Lunar Control Densification with Panoramic Space Photography", Proceedings of the Fall Convention, ASP, Oct., 1972.

44. Schut, G., "Formation of Strips from Independent Models", Photogrammetric Engineering, July, 1968.

45. Leberl, F., "Untersuchung uber die Geometrie und Einzelbildauswertung von Radarschragaufnahmen", Dissertation, Technical University Vienna, 1971.

46. Suits, G., "The Nature of Infrared Radiation and Ways to Photograph It", Photogrammetric Engineering, Vol. XXVI, No. 5, Dec. 1960.

47. Colwell, R., et. al., "Basic Matter and Energy Relationships Involved in Remote Reconnaissance", Photogrammetric Engineering, 1963, pp. 761-799.

48. Leonardo, E., "Capabilities and Limitations of Remote Sensors", Photogrammetric Engineering, 1064, pp. 1005-1010.

49. Harris, D., and Woodbridge, C., "Terrain Mapping by Use of Infrared Radiation", Photogrammetric Engineering, Vol. XXX, No. 1, Jan., 1964.

50. Suits, G., "Declassification of Infrared Devices", Photogrammetric Engineering, Vol. XXXII, No. 6, Nov., 1966.

51. Holter, Nudelmann, Suits, Wolfe, & Zissis, "Fundamentals of Infrared Technology", McMillan Co., New York, 1962.

52. Levine, D., "Radargrammetry", McGraw-Hill Book Co., New York, 1960.

53. Laboratory for Applications of Remote Sensing (LARS), Purdue University Research Bulletin, No. 831, July, 1967.

54. Laboratory for Applications of Remote Sensing (LARS), Purdue University Research Bulletin, No. 832, July, 1967.

55. Laboratory for Applications of Remote Sensing (LARS), Purdue University Research Bulletin, No. 844, 1968.

56. Laboratory for Applications of Remote Sensing (LARS), Purdue University Research Bulletin, No. 973, Dec., 1970.

57. Proceedings: "Third Symposium on Remote Sensing of Environment", University of Michigan, Oct. 14-16, 1964.
Also subsequent symposia.
4th - 1966
5th - April, 1968
6th - Oct., 1969
7th - May, 1971

58. Wilson, C., "Multispectral Data Processing and Results", Presented paper, Commission VII, International Congress of Photogrammetry, Ottawa, 1972.

59. Lapides, M., "Aircraft Multispectral Data Systems - Why Use Them?" Proceedings of the Spring Convention, ASP, Mar., 1973.

60. Carnes, R., "Advances in Scanners", Presented paper, Commission VII, International Congress of Photogrammetry, Ottawa, 1972.

61. Konecny, G., "Metric Problems in Remote Sensing", Proceedings of ISP Commission IV Symposium, ITC Series A, No. 50, Delft, 1971.

62. Konecny, G., "Geometrische Probleme der Fernerkundung", Bildmessung und Luftbildwesen, July, 1972.

63. Konecny, G., "Orientierungsfragen bei Streifenbildern und Aufnahmen der Infrarotabtastung", Bildmessung und Luftbildwesen, 1971, p. 60.

64. Taylor, J., "Rectification Equations for Infrared Line-Scan Imagery", Proceedings of the ISP Commission IV Symposium, ITC Series A, No. 50, pp. 178-194.

65. Leberl, F., "Metric Properties of Imagery Produced by Side-Looking Airborne Radar and Infrared Linescan Systems", ISP-Commission IV Symposium, ITC Publication A-50, Delft, 1970.

66. Leberl, F., "Vorschlarg zure Instrumentellen Entzerrung Von Abbildungen mit Seitwarts-Radar (SLAR) und Infrarotabtastsystemen (IRLS), Bildmessung und Luftvildwesen, 1971/2.

67. Leberl, F., "Remote-Sensing, Neue Entwicklungen zur Wohrnehmung auf Abstand", Osterreichische Zeitschrift fur Vermessungswesen, 1971/2.

68. Leberl, F., "Evaluation of Single Strips of Side Looking Radar Imagery," Invited paper, 12th International Congress for Photogrammetry, Ottawa, 1972.

69. Markarian, H., Bernstein, R., Ferneyhough, D., Gregg, L., and Sharp, F., "Implementation of Digital Techniques for Correcting High Resolution Images", Proceedings of the Fall Meeting, ASP, Sept., 1971.

70. Masry, S., and Gibbons, J., "Rectification of Infrared Imagery", Presented paper, Commission I, International Congress of Photogrammetry, Ottawa, 1972.

71. Forrest, R., "The LR-2 Line-Drawing Rectifier", Presented paper, Commission II, International Congress of Photogrammetry, Ottawa, 1972.

72. Bosman, E., et. al., "KARIN - A Programme System for the Mapping of Remote Sensing Information", Presented paper, Commission III, International Congress of Photogrammetry, Ottawa, 1972.

73. Graham, L., "An Improved Orthographic Radar Restitutor", Presented paper, Commission II, International Congress of Photogrammetry, Ottawa, 1972.

74. Yoritomo, K., "Methods and Instruments for the Restitution of Radar Pictures", Presented paper, Commission II, International Congress of Photogrammetry, Ottawa, 1972.

75. Forrest, R., "Mapping from Space Images", Bendix Technical Journal, Vol. 3, No. 2, 1970.

76. Beilock, M., "An Orbiting Line-Scanning System for Cartographic Data", Bendix Technical Journal, Vol. 3, No. 2, 1970.

77. McEwen, R., "Geometric Calibration of the RBV System for ERTS", Proceedings of the 7th Symposium for Remote Sensing of the Environment, University of Michigan, May, 1971.

78. Wong, K., "Fidelity of Space T. V.", Photogrammetric Engineering, Vol. 36, No. 5, May, 1970.

79. National Aeronautics and Space Administration, "ERTS Data Users Handbook", NASA Goddard Space Flight Center, Document No. 71SD4249.

80. National Aeronautics and Space Administration, "Design Study Specifications for ERTS-A and -B", 1970.

81. Doyle, F., "Imaging Sensors for Space Vehicles", Presented paper, 12th International Congress for Photogrammetry, Ottawa, 1972.

82. Doyle, F., "Instruments and Techniques for Cartographic Processing of Space Photography", Presented paper, 12th International Congress for Photogrammetry, Ottawa, 1972.

83. Colvocoresses, A., "Image Resolution for ERTS, Skylab, and Gemini/Apollo", Photogrammetric Engineering, Vol. XXXVIII, No. 1, Jan., 1972.

84. Colvocoresses, A., "ERTS - A Sattelite Imagery", Photogrammetric Engineering, Vol. 36, No. 6, April, 1970.

85. Kratky, V., "Photogrammetric Aspects of Precision Processing of ERTS Imagery", Proceedings of the First Canadian Symposium on Remote Sensing, Ottawa, 1972.

86. Kratky, V., "Photogrammetric Solution for Precision Processing of ERTS Images", Presented paper, International Congress of Photogrammetry, Ottawa, 1972.

87. Kratky, V., "Cartographic Accuracy of ERTS Imagery", Proceedings of Spring Convention, ASP, March, 1973.

88. Johnson, R., "The Image Processing System for the Earth Resources Technology Satellite", Presented paper, Commission II, International Congress of Photogrammetry, Ottawa, 1972.

89. Chapelle, W., et. al., "The Precision Processing Subsystem for the Earth Resources Technology Satellite", Presented paper, Commission II, International Congress of Photogrammetry, Ottawa, 1972.

90. American Society of Photogrammetry, "Manual of Photographic Interpretation", Falls Church, Va., 1960.

91. Lucas, J., "Differentiation of the Orientation Matrix by Matrix Multipliers", Photogrammetric Engineering, Vol. XXIX, No. 4, July, 1963.

92. Finsterwalder, S., "Die Geometrischen Grundlagen der Photogrammetric", Jahresbericht der Deutschen Mathematisch Vereinigung, VI, 2, Leipzig, 1899.

93. Von Gruber, O., "Photogrammetry, Collected Lectures and Essays", American Photographic Publishing Co., Boston, 1942.

94. Doyle, F., "The Historical Development of Analytical Photogrammetry", Photogrammetric Engineering, Vol. XXX, No. 2, Mar., 1964.

95. Phillips, T., "EQUDST, LARS Program Abstract", Unpublished program and documentation written at LARS, Sept., 1970.

96. Trinder, J., "EQUDST, A Generalization", Unpublished document written at LARS, Jan., 1973.

97. Pinkwart, E., "Die Umformung ungleichartiger Koordinaten in der Praxis", Allgemeine Vermessungs-Nachrichten, 1938.

98. Schatz, U., "Das Problem der optimalen Stutzpunktdichte und der optimalen Maschengrosse bei Transformationen ungleighartiger Koordinaten", Ph.D. Thesis, Bonn, 1970.

99. Kraus, K., and Mikhail, E., "Linear Least-Squares Interpolation" Presented paper, Commission II, International Congress of Photogrammetry, Ottawa, 1972.

100. Moritz, H., "Zur Fehlertheorie in der physikalischen Geodasie", Zietschrift fur Vermessungswesen, 1963.

101. Moritz, H., "Schwerevorhersage und Ausgleighsrechnung", Zeitschrift fur Vermessungswesen, 1965.

102. Wolf, H., "Pradiktion und Punktausgleichung", Zeitschrift fur Vermessungswesen, 94/5, 1969.

103. Hardy, R., "Multiquadric Equations of Topography and Other Irregular Surfaces", Journal of Geophysical Research 76, 1971.

104. Hardy, R., "The Analytical Geometry of Topographic Surfaces", Proceedings of the Spring Convention, ASP, Mar., 1972.

105. Jancaitis, J., and Junkins, J., "Modeling Irregular Surfaces", Photogrammetric Engineering, Vol. XXXIX, No. 4, April, 1973.

106. Johannsen, C., Bauer, M., et. al., "Corn Blight Watch Experiment and Results", LARS Print 012372.

107. Phillips, T., et. al., "1971 Corn Blight Watch Experiment Data Processing, Analysis, and Interpretation" LARS Print 012272.

108. Shapiro, S., and Wilk, M., "An Analysis of Variance Test for Normality (Complete Samples)", Biometrika, Vol 52, 1965.

109. Yaglom, A., "An Introduction to the Theory of Stationary Random Functions", Prentice Hall, Engleweed Cliffs, N. J., 1962.

110. Anuta, P., "OVERLA", Unpublished program and documentation written at LARS.

111. Brown, D., et. al., "Research in Mathematical Targeting. The Practical and Rigorous Adjustment of Large Photogrammetric Nets", Technical Documentary Report No. RADC-TDR-353, Oct., 1964.

112. Mikhail, E., Class notes for CE 604, Analytical Photogrammetry, Purdue University, June - Sept., 1971.

113. Greenwalt, C., and Shultz, M., "Principles of Error Theory and Cartographic Applications", ACIC Technical Report No. 96, Feb., 1962.

114. Bendat, J., and Piersol, A., "Measurement and Analysis of Random Data", John Wiley and Sons, Inc., New York, 1966.

APPENDICES

APPENDIX A

DIFFERENTIAL FORMULAS FROM LINEARIZED COLLINEARITY EQUATIONS

If the collinearity equations of (2.19) are linearized using the procedures of Section 2.4, the resulting linearized form of the equations is

$$\underline{F} = \underline{F}'^{o} + \dot{\underline{B}}'_{o}\,\underline{D}\,\delta x + \underline{A}'_{1}\,\delta y + \ddot{\underline{B}}'\,\ddot{\underline{\Delta}} + \dot{\underline{B}}'_{o}\,\underline{C}\,\dot{\underline{\Delta}} \tag{A.1}$$

in which the $\underline{B}'_{o}$, $\underline{A}'_{1}$, $\ddot{\underline{B}}'$, $\underline{C}$, $\underline{D}$ Jacobian matrices and $\underline{F}'^{o}$, $\ddot{\underline{\Delta}}$, $\dot{\underline{\Delta}}$ vectors are as defined in Section 2.4. These equations may be written in the form

$$\underline{F} = F'^{o} + \dot{\underline{B}}'_{o}\,\underline{D}\,\delta x + \underline{A}'_{1}\,\delta y - \underline{I}\begin{bmatrix}\delta X\\ \delta Y\end{bmatrix} + \ddot{\underline{B}}'_{3}\,\delta Z + \dot{\underline{B}}'_{o}\,\underline{C}\,\dot{\underline{\Delta}} \tag{A.2}$$

in which

$$\ddot{\underline{B}}'_{3} = \begin{bmatrix}\frac{\partial F_1}{\partial Z}\\ \\ \frac{\partial F_2}{\partial Z}\end{bmatrix} = \begin{bmatrix}U'/W'\\ \\ V'/W'\end{bmatrix} \tag{A.3}$$

and is obtained by partitioning the $\ddot{\underline{B}}'$ matrix ($\ddot{\underline{B}}' = [-\underline{I}\ \ddot{\underline{B}}'_{3}]$).

This linearized form of the collinearity equations is useful, as it may be solved directly for (δX, δY) object space differential changes, which results in the form

$$\begin{bmatrix} \delta X \\ \delta Y \end{bmatrix} = \underline{F}'^{o} + \dot{\underline{B}}'_{o}\,\underline{D}\,\delta x + \underline{A}'_{1}\,\delta y + \ddot{\underline{B}}'_{3}\,\delta Z + \dot{\underline{B}}'_{o}\,\underline{C}\,\dot{\underline{A}} \qquad (A.4)$$

which may be used to investigate object space planimetric coordinate displacements resulting from small changes in the parameters of exterior orientation.

As an example, consider the case of a single scan line for which the elements of exterior orientation may be assumed constant, due to the short time interval needed to record a single line. For this case

$$\begin{aligned} X &= X^{o} + \delta X \\ Y &= Y^{o} + \delta Y \end{aligned} \qquad (A.5)$$

The term $h = Z_c - Z$ is introduced, and the initial approximations of (X, Y) may be defined as (using $\theta = y/c$)

$$\begin{bmatrix} X^{o} \\ Y^{o} \end{bmatrix} = \begin{bmatrix} X_c \\ Y_c + h \tan\theta \end{bmatrix} = \underset{2,1}{0} \qquad (A.6)$$

and the initial approximations of the angular orientation elements (ω, ϕ, κ) may be taken as zero ($\underline{M} = \underline{I}$). The $\underline{F}'^{o}$ vector becomes

$$\underline{F}'^{o} = \begin{bmatrix} X_c - X_c \\ Y_c - Y_c - h \tan\theta^{o} + h \tan\theta^{o} \end{bmatrix} = \underset{2,1}{0}$$

Evaluating the Jacobian matrices of Equation (A.4),

$$\underset{2,6}{\dot{B}'_o} = \begin{bmatrix} 1 & 0 & 0 & 0 & -h & -h\tan\theta \\ 0 & 1 & \tan\theta & h(1+\tan^2\theta) & 0 & 0 \end{bmatrix}$$

$$\underset{2,1}{A'}_1 = \begin{bmatrix} 0 \\ \frac{h}{c}\sec^2\theta \end{bmatrix} \qquad \underset{2,1}{\ddot{B}'}_3 = \begin{bmatrix} 0 \\ -\tan\theta \end{bmatrix}$$

$$\underset{6,1}{D} = \underset{6,1}{0} \qquad \underset{6,6}{C} = \underset{6,6}{I}$$

Substituting these results into Equation (A.4) results in

$$\begin{aligned} \delta X &= \delta X_c - h\delta\phi - h\tan\theta\delta\kappa \\ \delta Y &= h/c\sec^2\theta\,\delta y - \tan\theta\,\delta Z + \delta Y_c + \tan\theta\,\delta Z_c + h(1+\tan^2\theta)\delta\omega \end{aligned} \tag{A.7}$$

If it is assumed that terrain elevation (Z) is constant in order to accomplish the transformation of a two dimensional vector then $Z = 0$. If it is desired to investigate the effects of changes of exterior orientation elements only, then the image y coordinate is assumed to have no error, so that $\delta y = 0$. Making the substitution $\sec^2\theta = 1 + \tan^2\theta$, the resulting equations become

$$\begin{aligned} \delta X &= \delta X_c - h(\delta\phi) - h\tan\theta(\delta\kappa) \\ \delta Y &= \delta Y_c + \tan\theta(\delta Z_c) + h\sec^2\theta(\delta\omega) \end{aligned} \tag{A.8}$$

If these results and those of Equations (A.6) are substituted directly into Equations (A.5), the resulting differential form of these equations becomes

$$X = X_c + \delta X_c - h\delta\phi - h \tan\theta \, \delta\kappa \qquad (A.9)$$

$$Y = Y_c + h \tan\theta + \delta Y_c + \tan\theta \, \delta Z_c + h \sec^2 \delta\omega$$

Equations (A.8) may be seen to be identical in form to those of Equations (2.16), demonstrating the validity of the linearized collinearity equations as a general form from which specific cases may be examined.

APPENDIX B

DERIVATION OF RESAMPLING ALGORITHM TO INCLUDE TOPOGRAPHIC EFFECTS [96]

Referring to Figure 3.4, the scan line length is given by

$$W = h_1 \tan(n\gamma) + h_N \tan(N\gamma - n\gamma) \tag{B.1}$$

After resampling, every sample has an equal length in the direction along the scan.

$$\Delta Y = \frac{W}{N} \tag{B.2}$$

From Figure 3.4, the distance d_j may be written, in terms of sample widths as

$$d_j = j(W/N) - 1/2(W/N) \tag{B.3}$$

Introducing the term $h_{L_j} = Z_c - Z_{L_j}$, the distance may also be written in terms of sample angle γ as

$$d_j = h_1 \tan n\gamma + h_{L_j} \tan(U_j\gamma - n\gamma) \tag{B.4}$$

Equating the right hand sides of (B.3) and (B.4) and solving for U_j yields

$$U_j = n + \frac{1}{\gamma} \tan^{-1}\left[\frac{W}{Nh_{L_j}}\left(\frac{2j - 1}{2}\right) - \frac{h_1 \tan n\gamma}{h_{L_j}}\right] \tag{B.5}$$

If Equation (B.1) is substituted into (B.5), the final resulting expression is

$$U_j = n + \frac{1}{\gamma} \tan^{-1} \left[\frac{1}{h_{L_j}} \left(\frac{2j - 1}{2N} h_1 \tan n\gamma + \frac{2j - 1}{2N} h_N \tan(N\gamma - n\gamma) - h_1 \tan n\gamma \right) \right] \tag{B.6}$$

The solution of this algorithm requires an iterative approach, since the value h_{L_j} is not known until the algorithm has been solved for U_j. As a first approximation,

$$\Delta h_{L_j} = h_j - h_1$$

The algorithm is solved, the updated value h_{L_j} is found, and the algorithm is reapplied for an updated U_j value.

As an example, consider a typical aircraft flight in which Z_c = 5000 ft. (1.52 km), γ = 6 mrad, and symmetric scanning for which N = 222, n = N/2 = 111. If it further assumed that $Z_1 = Z_n$ = 600 ft. (183 m), then $h_1 = h_N$ = 4400 ft. (1.34 km). For this example the value of U will be computed for j = 50, a value which results in a near maximum displacement (see Figure 3.3) and it is further assumed that Z_{50} = 600 ft. (183 m) in the unprocessed array and that the ground slope (λ) in the vicinity is 0.5, a relatively extreme case. Using these values in Equation (B.6), the first solution for U_j results in

$$U_j = 111 + 1/.006 \tan^{-1}\{(1/4400)[(99/444)(4400)\tan(0.666) + (99/444)(4400)\tan(0.666) - 4400 \tan 0.666]\}$$

$$U_j = 42.6$$

For the next iteration the value of $Z_{L_j} = Z_{42}$ is utilized instead of Z_{50}. The size of a ground element in the vicinity for this case (from Figure 1.19) is approximately 30 ft. (9.1 m), and would result in a change in elevation over the eight elements of 120 ft. (36.6 m). If the ground slope is positive then Z_{42} = 720 ft. (219.5 m). Utilizing this updated value in Equation (B.6) results in

$$U_j = 40.9$$

a change of approximately 1.7 elements. If one further iteration is carried out using $Z_{L_j} = Z_{40}$, the value becomes

$$U_j = 40.7$$

If the ground slope is negative, then for the second iteration Z_{42} = 480 ft. (146.3 m). Utilizing this updated value in (B.6) results in

$$U_j = 41.8$$

and a further iteration produces negligible change. It was found during the investigation that a single iteration is sufficient to refine the resampled position within one array element.

APPENDIX C

ADDITIONAL BIBLIOGRAPHY

The major portion of the literature survey included in the thesis was completed in mid year of 1973. The following represents publications relevant to the investigation which have appeared since that time.

Bair, L. and Carlson, G., "Height Measurement with Stereoradar", Photogrammetric Engineering, Vol. XLI, No. 2, Feb. 1975.

Baker, J., Marks, G. and Mikhail, E., "Analysis of Digital Multispectral Scanner (MSS) Data", Bildmessung und Luftbildwesen (special English edition), March 1975.

Colvocaresses, A., "The Map Projection of the ERTS Multispectral Scanner", Proceedings of Spring Convention, ASP, March 1974.

Derenyi, E., "SLAR Geometric Test", Photogrammetric Engineering, Vol. XL, No. 5, May 1974.

Derenyi, E., "Planimetric Accuracy of Infrared Line Scan Imagery", The Canadian Surveyor, Vol. 28, No. 3, Sept. 1974.

Derochie, W. and Forrest, R., "Potential Positioning Accuracy of ERTS 1 MSS Images", Proceedings of Spring Convention, ASP, March 1974.

Kalensky, Z. and Sayn-Wittgenstein, L., "Thematic Map of Larose Forest from ERTS-1/MSS Digital Data", The Canadian Surveyor, Vol. 28, No. 2, June 1974.

Kratky, V., "Cartographic Accuracy of ERTS", Photogrammetric Engineering, Vol. XL, No. 3, Mar. 1974.

Malhotra, R., "Absolute Spatial Registration of Skylab S192 Conical Scanner Imagery by Means of Dynamic Geometric Modeling", Proceedings of Spring Convention, ASP, March 1974.

Masry, S., "Digital Correlation Principles", Photogrammetric Engineering, Vol. XL, No. 3, Mar. 1974.

Rader, M., "A General Solution for the Registration of Optical Multispectral Scanners", Proceedings of the Spring Convention, ASP, March 1974.

Shmutter, B. and Ertog, U., "Analysis of Panoramic Photographs", Photogrammetric Engineering, Vol. XL, No. 4, April 1974.

Schoonmaker, J., "Geometric Evaluation of MSS Images from ERTS-1", Proceedings of the Spring Convention, ASP, March 1974.

van Roessel, J. and de Godoy, R., "SLAR Mosaics for Project RADAM", Photogrammetric Engineering, Vol. XL, No. 5, May 1974.

Woolnough, D., "A Simple Method of Digitizing Line Drawn Maps Using Densitometric Data", The Canadian Surveyor, Vol. 28, No. 1, March 1974.